An investigation of the role of Neuronal PAS Domain Protein 2 (NPAS2) in peripheral circadian clocks

Mitchell Masterson, BSc.

Submitted to the University of Nottingham for the degree of

Doctor of Philosophy

March 2021

Abstract

Circadian cycles are 24-hour biological oscillations, observable in an array of physiological and behavioural systems including the sleep wake cycle, metabolism, cardiovascular activity, and cognition. The core circadian clock, located in the suprachiasmatic nucleus (SCN) of the brain, is entrained by environmental light and is responsible for entrainment of oscillators in other tissues, known as peripheral clocks. Light entrainment via the SCN is not the only signal that can entrain circadian cycles, they can also be entrained by other cues such as time of feeding (reflecting environmental food availability), which acts to entrain peripheral cycles without requirement of the SCN. The molecular underpinnings of these peripheral clocks, responsible for this entrainment and various tissue-specific circadian effects, are incompletely understood. In these studies, we focused on investigation of the functional role of the transcription factor NPAS2 in liver and fibroblast peripheral clocks.

NPAS2 is a bHLH-PAS domain transcription factor and heterodimeric partner of BMAL1 that forms part of the positive arm of the core circadian feedback loop. Expression of either NPAS2 or its more well characterised paralog CLOCK have been shown in mouse gene KO studies to be required for functional circadian cycles. Constitutive KO of the NPAS2 gene in mice has also been found to severely delay circadian entrainment to time of feeding and enhance the entrainment to light but the precise role of NPAS2 in this entrainment is unclear. As feeding entrainment of behaviour is closely associated with the entrainment of peripheral clocks it is unknown if this effect is due to the loss of NPAS2 in the peripheral tissues or in the core clock in the constitutive KO. We aimed to investigate the function of NPAS2 in the molecular feedback cycle in peripheral clocks, and how it contributes to circadian behavioural entrainment. As loss of NPAS2 expression has also been found to impair long term fear conditioning performance we investigated the potential contribution of the liver peripheral

clock to this, and latent inhibition of fear conditioning.

To investigate NPAS2 function we utilised both cellular and mouse models. For cellular studies in NIH3T3 fibroblasts, *NPAS2* or *CLOCK* genes were targeted using CRISPR-Cas9 editing. Clonal lines were selected that showed loss of expression/function as confirmed by allele genotyping, western blots and RT-qPCR. It was observed that ablation of NPAS2 in NIH3T3 cells resulted in alterations in rhythmic expression of other core clock genes, including *CRY2* and both *REV-ERBα* and *REV-ERBβ* genes of the negative arm of the feedback loop. Indeed, robust increases of the endogenous *REV-ERBα* and *REV-ERBβ* genes were observed, suggesting that NPAS2 may negatively regulate these genes.

A liver-specific NPAS2 cKO mouse model was used to investigate expression of select core clock genes in liver and brain tissues, and also correlate this with behavioural effects of the loss of NPAS2 in the liver. In this mouse model we observed modulated expression levels of the *REV-ERB* genes in the liver across circadian time points. Interestingly however, we also observed significant changes in rhythmic expression of selected core clock genes in brain samples that included tissue from the prefrontal cortex and from other cortical (including motor cortical) and subcortical regions of the liver-specific cKO mice. We observed the appearance of variance in expression of *BMAL1* at different times of day and the loss of similar time variance in the expression of *REV-ERBβ*. This raises the novel suggestion that ablation of NPAS2 in the liver clock can influence rhythmic gene expression in the brain.

In contrast to the constitutive KO model, we found no effect of loss of liver NPAS2 on light entrainment but observed an enhancement of restricted feeding entrainment, although this effect was restricted to female mice. This suggests a sex-specific mechanism is involved in feeding entrainment and that loss of NPAS2 in the liver is beneficial for food entrainment. Investigation of fear conditioning and latent inhibition identified no effect of the loss of NPAS2 in the liver although a genotype independent sex effect on fear conditioning supports further

sex-specific investigation.

These findings suggest a systemic effect of loss of NPAS2 expression within the liver, influencing behavioural cycles and gene expression in separate tissues. This suggests the liver peripheral clock contributes to circadian behavioural cycles and entrainment of other tissues and that NPAS2 contributes to these activities of the liver clock. The mechanism behind this effect is unknown but it may be through effects on endocrine or metabolite signalling. The potential exists to breed mice with a brain specific NPAS2 KO in the future to complement these findings and investigate the specific effect of loss of NPAS2 from the central clock.

Acknowledgements

I owe huge amounts of thanks to my primary supervisor Dr Paula Moran for her assistance, guidance, advice and motivation whenever I needed it throughout my time working with her. Similarly, I am thankful to my second supervisor Prof David Heery for his advice and support throughout the project. I am very fortunate to have had two excellent supervisors for my project that I've worked so closely with.

A huge amount of thanks goes to Ruby Chrisp, both for her significant contributions to the work included here and her availability as someone to discuss any piece of work with be it the meanings of results, future directions or troubleshooting.

Thanks to Dr Hilary Collins who has been a constant and invaluable friendly source of advice for any situation. I think the very foundations of the GRRB lab would crumble to the ground without her around. DMH group, most notably Dr Jonathan Whitchurch who trained me and got me through my earliest issues as I started in the lab. Dr Bismoy Mazumder, Christopher Roberts and Ryan Morris have throughout my time been supportive and helpful in various ways and I'm very fortunate to have had them around. I would also like to thank all other members of the GRRB lab for forming such an amazing community and especially the close friends I've made in my time here.

I would like to thank Patrick Nolan and the whole Nolan group at MRC Harwell, for hosting me for my PIP and helping me in my time there to develop as a researcher.

Finally, I'd like to thank my wife Emily Masterson for her support throughout, especially while I was writing up through COVID lockdowns and working odd timed circadian experiments. I can't imagine having to write a thesis without her making sure I was able to keep working and stay focused through such a long stretch of time. I'm so thankful we were able to manage a wedding despite all the setbacks and I'm looking forward to our next adventure.

List of abbreviations

AD	Alzheimer's Disease
ANOVA	Analysis of Variance
bHLH	Basic Helix-Loop-Helix domain
Bp	Base pairs
Cas9	CRISPR-associated protein 9
Cas9n	Cas9 nickase variant
CCGs	Clock-controlled genes
ChIP-seq	Chromatin Immunoprecipitation Sequencing
cKO	Conditional knockout, within this thesis cKO is used exclusively to refer to the *NPAS2*$^{fl/fl}$/*Alb-cre* liver NPAS2 KO mouse
CLOCKΔ19	Mutant mouse model which express CLOCK lacking exon 19
CRISPR	Clustered regularly interspaced palindromic repeats
CS	Conditioned stimulus in fear conditioning experiments, in our experiments this takes the form of a tone
CT	Circadian time, a standard unit of hours of time based on an animal's free-running period. The onset of activity of mice, as nocturnal animals, is CT12
DD	Constant dark conditions
FAA	Food anticipatory activity
FEO	Food entrainable oscillator
GEE	Generalised estimating equations
GFP	Green Fluorescent Protein
HAT	Histone acetyl transferase
HDAC	Histone deacetylase
KO	Knockout; model with functional deletion of a gene
LD	Cycling light dark conditions
LI	Latent Inhibition
LL	Constant light conditions
MW	Molecular weight
NAc	Nucleus Accumbens
NPE	Non-pre-exposed to the tone stimulus in LI experimentation
PAM	protospacer adjacent motif
PAS	Per-ARNT-Sim domain

PCR	polymerase chain reaction
PE	Pre-exposed to the tone stimulus in LI experimentation
PFC	Pre-frontal cortex
RHT	Retinohypothalamic Tract
RF	Restricted feeding
RT-qPCR	Quantitative reverse transcription PCR
SAD	Seasonal Effective Disorder
SCN	Supra-chiasmatic nucleus
SEM	Standard error of the mean
sgRNA	Single Guide RNA
WT	Wild type
ZT	Zeitgeber time, a standard unit of hours of time based on cycling stimuli provided to the animals, the time at which lights turn on is ZT0, when in LD ZT and CT should be identical provided synchronisation is complete

Table of contents

List of figures

List of tables

Chapter 1: Introduction

1.1 Circadian cycles

Circadian cycles allow organisms to anticipate daily changes and pre-emptively respond with variating behaviour and physiology. These cycles match the organism to the 24-hour daily cycles of the environment due to the Earth's rotation. Circadian cycles are seen in many biological processes and behaviours in multicellular organisms. These biological circadian cycles include cycling of behaviour, physiology, and metabolism to match optimum timing within the day and provide a survival advantage (Xie et al., 2019, Panda et al., 2002b). External stimuli, known at zeitgebers, such as light (sunlight or artificial) and feeding can induce entrainment of these cycles to environmental time. Importantly, these zeitgebers entrain the cycles but are not responsible for them. In the absence of stimuli, i.e., in constant environmental conditions, circadian cycles persist with a period length (time taken for one repetition of the cycle) of approximately 24 hours. Any daily cycles in behaviour or physiology which do not persist in the absence of zeitgebers are not true circadian cycles, just responses to cycling stimuli. The capacity for entrainment allows adaptation of an organism's daily cycles with seasons and with changes in location on the earth (Panda et al., 2002b).

In mammals the suprachiasmatic nucleus (SCN) is the key brain region responsible for orchestrating circadian cycles throughout the organism. The SCN is located just above the optic chiasm at the base of the hypothalamus and is formed of an identical pair of regions, each with a core and shell subdivision. The SCN responds to information about changes in ambient light absorbed by the retina, received through the retinohypothalamic tract (RHT), to synchronise its output rhythms. The SCN then acts to synchronise the rest of the body. It does this through a combination of neuronal (primarily GABA) and hormonal signals, control of body temperature and by influencing behaviour (Takahashi et al., 2008).

Evidence to support the role of the SCN in circadian rhythms comes from a variety of sources. Ablation of the SCN in rats results in complete arrhythmicity of adrenal corticosterone

rhythm (Moore and Eichler, 1972) and sleep-wake cycles (Mistlberger, 2005) but food-entrained rhythms survive (Krieger et al., 1977). Transplantation of a functional SCN into animals with an ablated SCN also restores the circadian behavioural cycles (Ralph et al., 1990). Even outside of the brain SCN structure, isolated SCN neurons from rats continue to cycle in their expression of action potentials for several weeks in *ex vivo* culture (Welsh et al., 1995). These findings have cemented the SCN as a key tissue responsible for circadian cycles in mammals.

1.2 Circadian study methods *in vitro* and *in vivo*

Molecular mechanisms relevant to circadian cycles can be studied, at least partly, outside of *in vivo* systems. Cells growing *in vitro* retain circadian cycles, although in most cell types the cells all cycle individually, without synchronisation from the SCN and nervous system. This means that no significant cycling can be observed in cell cultures without manual synchronisation or investigation of a single cell (Balsalobre et al., 1998). The exception to this is that some specific cell types, such as SCN and some other neuronal cells, do synchronise to each other in culture due to cell-cell communication, and in co-cultures can even synchronise the cycles of other cells (Allen et al., 2001).

The NIH3T3 mouse fibroblast cell line is frequently used in circadian studies and can be synchronised by use of multiple different shock treatments (Nagoshi et al., 2005). These treatments act by inducing the expression of genes involved in resetting circadian cycles *in vivo* through pathways such as the MAP kinase cascade (Akashi and Nishida, 2000) and action at the glucocorticoid receptor (Balsalobre et al., 2000). One of the treatments used to synchronise cell cultures is a serum shock, in which the cells are exposed to a high concentration of serum in the culture medium, factors present in the serum stimulate the expression of circadian genes by the cells at a specific time and the cells are then cultivated in serum free medium for a short

time while they cycle in synchrony (Allen et al., 2004). Treatment with forskolin (Menger et al., 2007), dexamethasone (Balsalobre et al., 2000), tetradecanoylphorbol acetate (Akashi and Nishida, 2000) or heat treatment have also been used to synchronise circadian cycles (Tsuchiya et al., 2003). The HEK293 human kidney cell line is not as commonly used in circadian studies but it has been shown that the cells can be synchronised by use of dexamethasone treatment or serum shock (Cox, 2012).

Once cells are induced to cycle in synchrony *in vitro*, gene and protein expression can be investigated in samples harvested at various time points to follow rhythmic expression. The circadian cycles can also be investigated by use of bioluminescence. A luciferase reporter under the control of a circadian gene promotor, such as that for *PER2*, will cause cycling of this luminescent reporter which can be monitored, allowing detailed assessment of the cycling behaviour including period length (Welsh and Kay, 2005). After synchronisation, cultured cells will slowly desynchronise from each other over time. This means that rhythmic measurements taken from cycling cell cultures will dampen as more time passes from when the cells were synchronised.

To study circadian cycles *in vivo* rodents can be kept under specific light/dark cycles, typically 12 hours of light and 12 hours of dark per day (12h:12h LD) or constant darkness (DD). Generally, the mice are raised in LD before being changed to DD for the period of the study. Mice then present their endogenous free-running circadian cycles in their cycles of activity. The free-running behavioural periods present slightly shorter than 24 hours, as the animals require resynchronisation to retain consistently accurate 24-hour cycles (LeGates and Altimus, 2011). The light cycle can be modified to shift earlier or later to investigate entrainment or mimic jetlag and light pulses allow close investigation of entrainment by time of presentation (LeGates and Altimus, 2011).

Most commonly, wheel running is used as a measure of the animals' activity and at

points where the wheel is spinning the animal is considered to be active, and inactive otherwise (Siepka and Takahashi, 2005). Since wheel running is an elective behaviour it should be noted that the animal may be active but not running in its wheel. This means there are periods when the animal is considered inactive as no wheel turns are recorded even though it is awake. The introduction of a running wheel to a rodent can also impact on a number of behavioural parameters, however it remains a robust assay for circadian periods (Bains et al., 2017).

To assess sleep-wake cycles the surgical implantation of electrodes for electroencephalography (EEG) and electromyography (EMG) can be used. These monitor electrical activity and the readings can be used to identify periods of neural activity reflecting sleep and wakefulness (Oishi et al., 2016). This provides very accurate measures of the sleep-wake cycle at the cost of requiring surgical procedures.

General home cage activity can be recorded by use of a camera placed at the roof of the mouse containment chamber. Cameras are used in combination with a red or infra-red light, which rodents are insensitive to, meaning the behaviour of the mice can be recorded while normal lights are off. Video tracking software can then maintain tracking location of each mouse and be used to produce data about distance travelled and time spent active or inactive, assessing sleep-wake states at a basic level without the need for electrode implantation (Pack et al., 2007, Fisher et al., 2012). General activity can also be recorded by IR beams through cages, interruption of these beams by the mouse allows placement of the mouse's location in the cage allowing similar data to be produced (Brown et al., 2016).

The molecular circadian cycle can be studied in animal models by sacrificing animals at specific time points and tissues harvested for analysis. Sacrificing groups of animals at each time point to give reliable molecular data does however require a great number of animals for appropriately powered experiments which can often restrict the number of time-points used (Zhang et al., 2014).

1.3 The molecular feedback cycle

The genetic basis for the circadian clock was initially identified in drosophila flies. Modifications of the *per* locus were identified to be associated with modified circadian behaviour (Konopka and Benzer, 1971). Within wild type flies the expression of the mRNA of *per* and its protein product were both shown to exhibit 24 hour cycles in expression showing the rhythmic expression contributes to behavioural circadian cycles (Baylies et al., 1987).

Following this, loops of the complex feedback system of clock proteins responsible for the mammalian circadian rhythms were identified. Components that have been identified as central to the mammalian circadian system are NPAS2 (neuronal PAS domain protein 2), CLOCK (circadian locomotor output cycle kaput) and BMAL1 (brain and muscle ARNT-like 1) which make up the positive arm of the circadian feedback loop. NPAS2 and CLOCK are paralogs, and either can heterodimerise with BMAL1 to form similarly acting NPAS2:BMAL1 and CLOCK:BMAL1 dimers (hereafter referred to as CLOCK/NPAS2:BMAL1 when referring to both dimers). CLOCK/NPAS2:BMAL1 dimers bind to the E-box element, a genetic sequence (CANNTG) conserved between flies and mammals, and act as transcription factors (Gekakis et al., 1998). This binding also mediates nucleosome removal, opening chromatin to facilitate the binding of other transcription factors or transcriptional repressors to exposed regions of DNA sequence. This means the binding of CLOCK/NPAS2:BMAL1 can positively or negatively influence expression of various genes (Trott and Menet, 2018).

CLOCK/NPAS2:BMAL1 action is negatively regulated by proteins whose expression is induced by the dimer's transcription factor activity, the interactions of these positive and negative arms are responsible for the 24-hour cycles of circadian rhythms. Transcription of the period proteins (PER1, PER2 and PER3) and the cryptochrome proteins (CRY1 and CRY2) is activated by the activity of CLOCK/NPAS2:BMAL1 (Jin et al., 1999, Kume et al., 1999) and as the concentration of each of the proteins increases PER:CRY heterodimers form in the

cytoplasm and translocate to the nucleus to negatively regulate CLOCK/NPAS2:BMAL1 transcription factor activity. As PER and CRY proteins are degraded and not replaced due to lack of transcription the repression of CLOCK/NPAS2:BMAL1 is relieved, beginning the cycle again (Shearman et al., 2000). The mechanism of PER and CRY negative regulation within the nucleus is different between the two gene families. CRY proteins bind to the E-box element associated CLOCK:BMAL1 and inhibit the transcription of genes by forming a stable promotor associated complex. PER proteins mediate repression of expression however, by removing CLOCK/NPAS2:BMAL1 from the E-box element in a CRY dependant manner (Ye et al., 2014). This feedback is considered the major driver of circadian rhythm although other feedback loops have been identified.

A second negative feedback loop involves the nuclear receptors REV-ERBα (*NR1D1*) and REV-ERBβ (*NR1D2*), whose expression is induced by CLOCK/NPAS2:BMAL1 through E-box association. These REV-ERB proteins repress BMAL1 and NPAS2 transcription, in competition with the ROR nuclear receptors (RORα, RORβ, and RORγ) which are activators of transcription at RORE sites (Sato et al., 2004, Preitner et al., 2002, Takeda et al., 2011). A representation of the core feedback loops is shown in Figure 1.1.

A paralog of BMAL1, BMAL2 is also able to dimerise with CLOCK and NPAS2 to function as a transcription factor, however, in BMAL1 KO models BMAL2 is unable to compensate for this loss (Bunger et al., 2000), as BMAL1 KO mice also show a knockdown of BMAL2 expression levels. In these mice it has been shown manipulation increasing expression of BMAL2 expression in BMAL1 KO mice was sufficient to recover circadian cycles (Shi et al., 2010). It is not as well identified how BMAL2 contributes to normal circadian cycles or if it differs significantly from BMAL1.

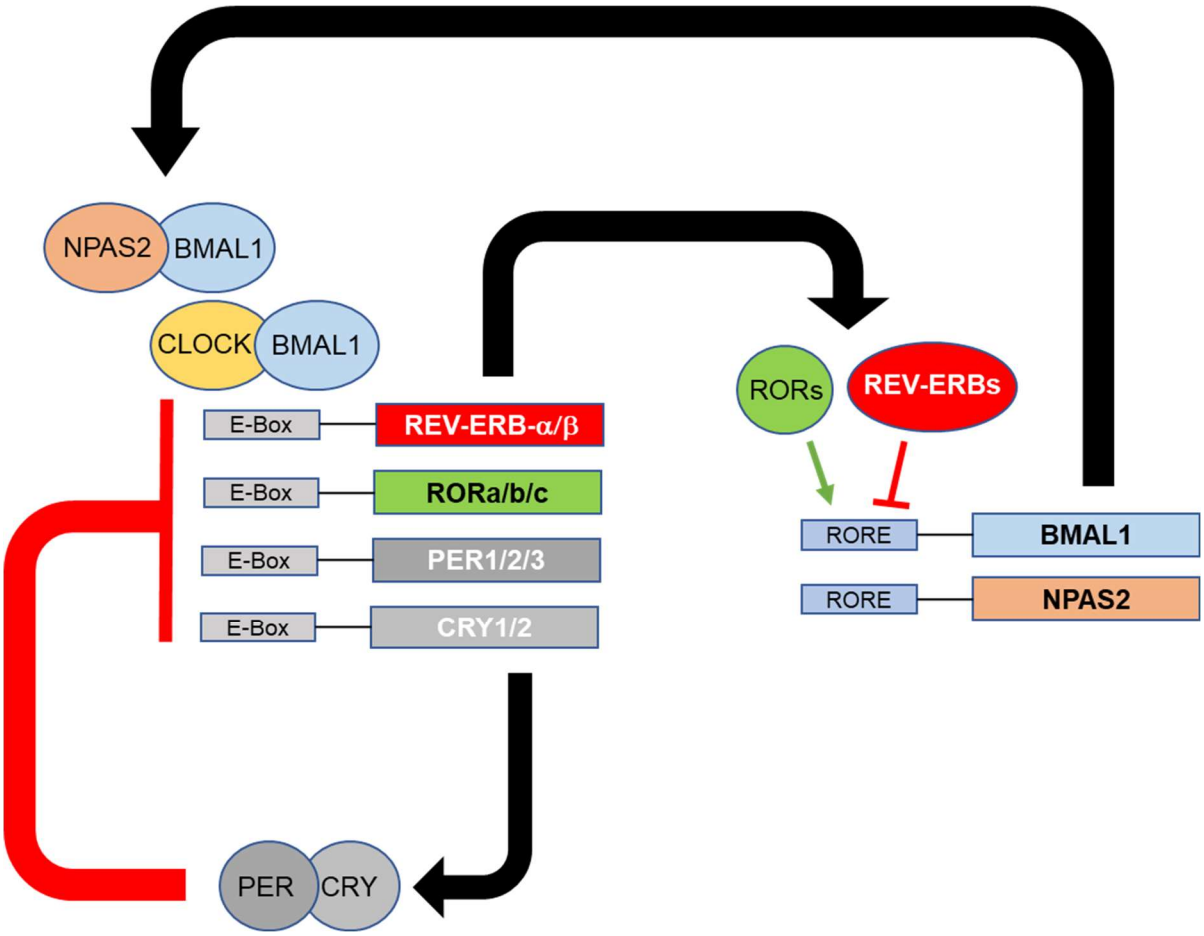

Figure 1.1: The transcriptional-translational feedback of the mammalian circadian clock. At the core of the circadian clock is the transcription factor activity of the CLOCK:BMAL1 or NPAS2:BMAL1 dimer acting at E-boxes. The PER and CRY proteins inhibit CLOCK/NPAS2:BMAL1 transcription factor activity, thereby inhibiting their own expression. The REV-ERB and ROR proteins have opposing effects on transcription at RORE sites influencing both BMAL1 and NPAS2 expression. These loops in combination with an array of other genes are responsible for ~24-hour circadian cycles in almost all cells.

Both NPAS2 and CLOCK also associate with the CLOCK interacting protein, circadian (CIPC) which is responsible for phosphorylation of the proteins required for normal function and is another possible level of circadian control (Yoshitane and Fukada, 2009). The circadian feedback loop is more complex than detailed here to permit the consistency of the 24-hour cycles and entrainment. Including these genes, more than 20 genes are considered to be 'core clock genes' which play a role in the regulatory network in mammals to produce circadian cycles (Takahashi et al., 2008).

1.4 Clock-controlled genes

The cycles of expression and activity of core clock proteins induce the cycling of physiological processes by modification of clock-controlled gene expression and protein activity. Genes which display a 24-hour cycle, including some of those which make up the molecular clock, are referred to as clock-controlled genes (CCGs). There is no clearly defined separation of CCGs from genes which make up the molecular circadian clock as a large amount of CCGs have an impact on the cycling of the cell clock (Pett et al., 2016, Li and Zhang, 2015). It has been observed that a significant fraction of the transcriptome is made up of CCGs within mouse tissues, 43% of protein coding genes and 32% of noncoding RNAs have been identified to present rhythmic expression depending on the tissue (Zhang et al., 2014).

The cycles of CCG expression are controlled by the core molecular clock in multiple ways. At the transcription level most significantly genes with an E-box promotor are induced to cycle through CLOCK/NPAS2:BMAL1 transcription factor action, while ROR and REV-ERB proteins have their nuclear receptor activity and CRY proteins can act as co-repressors for nuclear hormone receptors (Kriebs et al., 2017) all influencing gene transcription.

Circadian gene expression is also influenced at the epigenetic level. Dynamic changes

in chromatin structure are required to facilitate gene transcription and, as such, modification of chromatin is also an important step in circadian output. Chromatin modification is mediated by post-translational modifications of histones, commonly acetylation, regulated by histone acetyltransferases (HATs) which acetylate the histones and the opposing histone deacetylases (HDACs) which remove acetyl groups. Circadian rhythms of histone acetylation at promotor regions of CCGs have been shown to contribute to rhythmic gene expression (Etchegaray et al., 2003, Partch et al., 2014) and the specific histone modifications of H3K4me1, H3K4me3, H3K9ac, H3K27ac, and H3K36me3 all show diurnal variation (Vollmers et al., 2012). CLOCK/NPAS2:BMAL1 dimers have been shown to interact with the HATs CREB binding protein (CBP), p300 and the CBP-associated factor PCAF as well as HDACs including SIRT1. There are some differences in association between the two dimers, such as PCAF preferentially associating with the NPAS2:BMAL1 dimer in the vasculature clock (Curtis et al., 2004). Various HDACs also associate with other circadian genes such as SIN3-HDAC with the PER proteins (Duong et al., 2011) and HDAC3 with REV-ERBα (Feng et al., 2011), providing another level of circadian input to histone acetylation. It has also been reported that, without requiring recruitment of other proteins, CLOCK can itself act as a HAT, identified due to sequence similarity to ACTR, a member of the p160 family of transcriptional coactivators, also reported to have weak HAT activity (Chen et al., 1997). The HAT activity of CLOCK is dependent on heterodimerisation with BMAL1 and the major modification it is responsible for is H3K14ac (Doi et al., 2006, Aguilar-Arnal and Sassone-Corsi, 2015). The histone acetylation performed by CLOCK is opposed by the deacetylase activity of SIRT1 (Nakahata et al., 2008).

As well as lysine acetylation of histones, a variety of non-histone proteins can be acetylated reversibly as a post-translational modification, as part of the circadian control circuitry at the protein activity level. Acetylation can modulate protein functions, such as enzymatic activity, DNA binding capacity, protein:protein interactions or protein stability

(Masri et al., 2013). Reversible lysine acetylation has been shown to occur on both BMAL1 and PER2 modifying their function. CLOCK is responsible for the acetylation of BMAL1 on lysine 537 when associated and this acetylation appears to be required for normal circadian function (Hirayama et al., 2007). It is unknown if this acetylation occurs when NPAS2 and BMAL1 are associated or if another HAT is recruited to perform this function. The activity of the HDAC SIRT1 is responsible for deacetylation of the BMAL1 acetylation performed by CLOCK, modulating transcription factor function (Nakahata et al., 2008) and deacetylation of PER2, promoting degradation (Asher et al., 2008). In the liver various metabolic enzymes show circadian patterns of acetylation, several of which are dependent on the CLOCK protein (Masri et al., 2013).

1.5 The peripheral circadian clock

As detailed above the core circadian clock in mammals is that of the SCN, which is responsible for entrainment of all other oscillators. In terms of circadian cycles peripheral clocks refers to all oscillators which are not the SCN, including other regions of the brain. While almost all cells present circadian cycles, tissues with clear circadian involvement in their function include the vasculature, liver, kidneys, cardiac muscle, and the gastrointestinal system. Between tissues there is variation in the expression patterns of circadian genes and variation in which genes show rhythmic expression (Yeung et al., 2018). For example, *PER2* expression peaks 4-8 hours later in the liver compared to the SCN (Panda et al., 2002a). This variation is due to tissue-specific differences in chromatin accessibility and the activity of tissue-specific factors, including enhancers which associate with the CLOCK/NPAS2:BMAL1 dimer (Beytebiere et al., 2019).

Advancing or delaying the light cycle causes the rodent SCN to rapidly reset to the new timings while peripheral clocks can take longer than a week to resynchronise depending on the

tissue (Yamazaki et al., 2000). Melatonin and glucocorticoids have both been identified as acting to synchronise peripheral clocks to the SCN.

Melatonin synthesis is directly regulated by SCN inhibitory neuronal signals when exposed to light. In darkness this inhibition is alleviated and melatonin synthesis is facilitated (Korf et al., 2003). Melatonin receptors are found widely in peripheral tissues permitting entrainment through G protein-coupled receptor signalling. Melatonin signalling modifies the expression of certain core circadian genes, however, the exact mechanism by which the action at the receptor influences the circadian cycle has not been elucidated (Vriend and Reiter, 2015, Chen et al., 2020). Melatonin can also interact directly with RORα in the nucleus which may present a process for the entrainment of circadian cycles of gene expression (Carlberg, 2000). Showing the entrainment capabilities of melatonin, time restricted provision of melatonin to an *ex vivo* rat adipose culture has been shown to synchronise circadian cycles in the cells (Alonso-Vale et al., 2008).

Glucocorticoids are a group of steroid hormones which show a circadian peak of secretion around the time of activity onset and have been shown to synchronise peripheral clocks (Balsalobre et al., 2000). Expression of glucocorticoids are influenced by the SCN via direct neuronal connection to the hypothalamus–pituitary–adrenal axis (Son et al., 2011). Glucocorticoids act via binding to the glucocorticoid receptor which also presents circadian expression mediated by the action of CRY1 and 2 (Lamia et al., 2011). The activity of the glucocorticoid receptor at glucocorticoid response elements (GREs) has been identified to regulate the expression of the *PER* genes (Yamamoto et al., 2005, So et al., 2009) influencing the circadian cycle. In the liver similar activity at a GRE influences expression of HNF4α which then regulates the expression of other circadian genes (Reddy et al., 2007). The glucocorticoid receptor also regulates *REV-ERBα* expression without a GRE via interaction with the CLOCK:BMAL1 dimer at the E-box preventing transcription (Murayama et al., 2019). While

this was identified specifically at the *REV-ERBα* E-box with the CLOCK:BMAL1 dimer a similar effect may also modulate expression of other CLOCK/NPAS2:BMAL1 gene targets. The synthetic glucocorticoid dexamethasone can synchronise circadian cycles in cultured cells and is used in *in vitro* circadian research as detailed above in section 1.2 (Balsalobre et al., 2000). These functions are responsible for synchronising peripheral clocks to light cycles, the most common zeitgeber. Time of feeding is however another potent zeitgeber, especially in peripheral clocks.

1.6 Food entrainment

Time of feeding as a time cue in mice can be investigated through restriction of the times of food provision. In mice housed under a restricted feeding (RF) paradigm the peripheral oscillations of the liver, kidney, heart, and pancreas are entrained to the timing when feeding occurs, while the SCN is not. This peripheral entrainment leads to activity immediately prior to food provision on following days known as food-anticipatory activity (FAA) and overrides SCN control, showing the circadian clock network is controlled at multiple levels (Damiola et al., 2000, Carneiro and Araujo, 2009). This shows that these tissues are guided in their circadian pattern by the SCN but are not solely controlled by it. Under conditions where food is not restricted to a specific time the behavioural effect of the SCN means that eating times match the lighting pattern, this provides another mechanism of SCN entrainment of peripheral clocks.

The circadian cycles of the cells can be affected by metabolic state through multiple processes which likely contribute to food entrainment. The cellular redox state in the form of NAD+ and NADH levels affect the transcription factor activity of the CLOCK/NPAS2:BMAL1 dimer through direct interaction with CLOCK and NPAS2, NADH enhances DNA association while NAD+ inhibits it (Rutter et al., 2001). The activity of the HDAC SIRT1 is NAD+ dependent providing another route for metabolic state to influence

circadian cycling (Asher et al., 2008). The protein poly(ADP-ribose) polymerase 1 (PARP-1) which inhibits CLOCK/NPAS2:BMAL1 DNA association also participates in phase entrainment to metabolic state, though modulation of activity by NAD+ association (Asher et al., 2010).

The nutrient status of cells reflected in the AMP:ATP ratio can feed into circadian cycles through influencing adenosine monophosphate-activated protein kinase (AMPK) which can phosphorylate and destabilise CRY1 (Lamia et al., 2009). Both REV-ERBs have also been shown associate with haem which is required for their function. The activity of the proteins does not seem to be affected by the redox state of the haem; however, the levels of free haem may reflect the cellular metabolic state (Raghuram et al., 2007).

This peripheral entrainment is also associated with the food entrainable oscillator (FEO). The appearance of food anticipatory activity (FAA) while animals are under restricted food provision, as well as robust food entrained molecular rhythms across tissues, are observed effects of the FEO. FEO function is fully independent of the SCN, not requiring a functioning SCN and behavioural cycles entrained by feeding can be completely out of sync with SCN cycles (Mistlberger, 2020). As the shift in behavioural cycles requires that the influence of feeding needs to reach the brain it was assumed that a specific brain clock was the eventual endpoint for the information on the metabolic state and this region would then be responsible for synchronising behavioural cycles. However, the FEO has not been identified as a specific tissue despite various attempts (Pendergast and Yamazaki, 2018).

The noted complexity of the pathways which can allow entrainment to metabolic state means identification of individual contributors to the FEO are heard to identify, as any loss can be compensated for by other pathways. It has been found that knocking out BMAL1 in the brain leads to desynchronisation of peripheral tissues and a restricted food schedule restores synchrony in the liver and kidney tissues specifically (Izumo et al., 2014). This shows that the

liver and kidney clocks respond to feeding signals independent of entrainment signals from the clocks in the brain while other tissues still rely on them. This suggests the liver and kidneys may play a role in FEO entrainment. It is possible that the FEO itself, as has currently been identified, is a reflection of the communication between circadian cycles of multiple tissues and brain regions rather than a distinct tissue region. This peripheral clock communication, including to the brain, is made up of hormonal and afferent neuronal communication, as well as the influence of blood glucose and other signals more directly affected by food restriction (Carneiro and Araujo, 2009).

1.7 Clinical relevance of circadian cycles in humans

Investigation into circadian cycles has the potential to be of value in a variety of ways. Jetlag is an obvious example of disruption of circadian cycles with negative symptoms associated with loss of sleep due to desynchrony to the environment, as well as internal desynchrony due to different rates of entrainments of different tissues (Yamazaki et al., 2000). Another circadian disruption comes in the form of night shifts. In modern society humans are easily able to function at any time, regardless of the environmental daily cycles, and various industries employ workers who work night shifts. Even in ordinary life however, the use of electric lights late into the evening and night can impact normal circadian cycles. Long term disruption of circadian cycles has been associated with various health conditions (James et al., 2017). In shift workers with an established history of night work an elevated risk has been noted of type 2 diabetes (Vetter et al., 2018, Knutsson and Kempe, 2014), metabolic syndrome (Wang et al., 2014), various cancers (Straif et al., 2007, Erren et al., 2008), heart disease (Pimenta et al., 2012), stroke (Hermansson et al., 2007) and various mood disorders such as depression and anxiety (Kalmbach et al., 2015). Another contribution of circadian research is the field of chronotherapeutics. This aims to utilise knowledge of circadian cycles to identify

optimal timing of treatments to minimise toxicity or adverse events and enhance treatment efficacy (Ballesta et al., 2017).

Disturbed circadian rhythms are also presented in seasonal affective disorder (SAD). During winter months people diagnosed with SAD have been shown to have disturbed or damped circadian rhythms and morning bright light is often recommended as a treatment to help entrain the circadian cycles. A polymorphism in NPAS2, 471 Leu/Ser which is located outside of the conserved motif domains, has been identified to have a recessive effect on susceptibility to SAD with the leucine allele increasing susceptibility (Johansson et al., 2003).

In addition to cognitive decline people with Alzheimer's disease (AD) have also been found to present abnormal circadian cycles. At evening or night, a characteristic agitation and disruption in activity and sleep is commonly noted, known as sundowning. The daily cycles of body temperature are also often shifted in people with AD (Volicer et al., 2001). Amyloid β, which is responsible for the build-up of amyloid plaques, varies in concentration in the interstitial fluid and cerebrospinal fluid with time of day with a higher concentration at wakeful hours and lower concentration during sleep hours showing a potential circadian influence in AD development (Kang et al., 2009). Mouse models of AD can be generated by genetic modifications that lead to plaque formation such as APPswe/PS1dE9 mice (Jankowsky et al., 2004). The BACE1 and BACE2 genes, which are also linked to AD, have been found to be CCGs and their rhythmic expression is altered in the APPswe/PS1dE9 mouse strain (Ma et al., 2016). Within this strain it is also of note that in LD conditions a higher activity was seen at night compared to the wild type mice, and blunting of circadian variation in the clock proteins CRY1 and CRY2 in the medulla/pons was seen, even before amyloid plaques began to form. The mice also showed reduced responsiveness to the change from LD to DD potentially suggesting a failure in circadian entrainment in the AD model (Oyegbami et al., 2017).

1.8 The significance of NPAS2 in circadian cycles

This thesis will focus specifically on NPAS2. NPAS2 as introduced above is a transcription factor, part of the positive arm of the core circadian feedback loop. In the brain NPAS2 is expressed primarily in the forebrain and also hippocampal regions, notably pyramidal neurons of CA1, cortex, striatum, amygdala, and thalamus (Garcia et al., 2000, Zhou et al., 1997) and within the striatum NPAS2 is preferentially expressed within neurons expressing the dopamine D1 receptor (Ozburn et al., 2015). Outside of the brain NPAS2 is present in almost all tissues (Papatheodorou et al., 2019, Smith et al., 2018). NPAS2 and CLOCK are very similar proteins sharing 50% identity in their overall amino acid sequences, notably they share high similarity within their helix-loop-helix and PAS functional domains (King et al., 1997), shown in Figure 1.2. NPAS2 is able to associate with interacting proteins such as HATs and generally act with functional similarity to CLOCK despite lacking the intrinsic HAT domain (Curtis et al., 2004).

The CLOCK gene has been heavily investigated, however, relatively little is known about the function of NPAS2. This is due historically to an initial CLOCK mutant mouse model lacking exon 19 (CLOCKΔ19) used to investigate the protein's function. This mouse model showed that the CLOCK protein was integral for the circadian clock, as these mutants develop a significantly longer circadian cycle and blunted molecular rhythms, thus identifying CLOCK as the first mammalian circadian gene (Vitaterna et al., 1994). However, it was found that the modified CLOCK protein, while unable to associate with CIPC preventing transcription factor activity, was still able to associate with BMAL1 making this a dominant negative mutation (Gekakis et al., 1998, Zhao et al., 2007).

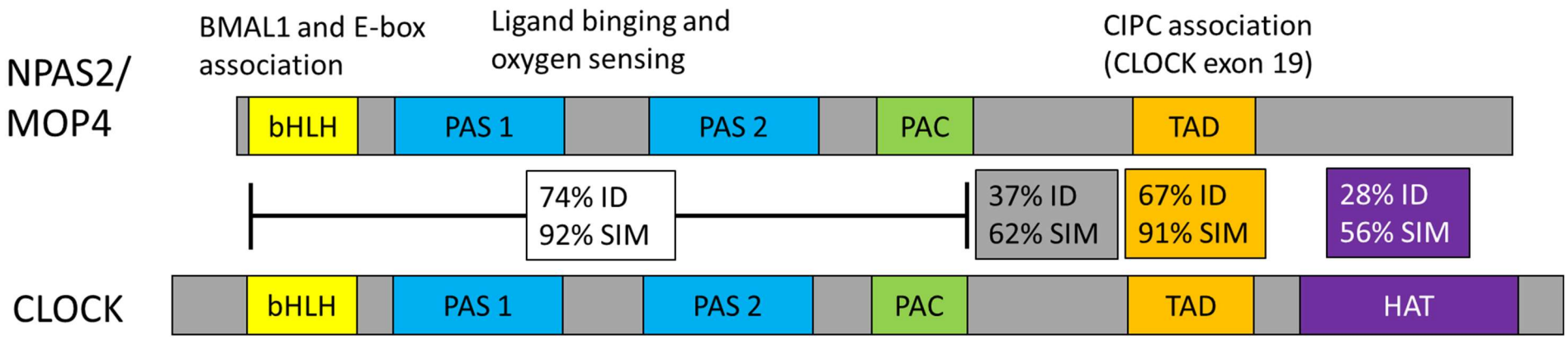

Figure 1.2: Functional domains of NPAS2 and identity and similarity comparison to CLOCK.

The areas of high similarity are the bHLH-PAS domain (including the PAS domain C-terminal or PAC), and the terminal activating domain (TAD) responsible for association with the CIPC. There is no observable similarity of the HAT domain of CLOCK with any of the amino acid sequence in NPAS2 following the TAD. Comparisons were performed using the LALIGN software (Madeira et al., 2019).

In mice with a homozygous CLOCK KO, rather than mutation, behavioural cycles remain and were shorted by only ~20 minutes (Debruyne et al., 2006). It was found that the capacity of the NPAS2 protein to act as an alternate dimerisation partner for BMAL1 could almost fully compensate for loss of the CLOCK protein. This suggests NPAS2 can compensate for CLOCK due to their overlapping function, overturning previous findings that CLOCK was crucial for circadian cycling (Debruyne et al., 2006, Debruyne, 2008). The expression of NPAS2 is upregulated in CLOCK KO mice in both neural and peripheral tissues (Debruyne et al., 2006, Landgraf et al., 2016), likely a compensatory mechanism in response to the loss of CLOCK. It should be noted that compensatory mechanisms, such as this, can be caused by the influence of the KO in development and can diminish the apparent role of the knocked-out gene (El-Brolosy and Stainier, 2017).

It had initially been suggested that NPAS2 is not expressed in the SCN despite enriched expression in the brain as NPAS2 transcripts could not be detected by *in situ* hybridisation (Shearman et al., 1999, Debruyne et al., 2006). However, following the discovery of the redundancy of CLOCK it was shown by quantitative reverse transcription PCR (RT-qPCR) that NPAS2 mRNA transcripts were present in the SCN (Kennaway et al., 2006) and NPAS2 was able to compensate for the loss of CLOCK through action in the SCN, independent of other tissues (DeBruyne et al., 2007a). NPAS2 or CLOCK KO mice under DD showed circadian cycles which only slightly vary from wild type mice while mice with both CLOCK and NPAS2 knocked out showed a loss of circadian cycles (DeBruyne et al., 2007a), see Figure 1.3.

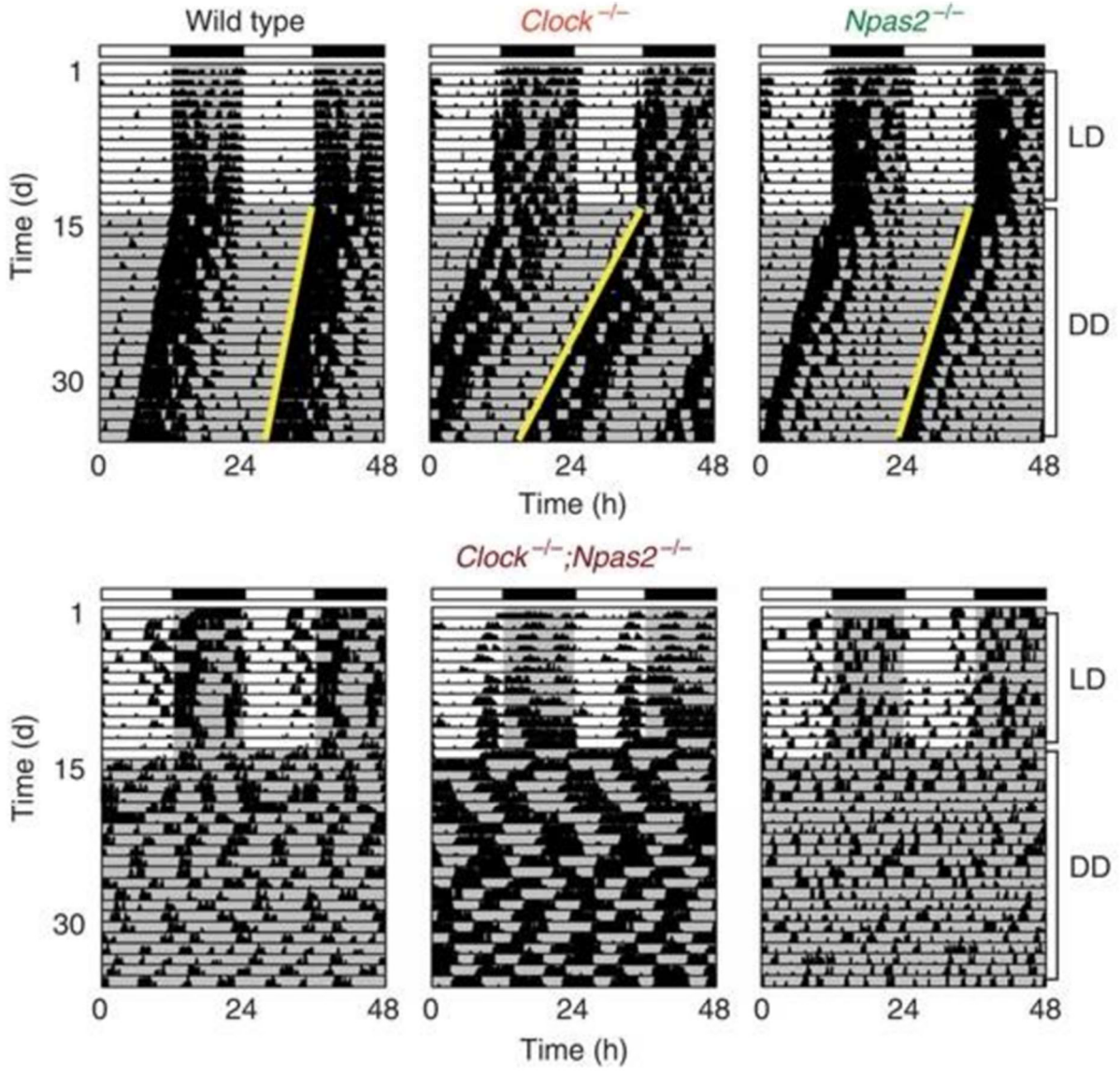

Figure 1.3: Actograms of wheel running activity in circadian gene mutant mice, adapted from DeBruyne et al. (2007a).

Plots are shown for wheel running activity in CLOCK-deficient (Clock−/−), NPAS2-deficient mice (Npas2−/−) and 3 different double KO (Clock−/−; Npas2−/−) mice. In the plots each horizontal line represents 48h; the second 24h period is plotted both to the right and below the first. Vertical bars represent periods of activity. Animals were initially housed in a 12-h light, 12-h dark cycle (LD) and were then transferred to constant darkness (DD), grey shading indicates darkness. Single CLOCK or NPAS2 KO mice retained some maintenance of circadian cycles even under constant darkness due to compensatory effects, however, double KO mice showed variable arrhythmicity in their behaviour.

Following these findings it was initially reported that NPAS2 could compensate for CLOCK in the SCN but not in peripheral clocks, shown by a loss of rhythmicity of luciferase under a *PER2* promotor in *ex vivo* liver identical in CLOCK and CLOCK/NPAS2 KO mice (DeBruyne et al., 2007b). However, in a separate report it was shown that loss of NPAS2 or CLOCK function individually had little impact on the cycling expression of factor VII, a protease involved in blood coagulation, but KO of both abolished this pattern (Bertolucci et al., 2008) showing peripheral circadian gene expression due to NPAS2 in the mouse liver. More recently, CLOCK deficient *in vitro* fibroblasts and *ex vivo* liver, lung, kidney and adrenal explants were all shown to exhibit NPAS2 dependant rhythmicity, while this cycling was impacted by the loss of CLOCK the cells do not behave arrhythmically without CLOCK, showing NPAS2 compensation (Landgraf et al., 2016).

While it is now commonly accepted that NPAS2 and CLOCK are similar genes it is of interest that there seem to be differences between the two genes that have not been fully explored. In the NPAS2 or CLOCK KO mice mentioned above, there were subtle differences between the SCN gene expression profiles suggesting different affinities for different circadian promotors between the CLOCK:BMAL1 and the NPAS2:BMAL1 heterodimers (Debruyne et al., 2006, DeBruyne et al., 2007a). This is despite the disrupted circadian cycles of behaviour seen in the mice being very similar between the two KO models. Chromatin immunoprecipitation sequencing (ChIP-seq) analysis in mouse liver has identified ~5900 BMAL1, ~4600 CLOCK and ~2300 NPAS2 unique DNA binding sites (Koike et al., 2012). This suggests a difference of the NPAS2:BMAL1 and CLOCK:BMAL1 DNA binding. This is explored in more detail in Chapter 3, section 3.1.2.

1.9 Role of NPAS2 in entrainment mechanisms

While NPAS2 KO mice under constant darkness present mostly unmodified rhythmic

behaviour due to the presence of CLOCK, changes in zeitgeber entrainment in these mice have been observed. NPAS2 KO mice adapt faster when the light schedule is shifted earlier compared to wild type mice with a more significant shift initially and a faster rate of adjustment. Entrainment due to RF was found to be compromised in the NPAS2 KO mice, with lower body weight, food intake and anticipatory locomotor activity compared to wild type mice when food is restricted under DD conditions to a six-hour window, during what had previously been light conditions. However, the mice did eventually show a shifted behaviour cycle in response to RF (Dudley et al., 2003).

These findings suggest that NPAS2 plays a role in entrainment of the FEO to food as a zeitgeber, this explains the deficit in food entrainment and a decreased contribution of the feeding zeitgeber or the FEO to the circadian cycles would permit faster entrainment to light as a zeitgeber or the SCN. This may reflect a role of NPAS2 in multiple different broad processes; entrainment of the molecular clock to the metabolic conditions and circadian signalling from entrained peripheral tissues to the brain, either outputting or responding to this signalling. NPAS2 as noted above interacts with NAD+/NADH meaning NPAS2 can play a role in entrainment of circadian cycles to the cells metabolic state. As a transcription factor, when molecular cycles of peripheral tissues are entrained by RF, NPAS2 activity may be required to appropriately output signals to entrain brain regions responsible for behavioural cycles. Finally, it may be that the signalling received at brain tissues to synchronise the circadian cycle act via influencing NPAS2 activity within the core circadian feedback loop. Investigation of these specific differences would likely require tissue collections over a significant number of time points on each of the days as the mice entrain to the zeitgeber which has not been performed. As the mice are still able to entrain eventually to RF there is clearly still some overlap of CLOCK and NPAS2 function. However, CLOCK is insufficient to completely compensate for NPAS2 in this function.

In contrast, mice with a conditional KO of NPAS2 in the neonatal liver showed less weight loss than wild types in male mice when feeding was restricted in a similar fashion under LD conditions (O'Neil et al., 2017) suggesting potentially faster entrainment in these mice. The mechanism of the process behind this has not yet been established.

1.10 Cognition and circadian cycles

As well as its role in behavioural circadian cycles, NPAS2 has been shown to have a role in memory and learning. This is not unexpected as memory and cognitive performance present physiological circadian cycles, observed as improvement at certain times of day. Human cognition is initially impaired following the transition from sleep to wakefulness but improves rapidly in the first 20 minutes and then continuing to improve at a slower rate over 2-4 hours from waking. Cognition is generally highest in the first 8 hours awake with an afternoon dip or slump after 8 hours followed by improved cognition right before habitual bedtime (Wertz et al., 2006, Wright et al., 2012). Mice have been observed to show improved acquisition of memory for maze navigation (Hoffmann and Balschun, 1992) and contextual fear conditioning (Valentinuzzi et al., 2001) in the dark phase of a light-dark lighting pattern when, as nocturnal animals, they are more active. However, it has been shown that mice acquire tone-cued fear conditioning more rapidly when trained in the light rather than dark phase (Chaudhury and Colwell, 2002). While circadian variation in performance in various cognitive tasks is often observed, differences in the phase of peak performance between tasks and breeds of mice have been reported, and other nocturnal rodents have been found to show different performance peaks to mice (Snider et al., 2018). This shows the complexity of circadian influence within cognitive tasks. Mouse performance in learned behavioural tasks such as the Morris water maze and contextual fear conditioning is also compromised when sleep is disrupted (Gerstner et al., 2009).

In humans long term memory performance is better during daylight hours and working memory shows clear circadian variation which follows diurnal body temperature fluctuation (Goel et al., 2013). Chronic disruption of circadian cycles leads to decreased cognitive performance in humans and mice. This is seen in mice subjected to shifting light cycles (Krishnan and Lyons, 2015), flight crews who routinely cross time-zones (Cho et al., 2000) and shift workers (Marquie et al., 2015). Working a night shift also has a noticeable temporary effect on short term memory (Meijman et al., 1993).

1.11 Roles of NPAS2 and other circadian genes in cognition

Mice with a functional NPAS2 KO under LD conditions were identified to perform similarly to mice in behavioural tests except for deficits in the long-term (24 hours later) cued and contextual fear task while short-term memory (half an hour later) remained intact. These mutant mice showed no change in Morris water maze performance or passive avoidance and step-down avoidance (Garcia et al., 2000). It was also noted that these mice showed no change in anxiety (open field, light/dark conflict, and elevated plus maze) (Garcia et al., 2000), but following this NPAS2 deficient mice have been shown to have decreased anxiety-like behaviour in the same tests (Ozburn et al., 2017). Using siRNA to knockdown NPAS2 in the nucleus accumbens also has the effect of reducing anxiety behaviours and also reducing expression of the GABAa alpha 1 subunit likely altering the GABAA receptor subunit composition which may alter inhibitory neurotransmission (Ozburn et al., 2017).

The effect of NPAS2 loss on fear conditioning suggests a specific role in long-term memory consolidation within this task, possibly as part of the role in circadian gene expression. The specific details of the mechanism of this effect have not however been identified. Cued and contextual fear conditioning have both been shown by to rely on the hippocampus (Maren et al., 1997), although lesions of the hippocampus in some reports is not associated with

modified cued fear conditioning behaviour (Kim and Fanselow, 1992, Phillips and LeDoux, 1992, Sanders et al., 2003). This suggests the impact was not a hippocampal defect however, performance in the Morris water maze, which requires hippocampal function (Vorhees and Williams, 2006), was unaffected.

The amygdala, which is essential for emotional responses, plays a role in both cued and contextual fear conditioning in acquisition, storage, and expression (Phillips and LeDoux, 1992, Marschner et al., 2008), so this may be a site of interest in the mechanism of how loss of NPAS2 induces deficits in fear conditioning performance. Dopamine signalling has also been shown to be required for both cued (Fadok et al., 2009) and contextual fear conditioning (Ikegami et al., 2014). Within the nucleus accumbens NPAS2 mRNA expression has been shown to be highly enriched specifically in dopamine receptor D1 (Drd1) containing neurons (Ozburn et al., 2015). Knockdown of *NPAS2* gene expression, specifically in the nucleus accumbens, disrupted diurnal mRNA expression of the dopamine receptors *Drd1*, *Drd2* and *Drd3* (Ozburn et al., 2015). Based on this it may be that an effect of loss on NPAS2 on dopamine signalling pathways is responsible for behavioural changes in NPAS2 mutant mice.

Other circadian genes also have an impact on cognition which should be noted. PER1 and PER2 KO mice exhibit defects in hippocampal-dependant learning tasks (Wang et al., 2009). BMAL1 KO and CLOCK dominant negative mutant mice have shown deficiencies in habituation while mice deficient in CRY1/2 have shown facilitated habituation, however at the circadian level all these mutant mice are similarly arrhythmic, showing unique roles of individual proteins above simply the interaction of circadian cycles with memory (Kondratova et al., 2010).

1.12 Aims & Objectives

The aim of this project was to first establish models of peripheral clocks with modified NPAS2 expression and second to use these models to investigate the role and function of NPAS2 in the circadian cycles of gene expression and behaviour. Two models were used, an *in vitro* cell culture and an *in vivo* mouse model. These models were intended to complement each other, with a cell model allowing more detailed molecular investigation than can be feasible in a mouse colony without exceptionally large numbers of mice, while the mouse model allows for investigation of behavioural effects and function within an organism.

The experimental aims can be summarised as: 1; Establish cells with modified NPAS2 expression. 2; Investigate expression of core circadian genes in modified cultured cells. 3; Investigate expression of core circadian genes in liver specific NPAS2 KO model mice. 4: Investigate circadian behavioural entrainment in the liver specific NPAS2 KO model mice. 5; Investigate latent inhibition of fear conditioning in liver specific NPAS2 KO model mice.

The cell culture model involved generation of mutant cells by use of CRISPR-Cas9 technology (Aim 1; Chapter 2). Due to relative ease of generation of modified cell models multiple were generated within this project. This allowed investigation of the NPAS2 gene as well as its paralogue CLOCK as a comparison of effects on a similar gene. Modification of these cells was confirmed by reduced protein expression levels and sequencing of the targeted region of the genome.

These modified cells were used to investigate the effect of modified expression of the core circadian genes on the expression of other genes of the circadian feedback loop (Aim 2, Chapter 3). Gene expression was investigated both under normal cell culture conditions and after circadian synchronisation to investigate any impact on rhythmic expression of core circadian genes. Having been established, the cells can be used in future research to investigate other potential effects, such as protein modifications and expression of various core clock genes

which may be of interest.

A liver-specific functional NPAS2 conditional KO mouse model colony was established in Nottingham. This previously generated model was floxed for NPAS2 and crossed for Cre expression in the liver to specifically KO functional gene expression in the liver. This mouse model was used in investigation of effect on core circadian gene expression in both the liver tissue as well as brain tissues to investigate the effect of the functional loss of NPAS2 in the liver (Aim 3, Chapter 4).

As constitutive NPAS2 mice have been identified to present modified entrainment to zeitgebers, entrainment was investigated in the liver-specific conditional KO mice (Aim 4, Chapter 5). The response in activity to light pulses and restricted feeding was investigated to identify the impact of the loss of NPAS2 in the liver on these entrainment processes. Performance in cued fear conditioning, which constitutive NPAS2 KO mice have shown deficits in (Garcia et al., 2000), and latent inhibition of fear conditioning was investigated to identify any potential effect on cognition of modification in a peripheral clock (Aim 5, Chapter 6). It is intended that this work will be complemented by development of a brain specific functional NPAS2 KO which can be produced by crossbreeding with mice which express a different tissue specific Cre. These two mouse models will allow comparative investigation of the effect of brain and non-brain peripheral tissue NPAS2 KO.

Together the *in vitro* and *in vivo* models can present a valuable resource for investigation of the NPAS2 gene and aid in understanding of its role in peripheral circadian cycles, as well as investigation of the contributions of peripheral clocks to overall circadian behaviour.

Chapter 2: CRISPR-Cas9 editing of circadian genes in mouse and human cells

2.1 Introduction

2.1.1 CRISPR-Cas9 modification

To study NPAS2 function in cell models we employed a genome editing approach using CRISPR-Cas9. CRISPR-Cas9 technology employs short (20 bp) guide RNAs (sgRNAs) to target the Cas9 nuclease to a specific target sequences that have an adjacent protospacer adjacent motif (PAM) (Ran et al., 2013b). The Cas9 enzyme contains two domains with nuclease activity (RuvC and HNH domains) that target opposing strands to achieve double-strand DNA cleavage near the PAM site. This activates the cells endogenous error prone non-homologous end joining repair pathway (NHEJ) which attempts to repair the double-strand break leading to insertions and deletions (indels) at the cleavage site.

In addition to editing events at the intended target site, studies have shown that partial mismatches in the sgRNA/DNA hybrids can be tolerated and lead to off-target mutations. To reduce the frequency of off-target events, we used the Cas9 nickase (spCas9n) variant harbouring the D10A mutation, in which the RuvC domain is inactivated. This enzyme introduces just a single strand break at the sgRNA target sequence. Single strand breaks produced with this enzyme are repaired without mutation of the DNA sequence by the high-fidelity base excision repair pathway (BER) (Ran et al., 2013a, Shen et al., 2014). Therefore, to achieve genome editing with Cas9n, pairs of guides were designed to target opposing strands at the target locus. The two single strand breaks generate a staggered cut that can be recognised as a double-strand break leading to NHEJ (See Figure 2.1). As the sgRNA pairs target distinct sequences, the likelihood of off-target events occurring on opposing strands at another locus is reduced by over 100-fold relative to wild type Cas9 (Ran et al., 2013a, Chiang et al., 2016, Shen et al., 2014). The orientation of the sgRNA target sequences, referred to as PAM-in or PAM-out designs, can alter the efficacy of editing with PAM-out showing higher efficiency of editing (Ran et al., 2013a).

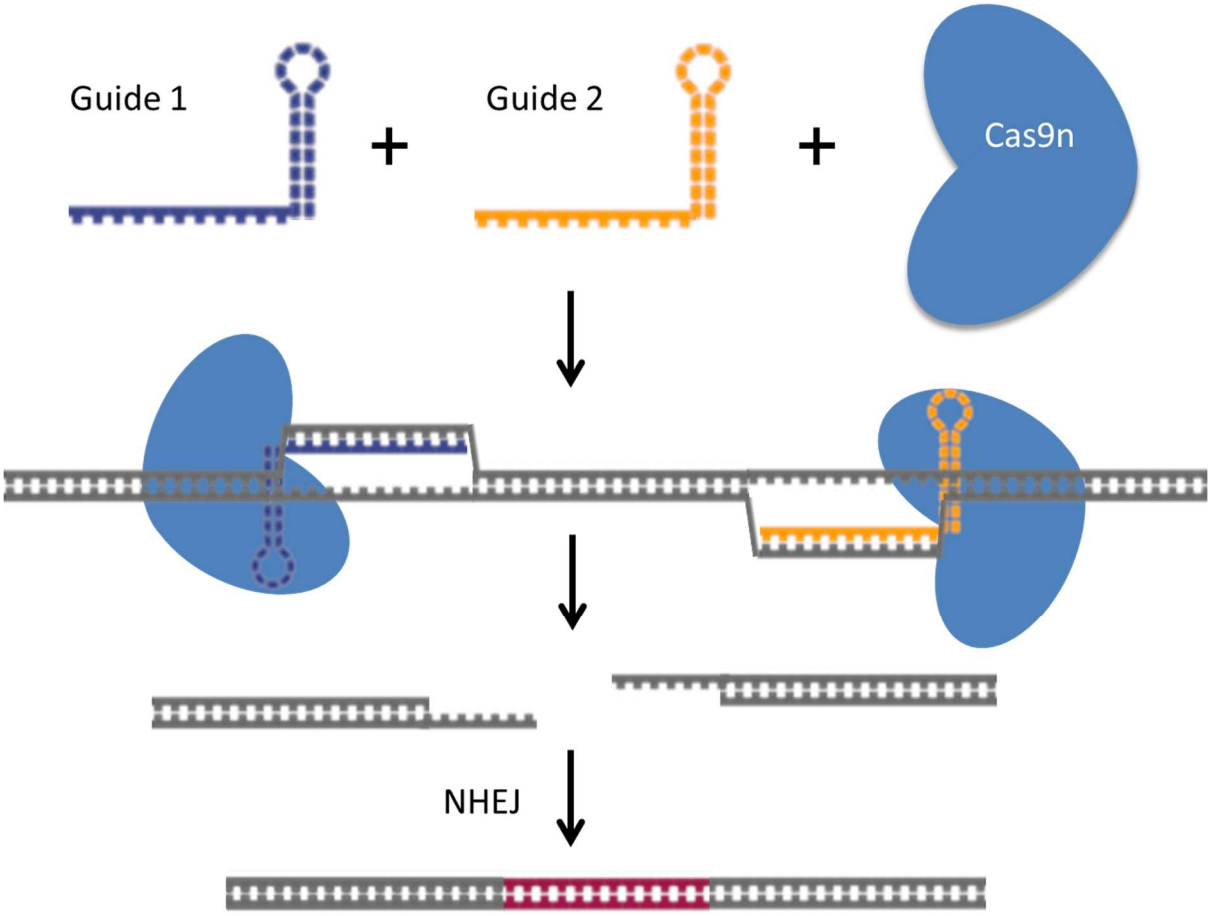

Figure 2.1: Schematic representation of Cas9n targeting.

sgRNA guide pairs are used to target opposing strands of the target sequence. Indels are generated randomly between these guides due to non-homologous end joining (NHEJ).

After we initiated this project, studies by Yan et al. (2017) using the D10A Cas9 in HEK293 cells showed that editing is more efficient with PAM-out designs with spacings of 40-70 base pairs between nicks, and that efficiency of targeting drops dramatically if nick distances are too close (<25 bp) or too distant (>85 bp) (Yan et al., 2017). All guide pairs designed for this work were PAM-out designs, with spacings between the PAMs of 50-80 bases. The D10A Cas9 has been shown to have a median deletion size of 36 nucleotides (Bothmer et al., 2017), so all nicks are targeted close to the region where modification was desired. Primers for PCR genotyping analysis were designed to amplify >100 bp fragments so that the primer binding sites would be less likely to bind within the indel region.

2.1.2 Clonal expansion

To generate modified cells, we relied on transient transfection of the Cas9 and sgRNA in a single expression vector, pSpCas9n(BB)-2A-GFP, also known as PX461. Different approaches are possible here; a polyclonal population can be selected with a mixture of targeted and untargeted cells with different indels. However, we chose to isolate and characterise clonally expanded cells, taking advantage of the eGFP gene on the PX461 vector. GFP+ cells are more likely to also express Cas9 protein and can be isolated using flow-assisted cell sorting (FACS). While antibiotic selection is also available that can facilitate selection of targeted clones, this may result in integration of the vector and sustained expression of the Cas9 protein, leading to higher incidence of off-target events.

2.1.3 Gene targeting

To enhance the chances of successful gene targeting of *NPAS2* and other circadian genes, it was decided to embark on this study using the well-characterised human HEK293 embryonic kidney and murine NIH3T3 fibroblast cell lines. Circadian cycling has also been experimentally induced in both cell types using serum shock (Cox, 2012, Allen et al., 2004).

Our preferred strategy was to target regions incorporating the start codon, where indels

could disrupt the start codon and thereby translation, or close by in the first coding exon, where indels could produce frame shift mutations, leading to a premature stop codon and early truncation of coding sequence or nonsense-mediated decay. Due to the random nature of indels generated by CRISPR-Cas9 technology, this process included screening many clones to successfully select those that showed reduced or absent expression of each target gene.

2.1.4 Aims

The main objectives for this chapter were to generate and characterise modified clonal cells derived from NIH3T3 and HEK293 cells. As well as *NPAS2*, the other two genes which make up the positive arm of the circadian transcription-translation feedback loop, *BMAL1* and *CLOCK*, were targeted for mutation. This strategy was to enable later comparisons to be made regarding the requirement of different circadian gene components for circadian regulation using RT-qPCR or reporter genes, and for follow-on studies, such as RNA-seq transcriptomics.

2.2 Materials & Methods

2.2.1 Sources of general chemicals and reagents

All general laboratory reagents were purchased as analytical grade quality from either Fisher Scientific or Sigma-Aldrich unless otherwise stated. Sterile Phosphate Buffered Saline (PBS) solution was prepared using tablets purchased from OXOID Ltd. All solutions were made in distilled water; purified by passage through a Millipore Elix® Essential 3 Water Purification System. The pH of solutions where specified was maintained by checking the pH with a pH meter (Jenway 3510), calibrated against standards of known pH. Sterilisation was achieved either by filtration through 0.2 µm filters, or via autoclaving at 121 °C for 20 minutes, as appropriate.

2.2.2 Bacterial preparation and culture

2.2.2.1 Bacterial strains & culture materials

The *Escherichia coli* strain DH5α (Hanahan, 1983) is a *recA* deficient strain used to propagate plasmid vectors and was cultured in the lab after initial purchase from Stratagene. Luria-Bertani bacterial growth medium (LB medium) was purchased from Fisher. Plates were made using LB medium with added 2% w/v bacteriological agar which had been autoclaved at 121 °C for 20 minutes. Solid medium was melted in a microwave for 5-10 minutes at full power. Where appropriate ampicillin was added to molten medium to a final concentration of 100 µg/ml. Approximately 20 ml was poured into each petri dish to cover the surface and allowed to solidify at room temperature. Plates were stored at 4ºC for up to 1 month.

Ampicillin was prepared as a 1000x stock solution made as 100 mg/ml in 50% ethanol, 50% sterile dH_2O. Stored in aliquots at -20 °C.

2.2.2.2 Preparation of competent cells (*Escherichia coli)*

Escherichia coli DH5α cells were streaked on an antibiotic-free LB agar plate and

incubated at 37 °C overnight. A single colony was used to inoculate a 10 ml volume of LB medium (antibiotic-free) and cultured overnight at 37 °C, with shaking. This was then used to set up a 300 ml total volume culture in the same medium and was incubated at 37 °C, with shaking until the optical density (measured at 600 nm; OD_{600}) reached 0.5. Cultures were chilled on ice and all further work was performed at 4 °C. The culture was centrifuged for 10 minutes, 4,000 rpm at 4 °C in separate 50 ml tubes and the supernatants removed. Each pellet was washed in 8.3 ml of 0.1 M $MgCl_2$, before the centrifugation was repeated. The supernatants were discarded, and each pellet was resuspended in 8.3 ml of 0.1 M $CaCl_2$. These suspensions were incubated on ice for a minimum of 20 minutes, before repeating the centrifugation. The supernatants were removed, and all pellets were resuspended together in a total of 8.6 ml of 0.1 M $CaCl_2$. 1.4 ml 100% glycerol was added to the suspension, inverted 5 times and 200 µl volumes were aliquot into microcentrifuge tubes. These were snap frozen immediately in liquid nitrogen and stored at -80 °C.

2.2.2.3 Bacterial transformations

Escherichia coli DH5α cells were utilised in all bacterial transformations. An aliquot of these heat-competent cells was allowed to thaw on ice for a maximum of 10 minutes after removal from storage at -80 °C. 50 ng of intact vector/plasmid, or 10 µl of ligation products was added to 50 µl of cells. The mixture held on ice for 30 minutes, then heat shocked at 42 °C for 2 minutes, before being placed on ice for a further 5 minutes. Pre-warmed LB medium was added to a final volume of 1 ml and each sample was cultured at 37 °C for 1 hour with shaking, before centrifugation for 2 minutes at 7,000 rpm. 900 µl of the supernatant was removed, the pellet was resuspended in the remaining liquid and (in the case of ligation mixes) the entire volume was plated on LB agar supplemented with 100 µg/ml ampicillin. Each agar plate was incubated overnight at 37 °C. For each transformation experiment, a negative control of 50 µl volume of DH5α cells, without added DNA, was included. When transforming ligation mixes,

additional controls included cut vector only (to ascertain background), insert only (to confirm no contaminating plasmid DNA) or vector/insert mix without ligase. Single Amp-resistant colonies were selected from plates for growth in LB-Amp broth for miniprep or maxiprep purification of the plasmid at 37 °C, with shaking. A positive control transformation using 50 ng of undigested PX461 vector was used to test the competence of the DH5α cells. This transformation mix was diluted 1:10, 1:100 and 1:1000 before plating, meaning the plates would grow colonies as transformed by 5, 0.5 and 0.05 ng. The colony counts of these plates were then used to calculate the transformation efficiency of the bacteria using Formula 2.1.

$$Colony\ forming\ units\ (CFU)\ = \frac{Colony\ count}{\mu g\ DNA}$$

Formula 2.1: Calculation of the transformation efficiency of competent bacteria

2.2.3 Computational design of sgRNAs

For each gene targeted for CRISPR-Cas9 modification the sequence of the genome was acquired from the Ensembl database (Zerbino et al., 2018, Cunningham et al., 2019). A specific region of the sequence where a mutation was desired was submitted to the MIT CRISPR design tool (Hsu et al., 2013) which identifies pairs of specific 23 base guide sequences ending in NGG, one on the forward and one on the reverse strand, in close proximity to each other. The design tool provides several guide pairs, and a single guide pair was selected based on locus in the genome and scoring provided by the tool. Later in the project alternative resources such as CHOPCHOP (Labun et al., 2019) or genome browser CRISPR track were also used due to the shutdown of the MIT CRISPR design tool.

The selected CRISPR-Cas9 sgRNA oligonucleotide sequences of 20 bases, not including PAM sequences, were ordered with the reverse complement with some additions. For sequences in which the first nucleotide was not guanine, a single guanine was added to the 5' end and a complementary cytosine added to the complementary strand. This was because a guanine at the 5' end of a sgRNA enhances its transcription when under the control of a U6

promoter, as in PX461 (Iijima et al., 2006, Chiang et al., 2016). In addition, "5'-CACC-3'" and "5'-AAAC-3'" sequences were added to the 5' ends of the respective forward and reverse sgRNA oligonucleotide sequences to form overhangs complementary to those formed by BbsI restriction digestion in PX461.

2.2.4 Molecular biology techniques

2.2.4.1 Sources and composition of reagents

All restriction enzymes, T4 polynucleotide kinase, calf-intestinal alkaline phosphatase and T4 DNA ligase enzymes and their relevant buffers were purchased from either Roche or New England Biolabs (NEB). Thermostable Taq DNA polymerase, along with reaction buffer, supplements and dNTPs were purchased from NEB. The 1 Kb Plus DNA Ladder was purchased from Invitrogen. Monarch® DNA gel extraction kits were purchased from NEB, Nucleospin® plasmid kits (miniprep kits) from Macherey-Nagel and plasmid maxi kits (maxiprep kits) from QIAGEN Ltd. The GenElute™ mammalian genomic DNA miniprep kits were purchased from Sigma-Aldrich. Oligonucleotides and primers were purchased from Sigma-Aldrich as lyophilised and desalted pellets. These were resuspended in sterile water to a 100 µM concentration and stored at -20 °C. The PX461 plasmid was a gift from Feng Zhang and generated plasmids are noted in the appendix Table A.2.

Agarose gel loading dye (10x) = 3.9 ml glycerol, 500 µl 10% (w/v) SDS, 200 µl 0.5 M EDTA, 0.025 g bromophenol blue & made up to a total volume of 10 ml with dH_2O. Used at a final concentration of 1x.

Tris-borate-EDTA (TBE) = 40 mM Tris-base, 40 mM boric acid, 0.5 mM EDTA (pH8.0) and made up to 1 L with dH_2O.

2.2.4.2 Annealing of oligonucleotides

100 µM CRISPR-Cas9 sgRNA single stranded oligonucleotides were individually

phosphorylated in the T4 Polynucleotide kinase reaction mixture shown in Table 2.1, incubated at 37 °C for 60 minutes. The mixture was then incubated at 65 °C for 20 minutes to inactivate the enzyme.

Table 2.1: Oligonucleotide phosphorylation reaction composition

100 µM Oligonucleotide	2 µl
10 x T4 DNA ligase buffer	2 µl (to make 1 x)
T4 Polynucleotide kinase	10 Units (1 µl)
dH_2O	To a total volume of 20 µl

Once complete, 5 µl of each complementary top and bottom oligonucleotide reaction mix were combined and made up to a total volume of 50 µl with sterile dH_2O. These mixtures were then placed in a thermocycler to heat the mixture to 95 °C for 3 minutes, then cooled by 1 °C each minute until a temperature of 25 °C was reached and held for additional 5 minutes at 25 °C to ensure correct annealing. The annealed and phosphorylated oligonucleotides were stored at -20 °C until required for ligation.

2.2.4.3 Restriction digestions

The PX461 Cas9 expression vector was digested with the BbsI restriction enzyme using NEBuffer 2.1 at 37 °C for 2 hours. Typical restriction enzyme digestions are shown in Table 2.2. The digestion reaction was then run on an agarose gel and extracted to purify the uncut vector from the excised fragment.

Table 2.2: Restriction digestion reaction composition

10 x Buffer	2.0 µl (to make 1 x)
Uncut PX461 vector	1 µg
BbsI enzyme	10 Units (1 µl)
dH_2O	To a total volume of 20 µl

The BbsI restriction enzyme cuts the PX461 vector so that non-compatible ends are produced, which means that the vector would be unable to self-ligate without inclusion an

insert. The cut vector was dephosphorylated at the 5' end by incubation with 1 µl TSAP (1 Unit) for 1 hour at 37 °C. The cut vectors were stored at -20 °C until required.

2.2.4.4 Agarose gel electrophoresis

Analysis and visualisation of PCR products and restriction enzyme digestions was performed via agarose gel electrophoresis. 0.8%-2% Agarose gels were made by mixing the relevant mass of agarose (w/v) required for the desired percentage agarose gel with 1 x TBE buffer, then heating in a microwave oven until agarose was dissolved and a clear liquid was formed (~3 minutes at full power). 1 µl of a 10 mg/ml ethidium bromide solution was added per 50 ml of liquid agarose, before pouring and allowing it to solidify at room temperature. 10 µl of the desired DNA ladder was loaded and all samples to analyse were mixed with the necessary volume of 10 x agarose gel loading dye to make a final concentration of 1 x loading dye, prior to loading in the gel. All agarose gels were run at 90 V in 1 x TBE buffer for the necessary length of time that would ensure good DNA band separation of the desired size, generally 1 hour. DNA bands were visualised and imaged using either a BIO-RAD Universal Hood II UV transilluminator or a Fujifilm LAS-4000 system.

2.2.4.5 Purification of DNA from an agarose gel

Desired band(s) of DNA were excised from the agarose gel under low power UV illumination using a sterile scalpel blade, removing as much agarose as possible and avoiding prolonged UV exposure of the DNA. DNA fragments were purified using the Monarch® DNA Gel Extraction Kit, following the manufacturer's instructions. The concentration of DNA in the eluate was determined using a NanoDrop 1000 Spectrophotometer. Purified DNA was stored at -20 °C until required.

2.2.4.6 Ligation of DNA fragments

Phosphorylated and annealed sgRNA linear dsDNA fragments were ligated to BbsI digested PX461 to generate Cas9 targeting constructs for the genetic regions of interest. A

typical ligation reaction is described in Table 2.3.

For each set of ligation reactions, a negative control was included to indicate the level of background undigested/re-ligated vector. This negative control contained all the reagents, with exception of the linear DNA insert. Since all ligations were of the same size insert, this process was not varied. Each sample was vortexed, centrifuged and allowed to ligate overnight at 4 °C. Following this, the products were stored at -20 °C until used for bacterial transformation (see 2.2.2.3).

Table 2.3: Ligation reaction composition

Linear DNA Insert	2 µl (1:3 insert:vector)
PX461 vector	100 ng
10 x T4 DNA ligase buffer	2 µl (to make 1 x)
T4 DNA ligase	3 Units (1 µl)
dH_2O	To a total volume of 20 µl

2.2.4.7 Small-scale purification of vectors & plasmids from bacteria (miniprep)

For the small-scale purification of ligated vector from bacterial colonies, a miniprep was performed. A 10 ml volume of LB supplemented with 100 µg/ml ampicillin was inoculated with a single bacterial colony from the relevant transformation plate. This was then allowed to grow at 37 °C overnight, with shaking. The culture was pelleted by centrifugation at 4,000 rpm for 10 minutes at 4 °C. Plasmid DNA was then recovered from the pellet by alkaline lysis and affinity purification using the NucleoSpin® Plasmid kit (Machery-Nagel) according to the manufacturer's protocol for low copy plasmids and the eluate DNA concentration determined using a NanoDrop 1000 Spectrophotometer. Purified plasmids were stored at -20 °C.

2.2.4.8 Sequencing of DNA

DNA was sequenced to identify that vectors purified from colonies had been ligated to correctly form PX461-sgRNAs and also to analyse the genetic sequence of targeted cells.

Plasmid or PCR DNA was sequenced by Source Bioscience Ltd using an Applied BioSystems 3730 DNA Analyzer and PeakTrace™ software. The volumes and concentrations used for sequencing as advised by Source Bioscience Ltd are shown in Table 2.4. Vectors were taken from miniprep stocks (see 2.2.4.7) and sequenced using a human U6 forward primer, whereas PCR products were taken from agarose gel purified stocks (see 2.2.4.5) and were sequenced using designed primers (See appendix section A.6, page 296 for primer details).

Table 2.4: The volume and concentration of vectors, plasmids, PCR products and primers for DNA sequencing

	Vector or plasmid	**PCR product**
DNA	5 µl (100 ng/µl)	5 µl (10 ng/µl)
Primer	5 µl (3.2 pmol/µl)	5 µl (3.2 pmol/µl)

2.2.4.9 Large-scale purification of vectors & plasmids from bacteria (maxiprep)

For the large-scale purification of PX461-gRNAs from bacteria, a maxiprep was performed. A 10 ml volume of LB supplemented with ampicillin (final concentration of 100 µg/ml), was inoculated with a single bacterial colony from a transformation plate made using the purified and sequenced PX461-gRNAs. This was then allowed to grow at 37 °C, with shaking, until the culture visually became turbid. This was then used to set up a 300 ml total volume culture in the same medium and was incubated at 37 °C overnight, with shaking. The Qiagen Plasmid Maxi Kit protocol was followed, with the exception of the centrifugation steps, which were all performed at 6,500 rpm for 50 minutes at 4 °C. The purified PX461-gRNAs was re-dissolved in 200 µl dH_2O and the concentration determined using a NanoDrop 1000 Spectrophotometer before storage at -20 °C ready for transfections into cultured cells.

2.2.4.10 Extraction of genomic DNA from mammalian cells and tissue

Genomic DNA was purified from mammalian cultured cells using the GenElute™ Mammalian Genomic DNA Miniprep Kit. Cells were harvested as described in 2.2.5.2, the

suspension was transferred to 15 ml tubes and centrifuged at room temperature at 1,500 rpm for 5 minutes. The supernatant was discarded and the pellet resuspended in 1 ml 1 x PBS, before repeating the centrifugation. Again, the supernatant was removed, and the pellet stored at -20 °C for <1 week and genomic DNA was then purified by use of the extraction kit following the manufacturer's instructions. Genomic DNA was stored at -20 °C until required. The concentration of DNA was determined using a NanoDrop 1000 Spectrophotometer.

2.2.4.11 Polymerase chain reaction (PCR)

PCR was utilised for genotyping of modified clones. Typical reaction mixtures and cycling protocols, as recommended by NEB, are shown in Table 2.5 and were performed in an Applied Biosystems 2720 thermal cycler. The Taq reaction buffer used includes $MgCl_2$ at a concentration of 15 mM for a 1.5 mM concentration in the final reaction. The annealing temperature was set at 5 °C below the lowest Tm of the primer pair(s). If the PCR reaction conditions were altered it is noted in the respective results section. PCR products were stored at -20 °C until use.

Table 2.5: Reagents used and composition of typical PCR reactions, along with typical thermocycler settings

	Reagents	**Cycle**	
DNA template	50 ng	95 °C – 30 seconds	
10 x standard Taq reaction buffer with $MgCl_2$	5 µl (to make 1 x)	95 °C – 10 seconds	x 35 cycles
10 µM Forward primer	1 µl (to make 0.2 µM)	55-65 °C – 30 seconds	
10 µM Reverse primer	1 µl (to make 0.2 µM)	68 °C – 1 min/kb	
10 mM dNTP mix	1 µl (to make 0.2 mM)	68 °C – 10 minutes	
Taq DNA polymerase	0.25 µl (1.25 units)		
Nuclease-free sterile dH_2O	To 50 µl final volume		

2.2.5 Mammalian cell culture

2.2.5.1 Sources of cell culture material and composition of reagents

All cell culture reagents were purchased from Lonza or Gibco and all plasticware was obtained from Corning. Lipofectamine™ 2000 Transfection Reagent was purchased from ThermoFisher.

2x HBS solution = 50 mM HEPES, 280 mM NaCl, 1.5 mM Na_2HPO_4 in dH_2O, pH adjusted to 7.07 using 1 M HCl. Filter sterilised and stored at -20 °C until use.

RIPA lysis buffer = 50 mM Tris base, 1% NP-40, 0.1% SDS, 150 mM NaCl, cOmplete™ mini protease inhibitor, pH adjusted to 8 using 1 M HCl.

2.2.5.2 Culturing of adherent cells

The human embryonic kidney (HEK293) and mouse fibroblast (NIH3T3) cells were typically maintained in Dulbecco's Modified Eagle Medium (DMEM). This medium was supplemented with either 10% (v/v) heat-inactivated fetal calf serum (FCS) for HEK293 cells or 10% (v/v) heat-inactivated newborn calf serum (NBCS) for NIH3T3 cells plus 1% (v/v) 0.2 M L-glutamine and 1% (v/v) Penicillin/Streptomycin antibiotics. Cells were cultured in sterile plastics at 37 °C, 5% CO_2 and passaged when at approximately 80% confluency. When cells were passaged and/or collected the medium was aspirated, and cells washed with 1 x PBS. HEK293 cells were then suspended in fresh medium while NIH3T3 cells were incubated for 5 minutes at 37 °C in 1 x trypsin and suspended in fresh medium. At this point, the cell suspension was diluted and split into other sterile plasticware and/or collected into 15 ml tubes if being used for other processes.

2.2.5.3 Cryopreservation of cells

For cryopreservation cells were collected into tubes in a media suspension as described in 2.2.5.2. A small volume of the cell media suspension was loaded onto a haemocytometer (Hawksley, BS.748) and counted under a light microscope. A volume containing the

appropriate number of cells was then centrifuged at 600 x g for 5 minutes to pellet the cells ($1x10^6$ cells/ml for NIH3T3 and 3 x 10^6 cells/ml for HEK293). These were then resuspended in freezing media (DMEM with 10% (v/v) DMSO and 20% (v/v) FCS for HEK293 or NBCS for NIH3T3) and moved to labelled cryovials. The vials were then stored at -20℃ until frozen solid. The cryovials were then placed at -80℃ overnight in bubble wrap to ensure slow freezing and then transferred to liquid nitrogen for long term storage.

2.2.5.4 Resuscitation of frozen cells

To recover cells from liquid nitrogen storage, cells were thawed at 37℃ and transferred into 10 ml of pre-warmed medium. The suspension was mixed thoroughly, and the cells pelleted by centrifugation at 600 x g for 5 minutes to remove residual DMSO which can impede growth. Cells were then resuspended in fresh media and incubated at 37℃, 5% CO_2. The day after cell plating the media was changed to remove dead and unattached cells, followed by another change of media after 24 hours. Cells were passaged at least three times after resuscitation, to ensure they have fully recovered, before use in experiments.

2.2.5.5 Calcium phosphate-mediated transfection of HEK293 cells

HEK293 cells were seeded at a density of 5 x 10^5 cells per well in a 6 well plate, 24 hours prior to transfection. On the day of transfection, the culture medium was replaced 3-4 hours before transfection. An aliquot of 200 µl 2 x HEPES Buffered Saline (HBS) solution, along with a separate mixture of 25 µl 2M calcium chloride solution & 1 µg of each vector/plasmid to be transfected, made up to a total volume of 200 µl with sterile dH_2O was prepared for each sample. The calcium chloride & DNA mixture was added in a dropwise fashion to the HBS solution, whilst gently vortexing the aliquot of HBS. This mixture was incubated at room temperature for 20 minutes, before being added to the relevant cells in a dropwise fashion. The cells were incubated for 16 hours at 37 °C, 5% CO_2. After incubation, the cells were washed three times with PBS, and then fresh medium was added. The cells were

then analysed for expression of the plasmid construct via fluorescent microscopy for GFP reporters after a further 24 hours and harvested for cell sorting within a further 36 hours.

2.2.5.6 Lipofectamine-mediated transfection of NIH3T3 cells

NIH3T3 cells were seeded at a density of 1.5 x 10^5 cells per well in a 6 well plate, 24 hours prior to transfection. On the day of transfection, the manufacturer's protocol for lipofectamine 2000 transfection was followed. The cells were then analysed for expression of the plasmid construct via fluorescent microscopy after 36 hours from transfection and were harvested for cell sorting as described for cell passaging within 72 hours.

2.2.5.7 Flow-Assisted Cell Sorting of GFP+ cells

Cell sorting of GFP+ single cells was achieved by the in-house fluorescence-activated cell sorting (FACS) facility using a FACSAria Cell sorter. Cell emission at 510 nm upon excitation using a 488 nm laser was used for analysis of GFP expression. To prepare transfected cells for FACS, they were harvested as for passaging in 2.2.5.2 and centrifuged at 600 x g for 5 minutes, prior to pellet resuspension in 500 µl of media appropriate for the cell type. These volumes were then transferred to separate BD Falcon FACS tubes with cellstrainer caps to remove clumps of cells and were kept on ice prior to sorting. Individual GFP expressing cells were sorted into 96 well plates containing 100 µl prewarmed media appropriate for the sorted cell type. An extra 100 µl of media was added after single-cell seeding.

2.2.6 Biochemical techniques

2.2.6.1 Sources and composition of biochemical reagents

The SDS-PAGE molecular weight protein marker, Color Prestained Protein Standard, Broad Range, 11–245 kDa was purchased from NEB. Nitrocellulose transfer membrane was purchased from Bio-Rad. The N,N,N,N-tetramethylethylenediamine (TEMED) was purchased from Sigma-Aldrich. 30% (w/v) ProtoGel acrylamide mix from National Diagnostics. The

developing solution used for imaging was Pierce™ ECL Western Blotting Substrate from ThermoFisher, used according to manufacturer's instructions.

SDS-PAGE loading buffer (4x) = 2.0 ml 1 M Tris-HCl pH 6.8, 0.8 g SDS, 4.0 ml 100% glycerol, 0.4 ml 14.7 M β-mercaptoethanol, 1.0 ml 0.5 M EDTA and 8 mg bromophenol blue, made up to 10 ml with dH_2O.

Ponceau S solution = 0.1% (w/v) Ponceau S in 5% (v/v) acetic acid. Made up to a total volume of 1 L with dH_2O.

5% milk blocking solution = 5% (w/v) Marvel 0% fat milk powder in 1x PBS.

Tris-glycine-SDS (TGS) buffer (10x) = 250 mM Tris base, 2 M glycine, 35 mM SDS, pH 8.3.

Transfer buffer = 48 mM Tris base, 39 mM glycine, 0.037% (w/v) SDS, 20% (v/v) methanol.

10% Ammonium persulphate (APS) solution = 10% (w/v) APS in dH_2O. Stored at -20 °C until use.

10% Sodium dodecyl sulphate (SDS) solution = 10% (w/v) SDS in dH_2O.

PBST = 1× PBS containing 0.1% (v/v) Tween 20.

2.2.6.2 Protein extraction from mammalian cell extracts

Mammalian cell-free extracts were prepared using RIPA buffer. HEK293 cells were harvested as described for passaging in 2.2.5.1, the suspension was transferred to 15 ml tubes and centrifuged at room temperature at 600 x g for 5 minutes. The supernatant was discarded and the pellet resuspended in 1 ml ice cold 1 x PBS, before repeating the centrifugation. The pellet was then resuspended in ice cold RIPA buffer. When harvesting NIH3T3 cells the medium was aspirated, and cells washed with ice cold 1 x PBS before being scraped into ice cold RIPA buffer. Cell suspensions in RIPA buffer were then stored at -80 °C until sonicated. The samples were defrosted and sonicated for 3 cycles of 30 second bursts in a Diagenode Bioruptor® before spinning down of the cell lysate and collection of the supernatant. The protein samples could then be stored at -80 °C until required or progressed directly into

Bradford assays to determine total protein concentration for SDS-PAGE and western blotting.

2.2.6.3 Antibodies

The primary antibodies mouse anti-CLOCK (sc-271603) and mouse anti-BMAL1 (sc-365645) were from Santa Cruz Biotechnology. Rabbit anti-NPAS2 (HPA019674) was from Atlas Antibodies. Mouse and rabbit anti-β actin (A5441 and A2066 respectively) were from Sigma-Aldrich. Primary antibody dilutions are detailed on western blot figures where they are used. Horseradish peroxidise (HRP) conjugated secondary antibody chicken anti-mouse (sc-2954, used at 1:5000) and secondary goat anti-rabbit (sc-2004, used at 1:2000) were purchased from Santa Cruz Biotechnology.

2.2.6.4 Protein concentration determination

Protein concentrations were determined using the Bradford assay method. Reactions were set up consisting of 2 µl of protein extract, 800 µl dH_2O & 200 µl of Sigma-Aldrich Bradford dye in cuvettes. The samples were mixed thoroughly and left to stand at RT for 15 minutes. The absorbance of each sample was then read at 595 nm and the concentration calculated relative to a standard curve created from reads of diluted Bovine Serum Albumin (BSA) standards of known concentrations, performed at the same time.

2.2.6.5 Sodium-dodecyl-sulphate polyacrylamide gel electrophoresis (SDS-PAGE)

SDS-PAGE gels were made as either 5% stacking, 6% resolving, 12% resolving two-part gel or 5% stacking, 12% resolving gel. The two-part gels were prepared as shown in Table 2.6, for a 12% gel all volumes for the 12% section were doubled.

The prepared protein extracts, which corresponded to 100 µg of protein made up to equal volumes with distilled water and SDS protein loading dye, were incubated for 5 minutes at 100 °C to denature the protein and resolved on a 6/12% or 12% SDS-PAGE gel ran at 180 V with 1 x TGS buffer.

Table 2.6: Reagents used and composition of SDS-PAGE gels. All volumes are in ml and are enough for one gel.

	5% Stacking gel	6% Resolving gel	12% Resolving gel
dH_2O	3.40	2.6	1.6
30% (w/v) Acrylamide	0.83	1.0	2.0
1.5 M Tris pH 8.8	-	1.3	1.3
1.0 M Tris pH 6.8	0.63	-	-
10% SDS solution	0.05	0.05	0.05
10% APS solution	0.05	0.05	0.05
TEMED	0.005	0.004	0.002

2.2.6.6 Western blotting

After removal from the gel apparatus and rinsing in transfer buffer, Proteins were transferred from SDS-PAGE gels onto a nitrocellulose membrane overnight at 30 V, 4 °C, with an ice block in the chamber and filled with transfer buffer. The membrane was covered with 1% Ponceau S solution for one minute, washed three times with dH_2O and checked by eye for successful protein transfer. Non-specific antibody binding was blocked by adding 5% milk to the membrane for 1 hour at room temperature, with agitation. The membrane was then incubated overnight at 4 °C, with agitation in 5% milk containing the primary antibody (typical concentration 1:500 see results for details). To remove excess antibody, the membrane was washed in PBST three times for 5 minutes each, with agitation at room temperature, then incubated for 1 hour with agitation at room temperature in 5% milk containing the secondary antibody (typical concentration 1:5,000). The washes with PBST were repeated to remove excess antibody. Developing solution was added to the nitrocellulose membrane and incubated at room temperature for 1 minute. The membrane was wrapped in clear plastic and excess developing solution removed. A Fujifilm LAS-4000 system was used immediately to detect and image the chemiluminescent signal. Exposure times are detailed in the legends for the specific western blots. The prestained protein marker (Color Prestained Protein Standard,

Broad Range, 11–245 kDa) was also imaged as a reference of molecular weight. The imaged membranes were then stored at 4 °C sealed in PBS and could be reprobed and imaged if required.

The molecular weight (MW) of the protein was calculated by use of a logarithmic regression analysis of migration distance. Briefly the migration distance of three of the known MW bands of the standard close to the band of interest were measured using ImageJ and a standard curve was made using the log of the distance travelled. This standard curve was then used to calculate the MW weight of the bands of interest using the migration distance calculated in ImageJ.

2.2.7 Generation and identification of modified cells process

2.2.7.1 Design of sgRNAs for targeting of murine and human circadian genes

CRISPR-Cas9 nickase-mediated genome editing (as discussed in the introduction section 2.1.1) requires the targeting of SpCas9n to proximal 20mer sequences on opposing strands of the target locus (Ran et al., 2013a). The generated single strand breaks on opposing strands invokes repair by the non-homologous end joining repair pathway leading to indels. Transcripts were compared using the Ensembl (Cunningham et al., 2019, Zerbino et al., 2018), RefSeq (O'Leary et al., 2016), and UniProt (Consortium, 2019) databases and sequences were acquired from the Ensembl database. Guide sequences were designed as described in section 2.2.3 to target *CLOCK*, *BMAL1* and *NPAS2* sequences in human kidney cells (HEK293) and *CLOCK* and *NPAS2* sequences in mouse fibroblast cells (NIH3T3). Details of the design process for the specific genes are included below in section 2.3 and detailed sequence information for the guides is included in the appendix section A.6 (page 296).

Our initial approach was to target indels close to or encompassing the initial ATG start codon (AUG in RNA) with the aim that sequence alterations disrupting the ATG should lead

to loss of expression. This was dependent on the availability of suitable guide sequences within the targeted region flanking the ATG. The alternative strategy, where required, attempted to introduce indels early in the coding sequence to produce premature stop codons or frame shifts leading to non-functional target proteins, the detailed process for each cell type below details the approach taken.

2.2.7.2 Generation of Cas9 targeting constructs for circadian genes

To generate Cas9 targeting vectors for *BMAL1*, *CLOCK* and *NPAS2* in human and mouse cell models, the designed oligonucleotide guide sequences were annealed and phosphorylated (2.2.4.1) and maxiprep DNA of the PX461 vector was digested with BbsI enzyme and purified by running on an agarose gel (2.2.4.3-2.2.4.5). Complete digestion was validated by identification that the linearised vector was the correct predicted size of 9.22kb and ran differently to the uncut vector (Figure 2.2). The purified cut vector was ligated to the annealed phosphorylated oligonucleotides comprising the guide sequences and the ligations transformed into DH5α cells (2.2.4.6 to 2.2.4.7). While consistently no colonies were obtained using the vector only control, tens to hundreds of ampicillin resistant clones were obtained with the vector insert mix, indicating successful ligation. Sequencing of cultures from several clones from each ligation confirmed successful generation of the targeting constructs (2.2.4.8). These verified cultures were then subjected to maxiprep purification for mammalian cell transfection (2.2.4.9).

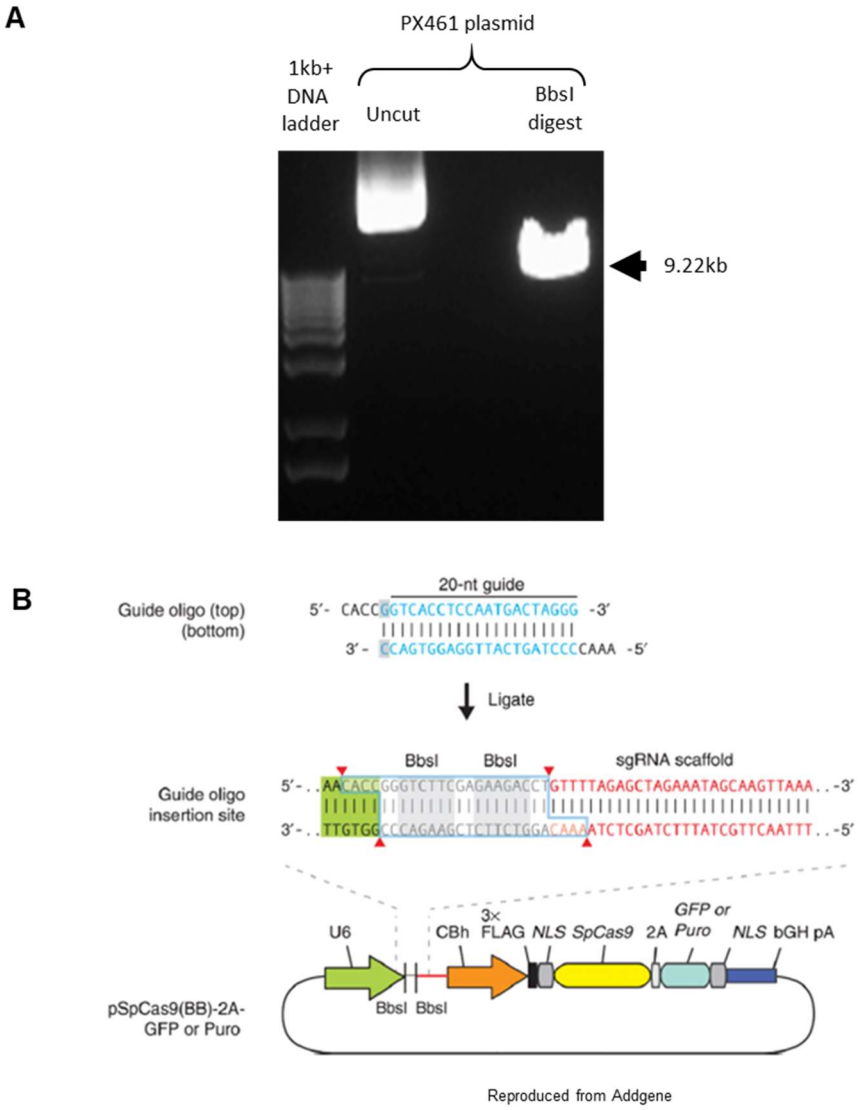

Figure 2.2: PX461 plasmid digestion

A: Agarose gel electrophoresis showing PX461 plasmid (1 mg), uncut or digested with BbsI. The linearised DNA runs with the band front at approximately the expected size of 9.2kb. **B:** Schematic of the BbsI cloning sites allowing insertion of the 20 bp guide sequences into the sgRNA scaffold. BbsI digestion generates incompatible ends preventing self-ligation of the cut vector. Design of annealed primers pairs is shown above. A schematic map of the PX461 vector is also shown detailing the FLAG-NLS-CAS9 and GFP coding sequences that are expressed under control of a CMV promoter.

2.2.7.3 Transfection of cells with generated PX461 vector to target circadian genes

For each target gene (human or mouse specific), the appropriate cell type was transfected with either the guide plasmid pairs or a single guide plasmid as a control (2.2.5.5 or 2.2.5.6). The PX461 vector carries eGFP, so after 2-3 days, transfection efficiency was scored by fluorescence microscopy (for example see Figure 2.3) and if the cells are seen to achieve at least 10% transfection efficiency, they were harvested for cell sorting. GFP positive cells were selected using a FACSAria Cell sorter (2.2.5.7). For each condition, individual GFP+ cells were sorted in 2 x 96 well plates and clonally expanded over 2-3 weeks.

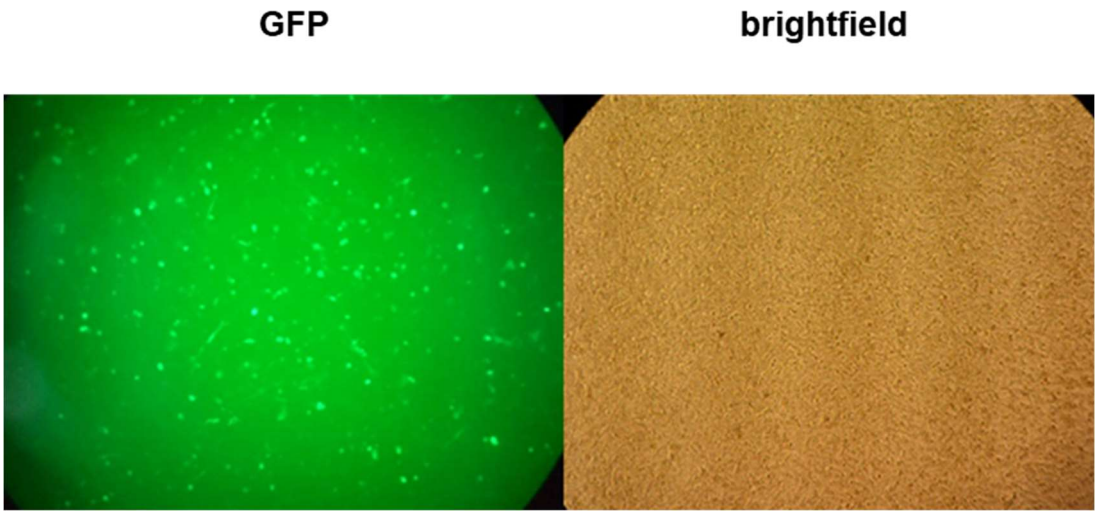

Figure 2.3: HEK293 cells transfected with PX461-*Homo sapiens CLOCK* sgRNA A and PX461-*Homo sapiens CLOCK* sgRNA B

A: Under a blue light viewed through a green filter. Cells visible here express the eGFP and have been successfully transfected. **B:** Under a white light showing total cells most of which are not expressing eGFP.

2.2.7.4 Identification of mutant clones

Identification of CRISPR-Cas9 targeted clones was performed to select specific mutants to use as models for research and characterise the specific mutations. This work was performed in collaboration with PhD student Ruby Chrisp. Surviving clones were named according to plate number and well position (e.g., 1E9). Once a sufficient number of cells were available (4-8 weeks) genomic DNA and protein extracts were collected for analysis of the control and targeted clones (2.2.4.10 & 2.2.6.2). Analysis of indels is detailed in section 2.3 but for each gene target a similar process is followed. The genomic DNA was amplified by PCR using primers flanking the targeted genomic region to characterise mutations by change in product size on an agarose gel (2.2.4.11 & 2.2.4.4). Due to the variability of insertions and deletions expected for the mutations, changes in product size are to be expected with the alleles presenting as different bands due to unique indels. PCR analysis also aids checking of the number of alleles, which is required as HEK293 cells show variable pseudotriploid karyotype and NIH3T3 cells are near tetraploid (Lin et al., 2014, Leibiger et al., 2013). The extracted protein was used for western blotting to assess impact on level of protein expression (2.2.6.4-2.2.6.6). Detection of changes in expression in the encoded proteins by western blots is reliant on the availability of high-quality antibodies, as well as knowledge of the different isoforms that may be expressed in each cell type or tissue. Sequencing of PCR products excised from the gels allowed complete identification of the induced mutation (2.2.4.8). These steps were necessary to enable selection of clones more likely to have gene inactivation in multiple alleles, rather than in-frame deletions/insertions etc.

2.3 Results of generation and characterisation of circadian gene edited clones

2.3.1 Targeting *NPAS2* gene expression in NIH3T3 fibroblasts

The mouse *NPAS2* gene is located on chromosome 1 and is made up of 21 exons, 20 of which are coding exons, and the major transcript is 4,234 bp (Figure 2.4 A). Only a single validated transcript is described for the mouse *NPAS2* gene in the NCBI and Uniprot databases, encoding an 816-residue polypeptide (NM_008719.2). However, the Ensembl database lists 2 more transcripts for mouse *NPAS2* generated by alternative splicing, thus other isoforms may be expressed in the cells although the other two transcripts are a short mRNA coding for a very short 60aa polypeptide and a non-protein coding processed transcript. Given the make-up of the major known transcript, the guide pairs were designed to target exon 2 which codes for the AUG initiation codon (Figure 2.4 B and C).

After transfection with the paired PX461 expression vectors encoding spCas9n-eGFP and specific sgRNAs, single GFP+ cells were isolated by FACs cell sorting and clonally expanded for analysis. Once clones had reached sufficient cell numbers, genomic DNA was extracted for PCR genotyping using the murine *NPAS2* primers outlined in the appendix section A.5.1 (page 291). The karyotype of NIH3T3 cells is considered tetraploid albeit with imbalances due to genomic rearrangements (Leibiger et al., 2013) meaning that when targeting events are investigated, multiple alleles may be present depending on the targeted chromosome and the location within the chromosome.

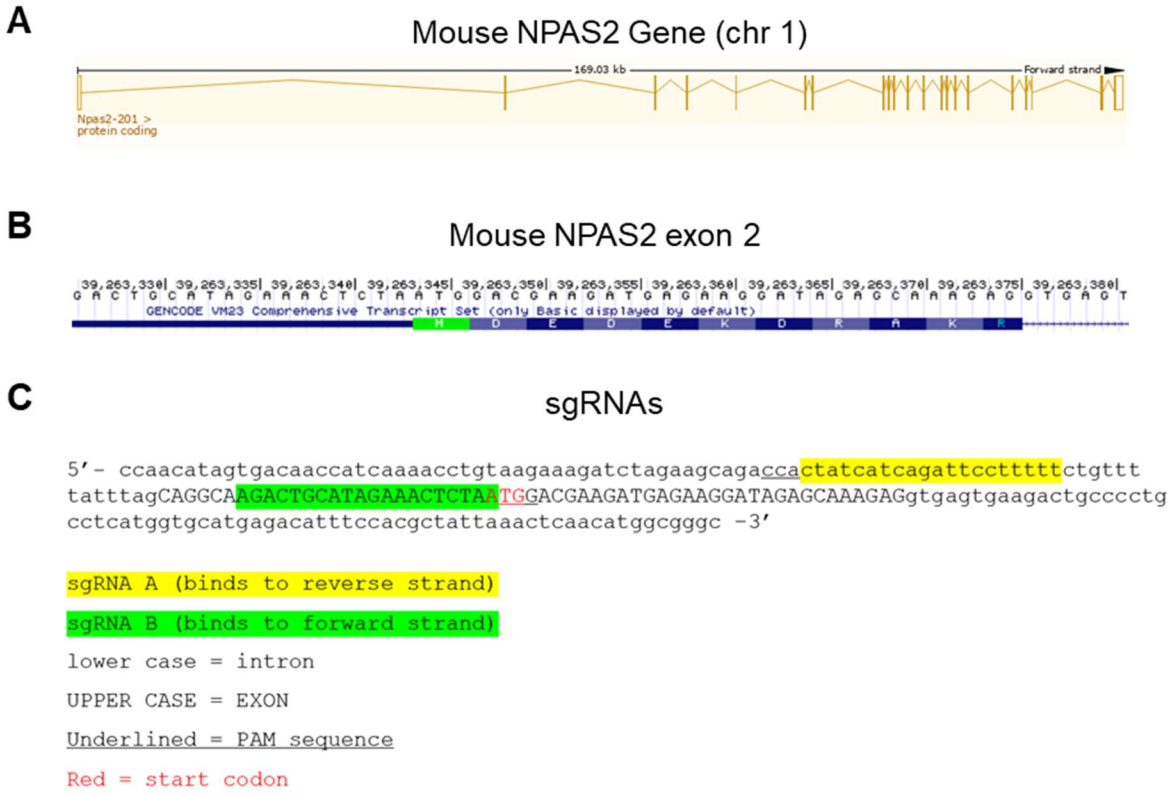

Figure 2.4: Targeting the mouse *NPAS2* gene

A: Exon structure of the mouse *NPAS2* gene from the Ensembl database. **B:** Sequence of the mouse *NPAS2* exon 2 from the UCSC genome browser showing the initiation codon and encoded 11 amino acids. **C:** sgRNA designs targeting opposite strands flanking exon 2 of *Mus musculus NPAS2*. Guide pairs were selected close to the ATG in a PAM-out arrangement with a 59 bp spacing.

Indels in the *NPAS2* exon 2 region were readily detected among the expanded clones (Figure 2.5) with at least three distinct alleles detected in some clones, as suggested by the number of distinct PCR products. In contrast, no obvious indels in this region were detected in controls (transfected with a single sgRNA vector). Some clones appeared to have amplified bands similar to expected size for unmodified *NPAS2*, such as the lower band of 1F3, which may mean not all alleles were targeted. However, gel electrophoresis is not sensitive enough to detect small alterations in targeted alleles. Nonetheless, several clones appeared to lack any unmodified product (242 bp) for example 1F12 clearly shows modification of sequence in the products.

Several clones were selected for further investigation based on the absence of a PCR band consistent with the size expected for the wild type product. Cell-free extracts from these clones were used for western blotting to assess whether the targeted mutations were successful in reducing levels of NPAS2 expression. Initial western blot experiments, using a polyclonal antibody directed against NPAS2, identified bands that were inconsistent with the expected MW of the NPAS2 protein, indicating the antibody was not reliable (see appendix for more information, section A.3, page 287). We contacted several groups that had reported NPAS2 western blots to request antibody samples, but personal communications indicated that none of the commercial antibodies available were specific. Indeed, the poor specificity of available NPAS2 antibodies precluded western blot confirmation in a KO model (O'Neil et al., 2017, pers. comms.).

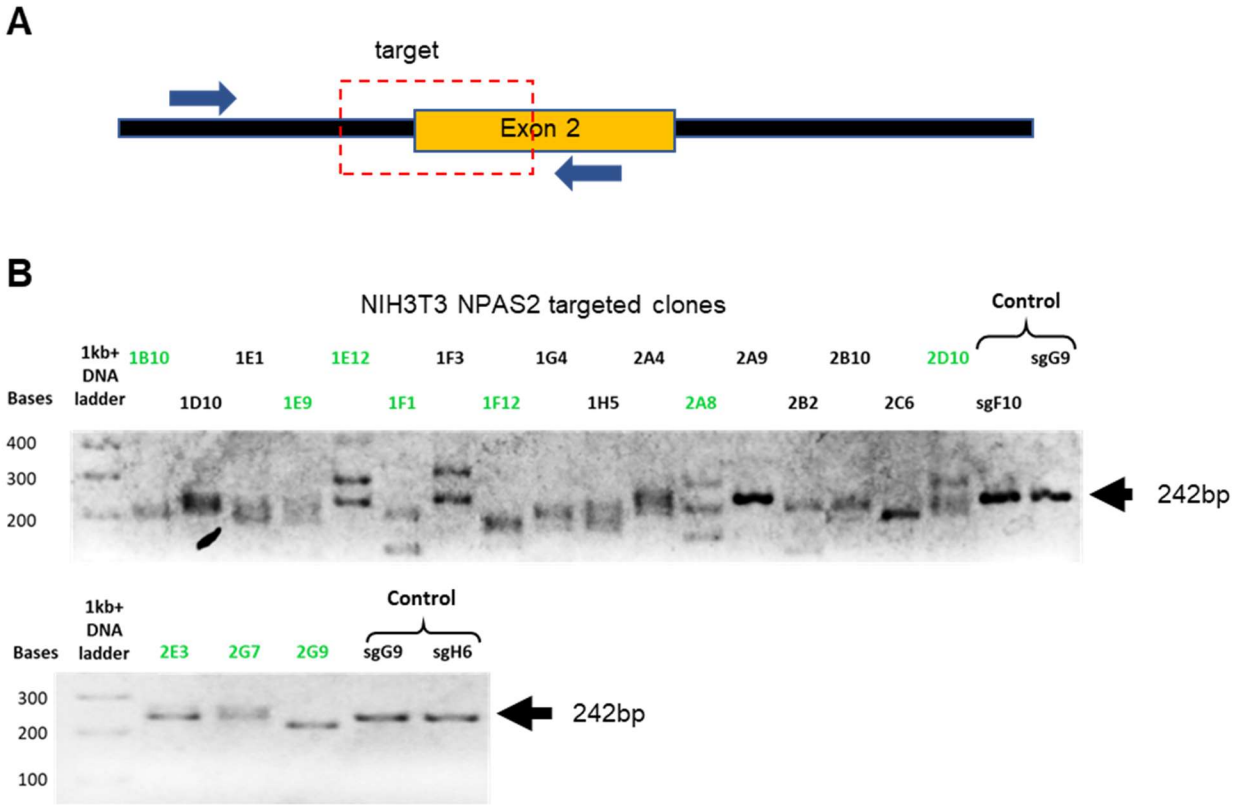

Figure 2.5: Genotyping mutations of murine *NPAS2*

A: Schematic showing the targeted region of the *NPAS2* gene. Blue arrows indicate the approximate positions of PCR analysis primers (F1 and R1, see section A.5.1). **B:** PCR genotyping gel of GFP+ *NPAS2* NIH3T3 clones. Clones transfected with single guide (Control, sgG9 and sgH6) all produced a single product of the expected size (242 bp) for wild type alleles. Up to three distinct bands are present in some clones indicating targeting of multiple alleles. All clones apart from 2A9 harbour obvious indels. Clones highlighted in green were selected for western blotting. (Note: the poor quality of the signal detection is due to this image being created using the Fujifilm LAS-4000 which used a less powerful UV bulb, due to a temporary defect in the BIO-RAD Universal Hood II UV transilluminator that was later repaired.)

Based on the PCR genotyping data, several *NPAS2* targeted clones (2G9, 1E9, 1F1 and 2D10) were selected for further investigation of the nature of the targeting events. Multiple PCR bands from clones 2G9, 1E9, 1F1 and 2D10 and a single band from an sgControl were gel purified and sent for sequence analysis. Sequencing of the sgControl band confirmed only wild type sequence as expected, indicating successful HDR repair and no editing events in single guide controls. The single band detected in 2G9 contained a 23 bp deletion upstream of the ATG. Clone 2D10 yielded 3 or 4 PCR products, the lower 2 or 3 bands ran very closely together meaning only the larger band with a 31 bp insertion upstream of the ATG was clearly sequenced. Since the ATG was unaffected and a frameshift could not be expected these two clones were eliminated from further analysis. Clone 1E9 produced three observable PCR products, mixed sequence was obtained for the larger products, which indicated co-migration of similar sized PCR products, while the lower allele harboured a deletion of 118 bases including loss of the ATG. Clone 1F1 sequencing revealed clear deletions of 33 bp and 109 bp in the lower sized products, removing part of or the entire exon 2 region respectively, thus both alleles detected would be predicted to have lost the mRNA AUG start codon.

The larger band detected in the 1F1 PCR is approximately 400 bp (A in Figure 2.6), suggesting an insertion in the sequence. However, sequence analysis of this product detected a mixed sequence. Surprisingly, deconvolution of the mixed sequence suggested that it consisted of both of the two smaller alleles 1F1.1 and 1F1.2 (see Figure 2.6.B). No other sequence was present. It is possible that during the PCR reaction overlap of sequence of these two products generated an artefactual recombined product. As such this is not a unique allele.

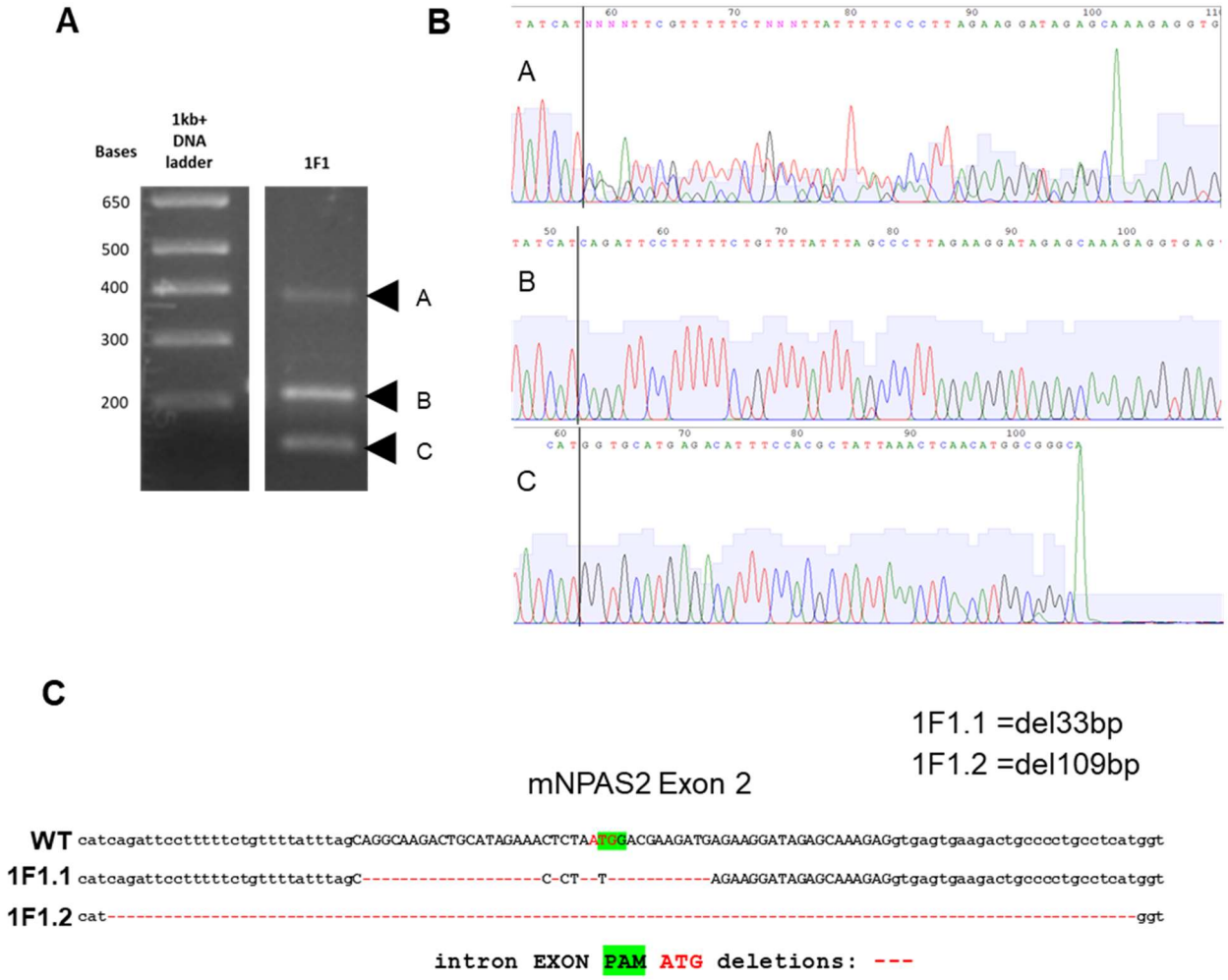

Figure 2.6: Sequencing murine *NPAS2* mutations

A: PCR genotyping of clone 1F1 produced three distinct bands A-C with no band at the wild-type position of 242bp. **B:** Electropherograms showing a section of sequence analysis of the isolated PCR products A-C, clear sequence can be seen for B and C but for product A the read shows only a mix of B and C within the targeted region which becomes clear B sequence after the end of the C sequence. **C:** Sequence alignments of bands B (1F1.1) and C (1F1.2) to wild type sequence indicate two targeted alleles harbouring 33 bp and 109 bp deletions respectively.

Following this analysis, we obtained a different polyclonal NPAS2 antibody (Atlas antibodies; HPA019674), which detected multiple bands of varying size, but only one band between 80-135 kDa in NIH3T3 cell extracts, calculated to represent a protein of ~104 kDa, close to the predicted molecular weight of the NPAS2 main isoform (91 kDa). This band was assumed to be the NPAS2 protein based on no other proteins being observed in the correct range. Blots with this antibody showed variation of NPAS2 expression in selected clones including a strong reduction in the expression of endogenous NPAS2 protein in the clone 1F1 compared to the wild type (WT) control. In contrast, western blot detection of β actin confirmed equal loading (Figure 2.7). As well as highlighting 1F1 as a candidate clone the variation of the protein in our NPAS2 modified lines also provides additional confidence that this is a true NPAS2 protein band observed.

Similar western results were observed independently in our lab (Ruby Chrisp, pers. comm.). NPAS2 expression is not completely ablated which may indicate expression from an undetected allele or reinitiation from a downstream AUG. We did note that the band in Figure 2.7 for 1F1 appeared to have travelled slightly further than other clones, possibly indicating a truncated product, calculated as ~101 kDa. Interestingly, the next available AUG that could potentially be used to initiate translation would generate a polypeptide lacking the N-terminal 34 amino acids. This would truncate the NPAS2 protein within the bHLH domain, comprised within residues 1-77, required for DNA binding and BMAL1 association (Yoshii et al., 2013), and likely abrogate these functions. Thus, the NIH3T3-NPAS2-1F1 clone is likely to be deficient in functional NPAS2.

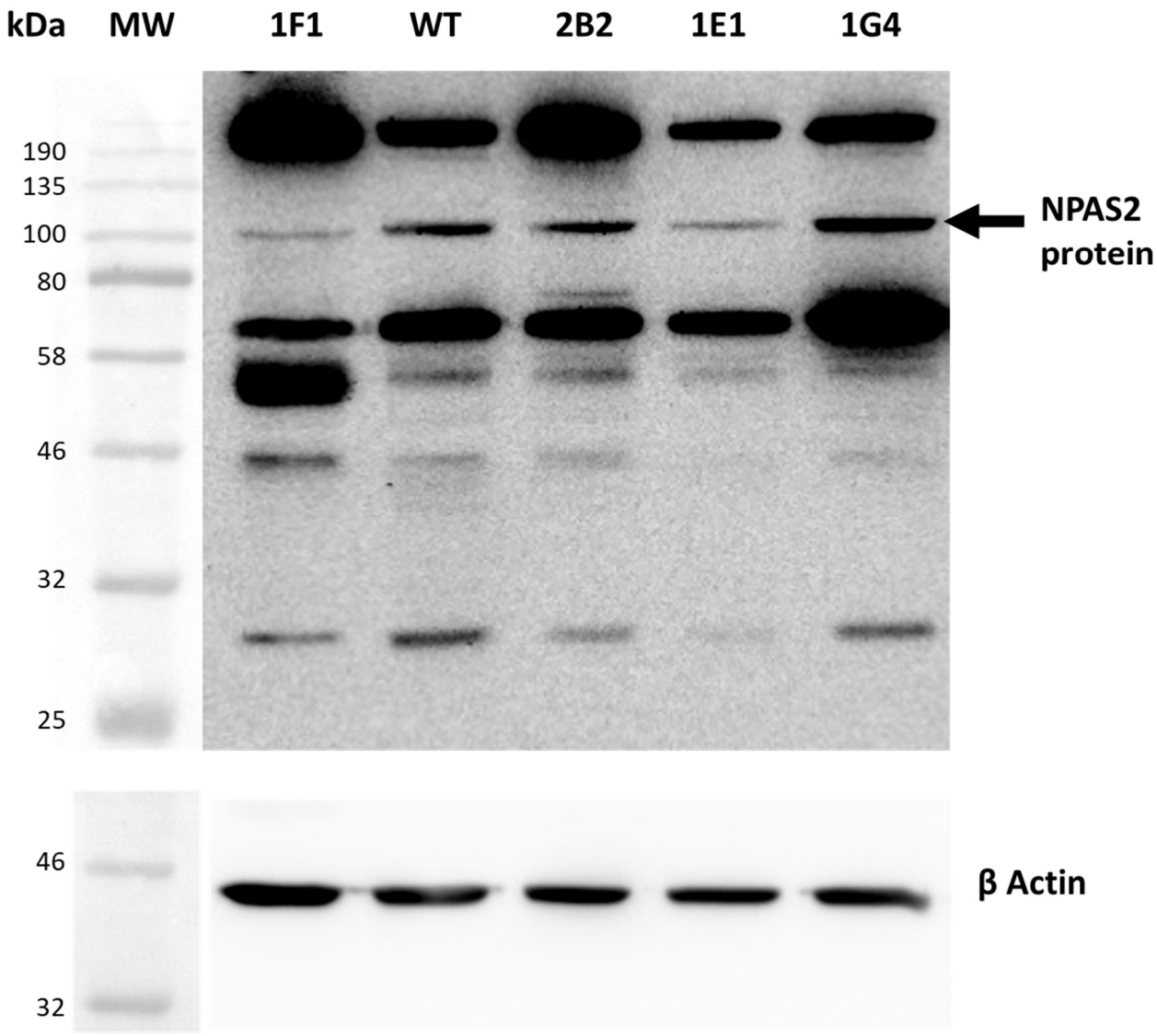

Figure 2.7: NPAS2 protein expression in targeted NIH3T3 clones

Western blot of protein extracts from selected *NPAS2* targeted NIH3T3 clones, probed for NPAS2 (Atlas antibodies, HPA019674, batch: A115419, predicted MW 91 kDa, 1:1000 dilution, 1000 sec exposure) and β actin (Sigma-Aldrich, A2066, batch: 018M4853V, predicted MW 42 kDa, 1:1000 dilution, 60 sec exposure) as a loading control. A large number of bands were picked up by the NPAS2 antibody but the band closest to the estimated size for NPAS2 is marked with an arrow. 1F1 is presented first next to the wild type control and a clear reduction in expression is visible in both 1F1 and 1E1 in the NPAS2 band on the western. It also appears that the putative NPAS2 band in 1F1 may have a slightly lower MW compared to other clones and control.

2.3.2 Targeting *CLOCK* gene expression in NIH3T3 fibroblasts

The murine *CLOCK* gene is located on chromosome 5 and is made up of 23 exons, 20 of which are coding exons, and the major transcript is 9,744 bp (Figure 2.8 A). Multiple isoforms are listed in the NCBI and Uniprot databases, but all share the same start codon, located within exon 4 of the major transcript (Figure 2.8 B). Based on this, guide pairs were designed to target exon 4 as shown below (Figure 2.8 C).

After transfection with the paired PX461 expression vectors for the specific sgRNAs GFP+ cells were sorted by FACs and single clonal cells expanded for PCR genotyping, as described previously, using the murine *CLOCK* primers outlined in appendix section A.5.2 (page 292)271. Indels in the *CLOCK* exon 4 region were detected in the expanded clones (Figure 2.9), with two to three distinct products detected in most clones (or in one case four products). No obvious indels were observed in the control clone transfected with a single sgRNA vector (sgG9).

Several clones were selected for further analysis based on the absence of a PCR band consistent with the size expected for the wild type product (243 bp). However, most of the clones were lost at this stage due to growth failure or contamination, limiting those available for investigation to the three clones 2C1, 2H8 and also 1D12 which had not been included in the initial gel shown in Figure 2.9 B.

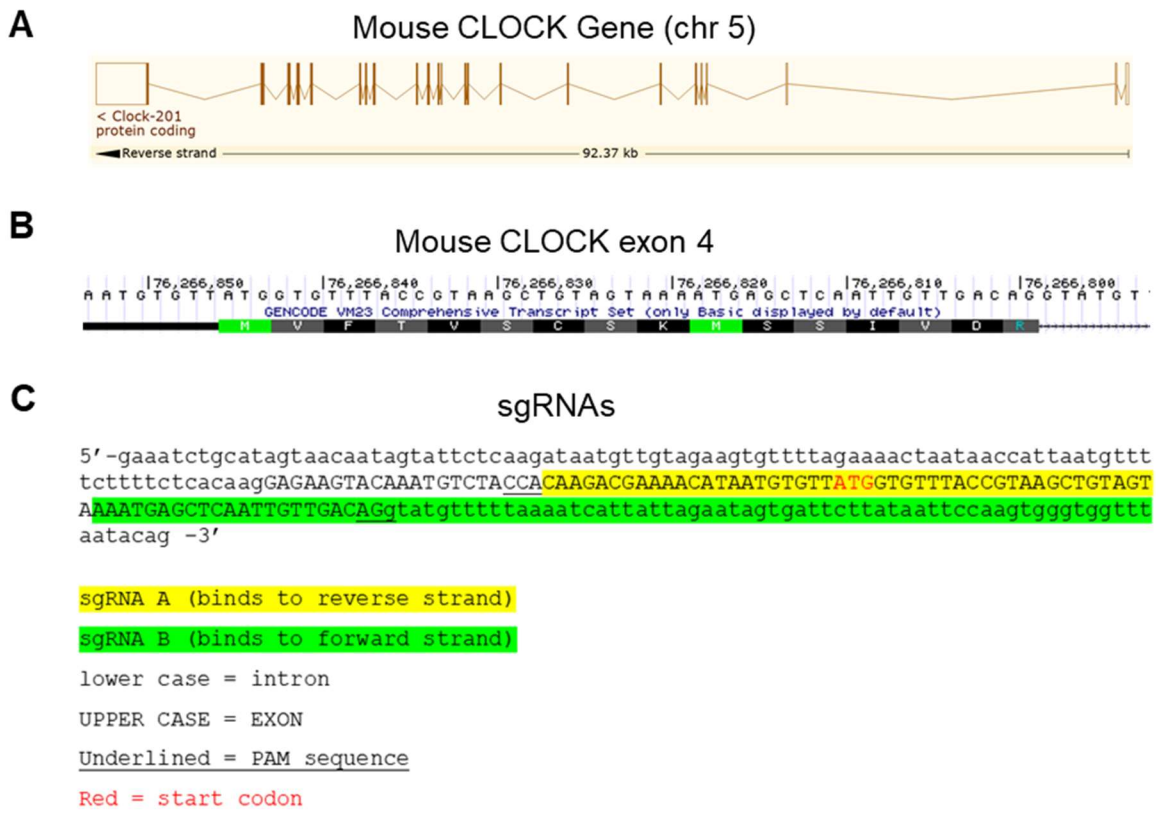

Figure 2.8: Targeting the mouse *CLOCK* gene

A: Exon structure of the mouse *CLOCK* gene from the Ensembl database **B:** Sequence of the mouse *CLOCK* exon 4 from the UCSC genome browser showing the initiation coding and encoded 16 amino acids. **C:** sgRNA designs targeting opposite strands flanking murine *CLOCK* exon 4. Guide pairs were selected to flank the ATG in a PAM-out arrangement with a 67 bp spacing.

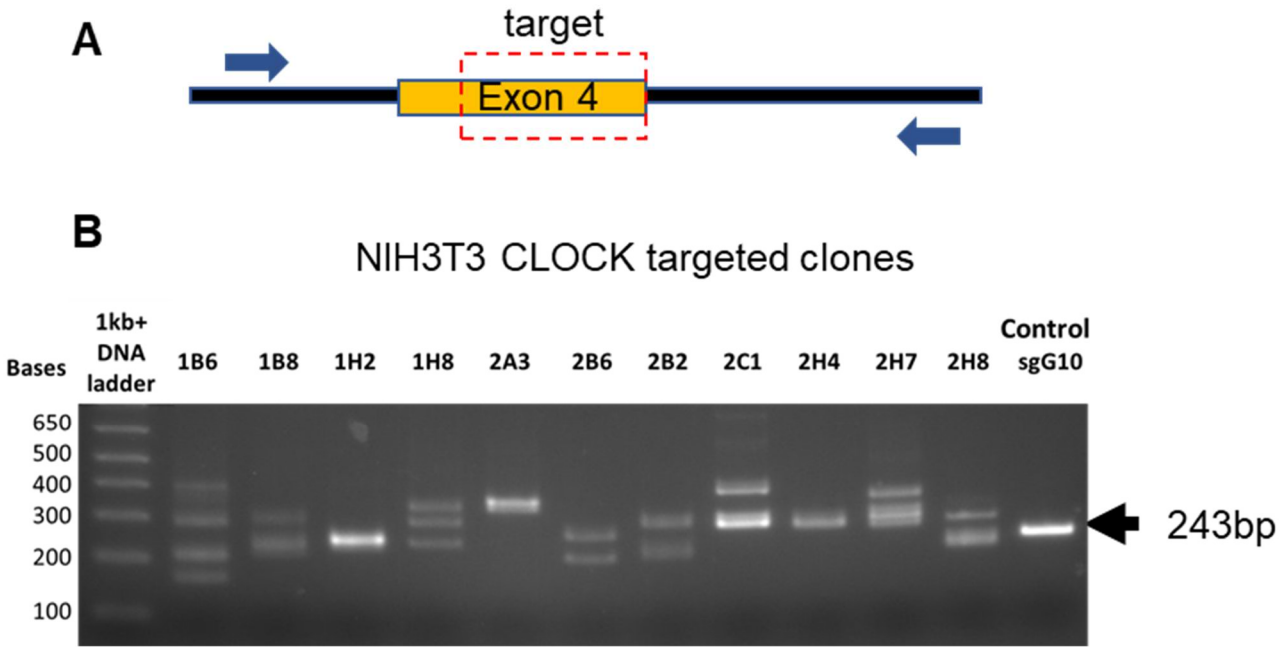

Figure 2.9: Genotyping mutations of murine *CLOCK*

A: Schematic showing the targeted region of the *CLOCK* gene. Blue arrows indicate the approximate positions of PCR analysis primers (F2 and R2, see section A.5.2). **B:** PCR genotyping gel of GFP+ *CLOCK* NIH3T3 clones. The control (sgG10) transfected with single guide produced a single product of the expected size (243 bp) for wild type alleles. Several distinct bands are present in some clones indicating targeting of multiple alleles. All clones (with the possible exception of 1H2) harbour obvious indels. As detailed above most of these clones were lost before they could be carried forward for further testing.

A western blot was performed on cell-free extracts from these three clones using a monoclonal CLOCK antibody (Santa Cruz; sc271603) to assess whether the targeted mutations were successful in reducing levels of CLOCK expression. As shown in Figure 2.10 A, two bands were detected in the WT control, calculated as ~85 and ~95 kDa. The Uniprot database also describes 2 isoforms of murine CLOCK of 855 (96 kDa) or 825 (93 kDa) residues which may be what we observe. The antibody supplier (Figure 2.10 B) and other studies also reported the detection of multiple CLOCK bands 90-120 kDa, indicating expression of isoforms and posttranslational modifications that affect mobility (Lee et al., 2001). Clone 2H8 shows a clear reduction in the intensity of these bands but no change in β actin protein levels. While reduced CLOCK expression was also observed for clones 2C1 and 1D12, the loading control was also less in these, thus we could not make a confident conclusion as to whether CLOCK expression has been reduced in these clones, based on this western blot.

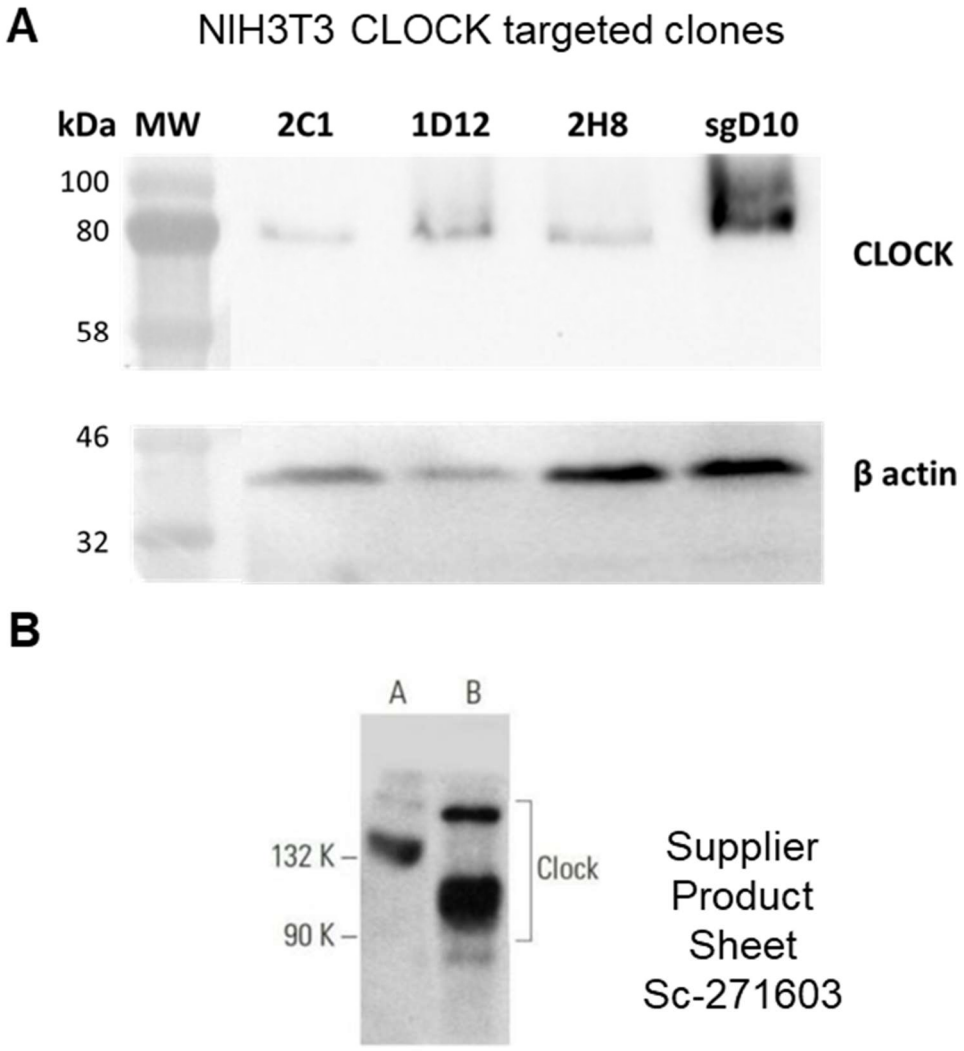

Figure 2.10: CLOCK protein expression in targeted NIH3T3 clones

A: Western blot of protein extracts from selected CLOCK targeted NIH3T3 clones, probed for CLOCK (Santa Cruz, sc-271603, batch: I2917, predicted MW 93 kDa, 1:250 dilution, 600 sec exposure) and β actin (Sigma-Aldrich, A2066, batch: 018M4853V, predicted MW 42 kDa, 1:1000 dilution, 60 sec exposure) as a loading control. CLOCK expression is clearly reduced in 2H8 compared to the control. While CLOCK seems to be reduced in 2C1 to a similar level and also in 1D12 to some extent, the imbalanced intensity of the β actin band means this is at least in part due to loading error. Multiple bands for CLOCK can be seen in the more intense lanes (WT and 1D12) potentially due to post translational modifications. **B:** Supplier image showing multiple CLOCK bands detected with this antibody from human A-673 (A) and mouse Sol8 (B) cell model lysates.

To further investigate the nature of targeting events in clones 2C1 and 2H8, PCR genotyping was performed for these clones and the sgControl (Figure 2.11 B), individual bands were gel-purified and sent for sequencing. Surprisingly, initial attempts to sequence 2H8 PCR products failed which we suspected might indicate indels spanning the region where the sequencing primer anneals. As this was the most promising candidate in terms of the western blot result, additional forward and reverse primers were designed the amplify the targeted region (Figure 2.11 C) Surprisingly, we continued to encounter poor yields, although the best yield was achieved using the F3,R3 primer set. We hypothesised that this might indicate some problems with Taq Polymerase amplification of the region.

To investigate this, we decided to optimise the PCR conditions by varying the concentration of $MgCl_2$ in the reaction, and/or adding 0.5M betaine. Magnesium ions are essential for Polymerase function, thus the presence of chelating agents or magnesium binding contaminants in the genomic DNA preps can hamper amplification or sequencing. Increasing the amount of $MgCl_2$ in the reaction can counter this. Betaine facilitates amplification of DNA regions that are GC rich by disruption of secondary structures which can block polymerase action. As shown in Figure 2.11 D, addition of these reagents helped to optimise the 2H8 PCR product yield. Successful sequencing was then performed on products of the PCR reaction performed in the presence of 5 mM $MgCl_2$ and 0.5M betaine.

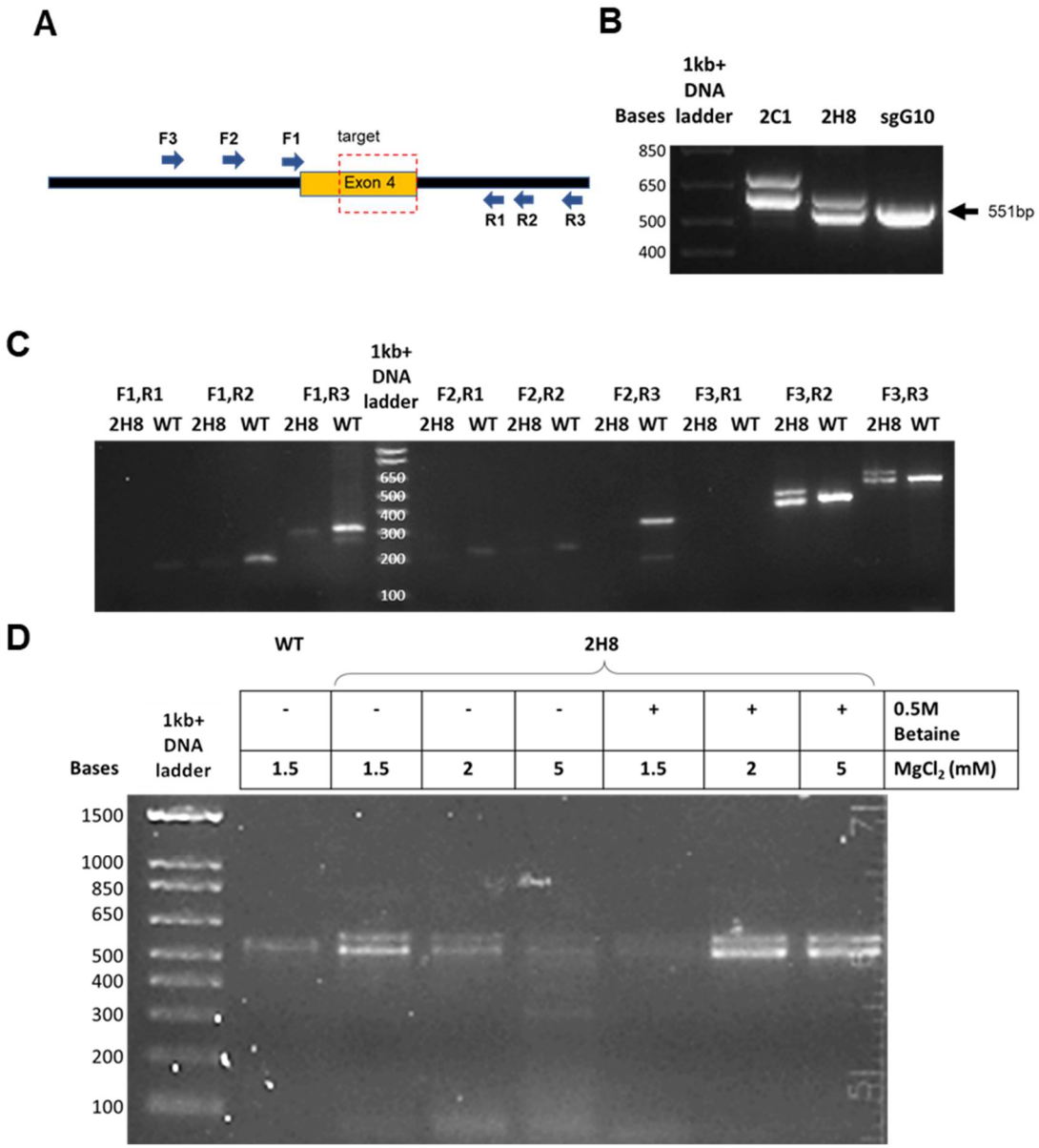

Figure 2.11: Further genotyping of murine *CLOCK* mutations

A: Schematic of the *CLOCK* exon 4 targeted region showing forward and reverse primers, for more detail see section A.5.2. **B:** PCR genotyping of NIH3T3 *CLOCK* targeted clones using the F3 and R3 primers. The control (sgG10) produced a single product of the expected size (551 bp) for wild type alleles. **C:** Comparison of PCR product yields using different *CLOCK* exon 4 primer combinations. For details on primers see section A.5.2. **D:** Optimisation of the 2H8 PCR product yield in the presence of different concentrations of $MgCl_2$ and /or 0.5M betaine. Primers F3 and R3 were used.

Sequencing of the sgControl band confirmed only wild type sequence while the two clones showed alterations in the targeted region. Clone 2C1 contained two distinct alleles with large insertions of 153 bp, introducing 51 in-frame amino acids after Val2, and 42 bp, introducing 7 in-frame amino acids after Val14 and a premature in-frame stop codon (Figure 2.12). Expression of the first allele is likely to be unaffected while expression of the second allele would be inhibited explaining the reduced protein expression seen in the western blot. Taken together with the western blot result however, the 2C1 clone is not favourable as a CLOCK modified model, so investigation was focused on the 2H8 clone which appeared to show more significantly reduced protein expression.

Sequencing of the two clear bands in clone 2H8 detected the presence of 3 alleles due to a mix of sequences in the lower band which could be individually identified after forward and reverse sequencing (see Figure 2.13). Allele 1 was found to have an insertion of 103 bp replacing 59 bp of the wild type sequence, resulting in complete deletion of exon 4. A potential open reading frame was generated that would produce a truncated 20 residue sequence unrelated to CLOCK. This allele is therefore likely to be non-functional. Allele 2 was found to have a 13 bp deletion generating a frameshift. If expressed this would destroy the exon 4 coding sequence after Serine 11, leading to an out of frame open reading frame that terminates at 108 codons downstream (S11fs108*). Again, this is likely to be a non-functional allele. Allele 3 has a 24 bp in-frame deletion that removes residues between Ser-6 and Arg-17, replacing this with a Tyr codon (S6-Y-R17). While this could produce a functional truncated product, it is possible that indels may also destabilise the gene transcription, mRNA transcript stability or protein stability, leading to loss of expression as is observed in the western blot.

Based on these findings, we conclude that the NIH3T3-CLOCK-2H8 clone is strongly deficient in functional CLOCK expression.

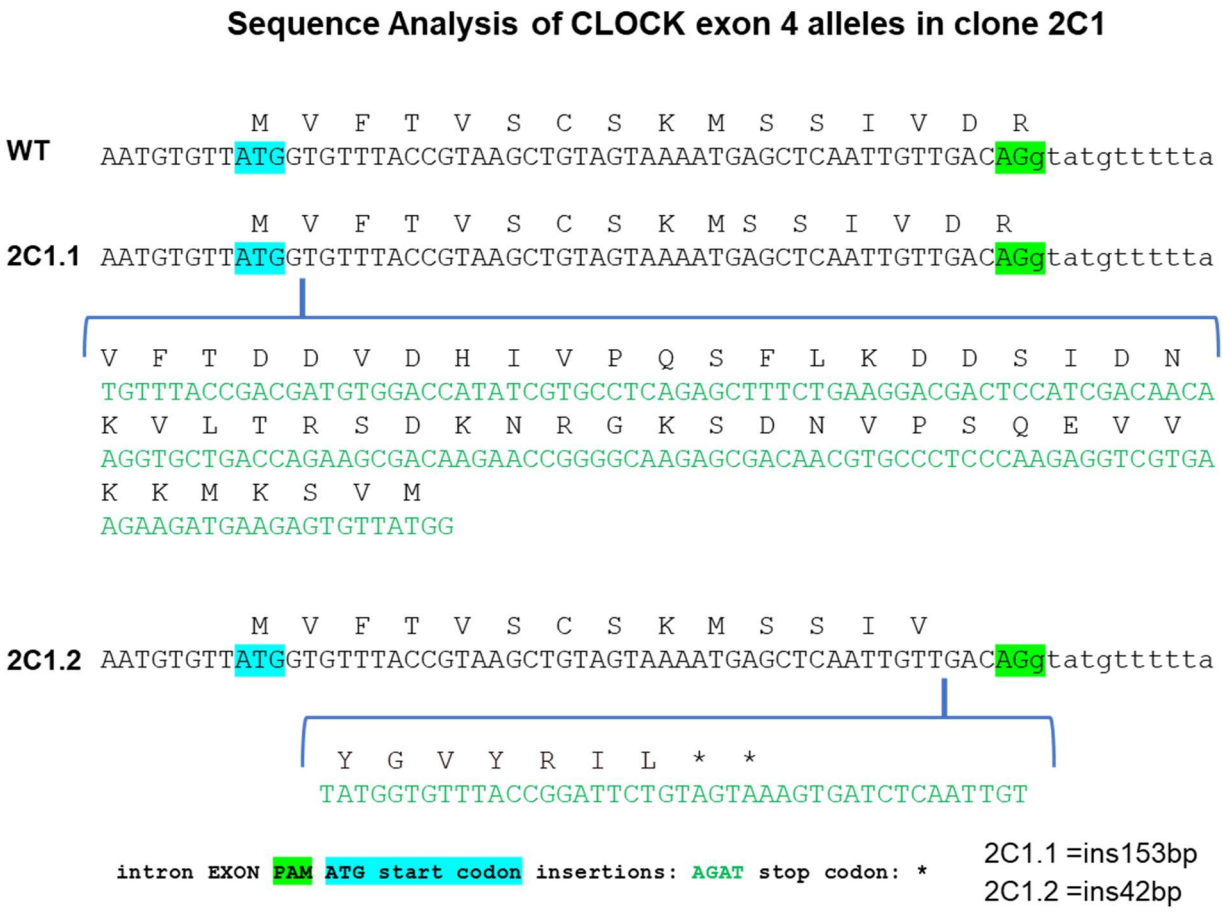

Figure 2.12: Sequencing murine *CLOCK* mutations in NIH3T3 clone 2C1

Sequence analysis of the exon 4 region of two *CLOCK* gene alleles. Allele 1 has a 153 bp in-frame insertion at codon Val-2 whereas Allele 2 has a 42 bp insertion at the codon Val-14 which introduces an in-frame premature stop codon.

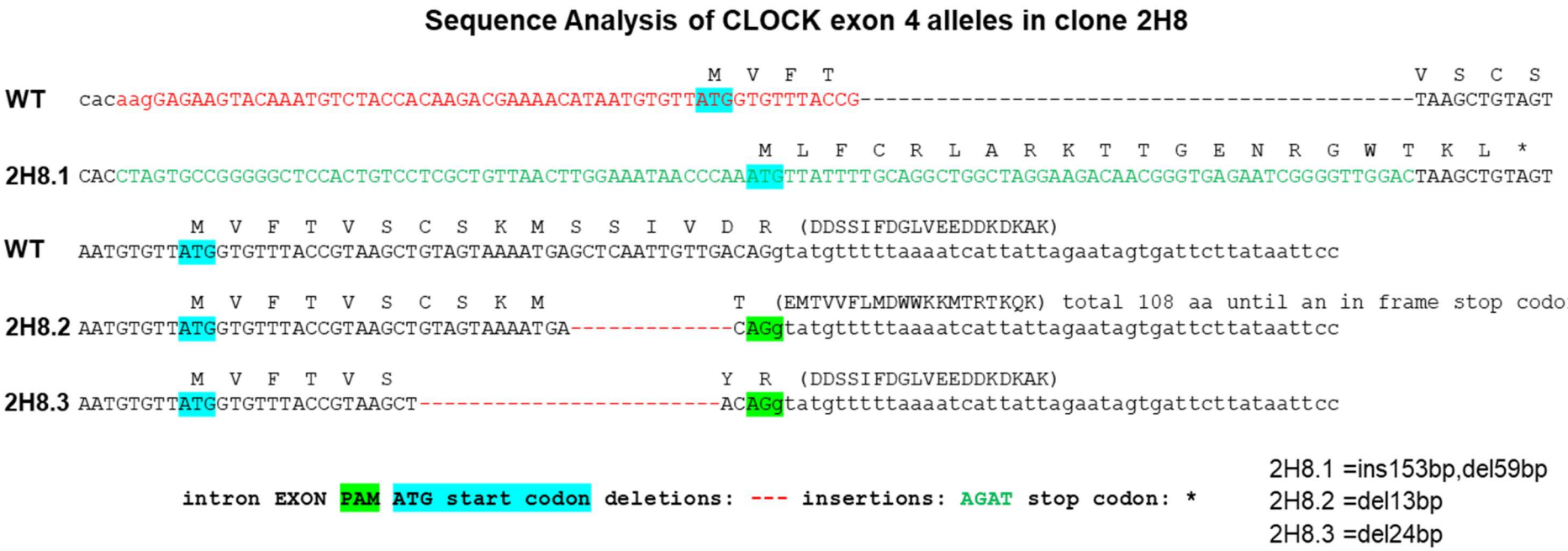

Figure 2.13: Sequencing murine *CLOCK* mutations in NIH3T3 clone 2H8

Sequence analysis of the exon 4 region of three *CLOCK* gene alleles. Allele 1 has a 59 bp deletion and 153 bp insertion that disrupts CLOCK expression due to loss of the start codon. Allele 2 has a 13 bp deletion at codon Ser-11 generating a frameshift and an incorrect 108aa protein product (S11fs108*). Allele 3 has a 24 bp deletion at codon Cys-7 which is an in-frame deletion (S6-Y-R17).

2.3.3 Targeting *CLOCK* gene expression in HEK293 cells

The human *CLOCK* gene is located on chromosome 2 and is made up of 22-24 exons depending on the specific transcript, 20 of which are coding exons, and the major transcript is 10,470 bp (Figure 2.14 A). Multiple splice variant isoforms are listed in the NCBI, Uniprot and Ensembl databases but all coding transcripts share the same start codon, located within exon 4 of the major transcript (Figure 2.14 B). No suitable target sequences for guides were available flanking the ATG in exon 4, therefore guides were designed to target exon 5, which is included in all isoforms, as shown below (Figure 2.14 C).

After transfection with the paired PX461 expression vectors for the specific sgRNAs GFP+ cells were sorted by FACs and single cells clonally expanded for PCR genotyping, as described previously, using the human *CLOCK* primers outlined in appendix section A.5.3 (page 292). The karyotype of the HEK293 cells is considered variable pseudotriploid (Lin et al., 2014) meaning that when targeting events are investigated, multiple alleles may be present. Indels in the *CLOCK* exon 5 region were detected in the expanded clones, with two to three distinct PCR products detected in most clones. No detectable indels were observed in the control clones transfected with a single sgRNA vector (sgF3 and sgG7) (Figure 2.15). 2D6 was specifically identified as potentially containing a wild type allele and a modified allele meaning it is potentially a heterozygous KO which could be a valuable model to have in combination with a homozygous KO.

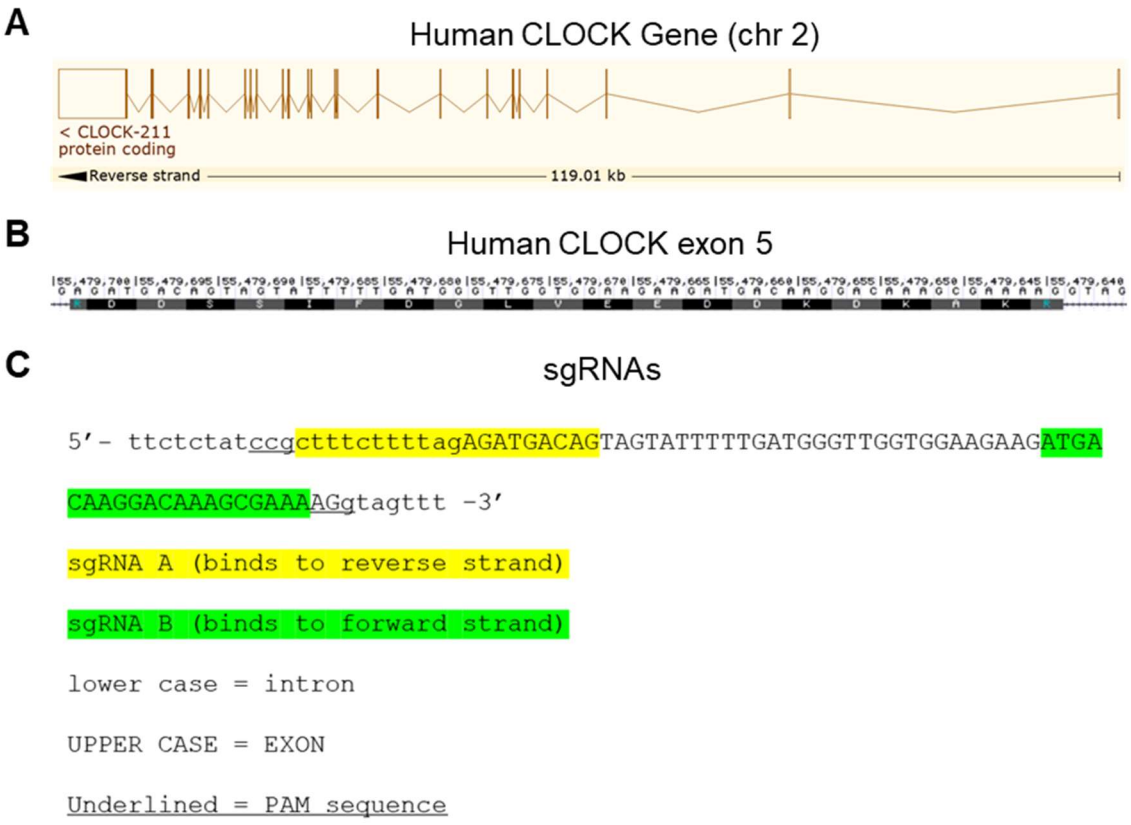

Figure 2.14: Targeting the human *CLOCK* gene

A: Exon structure of the human *CLOCK* gene from the Ensembl database **B:** Sequence of the human *CLOCK* exon 5 from the UCSC genome browser showing the encoded 21 amino acids **C:** sgRNA designs targeting opposite strands flanking exon 5 of *Homo sapiens CLOCK*. Guide pairs were selected targeting the second coding exon in a PAM-out arrangement with a 69 bp spacing.

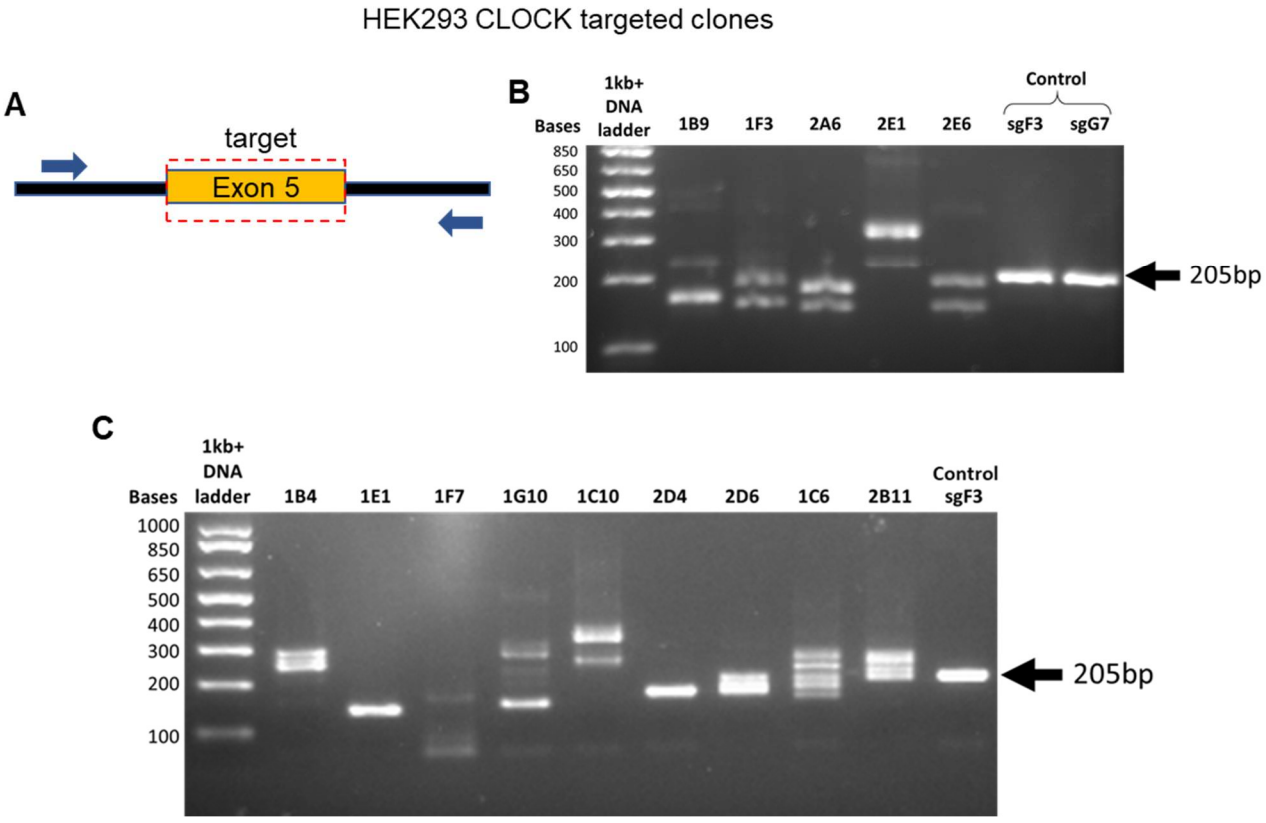

Figure 2.15: Genotyping mutations of human *CLOCK*

A: Schematic showing the targeted region of the human *CLOCK* gene. Blue arrows indicate the approximate positions of PCR analysis primers (F2 and R1, see section A.5.3). **B & C:** PCR genotyping of GFP+ *CLOCK* HEK293 clones. The controls (sgF3 and sgG7) transfected with single guides produced a single product of the expected size (205 bp) for wild type alleles. Several distinct bands are present in some clones indicating targeting of multiple alleles. All clones tested harboured obvious indels. Notably 1C6 presented at least 5 products. This may be due to duplication of one of the primer binding sequences meaning multiple products are produced or the clonal expansion may be a mixture of two differently modified clones.

Initially all clones genotyped on the first gel were taken for further analysis to assess whether the targeted mutations were successful in reducing levels of CLOCK protein expression by western blot using the monoclonal CLOCK antibody detailed in 2.3.2. As shown in Figure 2.16 three bands for CLOCK were identified in all clones. Using the blot of Figure 2.16 A the lower band was calculated to present the expected MW of ~95 kDa and the two higher bands to have MWs of ~122 and ~144 kDa. These larger bands are potentially due to isoforms or posttranslational modifications as noted for murine CLOCK. Clone 2A6 consistently showed the lowest level of CLOCK expression (Figure 2.16 A-C), albeit in one of the blots poor detection of β actin (Figure 2.16 B) suggests suboptimal protein extraction. Reduced CLOCK expression was confirmed for clones 1G10 and 2A6 (Figure 2.16 C).

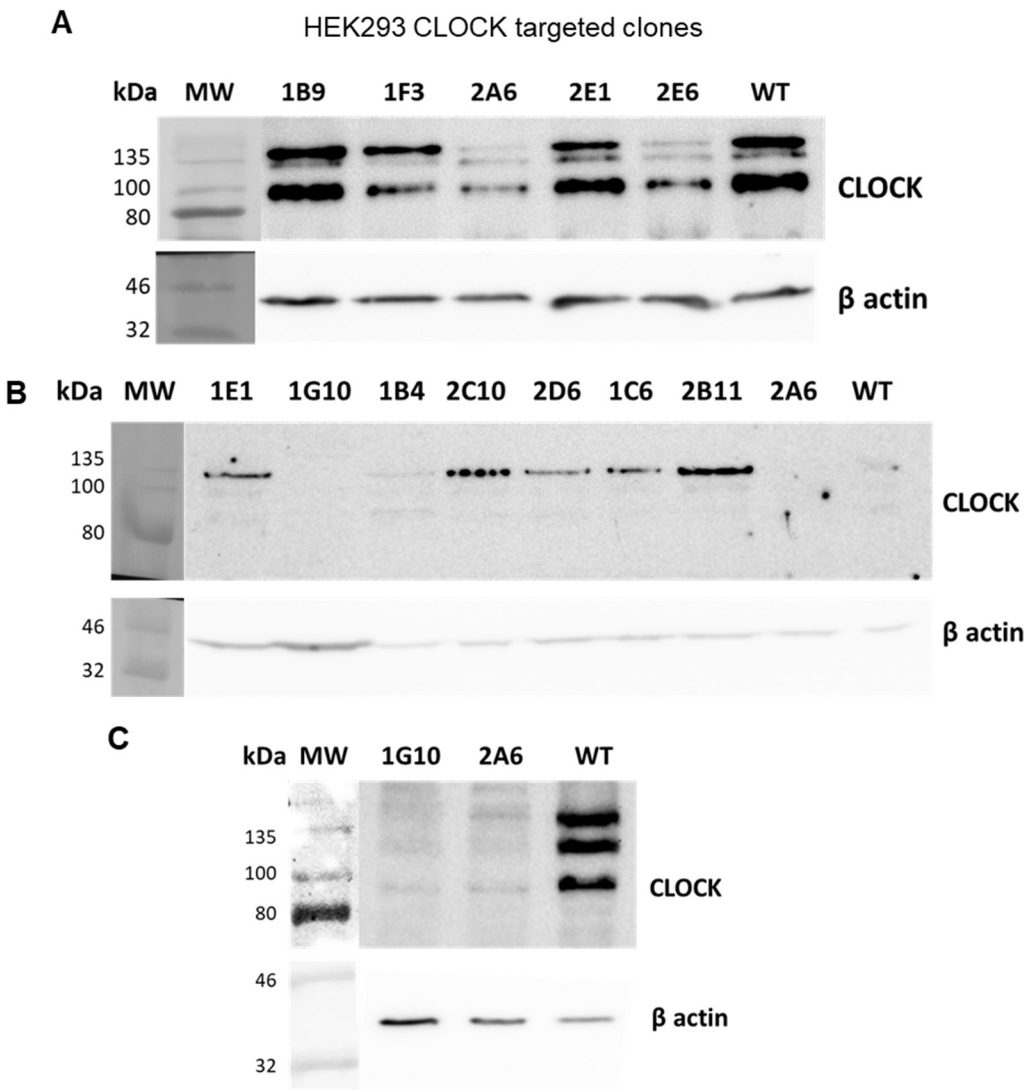

Figure 2.16: CLOCK protein expression in targeted HEK293 clones

Multiple western blots of protein extracts from selected CLOCK targeted HEK293 clones, probed for CLOCK (Santa Cruz, sc-271603, predicted MW 95 kDa batch: I2917, 1:250 dilution, 500 sec exposure) and β actin (Sigma-Aldrich, A2066, batch: 018M4853V, predicted MW 42 kDa, 1:1000 dilution, 60 sec exposure) as a loading control. As above multiple bands are observed for CLOCK **A:** Expression appears most reduced in the 2A6 clone. The other clones were excluded from further analysis. **B:** Expression appears most reduced in the 1G10 and 2A6 clones however these could not be compared to the control lane in which there appears to be an issue with the protein sample. Only the upper band for CLOCK is seen in this blot as well suggesting an issue with the antibody binding. **C:** Western blot of extracted protein for the 1G10 and 2A6 clones. Expression of CLOCK is clearly reduced in both clones compared to the WT control.

To further investigate the nature of targeting events, PCR products from the clones 1G10, 2A6 and 2D6 and an sgControl clone (Figure 2.17 A) were sequenced. Clone 2D6 was included due to the possibility, based on initial PCR genotyping and western blot results, that it may be a heterozygous KO. Sequencing of the sgControl band confirmed only wild type sequence as expected and modified sequences within the target region for alleles from the other clones (Figure 2.17). As was seen for the NPAS2 3T3 clone 1F1 in section 2.3.1 the higher band in both of 1G10 and 2A6 clones when sequenced was a mixture of the two lower bands, so does not represent a unique allele.

Clone 2A6 presented two alleles, one with a deletion of 23 bases and the other with a deletion of 53 bases. 1G10 presented 2 alleles one with a deletion of 7 bases and the other with a deletion of 56 bases. All the deleted sequences from these two clones included splice junctions; loss of these may cause issues in mRNA splicing responsible for the reduced or altered expression. Deletions of the splice junction means it is difficult to predict what amino acid sequence the protein will have and possibly just that exon will be skipped. Neither allele of 2D6 showed wild type sequence meaning it was not of interest as a heterozygous clone, allele 1 had a deletion including the intron-exon junction and allele 2 a deletion at Glu-28 generating a frameshift (E28fs30*). Based on this information we can conclude that the clones HEK293-CLOCK-1G10 and HEK293-CLOCK-2A6 are likely to have major CLOCK inactivation.

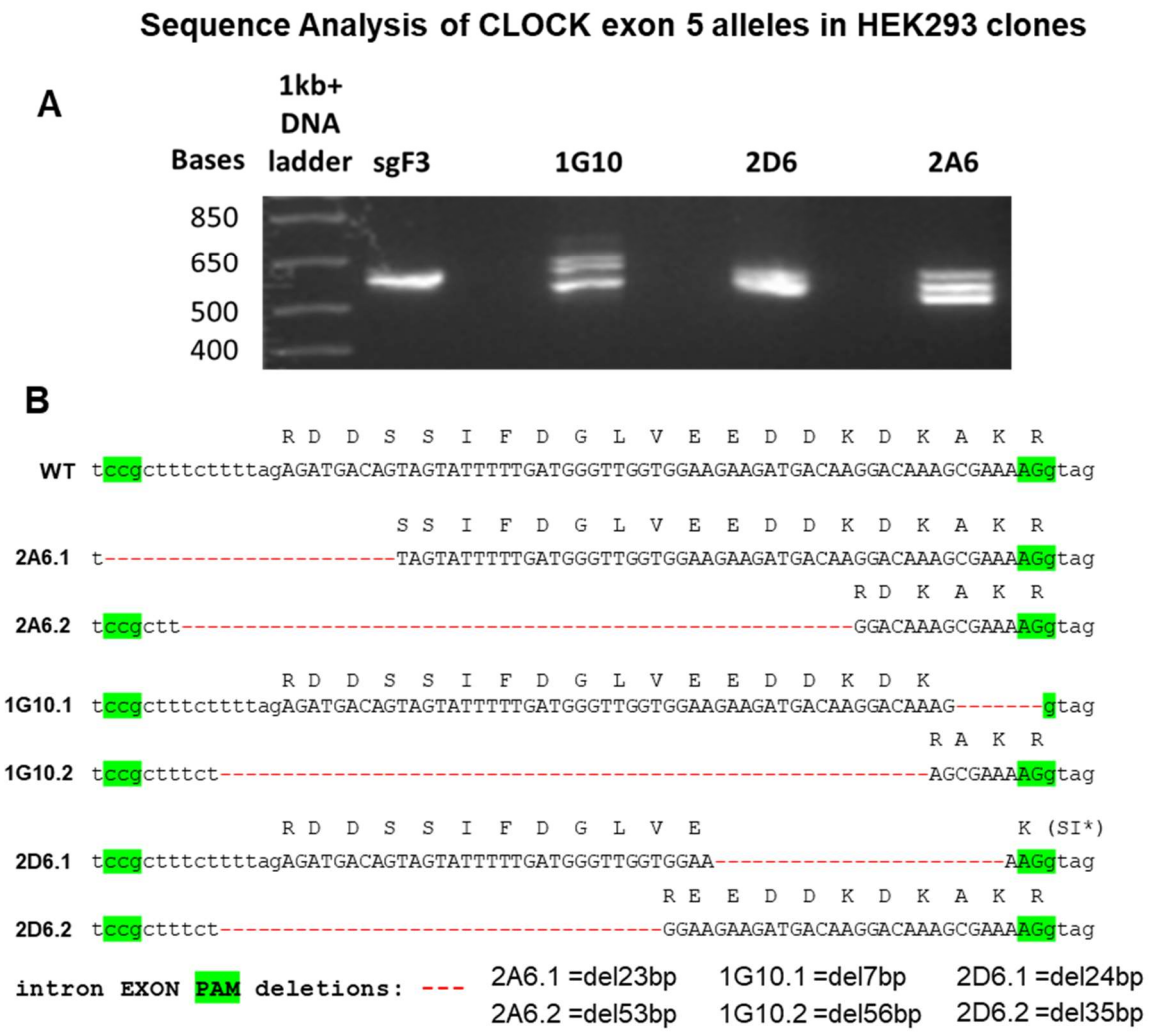

Figure 2.17: Sequencing human *CLOCK* mutations

A: PCR genotyping of HEK293 *CLOCK* targeted clones. The control (sgF3) produced a single product of the expected size (575 bp) for wild type alleles. **B:** Sequence analysis of the exon 5 region of *CLOCK* gene alleles present in HEK293 clones. All alleles sequenced excluding 2D6 1 show splice junction mutations, it is likely that these would cause differential splicing of the transcript as such the amino acid predictions would be inaccurate. The 2D6 1 allele shows a deletion causing a frame shift which will lead to a premature stop codon and likely prevent functional CLOCK expression (E28fs30*). The highest of the three bands on the gel for both 1G10 and 2A6 were found to consist of mixed sequence of the alleles in the lower bands so was not a unique third allele similar to that shown above for NIH3T3-NPAS2-1F1 in Figure 2.6.

2.3.4 Targeting *BMAL1* gene expression in HEK293 cells

The human *BMAL1* gene (also known as *ARNTL*-aryl hydrocarbon receptor nuclear translocator like) is located on chromosome 11 and is made up of 18-21 exons depending on the specific transcript, 16 of which are coding exons, and the major transcript is 2,776 bp (Figure 2.18 A). Multiple protein coding isoforms (at least 27) are listed across the NCBI, Uniprot and Ensembl databases. All identified isoforms utilise the same start codon in exon 5 of the major transcript, however, multiple potential in-frame start codons exist, encoded in the first 20 amino acids (Figure 2.18 B). Guides were therefore designed to target within exon 5 but downstream of these start codons with the intention of introducing a frameshift mutation (Figure 2.18 C). After transfection of HEK293 cells with the paired PX461 expression vectors for the specific sgRNAs GFP+ cells were sorted by FACs and single cells clonally expanded for PCR genotyping, as described previously, using the human *BMAL1* genotyping primers outlined in appendix section A.5.4 (page 293). Indels in the *BMAL1* exon 5 region were detected in the expanded clones, with three distinct products detected in most clones (Figure 2.19). PCR amplification from wild type NIH3T3 cells showed an expected wild type product. Amplification from the single guide transfected clones produced this band and also a shorter product, which may indicate an indel caused by the single guide expression, or possible contamination with DNA from a targeted clone.

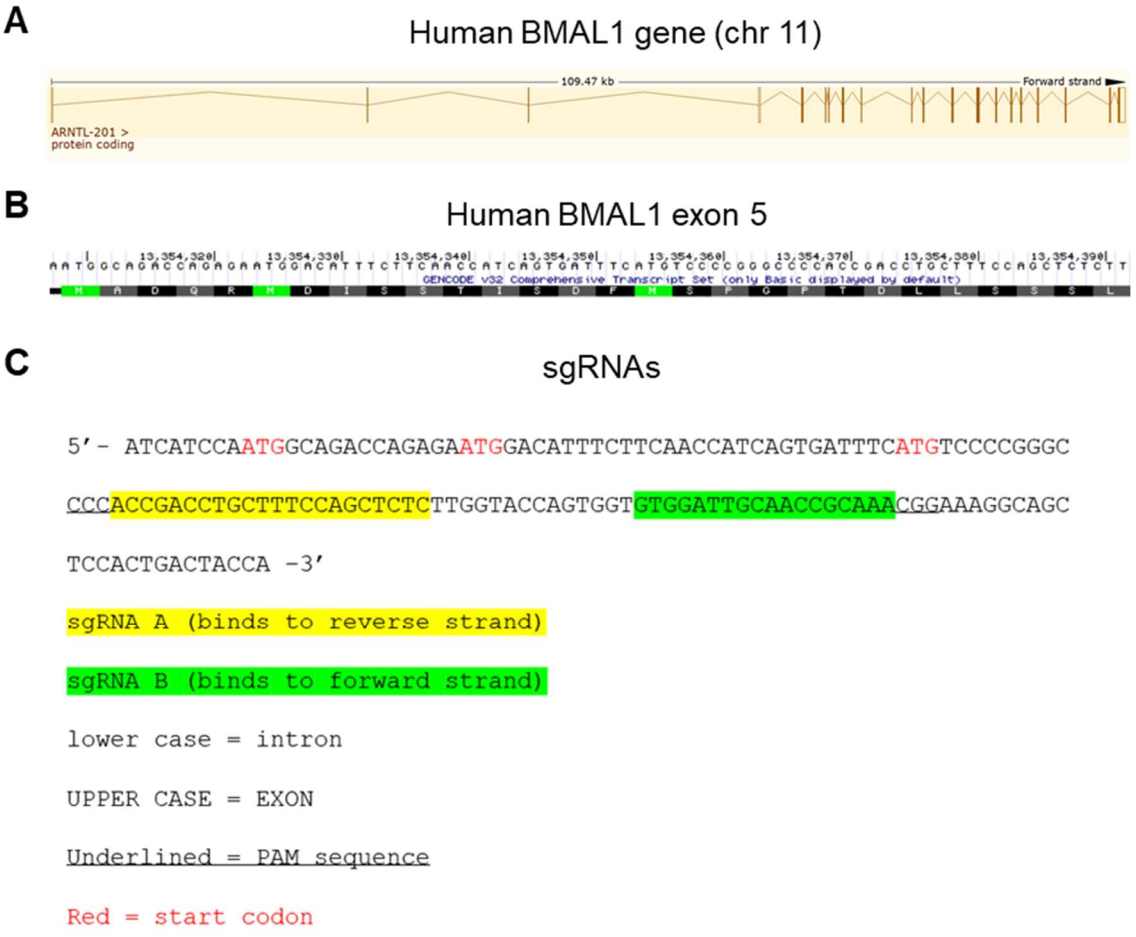

Figure 2.18: Targeting the human *BMAL1* gene

A: Exon structure of the human *BMAL1* gene from the Ensembl database **B:** Sequence of the start of the human *BMAL1* exon 5 from the UCSC genome browser showing the encoded amino acids and multiple in-frame start codons **C:** sgRNA designs targeting opposite strands in exon 5 of *Homo sapiens BMAL1*. Guide pairs were selected downstream of the ATGs in a PAM-out arrangement with a 54 bp spacing.

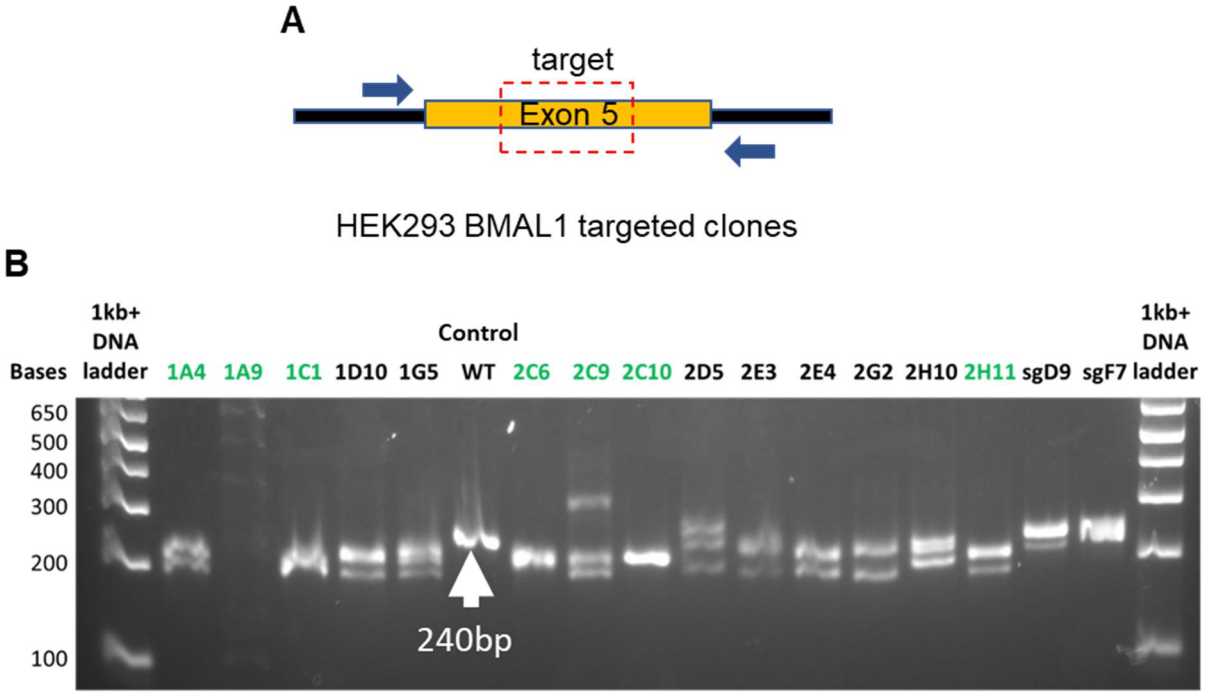

Figure 2.19: Genotyping mutations of human *BMAL1*

A: Schematic showing the targeted region of the human *BMAL1* gene. Blue arrows indicate the approximate positions of PCR analysis primers (F2 and R1, see section A.5.4). **B:** PCR genotyping of GFP+ *BMAL1* HEK293 clones. A WT control shows the expected size (240 bp) for wild type alleles. The clones transfected with single guides (sgD9 and sgF7) produced multiple products including one of the expected size suggesting contamination with one of the modified clones. Several distinct bands are present in most clones indicating targeting of multiple alleles. All clones tested harboured obvious indels. Clones highlighted in green were selected to be carried forwards for initial western blotting.

Several clones were taken for further investigation by western blot based on the absence of a PCR band consistent with the size expected for the wild type product. Cell-free extracts from these clones were used for western blotting to assess whether the targeted mutations were successful in reducing levels of BMAL1 protein expression using a monoclonal BMAL1 antibody (Santa Cruz; sc-365645). A single band of ~69 kDa was detected in HEK293 control extracts, consistent with the predicted MW of the largest isoform (BMAL1b; 68.7 kDa) described in Uniprot. The western blot showed reduced band intensity in multiple targeted clones, with clones 1A9 and 2C9 appearing to show the most significant reduction, however some variation in β actin loading controls suggests this blot is not conclusive (Figure 2.20 A). A second blot including the two low expression clones and other potential clones identified 2C9 and 1A9 remained the clones with the most notable reduction in BMAL1 expression (Figure 2.20 B).

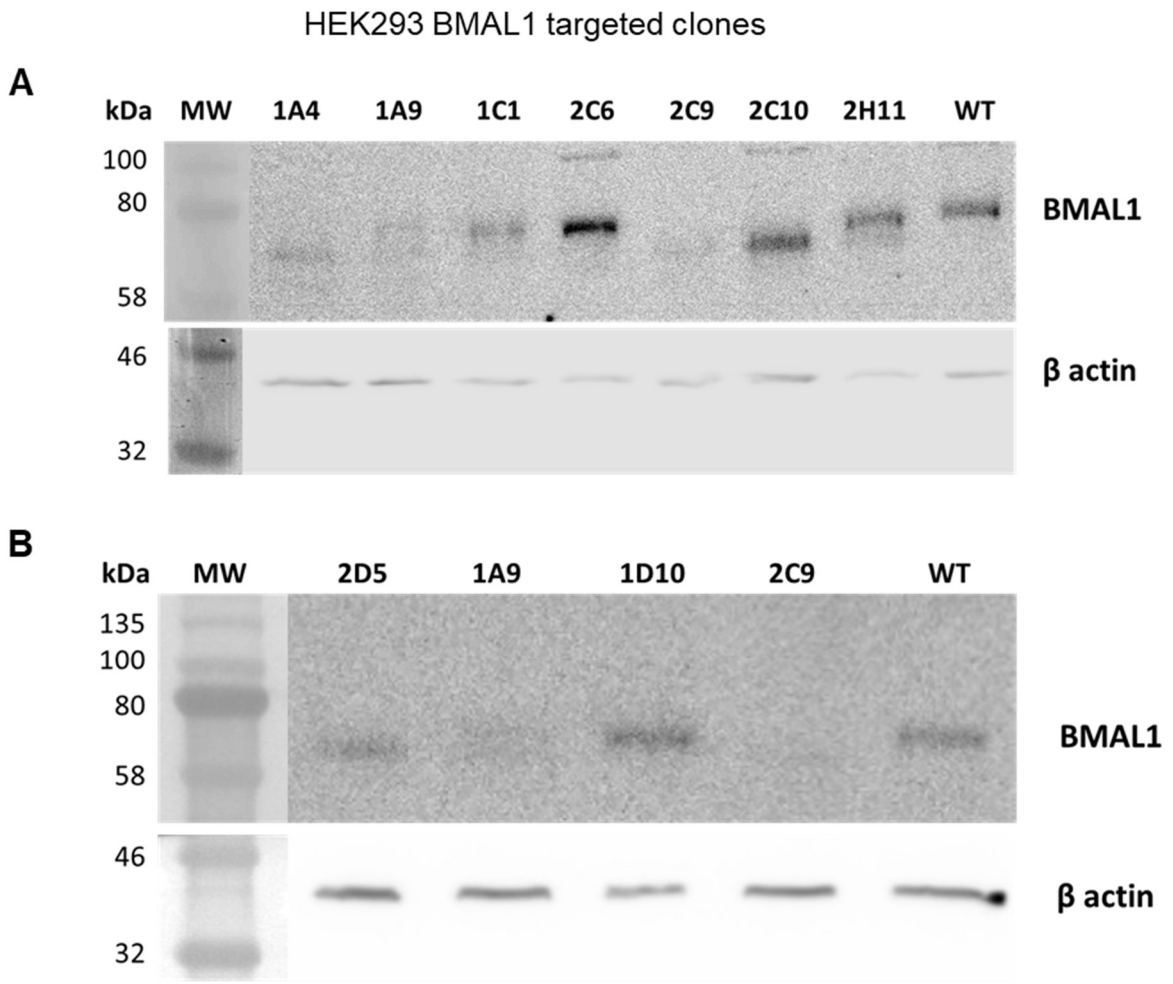

Figure 2.20: BMAL1 protein expression in targeted HEK293 clones

Western blots of protein extracts from selected BMAL1 targeted HEK293 clones, probed for BMAL1 protein (Santa Cruz, sc-365645, batch: B2318, predicted MW 69 kDa, 1:500 dilution, 1000 sec exposure) and β actin (Sigma-Aldrich, A5441, predicted MW 42 kDa, batch: 11SM4835V, 1:1000 dilution, 60 sec exposure) as a loading control. **A:** Expression of BMAL1 can be seen to be reduced compared to the wild type control in the clones 1A4, 1A9, 1C1 and 2C9 while 2C6 shows increased expression. Some of the bands, most noticeably 2C10, appear to show a smaller MW compared to the WT band. This may reflect isoforms or modified protein. The β actin loading control varies a bit across the blot meaning it is hard to be fully confident in interpreting BMAL1 expression levels. **B:** Western blot showing reduced expression of BMAL1 in clones 1A9 and 2C9 as compared to the wild type control.

To further investigate the nature of targeting events in these clones, PCR genotyping was performed, as this first gel was performed concurrently it included all clones from the first western blot. Individual bands were gel-purified (excluding the 1A9 clone for which no products were produced) and then based on the western blot findings the three bands from 2C9 were sent for sequencing. Sequencing of the unmodified cells revealed only the expected wild type sequence detailed in databases while sequencing of the 2C9 clone presented 3 distinct modified alleles (see Figure 2.21). The higher band showed a 38 base insertion introducing 13 amino acids and generating a frame shift which leads to a premature stop codon occurring in exon 6 potentially resulting in a 73 amino acid protein (D22fs73*). The second band showed a 29 base pair deletion and frame shift leading to a premature stop codon after 34 codons (P20fs34*). The third band showed a 46 base pair deletion leading to a frame shift the same as the first allele and reading frame which terminates 45 codons downstream (M16fs44*). These premature stop codons mean that either expression of non-functional protein or nonsense mediated decay of the transcripts would occur and there would be no expression of BMAL1 protein. An attempt was made following this to amplify 1A9 products using alternate primers which was unsuccessful so 2C9 was chosen as the favoured clone. Based on this information we can conclude that the HEK293-BMAL1-2C9 clone is likely to have a major loss of BMAL1 expression.

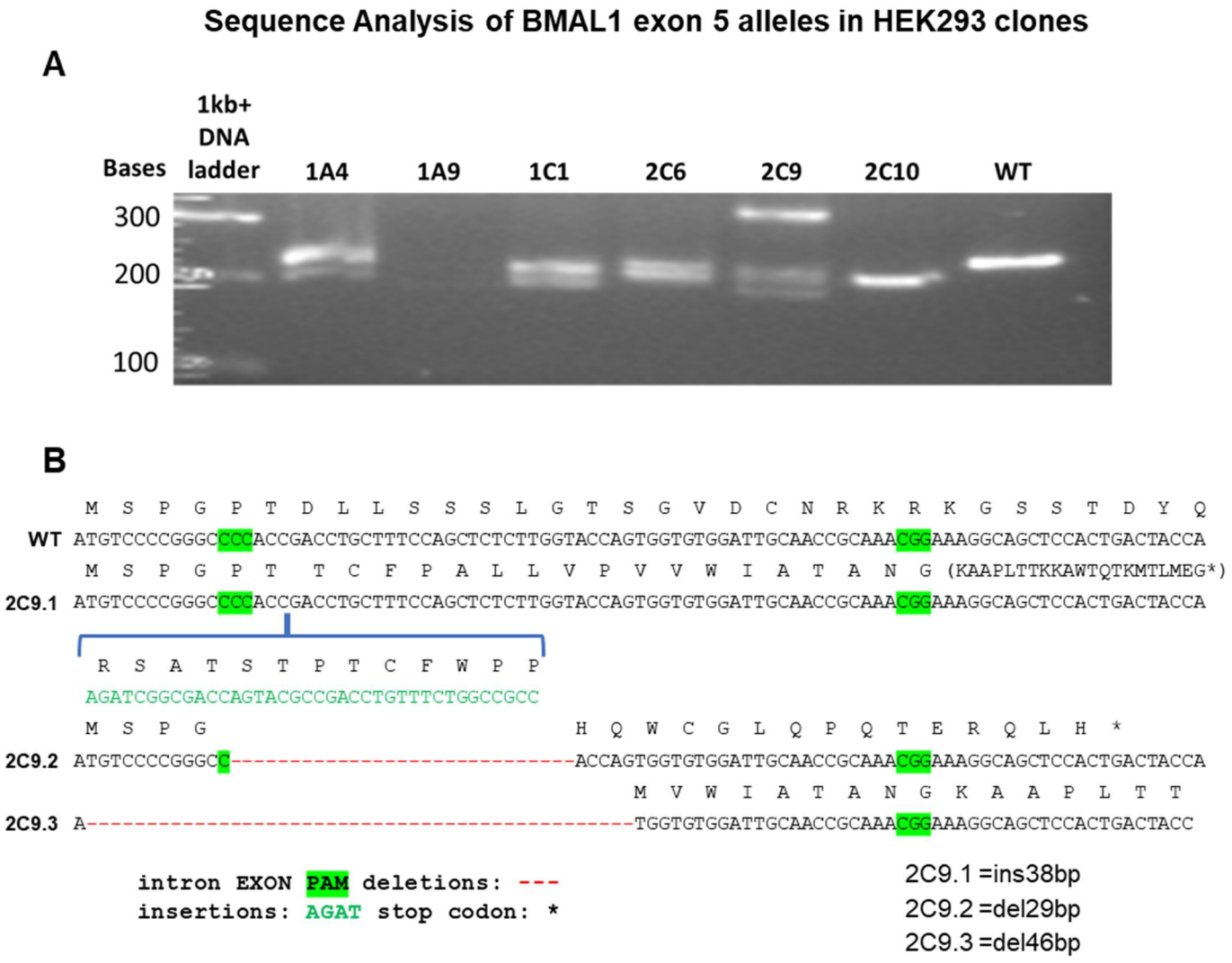

Figure 2.21: Sequencing human *BMAL1* mutations

A: PCR genotyping of HEK293 *BMAL1* targeted clones. The WT control shows a single product of the expected size (240 bp) for wild type alleles. **B:** Sequence analysis of the exon 5 region of *BMAL1* gene alleles present in the 2C9 clone. Allele 1 has a 38 bp insertions immediately after codon Thr-21 generating a frameshift and an incorrect 73aa protein product (D22fs73*). Allele 2 has a 29 bp deletion at codon Pro-20 generating a frameshift and an incorrect 34aa protein product (P20fs34*). Allele 3 has a 46 bp deletion at Met-16 generating the same frameshift as in allele 1 and an incorrect 44aa protein product (M16fs44*).

2.3.5 Targeting *NPAS2* gene expression in HEK293 cells

The human *NPAS2* gene is located on chromosome 2 and is made up of 21 exons, 20 of which are coding exons, and the major transcript is 4,020 bp (Figure 2.22 A). Similar to mouse *NPAS2* gene detailed in 2.3.1 there is only one validated transcript described for human *NPAS2* gene in the NCBI and Uniprot databases encoding an 824 residue polypeptide with the start codon present in exon 2 (NM_002518.4, Figure 2.22 B) while the Ensembl database lists 12 transcripts. These 12 transcripts are the one major transcript from NCBI and Uniprot, 6 non-coding transcripts and 5 transcripts which code for much shorter proteins with under 300 residues. The gnomAD database (Karczewski et al., 2020) indicates the longest isoform as the most abundant human transcript in sequencing studies (Figure 2.22 C). No suitable target sequences for guides were available flanking the ATG in exon 2, therefore guides were designed targeting downstream of the ATG within the same exon (Figure 2.22 D).

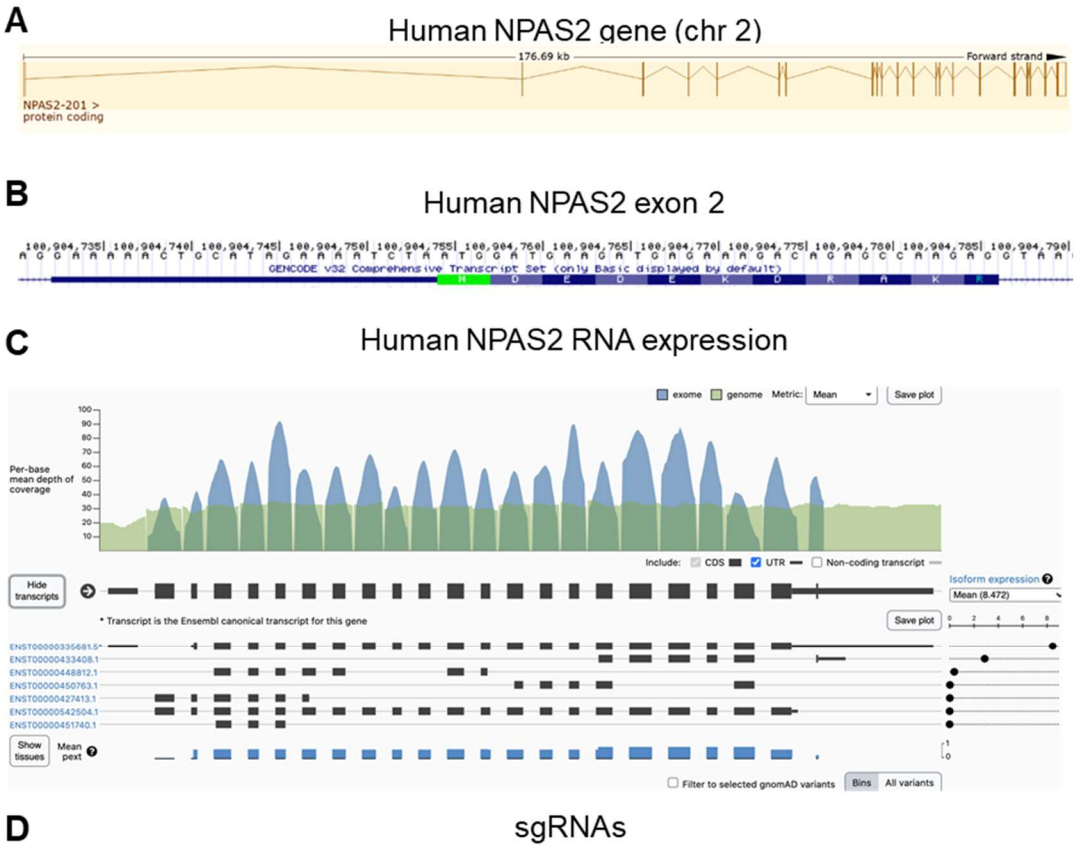

Figure 2.22: Targeting the human *NPAS2* gene

A: Exon structure of the human *NPAS2* gene from the Ensembl database **B:** Sequence of the human *NPAS2* exon 2 from the UCSC genome browser showing the encoded amino acids. **C:** *NPAS2* exon RNA expression depiction from the GnomAD database **D:** sgRNA designs targeting opposite strands in exon 2 of *Homo sapiens NPAS2*. Guide pairs were selected downstream of the ATG in a PAM-out arrangement with a 51 bp spacing.

After transfection with the paired PX461 expression vectors for the specific sgRNAs GFP+ cells were sorted by FACs and single cells clonally expanded for PCR genotyping, as described previously, using the human *NPAS2* primers outlined in appendix section A.5.5 (page 293). Indels in the *NPAS2* exon 2 region were detected in the expanded clones, with two distinct products detected in most clones. No obvious indels were observed in the control clones transfected with a single sgRNA vector (sgD7, sgE2 and sgG3) (Figure 2.23).

Several clones were taken for further investigation based on the absence of a PCR band consistent with the size expected for the wild type product. Western blots to assess whether the targeted mutations were successful in impacting levels of NPAS2 expression were performed. However, these blots used the initial NPAS2 antibody mentioned in 2.3.1 and detailed in the appendix (see section A.3, page 287) which was not specific for NPAS2.

At this stage in the identification process the choice was made to focus on the NIH3T3 targeted clones for inclusion in this PhD project due to the more advanced stage of identification and amenability to cycling experiments.

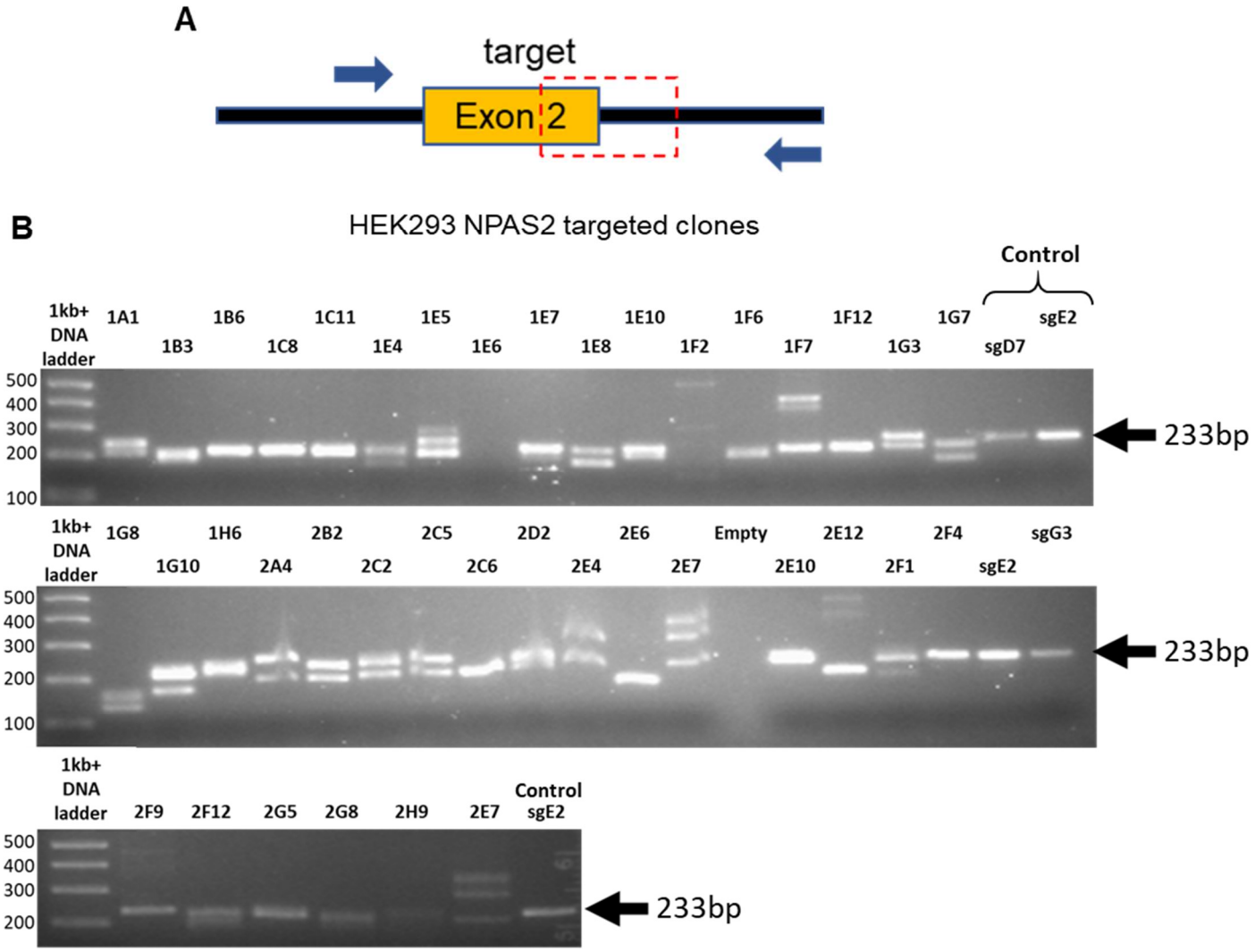

Figure 2.23: Genotyping mutations of human *NPAS2*

A: Schematic showing the targeted region of the human *NPAS2* gene. Blue arrows indicate the approximate positions of PCR analysis primers (F1 and R1, see section A.5.5). **B:** PCR genotyping of GFP+ *NPAS2* HEK293 clones. The controls (sgD7, sgE2 and sgG3) transfected with single guides produced a single product of the expected size (233 bp) for wild type alleles. Several distinct bands are present in some clones indicating targeting of multiple alleles. Multiple clones such as 2F4 showed no modification from wild type sequence.

2.4 Discussion

These results show that we have successfully modified the genetic sequences of circadian regulator genes in cells leading to clearly reduced or ablated protein expression. Mutant clones for mouse *NPAS2*, mouse *CLOCK*, human *BMAL1* and human *CLOCK* have been clearly identified. The NIH3T3-NPAS2-1F1 clone is likely a functional NPAS2 KO and is demonstrably at least a clone with significant reduction of NPAS2 expression. The NIH3T3-CLOCK-2H8 clone is strongly deficient in functional CLOCK expression. The HEK293-CLOCK-1G10 and 2A6 clones should have major CLOCK inactivation. The HEK293-BMAL1-2C9 clone should have major loss of BMAL1 function. Mutants for human NPAS2 have likely been produced but full characterisation was not completed due to time constraints and the decision to focus on the mouse NIH3T3 cells.

These generated cells provide models that can be used for investigation of the role of the modified genes in gene expression and cell biology. Utilising comparable WT cells, changes in mutant cells can be investigated in gene and protein expression and the presentation of in vitro circadian cycles, among other factors which can be investigated in *in vitro* models which may be of interest. Within a similar timeframe of this project targeting genes within the modified cells could be used to produce double knockout models, this may be of interest to produce CLOCK;NPAS2 double KO cells. The modified NIH3T3 clones produced here are used in the following chapter, as models to investigate the impact of loss of the *NPAS2* and *CLOCK* genes on the expression of core circadian genes.

Chapter 3: Investigation of the roles of CLOCK and NPAS2 in expression of core circadian genes using mutant NIH3T3 models

3.1 Introduction

3.1.1 Modelling circadian cycling in cultured cells

Cells in culture maintain circadian oscillations of core clock genes and clock-controlled genes (CCGs). However, the cultured cells are normally asynchronous, meaning gene expression analysis effectively gives an average across the circadian period (Nagoshi et al., 2004). To model circadian gene expression *in vitro* cell cultures can be induced to synchronise, for example by treatments such as a brief serum shock in 50% horse serum which acts to reset the clocks of the cells all at the same time (Balsalobre et al., 1998). After replacement of the high serum media with serum free media cultured cells show a persistent circadian rhythm which gradually flattens over several days due to loss of synchrony within the culture. NIH3T3 cells have in fact been shown to present circadian rhythmicity after simply prolonged culture at confluence when media changes always occurred at fixed times of day, without requiring a serum shock. This effect is likely due in part to the inhibition of cell division in confluent cells, which can modulate circadian rhythms, and some cell-cell communication along with a subtle repeated entrainment effect of media changes (O'Neill and Hastings, 2008).

To facilitate the detection of circadian rhythms a circadian luciferase vector can be introduced into the cells, either by transient or stable transfection methods. The typical reporter utilises a modified luciferase cDNA (dLuc) which encodes a Luciferase destabilised by introduction of a hPEST destabilising sequence so that it is degraded rapidly in cells (Leclerc et al., 2000). This is useful in following circadian expression as long-term stability of the luciferase protein would interfere with observation of the circadian expression pattern. This luciferase system can be used to follow circadian cycling when expressed under the promotor of a circadian regulated gene (commonly *PER2* or *BMAL1*) meaning luciferase expression is subject to circadian regulation. This can allow identification of the circadian period by collection of protein for luciferase assays at time points after synchronisation or detailed period

identification by real-time bioluminescence recordings of live cultures (Fang et al., 2017).

3.1.2 NPAS2 in the circadian transcriptional feedback cycle

NPAS2 is a core circadian gene and functions as part of the positive arm of the transcriptional feedback cycle. The NPAS2 protein acts as a transcription factor when dimerised with the BMAL1 protein by binding to genomic E-boxes, both the BMAL1 and DNA association are dependent on the NPAS2 bHLH domain (Hogenesch et al., 1998). CLOCK is a paralog of NPAS2 and an alternate dimerisation partner for BMAL1 (Gekakis et al., 1998). Circadian cycles are primarily maintained by the transcription of genes of the negative arm of the feedback loop through the positive arm activity at E-boxes. This includes the CRY and PER proteins which act to prevent the transcription factor activity of the CLOCK/NPAS2:BMAL1 dimer. Also involved in circadian maintenance are the *REV-ERB* and *ROR* genes, also under E-box promotors, which have opposing activity influencing the transcription of *NPAS2* and *BMAL1* (Shearman et al., 2000), for more details refer to section 1.3 (page 26). The activity of both CLOCK and NPAS2 has been shown to be influenced by interactions with CO (Dioum et al., 2002) and NAD+/NADH (Rutter et al., 2001).

While it has been proposed that NPAS2 and CLOCK have overlapping roles in gene expression in the SCN and are therefore at least partially redundant (Bertolucci et al., 2008), other studies using ChIP-seq of mouse liver samples have identified unique binding sites of CLOCK:BMAL1 and NPAS2:BMAL1 presented in Figure 3.1 (Koike et al., 2012). Most of the core circadian genes are identified as targets of both CLOCK and NPAS2 dimers, as would be expected, with the exception of a few genes (see Figure 3.1 legend for specific genes). However, the observation of subsets of genes that are specific targets for CLOCK:BMAL1 or NPAS2:BMAL1 heterodimers indicates differential recruitment to some gene regulatory regions. It remains unclear if this involves differences in DNA binding specificities or the involvement of additional cofactors.

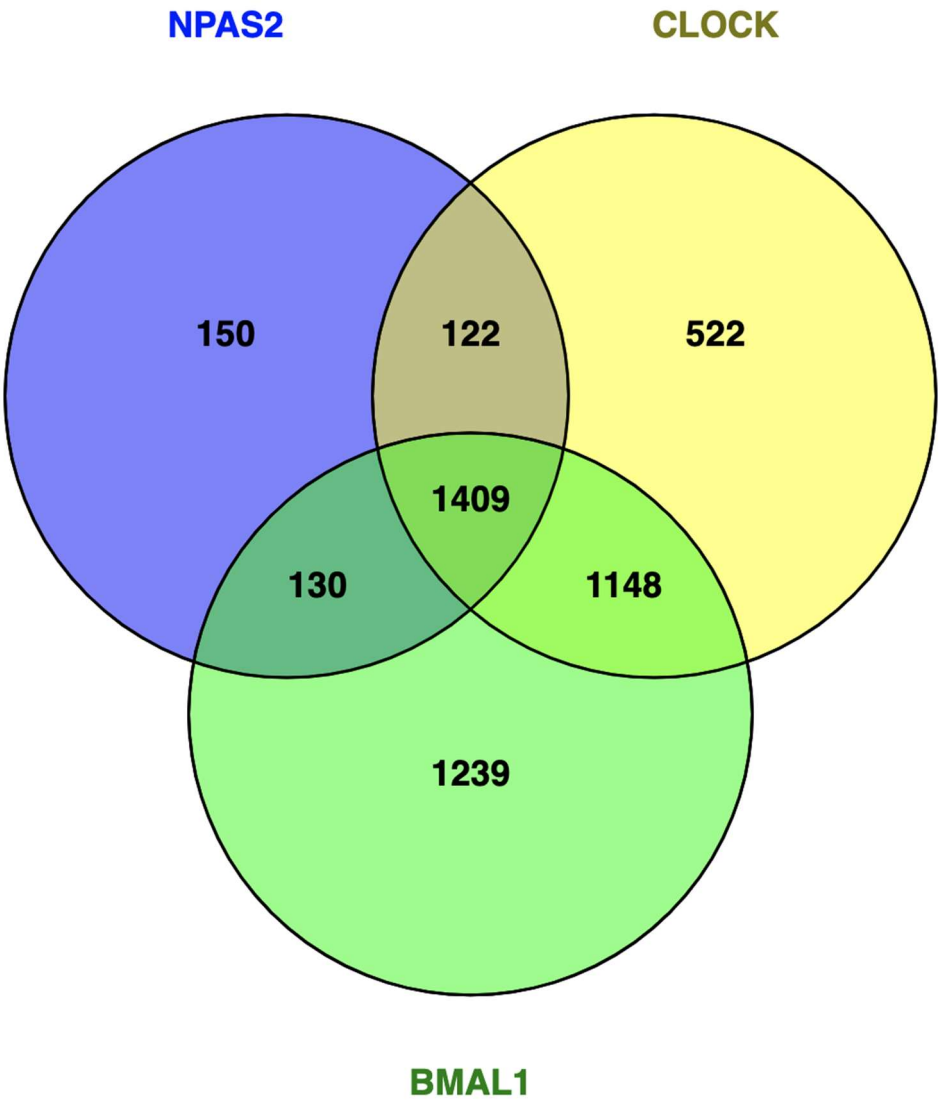

Figure 3.1: Unique and overlapping target genes of BMAL1, CLOCK and NPAS2

Based on ChIP-seq data from Koike et al. (2012), image generated using Venny software (Oliveros, 2007). The majority of genes fall in the overlaps of CLOCK and BMAL1 with the circadian genes *PER1*, *PER2*, *CRY2* and *REV-ERBα* all identified as target genes of all three. Notably *CRY1* and *REV-ERBβ* were only identified as targets of CLOCK and BMAL1 and *PER3* was identified as a target of BMAL1 only. The full gene lists as sorted in the diagram are included in the appendix (section A.7, page 305). Not all binding sites necessarily suggest transcription factor activity at these sites however in genes targeted by both BMAL1 and either NPAS2 or CLOCK there is an increased likelihood.

Another functional difference between CLOCK and NPAS2 has been reported in the subtle differences of circadian gene expression profiles in the SCN of NPAS2 and CLOCK KO mice. For example, the CLOCK KO was associated with a subtle phase shift but no change in expression levels of *PER2* and a reduction in the amplitude of *REV-ERBα* expression while NPAS2 KO mice presented a reduction of *PER2* cycling expression but no change in *REV-ERBα* expression pattern in the SCN (Debruyne et al., 2006, DeBruyne et al., 2007a). CLOCK also has intrinsic HAT activity, described in section 1.4 (page 29), which plays a role in regulation of gene expression and activity (Doi et al., 2006). In contrast NPAS2 has not been shown to perform any acetyltransferase activity and investigation of the amino acid sequence suggests NPAS2 lacks this HAT domain (see Figure 1.2, page 38) so is unable to perform these same activities without HAT recruitment.

These observed differences between CLOCK and NPAS2 make it likely these genes have both overlapping and distinct functions, even in how they influence the core circadian feedback loop.

3.1.3 Previous investigations of CLOCK and NPAS2 function in fibroblasts

CLOCK and NPAS2 functions in gene expression have been investigated previously in various cell culture models, including fibroblast cells. For example Ramanathan et al. (2014) reported the effects of lentiviral shRNA knockdown of core circadian genes on cycling of a BMAL1-dLuc reporter in NIH3T3, a mouse fibroblast cell line. While suppression of CLOCK or BMAL1 lead to rapid arrhythmicity, knockdown of NPAS2 expression was reported to have no detectable effect on the circadian cycling period of the reporter in NIH3T3 cells nor in the adipocyte or hepatocyte cell lines tested. A caveat of this study is that the endogenous levels of NPAS2 protein were not determined; the efficacy of the shRNAs were identified by co-transfection of FLAG-tagged NPAS2 expression vectors with the shRNA or control shRNA. This means that the reduction of protein expression presented only reflects the reduction of the

introduced FLAG-tagged NPAS2 which may not reflect endogenous levels in the control. The mRNA level of *NPAS2* determined by RT-qPCR was only reduced to ~50% of the endogenous expression while the mRNA levels of CLOCK were reduced to ~40% or <10% in the two different shRNA models (Ramanathan et al., 2014) The reported effects were limited to the effect on the BMAL1-dLuc reporter and no investigation was performed on either the cycling or expression levels of the circadian genes.

Primary dermal fibroblast cultures from NPAS2 constitutive KO mice showed an increase in expression of *PER2*. No change was observed in the expression of *BMAL1*, *CLOCK*, *PER1*, *PER3* or *CRY1-2* or in the circadian expression patterns and periods (Sasaki et al., 2020).

3.1.4 Experimental aims and hypothesis

The aim of this chapter was to investigate the effect of modification of the expression of NPAS2 and CLOCK on expression of core circadian genes in a cell culture model. As described in Chapter 2, mutant NIH3T3 CRISPR-Cas9 modified clones NIH3T3-NPAS2-1F1 (ΔNPAS2) and NIH3T3-CLOCK-2H8 (ΔCLOCK) were developed for investigation of NPAS2 and CLOCK (2.3.1 & 2.3.2). The choice was made to focus on the NIH3T3 clones rather than the HEK293 clones as they are an easier experimental model to investigate circadian cycling due to the comparative ease of culturing the cells at confluence. While NIH3T3 cells can be cultured at confluence, due to contact inhibition preventing further growth, in HEK293 cultures cell death occurs due to continued growth when cultured past confluency. While circadian cycling has still been shown to be induced in these cells more care needs to be taken and results can be affected by the increasing cell death at later time points (Cox, 2012).

The expression of genes of the core circadian feedback loop were investigated in selected cells by RT-qPCR while in normal culture to investigate effects of the genetic modifications on the overall expression levels of the genes. As this measure cannot observe any effect on rhythmic expression of the genes a serum shock was also utilised to synchronise

the circadian cycles of the cells. The rhythmic expression of the genes and the influence of the modification of gene expression could then be investigated.

It was hypothesised that we would see changes in gene expression either in the total levels consistent across each time point or in a time point specific manner. As both NPAS2 and CLOCK act with circadian rhythmicity it was assumed most likely that primarily time point specific effects would be observed. However, the investigation of asynchronous cells would provide some insight into effects on gene expression levels through a much faster and easier initial experiment. It was expected that we would not see effects such as a change in circadian period or any gross change in circadian cycle as in each cell type the other gene of *CLOCK*/*NPAS2* would be present to compensate. Any change in circadian period was anticipated to be too subtle to be observed in the 6-hour window of these investigations.

3.2 Materials & Methods

Chemicals, reagents, and methodologies were as described in Chapter 2, with the following additional details.

3.2.1 Mammalian cell culture

3.2.1.1 Culture and transfection

NIH3T3 mutant clonal cells and the wild type (WT) NIH3T3 cells were cultured as described in section 2.2.5.2 (page 62). The ΔNPAS2 1F1 clones were identified to grow slower than the other cells so were passaged at 1:5 for general culture rather than the 1:10 used for the other cultured cells.

3.2.1.2 Light microscopy

Cell images were taken 1, 2 or 3 days after seeding $3x10^5$ cells in 10 cm dishes (or $6x10^5$ cells for the ΔNPAS2 cells). The images were taken using a Celestron HD digital microscope imager attachment for a light microscope and Celestron Digital Imager HD software.

3.2.1.3 Cell culture for RNA extraction (unsynchronised cells)

Cells were seeded in triplicate at $3x10^5$ cells in 10 cm dishes (or $6x10^5$ cells for the ΔNPAS2 cells) and grown for 3 days before RNA extraction. At the time of collection, the cells were collected into 1.5 ml cold PBS and 400 µl was taken, the cells spun down at 600 x g for 5 minutes at 4 °C and the pellet taken for RNA extraction as described in section 3.2.2.2.

3.2.1.4 Serum shock induction of circadian cycling

To investigate circadian gene expression, cells were seeded at $2x10^4$ (or $4x10^4$ for the ΔNPAS2 cells) in triplicate in 5 x 12-well plates. The cells were cultured to full confluence (2 weeks) in the plate, media changes were performed as required at a fixed time of day. The cells were then exposed to a serum shock; the media was removed, and the cells gently washed with 0.5 ml warm PBS and the media replaced with 1 ml DMEM made up as 50% horse serum. The

cells were incubated for 2 hours at 37 °C before the serum was removed, the cells were washed with 0.5 ml of serum free media, 2 ml serum free media added and incubated at 37 °C. The cells were collected for RNA extraction by collection into the lysis buffer from the RNeasy kit after a wash with cold PBS at specific time points of 0, 6, 12, 18 and 24 hours after the end of the serum shock. Note that due to COVID-19 SOPs, it was not possible to extend the experiment beyond the 24-hour period. Samples in lysis buffer were stored at -80 °C until the RNA extraction was performed. This serum shock induction of cycling method was primarily based on the protocol used by Allen et al. (2004).

3.2.2 Molecular biology techniques

3.2.2.1 Sources and composition of reagents

Primers for RT-qPCR were purchased from Sigma-Aldrich as lyophilised and desalted pellets. These were resuspended in sterile water to a 100 µM concentration and stored at -20 °C. Primers sequences were those previously designed (Oyegbami et al., 2017) or newly designed by use of the NCBI Primer BLAST software. The primers were designed to amplify across an exon-exon boundary preventing amplification of any genomic DNA. Primers are all between 17 and 26 bases in length and amplify products between 60 and 150 bases with Tm values between 60 °C and 70 °C. All primer sequences are detailed in Table A.1 (page 296). The primers were validated through cDNA dilution series and agarose gel electrophoresis to confirm the expected size of products and no alternate products, these are detailed in the appendix, section A.4 (page 288).

The RNA extraction RNeasy Mini kit and the QuantiTect Reverse Transcription kit were purchased from QIAGEN Ltd. The Brilliant II SYBR® Green QPCR Master Mix was purchased from Agilent Technologies.

3.2.2.2 RNA extraction

Total RNA was extracted from pelleted cultured cells using the QIAGEN RNeasy Mini

kit, ready for cDNA synthesis. Isolation of RNA was performed according to the manufacturer's protocol and the RNA eluted from the column in 2 spins of 30 µl RNase free water for a total 60 µl volume and stored at -80 °C until required. The concentration of RNA was determined using a NanoDrop 1000 Spectrophotometer.

3.2.2.3 Reverse transcription and cDNA to synthesis

To produce cDNA from the RNA for RT-qPCR analysis the QuantiTect Reverse Transcription kit (QIAGEN Ltd) was used. To prepare extracted RNA for use as a template to synthesise cDNA, potential contaminating genomic DNA was removed following the manufacturer's instructions. Samples were set up as shown in Table 2.3, mixed and incubated for 2 minutes at 42 °C, followed by immediate chilling on ice.

Table 3.1: Composition of genomic DNA wipeout reactions

7x gDNA Wipeout buffer	1 µl (1x)
Template RNA	500 ng
Sterile RNase-free water	To a total volume of 7 µl

To synthesise cDNA, reverse transcription reactions were prepared using the produced genomic DNA-free RNA samples for a final volume of 10 µl, as shown in Table 3.2. These were incubated for 15 minutes at 42 °C, then for 3 mins at 95 °C to inactivate the Quantiscript Reverse Transcriptase enzyme. 15 µl of sterile dH_2O was added to products of this reaction (1:2.5 dilution), thoroughly mixed and samples were stored at -20 °C until required. If more cDNA was required, for example when testing primers for standard curves, the reactions were scaled up appropriately.

Table 3.2: Composition of reverse transcription reactions

Quantiscript Reverse Transcriptase	0.5 µl
5x Quantiscript RT buffer	2 µl (1x)
RT Primer mix	0.5 µl
Genomic DNA wipeout reaction	7 µl
Total volume	10 µl

3.2.2.4 Quantitative reverse transcription PCR (RT-qPCR)

To analyse gene expression RT-qPCR was performed using the cDNA generated by reverse transcription and Brilliant II SYBR® Green QPCR Master Mix from Agilent Technologies. The reaction mixture is detailed in Table 3.3 and the cycling protocol in Table 3.4. All samples and reagents were kept on ice while the RT-qPCR reactions were prepared. The reactions were run on a Stratagene Mx3005P qPCR machine, programmed and data collected through the MXPRO software. In each plate for each gene ran, a no template control (NTC) was also included, with a reaction mix lacking cDNA but otherwise identical to that shown in Table 3.3, to check for contamination of the mastermix. The dissociation curves and amplification plots of each reaction were viewed in the MXPRO software to confirm no abnormal behaviour of the qPCR, such as multiple products. The software calculated an appropriate critical threshold for each run and quantified the cycle number at which the intensity of the fluorescence reached the critical threshold (Ct value). RT-qPCR analysis was performed in technical duplicates upon each of the biological triplicates, so a total of 6 readings were obtained for each data point. *18S* rRNA (*Rn18s*) expression was used as a normalisation gene as various other genes which can be used in this capacity, such as *GAPDH*, have been identified to show circadian variation which would influence the calculated results (Matsumura et al., 2014).

Table 3.3: Composition of RT-qPCR reactions

Sterile dH_2O	2 µl
10 µM Forward primer	0.5 µl
10 µM Reverse primer	0.5 µl
Brilliant II SYBR® Green QPCR Master Mix	5 µl
cDNA	2 µl
Total volume	10 µl

Table 3.4: Quantitative thermocycler setting for RT-qPCR experiments

No. Cycles	Time	Temperature
x 1	10 mins (initial denaturation)	95 °C
x 40	30 secs (denaturation)	95 °C
	1 min (primer annealing and extension)	60 °C
x 1	melt curve analysis	60-95 °C

Initially the qPCR testing for expression of *18S* rRNA was performed on a 1:40 diluted sample of the RT produced cDNA, the low dilution was used as 1*8S* rRNA is expressed at a high level so easily detected and saves on use of the cDNA. This read was used to calculate the amount to dilute the cDNA, to ensure all samples were appropriately comparable and that dilution of the samples to provide the volume required to investigate all genes would not dilute those genes below the limit of the detection. The diluted cDNA samples were then used for qPCR testing of *18S* rRNA for use as a normalisation gene and all genes of interest.

3.2.2.5 RT-qPCR analysis

Each sample was run in duplicate for each qPCR transcript analysis. The paired Ct values were confirmed to not vary more than 1.5 Ct, any instance where a greater difference was seen the qPCR was repeated. Data for each transcript were normalised to *18S* rRNA as an internal control using the $2^{-\Delta Ct}$ method. The respective average *18S* rRNA Ct values were taken

away from the transcript of interest Ct values and then converted to copy number as in Formula 3.1. The copy numbers were then divided by the average copy number of the control samples (the expression of the gene in WT cells or the WT cells at 0 hours in the synchronised time point experiment) to give the relative change in expression and the mean of the technical duplicates used for statistical analysis.

$$Normalised\ RNA\ expression\ level\ = 2^{-\Delta Ct}$$

Formula 3.1: Calculation used to analyse the relative gene expression of RT-qPCR targets. This formula can be explained as: 2 to the power of the negative value of (Ct of gene of interest - Ct of *18S* rRNA normalisation gene).

3.2.3 Statistical analysis

Tests were performed in biological triplicate based on previous procedures used in the lab for investigation of gene expression as 3 replicates is generally accepted as sufficient to identify biologically relevant changes in gene expression. Statistical tests were performed by use of IBM SPSS Statistics for Windows, Version 26.0. Normality was confirmed by visualisation on a graph. The significance level was set at 0.05. Gene expression in the modified clones was compared individually to expression in the WT cells. Independent t-tests were used for comparison of the unsynchronised gene expression between cell types and two-way ANOVAs were used to investigate the effect of time and genotype on rhythmic gene expression. Significant interactions identified by ANOVA were followed up by pairwise analysis of simple main effects between the cell types at individual time points.

3.3 Results

3.3.1 Growth and morphology of CRISPR-Cas9 edited NIH3T3 cells

Chapter 2 described the generation of CRISPR-Cas9 edited clones defective in expression of CLOCK and NPAS2. Due to their greater survival in synchronising procedures compared to HEK293 cells, we chose to take forward NIH3T3 modified clones for further analysis to assess the impact of NPAS2 or CLOCK deficiency on circadian gene regulation. Therefore, unmodified WT NIH3T3 cells, ΔNPAS2 1F1 and ΔCLOCK 2H8 cells were selected and maintained in culture. We noticed while passaging the three cell types that the ΔNPAS2 1F1 cells took longer to reach confluency, as compared to the WT NIH3T3 or ΔCLOCK 2H8 cells under normal culture conditions. To adjust for this, when passaging cells, the ΔNPAS2 cells were passaged to 1:5 rather than 1:10 and for each seeding of a specific cell count double the cell number was used as described in the methods sections. Assessment of the three cell types in culture by light microscopy did not reveal any gross phenotypic effects on morphology over 3 days of culture (Figure 3.2). It was noted that ΔCLOCK 2H8 cells took longer to recover after passage, perhaps due to delayed adherence, but all three cell cultures reached comparable confluency on day 3.

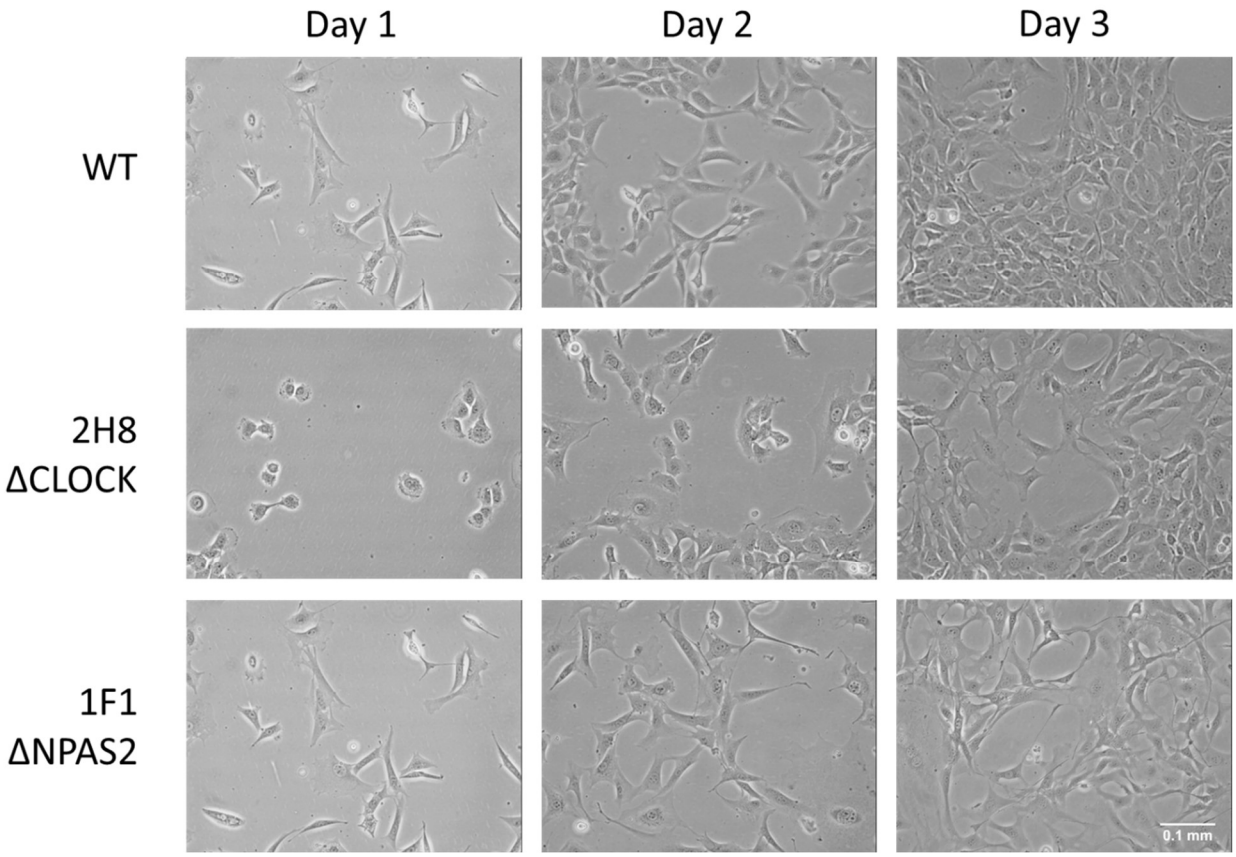

Figure 3.2: Cell growth images

Representative images of the cells on sequential growth days; note the ΔNPAS2 1F1 cells were seeded at a higher density (2x) to account for slower recovery. All cultures showed similar confluency and appearance on day 3, despite the appearance of the ΔCLOCK 2H8 cells on day one suggesting that they showed slower recovery from the passage procedure, in that the cells had not yet begun to extend filopodia as the other two cells had.

3.3.2 Expression of core circadian genes in unsynchronised edited NIH3T3 cells

To investigate the effect of the modified expression of NPAS2 and CLOCK on circadian regulation in NIH3T3 cells, mRNA expression levels of several core circadian genes were determined (Figure 3.3). As most circadian genes show rhythmic expression over a 24-hour period, expression levels detected in asynchronous cultures reflect the average gene expression across the cycling period.

Expression levels of *PER1*, *PER2*, *CRY1*, *CRY2*, *CLOCK*, *BMAL1*, *REV-ERBα* and *REV-ERBβ* genes in the ΔCLOCK and ΔNPAS2 cells were compared individually to their expression levels in WT cells. The ΔNPAS2 cells showed significantly increased expression levels of *REV-ERBα* and *CLOCK* and reduced expression of *BMAL1* compared to WT cells (Table 3.5 and Figure 3.3). These results suggest a possible negative regulation of *REV-ERBα* and *CLOCK* expression by NPAS2, and a positive effect on *BMAL1* expression levels. Some increase in the expression of *PER1* and *REV-ERBβ* was also observed, although not reaching significance.

In contrast, no significant changes were observed in the expression of these genes in the ΔCLOCK cells compared to the WT cells, at least under conditions of unsynchronised culture (Table 3.5). However, it should also be noted that the ΔCLOCK cells are a knockdown rather than KO model (see section 2.3.2, page 82). Thus, a more complete KO may be required to observe robust effects.

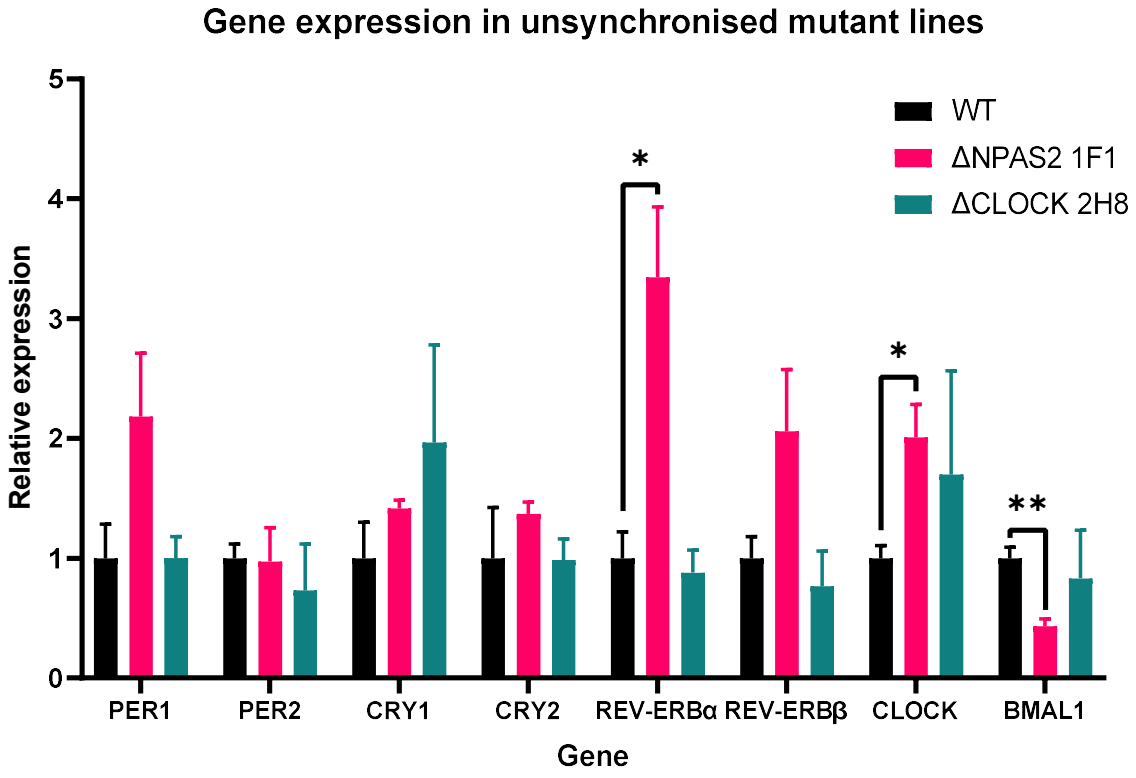

Figure 3.3: Expression of circadian genes in asynchronous NIH3T3 cells

Mean relative gene expression (±SEM) of ΔNPAS2 cells (red), ΔCLOCK cells (green) compared to WT NIH3T3 cells (black). Relative expression values are based on RT-qPCR reads after $2^{-\Delta Ct}$ transformation based on *18S* reads, relative to the WT sample for each gene. The significance of independent t-test comparisons between WT and the ΔNPAS2 cells are shown (*=p<0.05, **=p<0.01), identical t-tests were also performed comparing the WT and ΔCLOCK cells but no significant differences were observed, details in Table 3.5.

Table 3.5: Independent t-testing of expression of each gene in WT cells compared to modified ΔNPAS2 and ΔCLOCK cell lines

Gene	WT compared to ΔNPAS2 cells	WT compared to ΔCLOCK cells
PER1	t(4)=0.973, p=0.120	t(4)=-0.006, p=0.996
PER2	t(4)=-0.092, p=0.931	t(4)=-0.663, p=0.543
CRY1	t(4)=1.352, p=0.248	t(4)=1.117, p=0.326
CRY2	t(4)=0.846, p=0.445	t(4)=-0.035, p=0.974
REV-ERBα	t(4)=3.728, p=0.020*	t(4)=-0.416, p=0.698
REV-ERBβ	t(4)=1.942, p=0.124	t(4)=-0.678, p=0.535
CLOCK	t(4)=3.402, p=0.027*	t(4)=-0.798, p=0.470
BMAL1	t(4)=-5.185, p=0.007*	t(4)=-0.410, p=0.703

We also see that the levels of the *CLOCK* transcript appear unchanged in the ΔCLOCK cells. Note that the qPCR primers amplify a sequence from exons 15-16 of the *CLOCK* mRNA so will detect the modified transcripts from both alleles. While the modification clearly reduced protein levels (see Figure 2.10, page 86) the modification would not necessarily cause reduced expression of the transcript. In summary, this initial analysis of core clock genes in unsynchronised cells revealed that depletion of NPAS2 coincided with increased expression of *REV-ERBα* (>3-fold) and *CLOCK* (2-fold) transcripts as detected by RT-qPCR. This result suggests a possible role for NPAS2 in negative regulation of *REV-ERBα* and *CLOCK* expression in NIH3T3 cells. In contrast, depletion of NPAS2 resulted in a reduction (>2 fold) in *BMAL1* transcripts, suggesting NPAS2 may act to positively regulate expression of its heterodimeric partner.

3.3.3 Rhythmic expression of core circadian genes in synchronised edited NIH3T3 cells

Having established that we could detect changes in transcript levels of core clock genes (*REV-ERBα*, *BMAL1*, *CLOCK*) between the WT and the ΔNPAS2 cells in asynchronous conditions, the next goal was to assess how circadian expression of key genes was altered in these cultured cells after serum shock. Based on the data from the analysis of gene expression in asynchronous cells it was decided to focus on the expression of 6 genes. *REV-ERBα*, *BMAL1*, *CLOCK* (based on the significant change in gene expression in the ΔNPAS2 cells). *REV-ERBβ*, *PER1* (based on the sub-significant but observable change in expression in the ΔNPAS2 cells) and *CRY1* (based on the observable change in the ΔCLOCK cells) were also included, in addition to *18S* rRNA gene as a normalisation control.

3.3.3.1 Circadian expression of genes in WT NIH3T3 cells

Firstly, the expression of the genes across the time points in WT NIH3T3 cells was assessed to identify if we observe the expected rhythmic expression of genes to confirm to the model (Figure 3.4, Table 3.6). Looking at transcript levels of the 6 circadian genes, only *REV-ERBα* and *REV-ERBβ* showed robust and statistically significant circadian patterns, peaking at 18 hrs post serum shock. This pattern of expression is consistent with results from Osland et al. (2011) using serum shocked NIH3T3 cells, in which *REV-ERBα* expression peaked at 18 hours and 42 hours post shock.

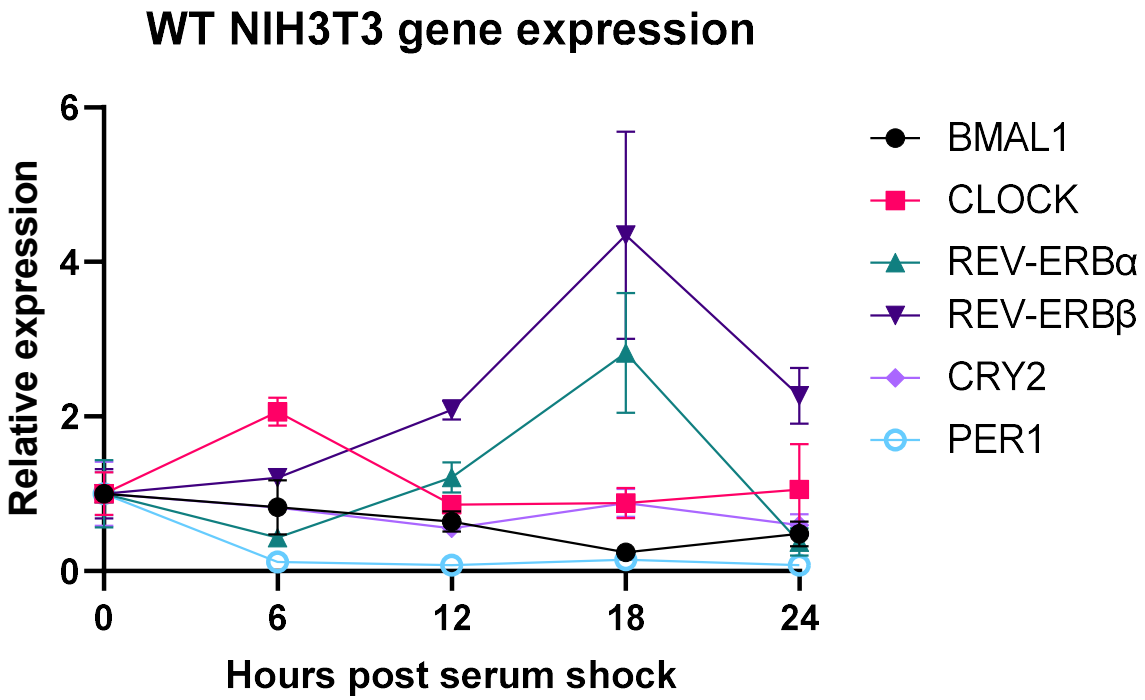

Figure 3.4: Expression of circadian genes in WT NIH3T3 cells following serum shock synchronisation.

Mean relative expression (±SEM) is shown for each of the genes of investigated; *BMAL1* (black), *CLOCK* (red), *REV-ERBα* (green). *REV-ERBβ* (blue), *CRY2* (violet) and *PER1* (cyan). Clear circadian peaks are seen in the expression of both *REV-ERB*s peaking at 18 hours. *CLOCK* and *BMAL1* both show antiphasic expression to the *REV-ERB* transcripts with highest expression seen at 6 hours for *CLOCK* and 0 hours for *BMAL1*. *PER1* shows decreased expression after 0 hours and *CRY2* does not present a notable variation across the time points.

Table 3.6: One-way ANOVA testing of time point effect on gene expression in serum shocked WT NIH3T3 cells

Gene	Effect of time point
PER1	F(4,10)=9.707, p=0.00179*
CLOCK	F(4,10)=2.528, p=0.107
BMAL1	F(4,10)=2.377, p=0.122
CRY2	F(4,10)=0.743, p=0.584
REV-ERBβ	F(4,10)=4.300, p=0.028*
REV-ERBα	F(4,10)=5.639, p=0.012*

The significant variation across time points observed for *PER1* expression is likely primarily due to 10-fold higher expression of the transcript initially after the serum shock compared to all other time points. This initial induction of the expression of *PER* genes has been reported in other serum shock synchronised cultured cells and is likely part of the response responsible for entrainment in cultured cells (Balsalobre et al., 1998). Although a subtle increase of *PER1* expression is observed at 18 hours, levels remained substantially lower than the expression at 0 hours. This pattern is consistent with that in the report by Osland et al. (2011) who noted no circadian expression of *PER1* in NIH3T3 cells once the initial peak of expression is passed.

No statistically significant effect of time was identified on expression of *CLOCK*. Despite this a potentially antiphasic expression pattern compared to the *REV-ERB*s can be seen, peaking at 6 hours within the time frame of the experiment. *BMAL1* showed no significant time point variation but showed a potentially antiphasic expression pattern as compared to the *REV-ERB*s, with lowest expression observed at the 18-hour time point. Again, these results for *CLOCK* and *BMAL1* are consistent with the observations in the Osland et al., 2011 study, albeit they had more time points.

In the Osland study, *CRY2* expression levels displayed a modest and less clear oscillation over time, being low at 6 hrs and highest at 18 hrs. The *CRY2* expression oscillations in WT NIH3T3 cells observed here were also modest and while they did not show a significant time point effect, we still observe subtle rhythmic fluctuations in expression.

Thus, across all genes investigated we concluded that at least for several of the genes in this study, circadian oscillation patterns were observed that were consistent with previous studies and confirm the efficacy of serum shock in synchronising cell autonomous circadian clocks.

3.3.3.2 Effect on circadian expression of genes in ΔNPAS2 NIH3T3 cells

We next assessed the role of NPAS2 in regulating circadian oscillations of these genes shown in Figure 3.5. Results of the analysis are presented in Table 3.7. Significant interaction effects of genotype x time point on the expression of *REV-ERB*s and *CRY2* were identified suggesting an impact of the loss of NPAS2 on the rhythmic expression of these genes. These interactions were investigated through post hoc pairwise analysis, the findings of which are shown on the respective graphs of Figure 3.5 and detailed in Table 3.8. Significant main effects of the loss of NPAS2 expression on *BMAL1* and *CLOCK* expression were observed suggesting an impact of NPAS2 loss on the general expression of these genes without an effect on the rhythmic expression. However, no significant effect of NPAS2 expression on *PER1* was observed.

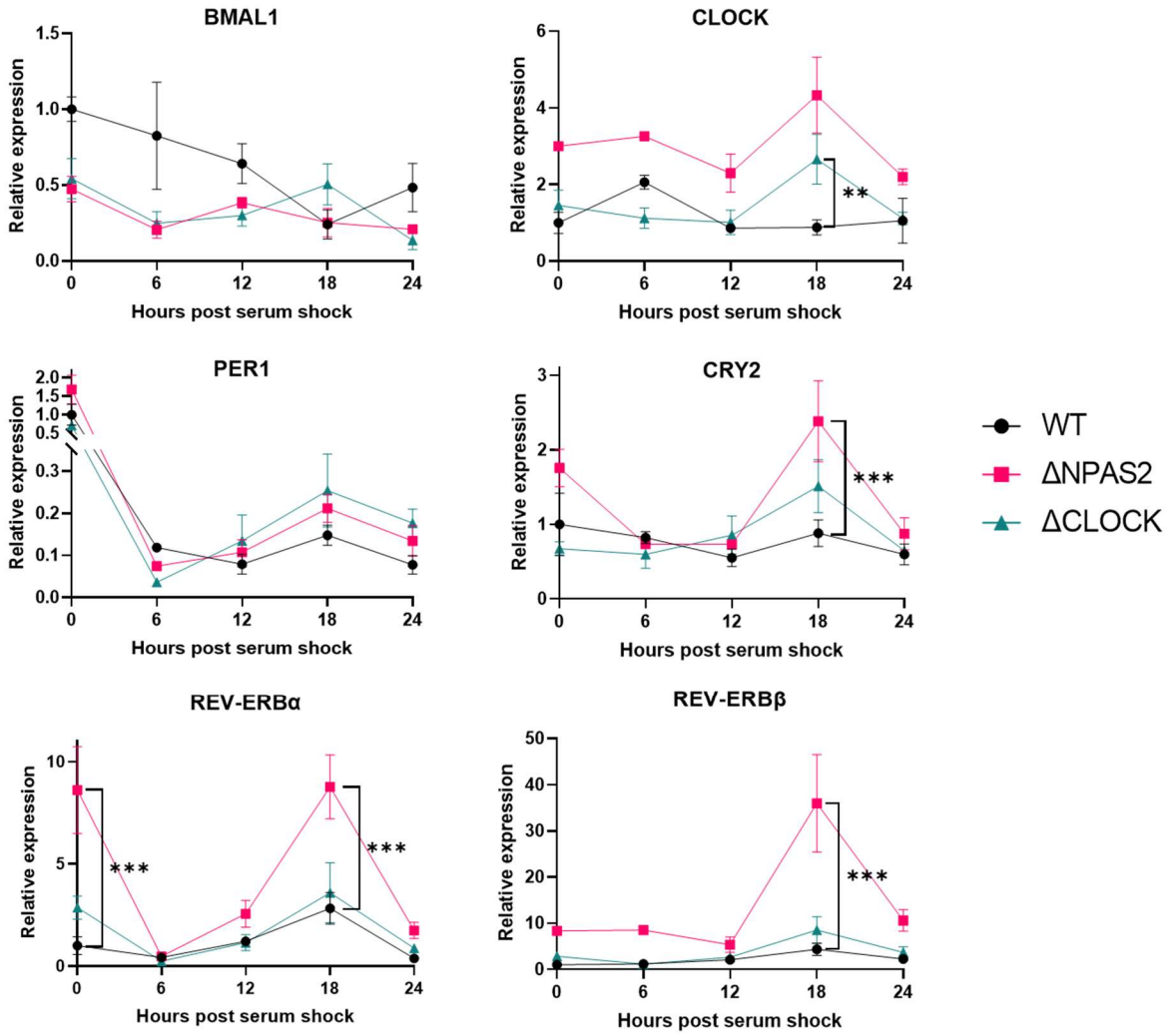

Figure 3.5: Expression of circadian genes in serum shock synchronised cells

Mean relative gene expression (±SEM) in ΔNPAS2 cells (red), ΔCLOCK cells (green) compared to WT NIH3T3 cells (black). Relative expression values are based on RT-qPCR reads after $2^{-\Delta Ct}$ transformation based on *18S* reads, relative to the WT sample at time point zero for each gene. Note *PER1* expression at 0 hours varies hugely from the other time points hence the split axis. The results of statistical analysis of main effects are shown in Table 3.7 and Table 3.9. The significance of pairwise post hoc comparisons of cell types at specific time points are shown (**=p<0.01, ***=p<0.001, details in Table 3.8 and Table 3.10).

Table 3.7: Factorial ANOVA comparison of gene expression in serum shock synchronised WT and ΔNPAS2 cells

Gene	Genotype	Time	Genotype x time interaction
BMAL1	F(1,20)=13.643, p=0.00144*	F(4,20)=3.442, p=0.027*	F(4,20)=1.518, p=0.235
CLOCK	F(1,20)=47.83, p<0.00001*	F(4,20)=3.015, p=0.042*	F(4,20)=2.574, p=0.069
PER1	F(1,20)=2.622, p=0.121	F(4,20)=25.503, p<0.00001*	F(4,20)=1.858, p=0.157
CRY2	F(1,20)=10.46, p=0.004*	F(4,20)=5.95, p=0.003*	F(4,20)=2.96, p=0.045*
REV-ERBα	F(1,20)=31.535, p=0.00002*	F(4,20)=13.236, p=0.00002*	F(4,20)=6.462, p=0.00166*
REV-ERBβ	F(1,20)=27.279, p=0.00004*	F(4,20)=7.717, p=0.00062*	F(4,20)=5.269, p=0.005*

Table 3.8: Post hoc pairwise comparison of gene expression in WT and ΔNPAS2 cells at individual time points for genes with a significant interaction effect identified by factorial ANOVA

Time point	***CRY2***	***REV-ERBα***	***REV-ERBβ***
0	p=0.050	p=0.00001*	p=0.153
6	p=0.810	p=0.971	p=0.157
12	p=0.620	p=0.310	p=0.518
18	p=0.001*	p=0.00018*	p<0.00001*
24	p=0.458	p=0.306	p=0.108

Significantly enhanced expression of *REV-ERBα* and *REV-ERBβ* in the ΔNPAS2 cells was observed at 18 hours after the serum shock (3-fold higher *REV-ERBα* & 8-fold higher *REV-ERBβ* expression compared to WT at 18 hours). This is consistent with our previous result in the asynchronous expression assay (Figure 3.3) showing that loss of NPAS2 causes an increase in the amplitude of *REV-ERB* cycles. This suggests that depletion of NPAS2 leads to a derepression of *REV-ERB* gene transcription primarily at times of peak *REV-ERB* expression. The circadian pattern peaking at 18 hours is seen for both genes, so the timing of the circadian pattern is not modified from WT cells. The expression of *REV-ERBα* is also significantly increased in the ΔNPAS2 cells immediately following the serum shock, while not obvious in

the WT data presented here, Osland et al. (2011) reported an initial early peak of *REV-ERBα* in serum shocked NIH3T3 cells so we are likely also observing an enhancement of this peak. For *REV-ERBβ* expression while the post hoc testing only identified a significant change at 18 hours the expression at every time point is several times greater than in the WT cells suggesting that while the major effect occurs at the time of peak expression there is a persistent increase in expression of *REV-ERBβ* in the ΔNPAS2 cells.

The expression of *BMAL1* at time zero is 2-fold lower in the ΔNPAS2 cells and it appears that the rhythmic expression of *BMAL1* seen in WT cells is lost with the loss of NPAS2, shown in Figure 3.5. Despite this, the statistical analysis identified that loss of NPAS2 caused a significant reduction of *BMAL1* expression however there was not a significant interaction effect with time point. As such this data only confidently shows that NPAS2 depletion causes decreased *BMAL1* expression but not loss of the rhythmic expression. This is likely due to the subtle change in BMAL1 expression across time points and variation in expression meaning that there was not a significant effect of time points observed in the WT cells by statistical analysis.

Figure 3.5 shows that the expression of *CLOCK* is increased between 2- and 4-fold in the ΔNPAS2 cells at each of the 5 time points, supporting the observed significant main effect of NPAS2 expression without a significant time point interaction. This suggests loss of NPAS2 significantly increases *CLOCK* expression across the cycle without a rhythmic effect.

The expression of *CRY2* was enhanced in the ΔNPAS2 cells specifically at the points of higher expression (0 and 18 hours) although a significant comparison is only seen at 18 hours. This means that the circadian pattern of expression is more obvious than was observed in the WT cells where a significant time point effect was not observed. As for the *REV-ERB* transcripts this suggests that depletion of NPAS2 leads to a derepression of *CRY2* gene transcription primarily at times of peak expression.

3.3.3.3 Effect on circadian expression of genes in ΔCLOCK NIH3T3 cells

The role of CLOCK in regulating circadian oscillations of these genes was investigated and results are shown in Table 3.9. Significant interactions of genotype x time point on the expression of the *CLOCK* transcript were identified suggesting an impact of the reduction of CLOCK protein expression on the rhythmic expression of its own modified transcript, or an effect of the modification on transcript stability. This interaction effect was investigated through post hoc analysis, the results of which are shown on the *CLOCK* expression graph of Figure 3.5 and detailed in Table 3.10. Significant main effects of the knockdown of CLOCK expression on the expression of the *BMAL1* and *REV-ERBβ* transcripts were observed suggesting an impact of reduced CLOCK on the general expression of these genes without an effect on the rhythmic expression. However, no significant effect of CLOCK expression on the expression of *PER1*, *CRY2* or *REV-ERBα* was observed.

As shown in Figure 3.5 the expression of *CLOCK* transcript in ΔCLOCK cells was ~2-fold higher that WT cells at 18 hours, with the significant increase only observed at this time point. While the WT cells do not present a clear circadian pattern there is a peak at 6 hours, which is lost in the ΔCLOCK cells with the 18-hour peak appearing instead, this may present a phase shift in the rhythmic expression of the *CLOCK* transcript. This suggests that the depletion of CLOCK protein causes a decrease in repressive functions affecting its own expression in a rhythmic manner.

The expression of *BMAL1* in the ΔCLOCK cells is similar to that seen in the ΔNPAS2 cells, although the expression in asynchronous ΔCLOCK cells did not present the statistically significant decrease in expression observed in ΔNPAS2 cells (Figure 3.3). Both ΔNPAS2 and ΔCLOCK cells appeared to show loss of the rhythmic *BMAL1* expression, however, as noted for ΔNPAS2 cells, statistical analysis did not identify a significant effect on the cycling behaviour. This means we observe that CLOCK depletion causes decreased *BMAL1*

expression.

Due to the substantially elevated expression of the *REV-ERB*s in the ΔNPAS2 cells another graph was created to clearly show the WT and ΔCLOCK comparison, Figure 3.6. *REV-ERBβ* was identified by analysis to show a significant increase in expression in the ΔCLOCK cells without it being a time dependent effect. However, it appears that expression is increased primarily at the time of peak expression similar to the expression in ΔNPAS2 cells suggesting a similar effect of CLOCK depletion. No significant effect of depleted CLOCK expression was observed on *REV-ERBα* expression although a 0-hour peak, possibly as part of the serum shock response, is observed in the ΔCLOCK cells similar to the larger peak in ΔNPAS2 cells.

The depletion of CLOCK expression was also not observed to significantly modify the expression levels of *CRY2* or *PER1* either overall or in a time specific manner.

Table 3.9: Factorial ANOVA comparison of gene expression in serum shock synchronised WT and ΔCLOCK cells

Gene	Genotype	Time	Genotype x time interaction
BMAL1	F(1,20)=9.127, p=0.007*	F(4,20)=2.736, p=0.058	F(4,20)=2.269, p=0.098
CLOCK	F(1,20)=1.778, p=0.197	F(4,20)=1.897, p=0.150	F(4,20)=3.721, p=0.020*
PER1	F(1,20)=0.106, p=0.748	F(4,20)=19.85, p<0.00001*	F(4,20)=1.263, p=0.317
CRY2	F(1,20)=0.385, p=0.542	F(4,20)=2.125, p=0.115	F(4,20)=1.573, p=0.220
REV-ERBα	F(1,20)=2.355, p=0.141	F(4,20)=7.474, p=0.00075*	F(4,20)=0.947, p=0.458
REV-ERBβ	F(1,20)=4.755, p=0.041*	F(4,20)=6.274, p=0.00193*	F(4,20)=0.993, p=0.434

Table 3.10: Post hoc comparison of *CLOCK* transcript expression in WT and ΔCLOCK cells at individual time points based on a significant interaction effect identified by factorial ANOVA

Time point	*CLOCK*
0	p=0.376
6	p=0.079
12	p=0.773
18	p=0.002*
24	p=0.904

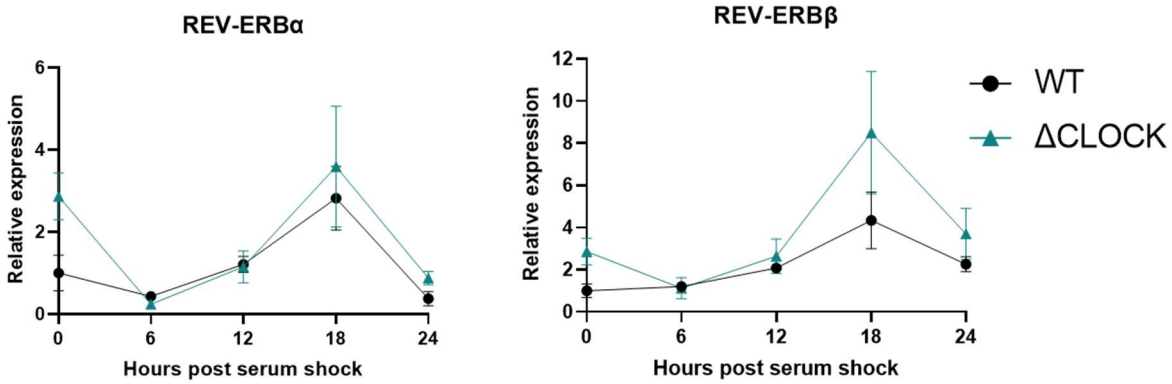

Figure 3.6: Expression of REV-ERB genes in serum shock synchronised ΔCLOCK cells

Mean relative expression (±SEM) of *REV-ERBα* and *REV-ERBβ* transcripts in serum shock synchronised ΔCLOCK cells (green) compared to WT NIH3T3 cells (black). Data is the same as that in Figure 3.5 without the data of ΔNPAS2 cells to allow clear comparison of the WT and ΔCLOCK cells. Relative expression values are based on RT-qPCR reads after $2^{-\Delta Ct}$ transformation based on *18S* reads, relative to the WT sample at time point zero for each gene.

3.4 Discussion

3.4.1 Results summary

In summary we have observed significant differences in the expression of various core circadian feedback genes between WT control cells and the ΔNPAS2 and ΔCLOCK cells. In unsynchronised cells it was identified that the expression of the *REV-ERBα* and *CLOCK* genes was significantly increased, and *BMAL1* significantly decreased in the ΔNPAS2 cells compared to the WT cells (Figure 3.3). Investigating the expression after circadian synchronisation we identified significantly different expression of *BMAL1*, *CLOCK*, *CRY2*, *REV-ERBα* and *REV-ERBβ* genes between the ΔNPAS2 and WT cells. The increase in *CRY2*, *REV-ERBα* and *REV-ERBβ* expression coincided with the times of peak expression (Figure 3.5). In ΔCLOCK cells, expression of *REV-ERBα* was similar to control levels, while *BMAL1*, *CLOCK*, and *REV-ERBβ* showed similar changes in expression to that in the ΔNPAS2 cells, although less substantial (Figure 3.5 & Figure 3.6).

3.4.2 NPAS2 KO may influence the cell cycle in NIH3T3 cells

Imaging of the cells identified no gross phenotypic effects in cell appearance. It was however noted in routine cell culture that the ΔNPAS2 clones take an increased amount of time to reach confluence (approximately 2x), although this has not been established experimentally. This may suggest loss of NPAS2 negatively influences cell growth. Various circadian genes have been linked to the cell cycle with various checkpoints affected by circadian timing which would influence cell growth (Farshadi et al., 2020). Upregulation of NPAS2 in hepatocellular carcinoma is associated with accelerated cell cycle progression (Yuan et al., 2017) and knockdown of NPAS2 in acute myeloid leukaemia cells supressed proliferation (Song et al., 2018) suggesting the slowing of growth rate is an effect of the loss of NPAS2. However silencing NPAS2 has been reported to enhance the growth of DLD-1 colorectal

adenocarcinoma cells (Xue et al., 2014) and a primary fibroblast culture from NPAS2 KO mice showed enhanced proliferation (Sasaki et al., 2020) so it appears this may be a tissue-specific effect and more complicated than a direct effect of NPAS2.

3.4.3 NPAS2 ablation impacts expression levels of *REV-ERBα*, *CLOCK* and *BMAL1* in unsynchronised NIH3T3 cells

Analysis of the expression levels of eight core clock components revealed significant changes in three genes in asynchronous ΔNPAS2 cells: *REV-ERBα*, *CLOCK* and *BMAL1*. While not reaching significance, expression levels of *REV-ERBβ* and *PER1* also showed a tendency toward increased expression (Figure 3.3). The increase in *CLOCK* expression may be a compensatory mechanism to overcome loss of its paralog, similar to the increase in *NPAS2* observed in studies of CLOCK KO mice, although the mechanism is unknown (see below). The change in overall expression of *REV-ERBα* and *REV-ERBβ* was unexpected and was not observed in the CLOCK deficient cell line. To our knowledge, this is the first reported observation of potential negative regulation of *REV-ERBα/β* genes by NPAS2, although REV-ERBs are known repress expression of BMAL1 and NPAS2 genes through binding ROREs in their promoters (Ikeda et al., 2019). Thus, our results may indicate another aspect of the autoregulatory interactions of core clock genes.

3.4.4 Serum shock model of circadian cycling in cell culture

We demonstrated in this study the successful reconstitution of circadian synchronisation of several core clock components in NIH3T3 cells induced by serum shock. The results were largely consistent with other studies (Osland et al., 2011), with the most robust time dependent changes observed for the *REV-ERB*s and *CRY2* which peak around 18 hours post shock (Figure 3.4). *BMAL1* and *CLOCK* showed an antiphasic expression compared to *REV-ERB*s. No clear cycling of *PER1* was observed over the time course of the experiment, despite an initial drop in *PER1* expression post shock (Figure 3.4), similar to previous studies

(Osland et al., 2011).

As shown in Figure 3.5, significant increases in the expression of both *REV-ERB* gene transcripts in the ΔNPAS2 cells were identified primarily at the time points of high expression, consistent with the observed modified expression in asynchronous cells. While in the ΔCLOCK cells an increase was observed in *REV-ERBβ* this change was very minor compared to the large change seen in the NPAS2 modified cells (2-fold compared to 8-fold increase). As such this may reflect an effect unique to NPAS2.

Although *CLOCK* gene transcripts shows a very moderate cycling pattern (Figure 3.4, Figure 3.5) it was noticeable that in the ΔNPAS2 cells the overall expression level was increased, consistent with the data from unsynchronised cells. As noted above, this increase may potentially be a compensatory effect, similar to the compensatory increase in NPAS2 expression which has been observed in the liver of CLOCK KO mice (Landgraf et al., 2016, Debruyne et al., 2006). It is noted that a decrease in expression of *REV-ERBα* is also reported in these mouse models which could be responsible for the increase in *NPAS2* expression through loss of REV-ERB repression of NPAS2 transcription. This does not however explain the mechanism in our model, nor is the observed increase of both *REV-ERB*s and *CLOCK* contradictory as the REV-ERB proteins have been reported to not directly influence CLOCK expression due to the absence of a RORE site (Ikeda et al., 2019). Similarly, an increase in *CLOCK* transcript levels was noted in the ΔCLOCK cells (Figure 3.5), likely the response of a similar compensatory process. However, this is not associated with an increase in CLOCK protein expression based on the previously detailed western blot investigation of the cells (Figure 2.10). The analysis of the target sites identified by Koike et al. (2012), used to produce Figure 3.1 (details in appendix section A.7, page 305), found that BMAL1 alone has a binding site potentially influencing expression of the *CLOCK* gene. However, as the *CLOCK* gene was not reported to be a target of CLOCK or NPAS2 this is unlikely to reflect regulation of *CLOCK*

expression directly by BMAL1 activity and the change in expression is more likely due to indirect effects.

BMAL1 showed reduced expression in both cell lines, primarily at the time points of higher expression in the WT cells meaning a loss of the variance of *BMAL1* expression across time points (Figure 3.5). A similar decrease in cycling of *BMAL1* transcript is observed in the liver and other peripheral clocks of CLOCK KO mice although cycling expression is still observed (Landgraf et al., 2016). In the SCN of NPAS2 KO mice rhythmic expression of *BMAL1* is lost, however this effect is due to an increase in *BMAL1* expression at lower expression time points rather than a decrease at the higher expression time points as seen in our cell model (DeBruyne et al., 2007a). As the REV-ERB proteins act to inhibit *BMAL1* expression the increased expression of *REV-ERB*s in both clones may be responsible for this effect, although the more substantial upregulation of the *REV-ERB*s in the ΔNPAS2 cells compared to the ΔCLOCK cells is not associated with a more substantial reduction of *BMAL1* expression.

An increase in the expression of *CRY2* was observed in the ΔNAPS2 modified cell line at the time of peak expression with a similar increase in the ΔCLOCK cells, although below significance (Figure 3.5). As CLOCK and NPAS2 both act as transcription factors for the *CRY* genes it is surprising that expression increases. However, this may suggest compensatory effects within the circadian cycles which then cause modifications in the expression patterns.

3.4.5 Mechanisms of NPAS2 knockout influence on the expression of the REV-ERB genes

Most notable of the gene effects is the substantial increase in expression of the *REV-ERB* transcripts in NIH3T3 cells with a KO of NPAS2. Possible mechanisms of this effect are shown in Figure 3.7.

Firstly, this could be due to alleviation in the ΔNPAS2 cells of competition between

NPAS2 and CLOCK, both in association with BMAL1 and binding to genomic E-boxes. If in normal function the NPAS2:BMAL1 dimer is unable to induce transcription of the REV-ERB genes (Figure 3.7 A) or is a weaker activator of REV-ERB transcription (Figure 3.7 B) then loss of NPAS2 as a competitor will allow increased association of the CLOCK:BMAL1 dimer and lead to higher levels of transcription. This is unlikely as, while less substantial, we also observed increased *REV-ERB* expression in the ΔCLOCK cells.

It may be a functional result of the compensation of loss of NPAS2, as noted above the ΔNPAS2 cells showed increased expression of the *CLOCK* transcript, if the levels of CLOCK expression are greater than the levels of NPAS2 and CLOCK expression combined in WT cells then this may enhance transcription of genes under E-box promotors, even if the NPAS2:BMAL1 and CLOCK:BMAL1 dimer are functionally similar, due to higher E-box occupation (Figure 3.7 C).

Finally, the results we present here may instead be an indication of a more complex effect caused via influences on the expression and activity of various CCGs rather than a direct effect. If expression of other unidentified genes is modified in the ΔNPAS2 cells then these genes may influence expression of *REV-ERB* transcripts. Other genes could affect transcription, potentially through influencing CLOCK:BMAL1 activity at E-boxes or activity at other promotors (Figure 3.7 D) or some may influence stability of the *REV-ERB* transcripts. It should be noted that a combination of these effects may be responsible and any of these effects may occur only as a tissue-specific function, as circadian cycles are controlled in a variety of ways, including tissue-specific influences on CLOCK/NPAS2:BMAL1 activity (Yeung et al., 2018). The potential tissue specificity of this relationship is highlighted by the fact than in the SCN of constitutive NPAS2 KO mice the expression of *REV-ERBα* was unaltered (DeBruyne et al., 2007a).

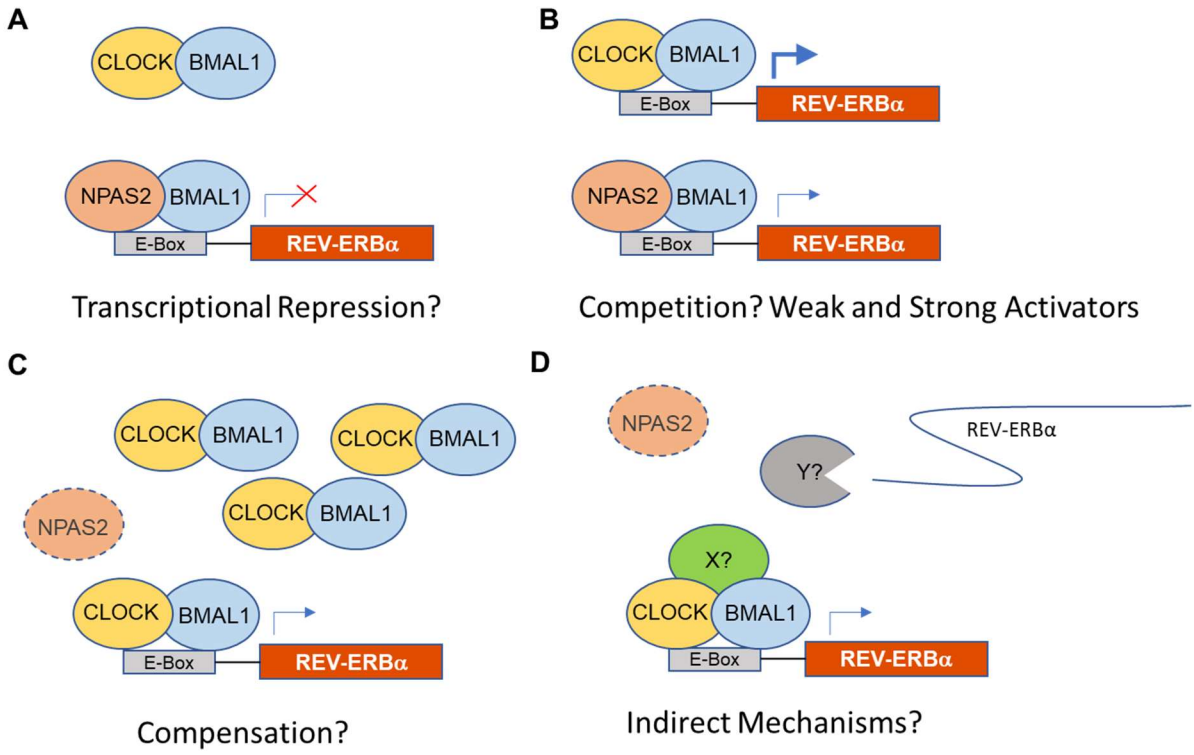

Figure 3.7: Possible mechanisms responsible for the increased REV-ERB expression in cells with a functional KO of NPAS2.

A: Transcriptional repression, if the NPAS2:BMAL1 dimer is a negative transcription factor of the genes then it will compete for CLOCK:BMAL1 E-box association. **B:** Competition, if the NPAS2:BMAL1 dimer is a weaker activator of gene transcription then absence of NPAS2 will alleviate competition for BMAL1 dimerisation for CLOCK allowing greater transcription through CLOCK:BMAL1 E-box association. **C:** Compensation, the ΔNPAS2 cells showed increased CLOCK transcript expression, if the expression of CLOCK protein is increased by more than the level of NPAS2 is decreased then this enhanced level of CLOCK:BMAL1 dimer will increase E-box occupancy and gene transcription. **D:** Indirect mechanisms, other gene expression levels may be positively or negatively influenced by loss of NPAS2, this may then affect the levels of gene transcripts through influencing transcription or transcript stability.

3.4.6 Future work

Effects on the expression levels of circadian genes have been identified, as follow up to this work it would be of value to perform rescue experiments, in which WT expression levels of the modified genes is restored via plasmid transfection. Reintroduction of the modified genes should change gene expression in the cells to levels similar to the WT cells. This would provide confidence that the findings are due to the gene modification effects, rather than any other change in the modified clones compared to the WT cells.

Observation of any effect on the circadian period of gene expression would not be expected to be observed here, due to the large time windows utilised. As loss of CLOCK or NPAS2 individually would likely only be associated with a subtle modification to the circadian cycles, substantially closer time points would be required to observe the effect. Alternatively using live luciferase recording the period of luminescence, as introduced in section 3.1.1, would reflect the circadian period and could be used to identify any change in period length.

Chapter 4: Establishing the *NPAS2*$^{fl/fl}$/*Alb-cre* liver knockout mouse model and investigating gene expression changes in the liver and brain regions

4.1 Introduction

4.1.1 Circadian rhythms in the liver

The core circadian transcription feedback loops are described in Chapter 1 (section 1.3, page 26). As addressed in section 1.5 (page 31), genes with rhythmic expression may exhibit differences in amplitude and phase across different tissues and some core clock genes and clock-controlled genes (CCGs) show rhythmic expression only in certain tissues (Yan et al., 2008). This is due primarily to the impact of tissue-specific factors (Yeung et al., 2018).

In the liver, circadian cycles play a significant role in metabolism, including rhythmic synthesis of cholesterol and bile acids (Ferrell and Chiang, 2015, Zhou et al., 2016). The liver is one of the peripheral oscillators which can be decoupled from the SCN cycles though preferential entrainment to restricted feeding (RF) schedules (Damiola et al., 2000) showing the sensitivity of liver circadian cycles to metabolic state. Liver-specific BMAL1 deletion causes loss of circadian transcription in the liver and also inhibits the oscillation of blood glucose levels leading to hypoglycaemia in the fasting phase (Lamia et al., 2008), showing the importance of the liver in metabolic circadian cycles and homeostasis. In mouse models which should only express a functioning clock in the liver due to constitutive KO of BMAL1 and reconstituted BMAL1 liver expression, it has been observed that the functioning genetic clock in the liver is not enough to fully restore the normal liver cycles of all rhythmic genes and even the cycling which does occur is quickly lost upon placement in constant darkness (Koronowski et al., 2019). The inverse has also been observed; even in liver-specific circadian KO models, the circadian cycling of some genes is retained in the liver tissue but lost when the liver is cultured *ex vivo,* while unmodified mice retain rhythmic expression of liver genes (Kornmann et al., 2007). This suggests liver cycles are dependent both on the contribution of circadian signals produced from other tissues as well as the internal circadian cycles for complete normal function.

Communication to other tissues of the circadian state of the liver has been shown to be performed by the liver-derived ketone body β-hydroxybutyrate. In mice under RF conditions, β-hydroxybutyrate production by the liver contributes to behavioural entrainment and artificial introduction of β-hydroxybutyrate to the brain, in a time restricted manner, causes a similar entrainment effect to that of RF (Chavan et al., 2016). Cycling levels of blood glucose have also been identified to influence behavioural cycles through effects on the brain (Yi et al., 2006, Burdakov et al., 2005)

4.1.2 NPAS2 in mouse models

The function of NPAS2 has previously been studied in constitutive mouse KO models. In the SCN the loss of NPAS2 has been found to cause little change in expression of some core circadian genes, a subtle dampening in the amplitude of *PER2* cycling and overall increase in *BMAL1* were observed without noticeable change in *PER1* or *REV-ERBα* expression (DeBruyne et al., 2007a). In the forebrain of NPAS2 KO mice, it has been reported that there was no change in the expression of *CLOCK* (which does not show cycling expression in the forebrain) (Dudley et al., 2003), while normal *PER2* cycling of expression was lost (Reick et al., 2001). A study of liver expression of genes in constitutive NPAS2 KO mice identified increased expression of *BMAL1* and decreased expression of *PER1* without any change in the expression of *CLOCK*, *CRY2* and *REV-ERBβ* (O'Neil et al., 2013). However, this study did not look at gene expression at time points or specify the time at which tissue collection was performed, so some effects may have been missed.

4.1.3 Genetics of the *NPAS2*$^{fl/fl}$/*Alb-cre* mouse model

To investigate gene functions within specific tissues, conditional KO mouse models can be employed in which a mutation is introduced into the genome in a way which modifies gene expression only in specific tissues. To investigate the role of NPAS2 in peripheral clocks a liver-specific KO was utilised.

The NPAS2^{TM2AAGAA} mouse model with floxed *NPAS2* was developed by the Aagaard group as part of their work investigating the interaction of NPAS2 with the microbiome (O'Neil et al., 2017). This liver-specific KO model NPAS2$^{TM2.1AAGAA}$ was generated by use of the Cre-LoxP system. Two LoxP sites within the introns up and downstream of exon 3 were introduced ('floxing' the exon) which should not affect the expression of NPAS2 protein nor change its structure. The Cre recombinase protein can then induce recombination of the DNA at the two LoxP sites, removing the DNA sequence between the two sites. This means that Cre under a tissue-specific promotor can be used to excise the *NPAS2* genomic sequence in any tissue of interest (Kim et al., 2018a). In the conditional liver-specific NPAS2 KO, Cre is expressed via the postnatal liver-specific Albumin promotor (cKO, *NPAS2*$^{fl/fl}$/*Alb-cre*). This leads to KO of NPAS2 after development reducing potential compensatory effects. Mice with floxed *NPAS2* but which lack the expression of Cre are used as controls from the same litters (Ctrl, *NPAS2*$^{fl/fl}$). This removal of exon 3 leads to loss of the functional protein expression; any protein expression from the common ATG start codon would present a frameshift due to the loss of the exon. This modification may lead to expression of a reported shorter NPAS2 protein (ΔbHLH-NPAS2) through an alternate exon 2 ATG becoming an in-frame start codon. However, this protein lacks exon 3 and without this substantial region of the bHLH domain would be unable to dimerise with BMAL1 or act as a transcription factor (Garcia et al., 2000). As such it is a non-functional protein and will also not compete with CLOCK for BMAL1 association.

4.1.4 Experimental aims and hypothesis

The liver-specific NPAS2 cKO mice were used to investigate the effect of loss of NPAS2 in a peripheral clock on circadian gene expression. As the mouse colony was established, various molecular tests were performed to investigate the model. Initially, establishment of the mouse genotypes using ear notches was required, both to confirm the

modifications to the genetic sequence, as had previously been reported for these mice, and establish genotyping procedures for use in maintenance of the breeding colony.

To assess the tissue-specific functioning of Cre in the liver, genomic DNA was obtained from the brain and the liver of wild type C57BL/6, floxed control and Cre expressing cKO mice. In the liver, due to the Cre activity, genotyping should show the loss of the floxed region of *NPAS2* while in the brain this genomic region should only present floxed sequence. In the control mice the floxed sequence should be present for both tissues, while for wild type mice both tissues will present the sequence without the LoxP insertion.

Finally, the effect of loss of liver NPAS2 on the expression of genes that make up the core circadian feedback loop was investigated. This was performed using a total of 18 female mice aged 2-5 months. Samples were collected from the liver at the time of lights on, which is defined as zeitgeber time 0 (ZT0) and lights off (ZT12). These time points were chosen as they reflect times of high and low expression for several circadian transcripts in the liver, based on information from the circadian expression profiles database, CircaDB (Pizarro et al., 2013, http://circadb.hogeneschlab.org/). Gene expression in the prefrontal cortex (PFC) was also investigated as a non-SCN clock in the brain with identified circadian oscillation (Chun et al., 2015) and one of the regions in the brain that clearly present NPAS2 expression (Reick et al., 2001). Specifically, the expression of the genes *REV-ERBα*, *REV-ERBβ*, *BMAL1* and *CLOCK* were investigated as these genes were identified to be influenced by the loss of NPAS2 in the modified cell models. Comparison of the gene expression levels between control and cKO mice was then used to inform conclusions as to how NPAS2 in the liver contributes to the circadian feedback loop.

It was hypothesised that we would see similar effects on gene expression in the cKO liver to those in the modified cells, as both are NPAS2 KO models of peripheral clocks, and gene expression within the brain would be unaltered due to retained NPAS2 expression.

4.2 Materials and Methods

4.2.1 *In vivo* methods

4.2.1.1 Animals

Mice were bred on site after establishment of the breeding colony using mice imported from the Baylor Institute, Texas. The control mice ($NPAS2^{TM2AAGAA}$) are floxed on exon 3 of *NPAS2* and cKO mice ($NPAS2^{TM2.1AAGAA}$) are floxed and are also heterozygous for Cre under an albumin promotor. This means the cKO mice express Cre specifically within the liver, resulting in a functional KO of NPAS2. Breeding cages were set up with two females and one male, either the male or both females were cKO mice and the remaining were control floxed mice. Other than breeders, mice were single sex housed in cages of up to five mice. The mice were provided with *ad libitum* water and 2018 Rodent diet (Envigo). The mouse holding room was kept on a light cycle of 12h:12h LD with lights on at 7am and constant temperature (20±2 °C) and humidity (40–60%). Wild type C57BL/6 mouse tissues for genotype analysis were taken from mice purchased from Charles River Labs UK aged 3-6 months.

4.2.1.2 Genotyping

From the breeding colony ear notches were collected from all mice when weaned. The ear notches were either used for genomic extraction and PCR testing (performed as detailed below) or sent off in well plates to Transnetyx, Inc., Cordova, TN, USA. Transnetyx provides automated genotyping services of the ear notch tissue using our established primer sequences.

4.2.1.3 Tissue collection

Liver and brain tissues were collected for genotype validation (5.1.1) and for investigation of mRNA expression (4.3.3); all mice were culled by cervical dislocation and tissue collected and placed directly onto dry ice before storage at -80 °C until needed. Sections were made to collect the PFC of the brain for gene expression analysis. These sections likely also included other cortical and subcortical regions of the brain including the motor cortex

while excluding the SCN. For genomic analysis a more general section encompassing a wider range of cortical and subcortical regions was made (see Figure 4.1). It should be noted that the brain region collected is likely to have included cortical regions outside of the PFC and some subcortical regions.

For investigation of gene expression, tissues were collected from female mice aged 2-5 months at lights on (ZT0) and lights off (ZT12).

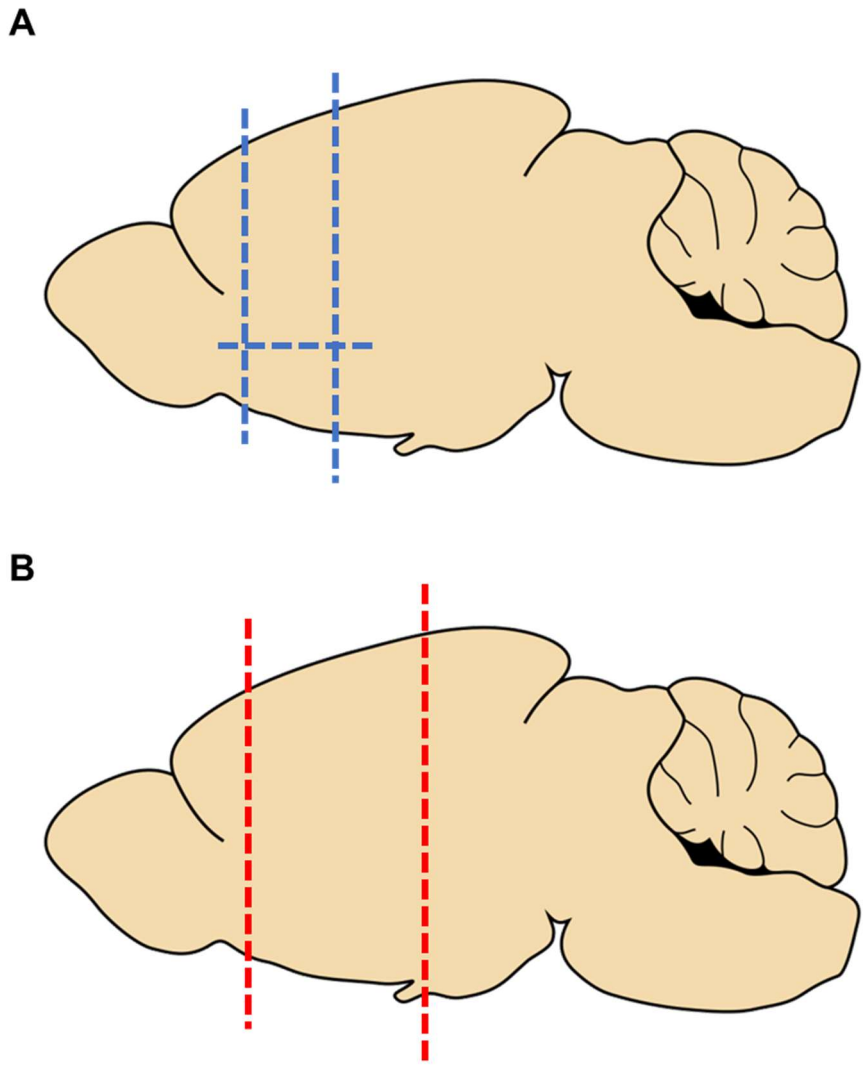

Figure 4.1: Brain sections for tissue collection

Sectioning of mouse brain used for tissue investigation. **A:** PFC sectioning used for investigation of gene mRNA expression levels. **B:** General brain section used for investigation of genomic DNA modifications.

4.2.2 Molecular biology techniques

Chemicals, reagents, and methodologies for molecular investigation were as described in Chapters 2 and 3, with the following additional details.

4.2.2.1 Composition of reagents

RNA agarose gel loading dye = 1 ml deionised formamide, 0.3 mg bromophenol blue, 0.3 mg xylene cyanol, 10 µl 1 M Tris-HCl pH 7.5-8.0. Stored at -20 °C.

4.2.2.2 Genomic extraction

Genomic DNA was purified from tissue using the GenElute™ Mammalian Genomic DNA Miniprep Kit. The tissue was cut minced on ice and digested in lysis solution T and genomic DNA extracted following the manufacturer's instructions for mammalian tissue. The concentration of DNA was determined using a NanoDrop 1000 Spectrophotometer.

4.2.2.3 Agarose gel electrophoresis

RNA agarose gels were performed similarly to DNA agarose gels as detailed in Chapter 2 (see 2.2.4.4). 1% agarose gels for RNA electrophoresis were made with 3 µl of 10 mg/ml ethidium bromide solution per 50 ml of liquid agarose rather than the 1 µl used for DNA gels. Prior to loading in the gel 0.2 µl RNA was added to 10 µl RNA agarose gel loading dye and incubated for 3 minutes at 70 °C to denature secondary structure. The gel was run for 1 hour at 90V or longer, as required for clear separation.

4.2.2.4 RNA extraction

For gene expression analysis, total RNA was extracted using Trizol (Sigma). The PFC brain sections and sections of the livers weighing ~100 mg were minced on ice immediately upon removal from -80 °C using cold tools. The tissue was immediately moved into preprepared 1 ml cold Trizol reagent and sonicated in cold water for a maximum of 3 x 15 second bursts as required to disrupt the tissue, using a Diagenode Bioruptor®. The RNA isolation was then performed according to the manufacturer's protocol, briefly this involved

separation of the RNA by addition of chloroform and taking the phase containing the RNA, precipitation of the RNA by addition of isopropanol, washing the RNA using 75% ethanol and resuspension in 30 µl or 200 µl of RNase free water for PFC and liver samples respectively.

4.2.2.5 RT-qPCR

Reverse transcription of RNA and RT-qPCR was performed exactly as detailed for cDNA from cultured cells in Chapter 3 (section 3.2.2.3, page 120). The primers used for analysis are the same used for investigation of gene expression in the NIH3T3 cells (validation in appendix A.4, page 288, sequences in appendix Table A.1, page 296). Reads were normalised to individual *18S* reads and the average of the specific gene expression in control mice at ZT0. Fold changes were calculated by dividing the reads at ZT12 by the average read at ZT0 for both genotypes individually.

4.2.3 Experimental design and statistical analysis

A power calculation using a Cohen's f of 0.908, based on a pilot study of genotype effect on gene expression in the liver of control and cKO mice, was performed in G power, for an ANOVA with an alpha value of 0.05 and power of 0.9 with 4 groups and a numerator df of 1. This large effect size was considered appropriate to identify biologically relevant influences on gene expression. Based on this a required total of 16 mice was calculated, equal to four mice per group. Due to greater availability within the litter more control mice were available for tissue collection and a total of five control mice were used at each time point.

Statistical analysis was performed using SPSS software as detailed in Chapter 3, section 3.2.3 (page 123). For investigation of the effect of the between-subjects factors of time and genotype on relative gene expression two-way ANOVAs were used. For investigation of fold changes across time-points independent t-tests were used to investigate the between-subjects factor of genotype.

4.3 Results

4.3.1 Validation of genotyping primers

To identify the genotypes of the mice for breeding and experimentation two genomic regions were investigated by PCR amplification. The inclusion of the inserted LoxP site shows that the mice are floxed for *NPAS2*. A region of genomic DNA where the LoxP site was inserted 5' of *NPAS2* exon 3 was amplified by PCR. This amplification produces products of different sizes, depending on the presence or absence or the LoxP site and will always produce a product if the PCR was successful for either genotype. The size of the product then identifies the genotype of the mouse with respect to the floxing. A second PCR test was designed for amplification of a region of the integrated Cre recombinase sequence, this PCR will only produce a product if Cre transgene is present. As genotyping is performed on the ear notches, the recombination events are not expected as they would be liver-specific, so there should be no modification of the *NPAS2* exon 3 region.

Using DNA from characterised mice without the LoxP insertion, with or without Cre genetic sequence, three different primer pairs all designed to amplify different arbitrary sequences within the Cre gene were tested (Cre1, Cre2 & Cre3) and the *NPAS2* LoxP primers (LoxP) were tested as internal controls (Figure 4.2 A). The use of an internal control is required for the Cre genotyping, due to a failure of PCR in a Cre positive sample and the absence of Cre appearing indistinguishable on a gel. Use of the LoxP amplification as the internal controls cuts down on the number of PCR tests required for genotyping. Based on the gel shown in Figure 4.2 A it was identified that the 408 bp product from the primers designated 'Cre2' showed most clear amplification in combination with primers to amplify the 5' LoxP site. Although the presence of observable primer dimers in the agarose gel also rose noticeably compared to the PCRs of only one primer pair it did not affect clear determination of the genotype. An exemplar gel showing genotyping of some mice from the breeding colony is presented in Figure 4.2 B

showing the larger LoxP product (246 bp) and the presence of Cre as identified by testing using the Cre2 primers. In amplification from DNA including the Cre genomic sequence, the LoxP product is fainter, suggesting the combined PCR amplification was less efficient, however it can still be seen and in this colony there should only be the LoxP inserted sequence present, meaning it purely acts as an internal control for the Cre negative samples.

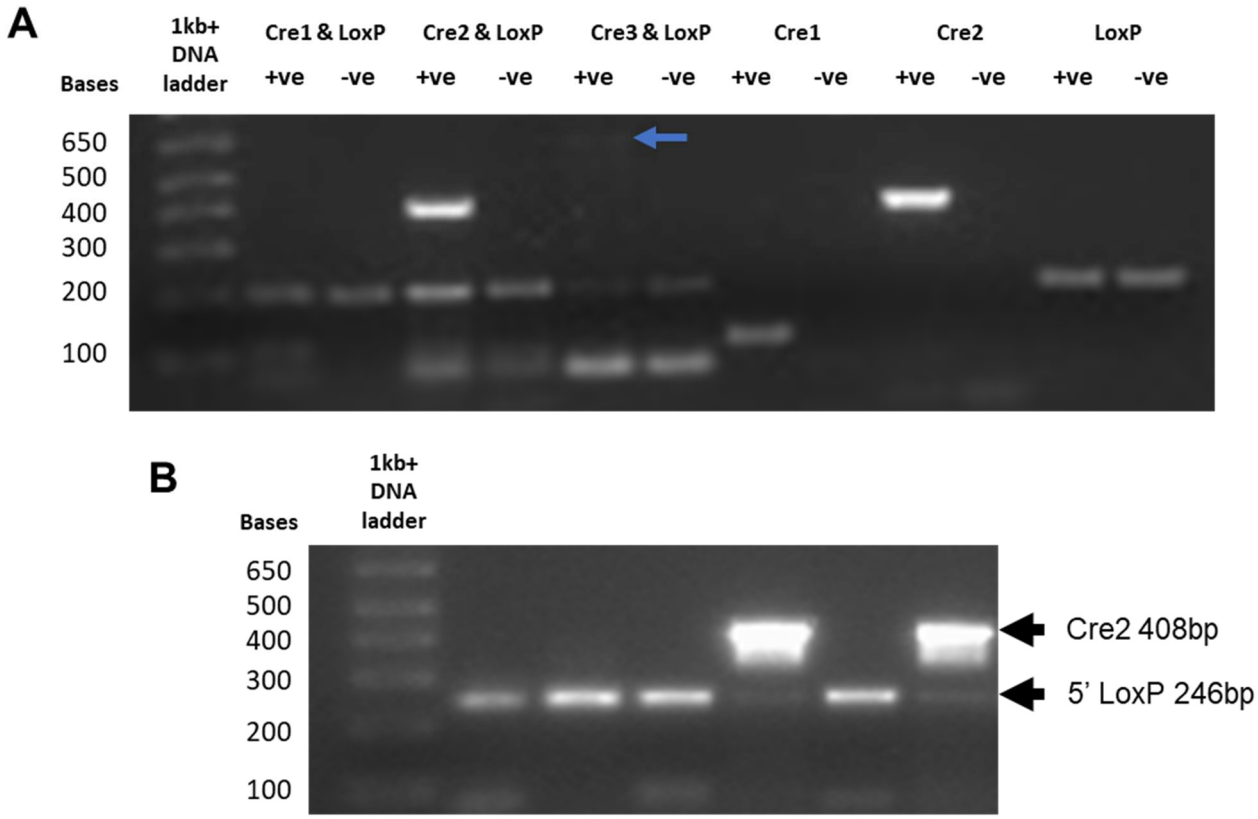

Figure 4.2: Agarose gels of mouse genotyping PCRs

A: Comparison of primers to genotype the presence of the Cre genomic sequence in combination with the LoxP primers. 3 different Cre primer pairs were used, Cre1 which amplifies a 100 bp product, Cre2 which amplifies a 408 bp product and Cre3 which amplifies a 643 bp product. These were run in combination with the *NPAS2* LoxP primer pair to validate that combination of both can be used to provide an internal positive. In this gel all PCRs were performed on genomic DNA lacking the inserted LoxP, meaning the LoxP primers amplify a product of 194 bp of unmodified *NPAS2* sequence (see Figure 4.3). The products of Cre1 primers are very small and hard to differentiate from primer dimers in the combination reaction and the products of Cre3 primers are barely visible and marked with a blue arrow. Cre2 primers however were able to amplify a product which appears very clearly on the agarose gel even when amplified in the combination reaction. **B:** An example genotyping gel of mice from the *NPAS2*$^{fl/fl}$/*Alb-cre* breeding colony. The LoxP primers produce a 246 bp product validating the inclusion of the *NPAS2* LoxP site. The Cre2 primers detect the 408 bp Cre sequence in the mice with Cre expression allowing clear differentiation.

4.3.2 Validation of conditional KO of NPAS2 in liver

The *NPAS2*$^{fl/fl}$/*Alb-cre* mouse model should present a liver-specific loss of *NPAS2* exon 3. To validate that this modification occurred, genomic DNA was extracted from liver and brain tissue of both control and cKO mice, as well as wild type C57BL/6 mice. A PCR was performed using primers up and downstream of either of the introduced LoxP sites, these will present different products depending on the genomic sequence present, explained in Figure 4.3 A. The agarose gel showed the expected 650 bp products for both wild type mouse tissues, as expected from amplifications of *NPAS2* exon 3 lacking the inserted LoxP site. Amplification from both tissues of the control *NPAS2*$^{fl/fl}$ mouse produced the expected 825 bp product, including the LoxP insertion. In the tissue from a cKO *NPAS2*$^{fl/fl}$/*Alb-cre* mouse the LoxP inserted 825 bp product was amplified from the brain DNA while the 220 bp product was amplified from the genomic DNA in the liver. This shows excision of the targeted region (including exon 3) in the liver specifically of mice expressing Cre under an albumin promotor. This work was performed by PhD student Ruby Chrisp.

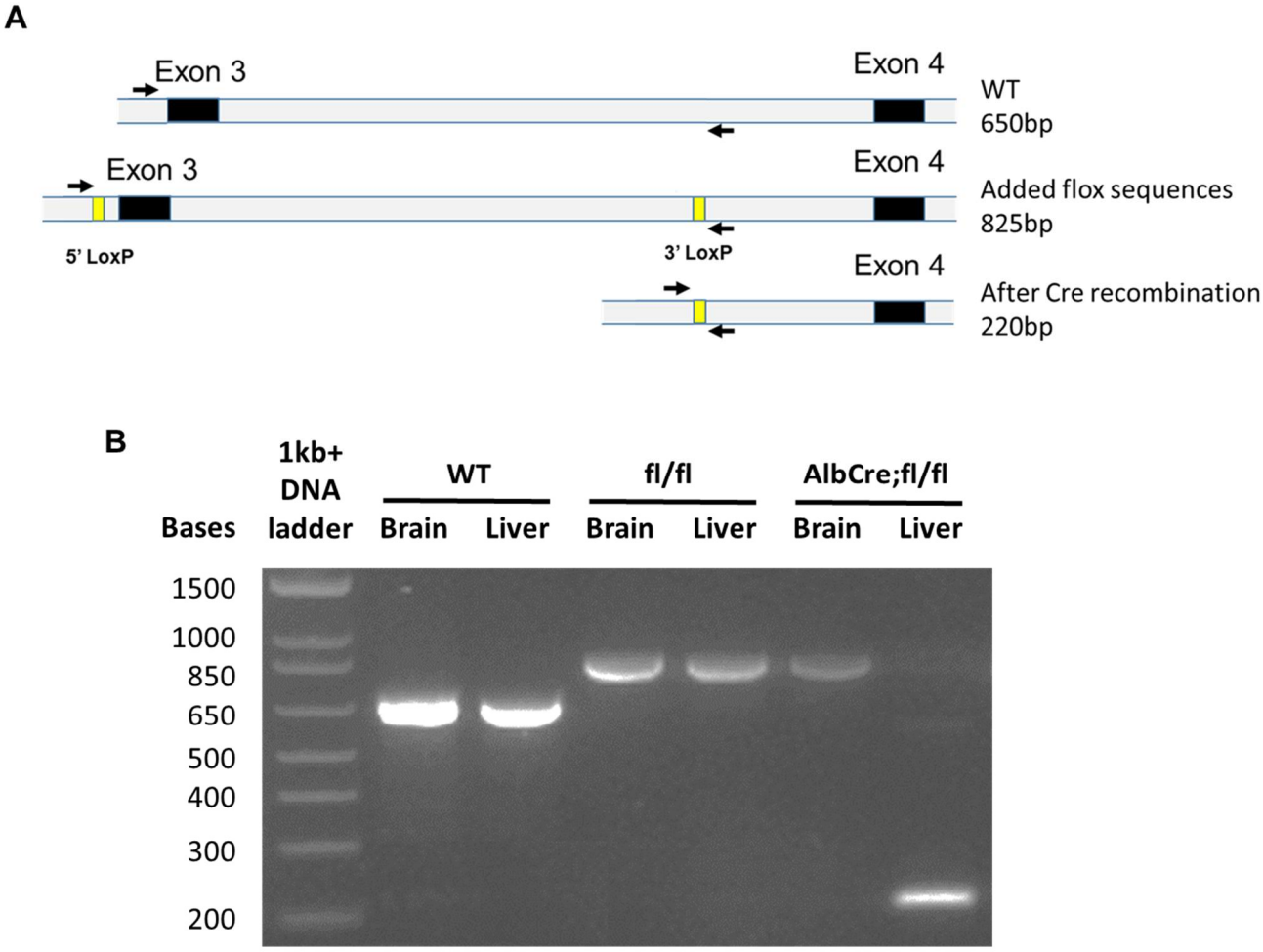

Figure 4.3: Confirmation of genetic modification in $NPAS2^{fl/fl}/Alb\text{-}cre$ cKO mice

A: Details of primers and expected product sizes for genomic amplification of wild type, floxed and excised *NPAS2* exon 3. **B:** Agarose gel of PCR products amplified from genomic DNA from brains and livers of specific genotype mice, performed by PhD student Ruby Chrisp. In both WT ($NPAS^{+/+}$) and floxed ($NPAS2^{fl/fl}$) mice both tissues present identical genomic DNA of the expected size and in mice expressing Cre under an Albumin promotor the 220 bp product amplified from the liver genomic DNA shows that Cre recombination has occurred while no recombination occurs in the brain.

4.3.3 RT-qPCR investigation of expression of core circadian genes in mouse tissues

Based on the detection of changes in the transcript levels of both *REV-ERB*s, *CLOCK* and *BMAL1* in ΔNPAS2 cell lines (see section 3.3.3.2, page 132), we assessed expression of these genes in female control and cKO mice. Gene expression was investigated at two time points; lights on (ZT0) and lights off (ZT12) to allow a measure of circadian effect. Gene expression was investigated in the liver as the tissue of interest with loss of NPAS2 expression in the modified mice, and the prefrontal cortex (PFC) as a non-SCN brain tissue. Along with the expression at the time points, the fold change in expression from ZT0 to ZT12 of each of the mouse genotypes was calculated and compared.

4.3.3.1 Core clock gene expression in the liver of control and liver cKO mice

Previously reported circadian expression of gene transcripts in the mouse liver are available in the circadian database CircaDB (Pizarro et al., 2013), this provides a normative base line against which the results can be compared. Note that ZT0 and ZT12 were used as time points here as they reflect peak and lowest expression of *CLOCK* and *BMAL1* and differences should be observable in the expression of both *REV-ERB*s between those time points with higher levels at ZT12. However, these time points do not reflect peak expression of the *REV-ERB* transcripts, *REV-ERBα* expression is highest as ~ZT7 and lowest at ~ZT20 while *REV-ERBβ* expression is highest at ~ZT9 and lowest at ~ZT0 (Pizarro et al., 2013).

In control floxed mouse livers the investigated transcripts showed the expected comparison in expression between time points; *CLOCK* and *BMAL1* both showed higher expression at ZT0 while the *REV-ERB*s showed higher expression at ZT12 (Figure 4.4). Analysis results are shown in Table 4.1.

A significant effect of time was observed for all genes. Supported by the comparisons of the expression between the time points consistent with the expression patterns from

CircaDB, this suggests we observed the normal circadian patterns of gene expression. The only significant genotype effect observed is the reduction of expression of *REV-ERBα* in the livers of cKO mice. Thus, ablation of NPAS2 was found to have a significant impact on expression of *REV-ERBα* in mouse liver.

Table 4.1: Factorial ANOVA comparison of gene expression in the liver of control and cKO mice

Gene	Genotype	Time	Genotype x time interaction
BMAL1	F(1,14)=0.008, p=0.932	F(1,14)=131.064, p<0.00001*	F(1,14)<0.001, p=0.991
CLOCK	F(1,14)=0.171, p=0.685	F(1,14)=54.666, p<0.00001*	F(1,14)=1.494, p=0.242
REV-ERBα	F(1,14)=8.05, p=0.013*	F(1,14)=39.862, p=0.00002*	F(1,14)=0.170, p=0.686
REV-ERBβ	F(1,14)=0.004, p=0.953	F(1,14)=126.683, p<0.00001*	F(1,14)=1.635, p=0.222

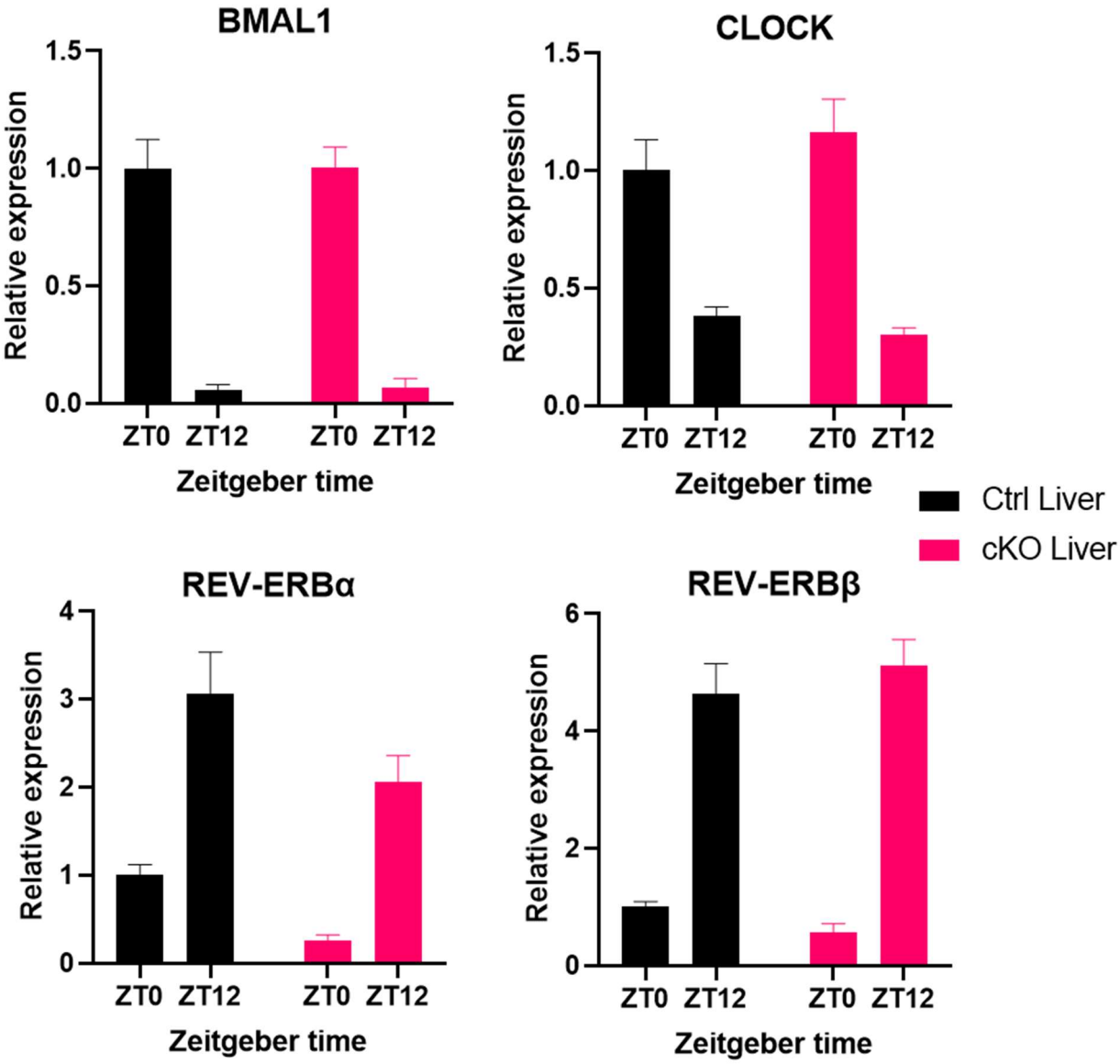

Figure 4.4: Liver gene expression in control and cKO mice

Mean relative expression (±SEM) of core circadian gene transcripts in the livers of control floxed (black) and conditional liver NPAS2 KO female mice (red) housed under 12h:12h LD conditions at ZT0 and ZT12. Relative expression values are based on RT-qPCR reads after $2^{-\Delta Ct}$ transformation based on *18S* reads, relative to the ctrl sample at ZT0 for each gene. Statistical analysis is presented in Table 4.1. A significant main effect of time was identified for the expression of all 4 genes, a separate main effect of genotype on *REV-ERBα* expression was also identified. No significant interaction effects were identified so pairwise comparisons were not investigated.

We also examined the fold change in expression of the four genes analysed from ZT0 to ZT12 (Figure 4.5, Table 4.2). This analysis identified significant increases in the fold change in expression of both *REV-ERB* transcripts in cKO mice. This observed increase of time-based variance in *REV-ERBα* is due to the decreased expression of the transcript in the cKO mice being more substantial at ZT0. This means that even though expression was reduced compared to control mice at both time points the difference between expression at the two time points is greater in cKO mice. The increase in fold change expression of *REV-ERBβ* is due to expression levels showing a subtle increase at ZT12 and a subtle decrease at ZT0 compared to expression in control mice. This suggests the amplitude of the rhythms of the *REV-ERB* genes may have increased even though the data suggests that the highest expression level of *REV-ERBα* has decreased. Although not reaching significance, the fold change in *CLOCK* expression is also further from 1 suggesting an increase in variation in the cKO mice.

Table 4.2: Independent t-testing of the effect of liver NPAS2 expression on the fold change in expression of circadian genes from ZT0 to ZT12 in the liver

Gene	Genotype fold change comparison
BMAL1	t(7)=-0.233, p=0.823
CLOCK	t(7)=1.923, p=0.096
REV-ERBα	t(7)=-2.663, p=0.032*
REV-ERBβ	t(7)=-7.704, p=0.00012*

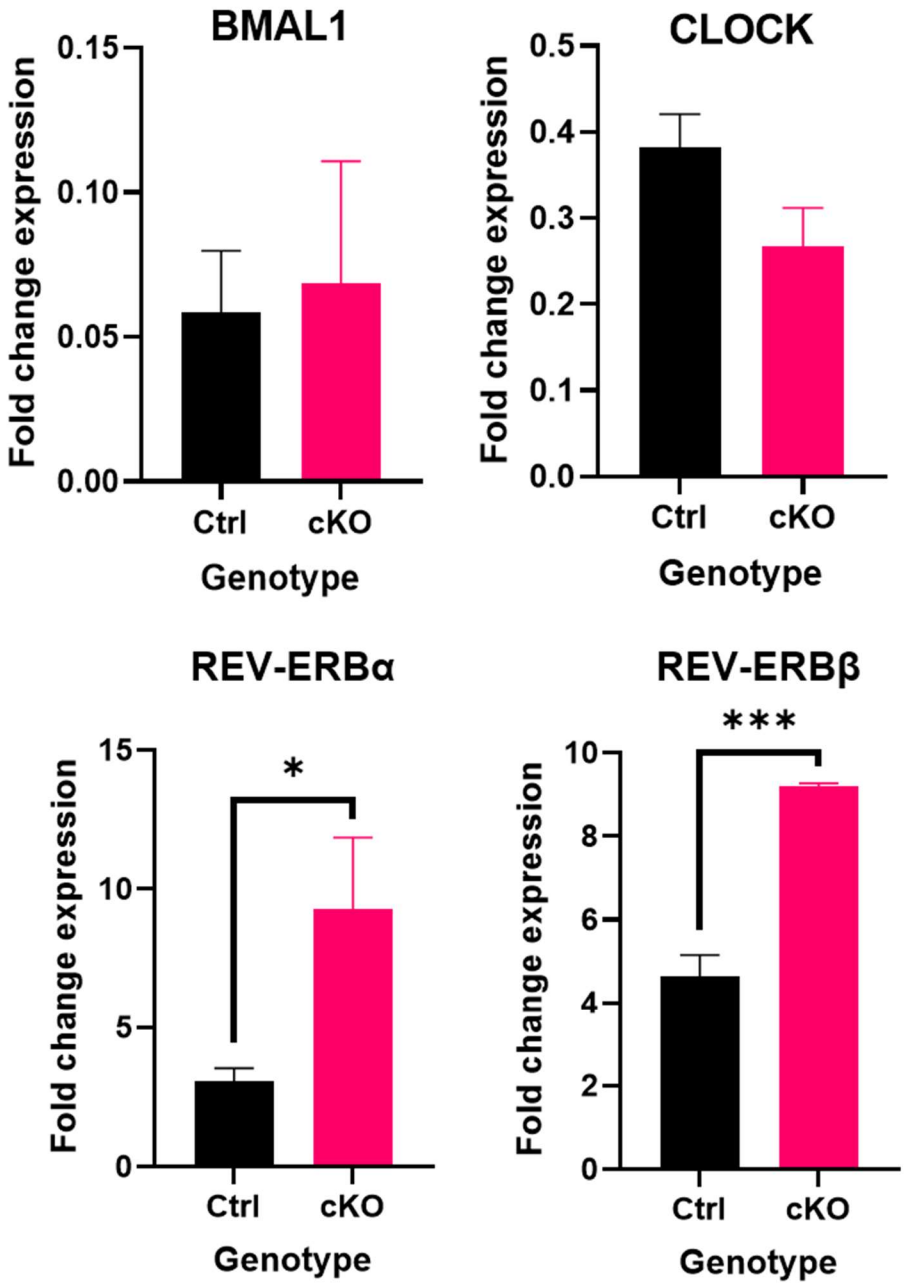

Figure 4.5: Rhythmic fold change in liver gene expression in control and cKO mice

Mean fold change (±SEM) in expression of circadian genes from ZT0 to ZT12 in the liver of control and cKO mice. Values higher than 1 reflect increased expression at ZT12 and less than 1 decreased expression at ZT12. The significance of independent t-test comparisons between WT and the ΔNPAS2 cells are shown (*=$p<0.05$, ***=$p<0.001$, details in Table 4.2).

4.3.3.2 Core clock gene expression in the prefrontal cortex (PFC) of control and liver cKO mice

Circadian expression of core circadian genes has been observed in the mouse PFC, and studies have shown that these cycles can be perturbed by circadian disorganisation (Otsuka et al., 2020). The reported gene expression patterns from this study provide a normative baseline of gene expression in the PFC. Both *CLOCK* and *BMAL1* were reported to show no rhythmic fluctuation in expression across time while *REV-ERBα* showed peak expression at ~ZT12 and low at ~ZT0 (Otsuka et al., 2020), *REV-ERBβ* expression was not investigated but it is assumed the expression pattern would be similar to *REV-ERBα* as is seen in most tissues.

We analysed the expression of four core circadian genes in the PFC of control and cKO mice at ZT0 and ZT12 (Table 4.3). Here we show that *CLOCK* and *BMAL1* expression in the PFC of control and cKO mice showed no significant change between ZT0 and ZT12, as a small apparent increase in *CLOCK* expression at ZT12 compared to ZT0 did not reach significance (Figure 4.6). Both *REV-ERBα* and *REV-ERBβ* showed ~2.5-fold higher expression at ZT12 compared to ZT0 (Figure 4.6). These observations are consistent with those previously reported (Otsuka et al., 2020).

Table 4.3: Factorial ANOVA comparison of gene expression in the PFC of control and cKO mice

Gene	Genotype	Time	Genotype x time interaction
BMAL1	F(1,14)=0.533, p=0.477	F(1,14)=8.079, p=0.013*	F(1,14)=5.885, p=0.029*
CLOCK	F(1,14)=0.001, p=0.974	F(1,14)=0.029, p=0.868	F(1,14)=7.353, p=0.017*
REV-ERBα	F(1,14)=0, p=0.987	F(1,14)=2.84, p=0.114	F(1,14)=2.439, p=0.141
REV-ERBβ	F(1,14)=0.914, p=0.355	F(1,14)=2.364, p=0.146	F(1,14)=4.985, p=0.042*

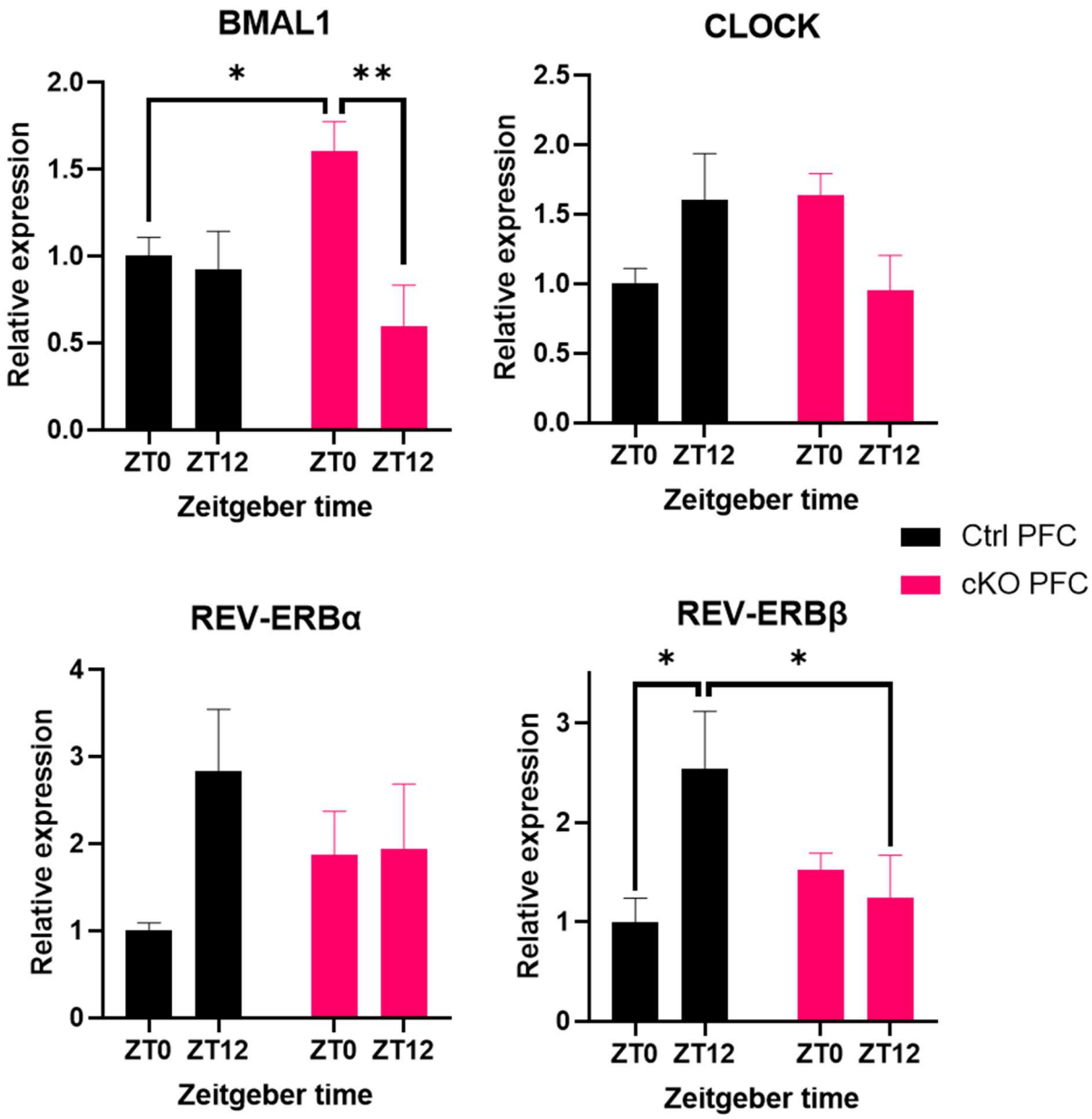

Figure 4.6: PFC gene expression in control and cKO mice

Mean relative expression (±SEM) of core circadian gene transcripts in the PFC of control floxed (black) and conditional liver NPAS2 KO female mice (red) housed under 12h:12h LD conditions at ZT0 and ZT12. Relative expression values are based on RT-qPCR reads after $2^{-\Delta Ct}$ transformation based on *18S* reads, relative to the ctrl sample at ZT0 for each gene. The results of statistical analysis of main effects are shown in Table 4.3. The significance of post hoc simple main effect comparisons within genotype or time point are shown (*=p<0.05, **=p<0.01, details in Table 4.4).

A significant interaction of genotype x time was observed in the expression of the *BMAL1*, *CLOCK* and *REV-ERBβ* genes. These interaction effects were further investigated by post hoc pairwise comparison, the results of this analysis are shown on the graphs of Figure 4.6 and in Table 4.4. These comparisons identified a significant change in *BMAL1* expression across time points specifically in cKO mice and a change in *REV-ERBβ* expression specifically in control mice. A significant change between genotypes at specific times was observed at ZT0 for *BMAL1* and ZT12 for *REV-ERBβ*. The appearance or loss of the time point difference is the most interesting, with the change between genotypes at time points primarily a reflection of this. Despite the significant interaction effect on CLOCK expression no significant pairwise comparison was identified. It appears changes were too subtle to be identified as statistically significant, although from the graph it appears an inversion of the timing of higher expression is observed in the cKO mice. Further time points would be required to understand these effects in more detail. No significant effect was identified on the expression of *REV-ERBα*, however the observed expression pattern suggests loss of variation in expression from ZT0 to ZT12, similar to *REV-ERBβ*.

Table 4.4: Post hoc pairwise comparison of gene expression levels in the PFC of control and cKO mice investigating the effect of genotype at each time point and the effect of time within each genotype

Comparison	***BMAL1***	***CLOCK***	***REV-ERBβ***
Ctrl:cKO @ ZT0	p=0.043*	p=0.079	p=0.382
Ctrl:cKO @ ZT12	p=0.250	p=0.073	p=0.041*
ZT0:ZT12 in ctrl mice	p=0.759	p=0.077	p=0.013*
ZT0:ZT12 in cKO mice	p=0.003*	p=0.074	p=0.648

The fold change in expression from ZT0 to ZT12 is shown in Figure 4.7, analysis results are presented in Table 4.5. This analysis identified significant changes in the fold change

expression of *REV-ERBβ* and *CLOCK* transcripts in cKO mice. Based on the fold change values this suggests we observe a loss of change in *REV-ERBβ* expression across timepoints but an inversion in the change in *CLOCK* expression across timepoints in cKO mice. It should be noted that the post hoc comparison analysis of *CLOCK* expression did not identify a significant effect of time in either control or cKO mice, and there is reported to be no rhythmic circadian expression of *CLOCK* in the PFC (Otsuka et al., 2020), as such this result will require further investigation. It is possible that the subtle effect observed is due to rhythmic expression of CLOCK in the other brain regions included in our investigation.

Table 4.5: Independent t-testing of the effect of liver NPAS2 expression on the fold change in expression of circadian genes from ZT0 to ZT12 in the PFC

Gene	Genotype fold change comparison
BMAL1	t(7)=2.057, p=0.079
CLOCK	t(7)=2.602, p=0.035*
REV-ERBα	t(7)=2.156, p=0.068
REV-ERBβ	t(7)=2.501, p=0.041*

The fold change in the expression of *REV-ERBβ* was reduced to ~1 suggesting a loss of the circadian rhythmicity, supported by the findings of the relative expression shown in Figure 4.6 and addressed above. Although not reaching significance, the fold change in *BMAL1* expression is numerically reduced from 1, combined with the significant pairwise analysis of the expression levels data, this suggests a circadian pattern of *BMAL1* expression in the cKO mouse PFC which is not seen in the PFC of control mice. In the inverse of this, the fold change in *REV-ERBα* expression is ~3 in the control mice but ~1 in the cKO. Taken together these data show a definite effect of loss of NPAS2 expression in the liver on rhythmic expression of core circadian genes in the PFC. This suggests both that expression of clock genes in the liver influences distant molecular tissue clocks and that NPAS2 contributes to this function of the liver.

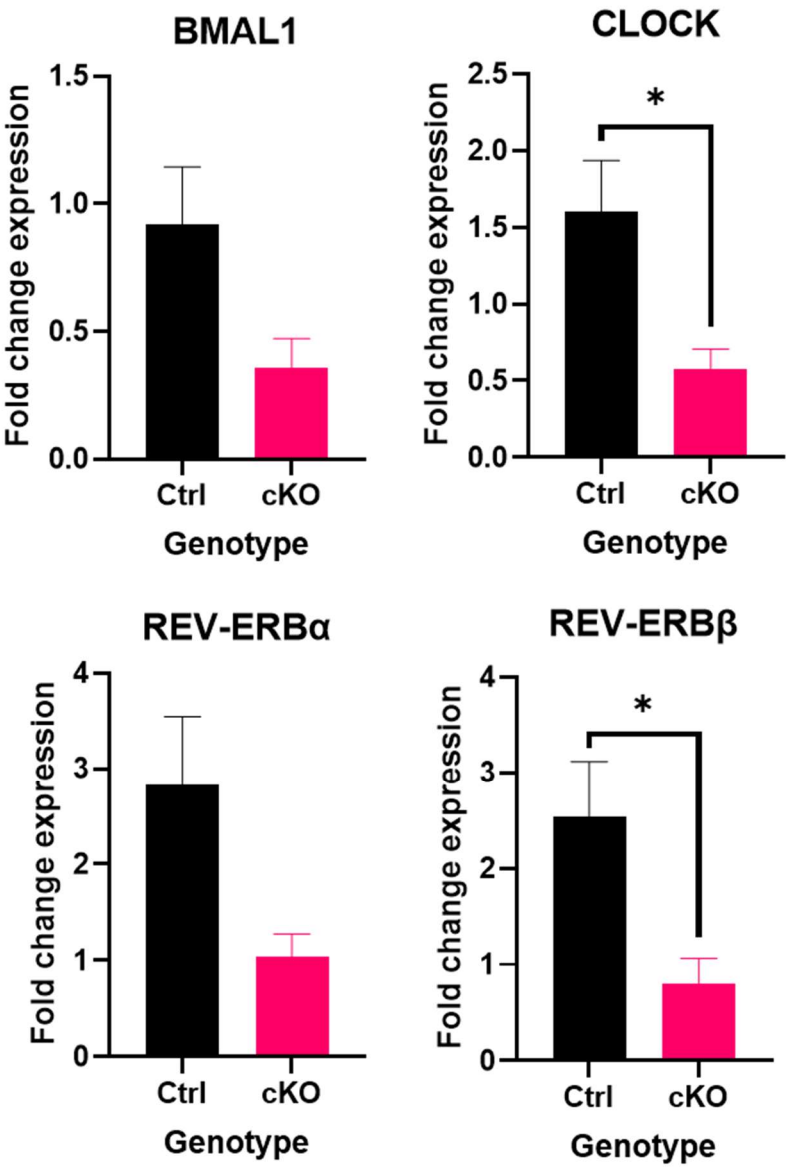

Figure 4.7: Rhythmic fold change in PFC gene expression in control and cKO mice

Mean fold change (±SEM) in expression of circadian genes from ZT0 to ZT12 in the PFC of control and cKO mice. Values higher than 1 reflect increased expression at ZT12 and less than 1 decreased expression at ZT12. The significance of independent t-test comparisons between control and cKO mice are shown (*=$p<0.05$, details in Table 4.5).

4.4 Discussion

4.4.1 Results summary

The expected genomic modifications were validated to occur within the liver tissue of the cKO mice but not in brain tissues (Figure 4.3). Investigation of gene expression found that in the liver of cKO mice the expression of *REV-ERBα* was decreased compared to the control mice (Figure 4.4). In the brain region investigated, genotype time interaction effects were identified on the expression of *BMAL1*, *CLOCK* and *REV-ERBβ*. A significant difference in the expression of *BMAL1* between timepoints was only identified in cKO mice while a significant timepoint difference in *REV-ERBβ* expression was only observed in cKO mice (Figure 4.6).

4.4.2 Model validation

We have validated the NPAS2 cKO mouse model, showing liver-specific loss of *NPAS2* exon 3 (Figure 4.3). A loss of exon 3 has been previously characterised, as this is utilised in the established constitutive KO mouse model, and while a truncated NPAS2 protein may still be expressed, this ΔbHLH-NPAS2 protein is unable to perform its normal function (Garcia et al., 2000). As such this mouse model shows functional KO of NPAS2 in the liver while in other tissues the gene is unaffected. These floxed mice also have the potential to be bred with alternative Cre expressing mice to produce various other tissue-specific KO models.

4.4.3 Knockout of NPAS2 expression in the liver modulates liver expression of the *REV-ERB* genes

In the liver of cKO mice, where NPAS2 function was lost, we observed significant effects on the fold change in expression between time points of both *REV-ERB* transcripts and a significant reduction in *REV-ERBα* expression irrespective of time point. This contrasts with the results in the cell culture model, where we observed increased expression of the transcripts

primarily at times of peak expression (see section 3.3.3.2, page 132). It is likely that the effects are modulated by unique tissue-specific factors between the liver and fibroblasts (Yeung et al., 2018, Beytebiere et al., 2019), such as the nuclear receptor hepatocyte nuclear factor 4 alpha (HNF4α) which is expressed in hepatocytes but not fibroblasts (Qu et al., 2018) but could also be the effect of synchronisation signals from other unmodified tissues present in the *in vivo* model but absent in the cell culture model.

Despite the differences it is still of note that in both models, where NPAS2 function is lost but CLOCK is unaltered, we see alterations in expression of the *REV-ERB* genes which results in an increase in variation of transcript expression across time. In the SCN constitutive NPAS2 KO was not associated with any change in *REV-ERBα* expression (DeBruyne et al., 2007a) supporting the contribution of tissue specific factors to this effect in peripheral clocks. The reduction of *REV-ERBα* expression levels suggests that in the liver NPAS2 normally acts to induce *REV-ERBα* expression, hence, the loss of NPAS2 then inhibits expression. The effect on *REV-ERBβ* expression is more subtle, appearing as an increase at the time of high expression and a decrease at the time of low expression.

The REV-ERB proteins have been shown to link circadian cycles and metabolism. Depletion of the expression of both REV-ERBs has been shown to derepress the expression of multiple metabolic genes and causes hepatic steatosis (Bugge et al., 2012). Interaction between NPAS2 and the REV-ERBs may be responsible for the metabolic importance of NPAS2, meaning it is of interest to identify what this change in expression can mean in terms of effects on the expression of other genes.

Both *BMAL1* and *CLOCK* transcripts in the liver retain their rhythmicity without significant changes in expression observed in the cKO mice. This again contrasts with the findings in the ΔNPAS2 cells which showed decreased *BMAL1* expression and increased *CLOCK* expression. As the significant increase in expression of the *REV-ERB* transcripts is not

observed in this model it may be unsurprising to note that we have not observed the repression of *BMAL1* expression which was likely to be, at least in part, due to increased repression though REV-ERB activity at RORE sites blocking *BMAL1* transcription. Based on some of the hypotheses proposed in Chapter 3 (section 3.4.5, page 143), it may be that the increased CLOCK protein expression is required for the increased *REV-ERB* expression through elevated transcription rates. As such we are not able to identify one specific effect responsible for the difference from the cell models. Whatever specific effect is responsible, the difference between this data and that from Chapter 3 may be due to tissue-specific variation in factors influencing the circadian cycle or even the presence of external signals to the liver which would occur in the mouse organism (Hughes et al., 2009). An effect of entraining signals from other tissues is very likely especially in a model where the circadian clock in all other tissues is genetically unmodified.

4.4.4 Distant clocks are influenced by the loss of NPAS2 expression in the liver

NPAS2 expression in the PFC is not expected to be modified, supported by the genotyping investigation (Figure 4.3). Despite this, significant alterations in *BMAL1*, *CLOCK* and *REV-ERBβ* expression in the PFC of cKO mice were observed, while expression of *REV-ERBα* also appeared modified although the data did not reach statistical significance. This result suggests a correlation between loss of liver NPAS2 expression and altered rhythmic expression of core circadian genes in the PFC. This is surprising as based on our data, the circadian cycles in the liver appear to have only changed subtly and under LD we would expect most tissues to retain entrainment to the light cycles via the SCN, without any modulation by the liver circadian clock. Importantly, in the liver, despite the observed changes, the pattern of time expression of the genes has remained, while in the PFC we saw loss of the time point variation of *REV-ERBβ* (and also *REV-ERBα*), the appearance of time point variation of

BMAL1 and the inversion of the fold change across time points of *CLOCK*. Expression of *BMAL1* was shown by Otsuka et al. (2020) to be constant without circadian rhythmicity in the PFC which our data from control mice also shows. The appearance of cycling BMAL1 protein levels in cKO mice will influence the core circadian cycle and many more cycling genes than the ones tested here will likely show modified expression patterns in the PFC of cKO mice.

The specific changes in gene expression may provide part of an explanation of the effects observed. A possible mechanism is presented in Figure 4.8. As the expression of the *REV-ERB*s depends on BMAL1, we know that in the PFC the arrhythmic expression of *BMAL1* means another factor must play a role in the circadian *REV-ERB* expression. In Figure 4.8 this is presented as a repressor, such as PER2, the *PER2* transcript has been reported show peak transcript expression a few hours after peak *REV-ERBβ* expression in the PFC (Otsuka et al., 2020), making this a reasonable candidate. However, any cycling input affecting *REV-ERBβ* expression could reasonably fill this role including activators of expression. As such, the cycling *BMAL1* expression in the cKO mice may then act counter to this regulation and act to balance it out, either due to similar phase expression to a repressor, or antiphasic expression to another activator. This then means that *REV-ERB* expression is constant. The reverse is also possible, in that the cycling expression of the REV-ERB proteins may contribute to the static expression of *BMAL1*, in conjunction with another circadian regulated factor. In Figure 4.8 this other factor is presented as an activator of *BMAL1* expression, such as ROR, however as stated above, a repressor of expression could also fill this role. A loss of the variation of REV-ERBβ protein expression in the cKO PFC would mean the complementary patterns of repression of *BMAL1* transcription, specifically by REV-ERB at RORE sites, is lost, leading to cycling expression. Potentially, any rhythmically expressed factors which affects the expression of *BMAL1* and *REV-ERBβ* can fill the gaps in this model as long as the circadian patterns of that factor are not modified in the cKO mouse. This model was kept simple for clarity, it is more is

likely there are transcription effects by multiple different proteins with different cycles of activity resulting the observe gene expression. While this hypothesised model could explain some of the expression patterns and show how modulation of any circadian gene expression can modify the whole feedback system, it is still unclear what causes this change in the PFC.

The apparent change in the expression of *CLOCK* is less clear due to the more subtle changes in expression levels meaning we do not directly observe a significant difference in expression between timepoints in ctrl or cKO mice (Table 4.4). However, it appears that we do see subtle time point variation in expression in control mice, although this was not observed by Otsuka et al. (2020). To further investigate this, more time points may be useful as we may be missing the times of peak and lowest expression which would be more useful in understanding the effect on the circadian cycles of the PFC.

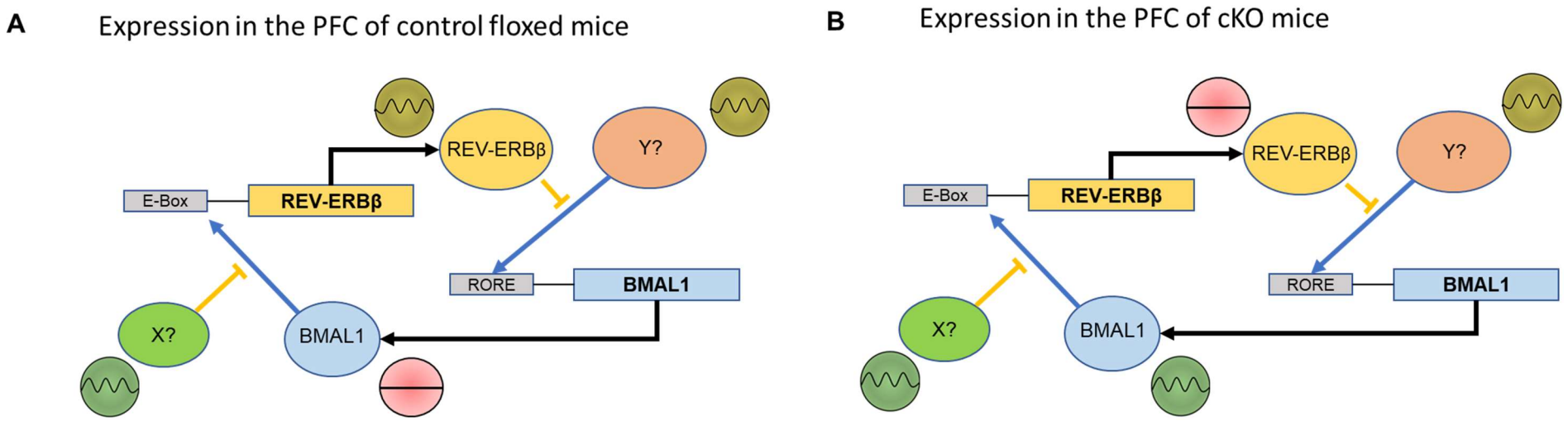

Figure 4.8: Hypothesised modifications to the feedback loop of RORE influenced BMAL1 expression

A: Hypothesised normal function of the feedback loop in the PFC of control mice. BMAL1 arrhythmically induces the expression of *REV-ERBβ*. The rhythmic expression of *REV-ERBβ* is due to rhythmic activity of a repressor of BMAL1 activity (X) such as the PER or CRY proteins. REV-ERBβ rhythmically represses the expression of *BMAL1* induced by an activator of *BMAL1* transcription (Y) such as RORα. The arrhythmic expression of *BMAL1* is due to the synchronous rhythmic expression of Y to REV-ERBβ meaning transcription rates remain comparable at all times due to increased repression of activity at time of higher induction of transcription. **B:** Hypothesised modified function of the feedback loop in the PFC of cKO mice. The rhythmic expression of BMAL1 would lead to rhythmic activation of transcription of *REV-ERBβ* however synchronous rhythmic expression of X leads to comparable transcription rates of *REV-ERBβ* at all times. This constant expression means that the rhythmic activation of transcription of *BMAL1* by Y leads to rhythmic expression.

4.4.5 Communication of the liver and the PFC

These results suggest that the loss of NPAS2 in the liver modifies circadian gene expression in the PFC. This could occur via nervous feedback through afferent nerves to the brain or hormonal/metabolite feedback, or a combination of these involving different tissues. No findings to date have identified circadian communication from the liver through any afferent nervous communication to the brain. Afferent nerves from the liver are however able to detect glucose levels and send signals which influence the initiation of food intake (Yi et al., 2010), suggesting that afferent nervous connections from the liver to the brain may play a role in circadian entrainment to the liver clock.

The liver plays a pivotal role in blood glucose circadian homeostasis due to its role in glucose uptake and forming the major site of glucose synthesis, with liver-specific BMAL1 KO leading to perturbations of cycling blood glucose levels (Lamia et al., 2008). If the cKO mice show a modulation of the metabolic output from the liver, then blood glucose levels may influence the circadian cycles in the brain. Information in the form of metabolites or hormones in the bloodstream can reach the brain without having to cross the blood brain barrier via the circumventricular organs: organum vasculosum of the lamina terminalis (OVLT), the subfornical organ (SFO), the area postrema (AP) and the arcuate nucleus (ARC). If the metabolic state of cells in these brain regions are modified, then the molecular clocks can be entrained in response to this through several metabolic effects on the metabolic feedback loop (as detailed in section 1.6, page 33). These brain regions can then influence circadian cycles throughout the brain. The ARC specifically has been reported to detect circulating glucose levels and even communicate directly to the SCN among other regions (Yi et al., 2006) making this a region that may be part of this liver influence on brain circadian cycles.

Elevated glucose levels within the brain have also been identified to influence melanin-concentrating hormone (MCH) and orexin neurons of the lateral hypothalamus (LH)

which exert opposing effects on arousal and metabolism. Glucose enhances the function of MCH neurons and has the opposite effect on orexin neurons (Burdakov et al., 2005). Despite the clear links between blood glucose levels and circadian cycles in the brain, in our model, our data does not suggest that normal metabolic liver function was modified in any way and no effects are noted on the mouse physiology, so it is not known whether blood glucose levels are affected.

As noted in section 4.1.1, the liver-derived ketone body β-hydroxybutyrate can also entrain other tissues and contributes to behavioural entrainment to RF (Chavan et al., 2016). If the loss of NPAS2 in the liver influences β-hydroxybutyrate production, then this may be responsible for the modulation of the separate circadian cycles.

Peripheral clocks have also been shown to be reset by hormones with circadian influence over their expression, notably insulin (Sato et al., 2014), glucagon (Sun et al., 2015), leptin (Wiater et al., 2013) and ghrelin (LeSauter et al., 2009) among others. Receptors for metabolic hormones like insulin, leptin and ghrelin allow the ARC to sense information from the periphery and signal it to the central nervous system (Buijs et al., 2006) and ARC leptin receptors have been found to contribute to circadian rhythmicity (Coppari et al., 2005). The liver can produce the hormone insulin-like growth factor 1 (IGF-1) which has been reported to influence circadian cycles in various tissues (Crosby et al., 2019). If the expression of IGF-1 is modified in cKO mice, then activity at the ARC may influence circadian cycles. Alternatively, indirect activity of IGF-1 at another tissue, such as the adipose, may influence leptin levels which could then affect brain circadian cycles. Any of these hypotheses would require further work to prove or invalidate them.

4.4.6 Future work

We have identified effects of the loss of NPAS2 in the liver on the expression of core circadian genes, both within the liver and also surprisingly within the PFC. Based on this data

across this chapter and Chapter 3 we have observed that loss of NPAS2 has effects on expression of the *REV-ERB* genes, however, the effects are different between the fibroblast cell culture and *in vivo* liver. As such it may be of interest to further characterise tissue-specific factors which influence NPAS2 activity. Since we are observing an effect on *REV-ERB* expression, part of a feedback loop which directly affects NPAS2 expression in normal conditions, it would be of interest to look at the expression of the *ROR* genes which act counter to REV-ERBs in this feedback loop.

For some of the changes in expression we see, it is possible that the effect is due to change in either amplitude or timing of the cycle. For instance, in the PFC our data cannot conclusively tell the difference between non-rhythmic expression and rhythmic expression where both ZT0 and ZT12 fall between peak and lowest expression. Although, since this then requires a very specific pattern this is unlikely. To validate or investigate our findings in more detail, RT-qPCR investigation of gene expression at more time points would be useful. RNA seq analysis could be used to investigate all transcripts in the tissues at multiple timepoints.

To further investigate the effect of the liver NPAS2 cKO, it may be of interest to investigate other tissues or brain regions to see if there is an effect on circadian cycles in other peripheral tissues. Investigation of the levels of blood glucose and β-hydroxybutyrate and metabolomics analysis of the serum and brain tissue throughout the day may provide insight into the cause of the modified gene expression in a separate circadian clock.

Chapter 5: Circadian behavioural entrainment in *NPAS2*$^{fl/fl}$/*Alb-cre* liver knockout mice

5.1 Introduction

5.1.1 Entrainment of circadian cycles and free-running

Circadian cycles are entrained by zeitgebers, meaning the cycles are synchronised to these signals to match the external environment (see section 1.1, page 22). Light is the primary zeitgeber which entrains and synchronises circadian cycles through the SCN (Takahashi et al., 2008). However, a variety of other signals have also been shown to synchronise behavioural cycles. In addition to light, time of feeding is a powerful zeitgeber which synchronises peripheral clocks and ensures the animal is awake and active at the time when food is available. Entrainment by zeitgebers is a daily process of resynchronising behaviour, when an animal is isolated from zeitgebers and under constant conditions it is no longer subject to the process of entrainment. In the absence of rhythmic zeitgebers patterns of behaviour are dependent on the intrinsic circadian free-running period, which tends to be close to, but not exactly, 24 hours, causing behaviour to steadily fall out of external daily synchrony (Panda et al., 2002b).

Light entrainment can easily be observed experimentally. Under normal light-dark cycling (LD) conditions, high activity at times of darkness is seen in nocturnal animals. When lighting cycles are modified, the entrainment to light can be seen in the shift of behavioural cycles, such that the active period of the animal occurs during the new dark phase. Acute shifts in behavioural cycles can also be caused by entrainment in response to short pulses of light when the animals are under constant darkness (DD) conditions in a time specific manner (LeGates and Altimus, 2011).

Food entrainment is observed when food is restricted to a specific time of day within a mouse's inactive phase. Under these conditions, rodents begin to show a period of activity in advance of the time of regular food provision. This is known as food anticipatory activity (FAA) (Richter, 1922). This FAA behaviour is controlled by the output of an incompletely identified circadian food entrainable oscillator (FEO), a biological clock entrained by food

availability, the output of which can be seen in FAA and molecular cycles in peripheral tissues (Mistlberger, 1994). The FEO is independent of the SCN, not cycling in synchrony nor requiring the function of the SCN, and has been shown to function even in the absence of canonical clock genes (Pendergast and Yamazaki, 2018).

The FEO has not been identified as existing as a single oscillator within one organ and while it has been posited that the FEO is possibly formed from the activity of multiple entwined loci, it is still possible that a final common circadian clock for food anticipation exists (Mistlberger, 2020). The liver has been suggested as an important organ for circadian entrainment to food as it is entrained to times of food availability and has been associated with RF entrainment of circadian endocrine signals (Hara et al., 2001, Díaz-Muñoz et al., 2000). It has been shown that a liver-specific KO of PER2 abolishes FAA as does a constitutive KO. This abolition is not seen in a brain specific PER2 KO (Chavan et al., 2016), suggesting a fully functional circadian clock in the liver may be more important than in the brain for FEO entrainment. However, it should also be taken into account that there is conflicting information as to the role of PER2 in FAA; under different food restriction conditions and with running wheel availability PER2 constitutive KO mice show normal FAA (Pendergast et al., 2017). It has also been shown in mice with a brain specific BMAL1 KO, effectively knocking out circadian cycles in the brain, that while most tissues become asynchronous under DD, the introduction of restricted feeding (RF) is sufficient to resynchronise liver and kidney circadian cycles while other peripheral tissues remain unsynchronised (Izumo et al., 2014). Since this suggests liver is entrained by RF independently of the brain it is possible that the entrained liver clock contributes to entrainment of circadian cycles in the brain to RF. The entrained brain clock would then be responsible for entrainment of other peripheral tissues.

These investigations of the responses of mouse models to the zeitgebers of light and food availability contribute to understanding the role of specific genes and tissues within

regular circadian maintenance. While the mechanisms of the core feedback loop are fairly well understood (e.g., how CRY and PER prevent the activity of the CLOCK/NPAS2:BMAL1 dimer) it is less well characterised how this feedback loop is externally influenced in the processes of entrainment. Nor is it fully known, especially as noted in the case of the FEO, how different tissues contribute to the circadian timing of an organism.

5.1.2 NPAS2 in circadian entrainment – studies in constitutive mouse models

Constitutive NPAS2 KO mice in DD have been shown to have a reduced free-running period compared to WT mice (23.7 (WT) and 23.5 (NPAS2 KO)) based on wheel running behaviour (Dudley et al., 2003). This shortening of the free-running period was likely due to the impact of loss of NPAS2 within the core feedback cycle, but the retention of rhythmic activity shows that the core clock feedback loop was still functional in these mice. The delay due to loss of NPAS2 appears similar to the impact of the CLOCK KO on free-running cycles while knocking out both genes renders mice arrhythmic (DeBruyne et al., 2007a). This suggests a similar effect of loss of one of the BMAL1 dimerisation partners on free-running period and that the overlapping functions of CLOCK and NPAS2 are sufficient to retain circadian free-running behaviour with minimal effect in the absence of the other gene.

The activity profiles of constitutive NPAS2 KO mice were also found to vary significantly from wild type mice; NPAS2 KO mice showed increased wheel-running activity and reduced sleep during the latter part of the dark phase of the LD cycle (ZT19-ZT22) (Dudley et al., 2003). This suggests a role of NPAS2 in the maintenance of normal activity patterns, as the normal circadian timings are, for the most part, retained it is likely that this is due to a role outside the SCN.

Constitutive NPAS2 KO mice have been shown to have an enhanced response to light entrainment but are deficient in entrainment to food availability. While wild type mice exposed

to a phase advance of the LD cycle of 4 hours shifted their activity to match the new light cycle over a few days, NPAS2 KO mice activity shifted almost completely within the first day. This showed that behaviour was more efficiently synchronised by light signals in NPAS2 KO mice (Dudley et al., 2003).

Although the NPAS2 KO model does not present increased expression of CLOCK as a compensatory protein, it was suggested that the contribution of CLOCK:BMAL1 to the circadian feedback cycle may be of greater importance for synchronisation to light in the SCN than NPAS2:BMAL1. According to this hypothesis the NPAS2 KO model favours entrainment to light as the feedback loop is entirely dependent on CLOCK:BMAL1 activity (Dudley et al., 2003). This is somewhat supported by a reported decrease in phase delay response to early active phase light entrainment in CLOCK constitutive KO mice, however a substantial increase in phase advance in response to late active phase light entrainment was also observed (Debruyne et al., 2006). This suggests specific directionality of the influence of the core circadian genes in light entrainment.

In contrast to light entrainment, the constitutive NPAS2 KO mice have been shown to have impairment in responding to time restricted food provision, although entrainment was not completely abolished. Under restricted feeding conditions NPAS2 KO mice showed a slower increase in FAA compared to wild type mice, taking three days longer to reach the peak activity level (Dudley et al., 2003). This suggests the phase shifting of FEO was less responsive to the restricted food entrainment in the KO mice. Although the mice were in constant darkness, the behavioural shift in KO mice still occurred faster than the shift due to the effect of free-running cycles alone and activity remained persistent after the shift to match the time of food availability. This shows that while entrainment was delayed, the FEO remained functional in these mice.

This suggests NPAS2 plays a role in entrainment of the FEO in response to feeding,

most likely contributing to pathways through which the cellular metabolic state influences circadian cycles (see section 1.6, page 33). The mechanism of this may include the influence of the redox state on the NPAS2:BMAL1 heterodimer (Rutter et al., 2001) and the influence of haem on the REV-ERB proteins (Raghuram et al., 2007), which can modulate NPAS2 expression.

Taken together this data suggests that NPAS2 primarily plays a role in food rather than light entrainment. Inhibiting entrainment to light cycles (by SCN ablation) has been associated with improved entrainment of circadian cycles to timed feeding (Saini et al., 2013). Any reduction of entrainment to feeding times may be the direct cause of the faster light entrainment, due to a similar mechanism of decreased competing circadian entrainment.

5.1.3 Restricted feeding response in conditional liver-specific NPAS2 knockout mice

The mouse model used in the following experiments, with a conditional KO of NPAS2 in the neonatal liver, has previously been investigated under conditions of RF. These studies measured body weight of the mice and the response in the microbiome. It was observed that recovery of weight after initial weight loss when food was restricted to the light/inactive phase under LD was accelerated in males or unchanged in females compared to floxed controls (O'Neil et al., 2017). This enhanced weight loss recovery may suggest enhanced entrainment. However, these experiments did not measure behavioural activity. Without knowledge of how activity was affected, the change in weight loss and recovery may be due to other effects of the genetic modification, potentially impacts on the microbiome (the primary focus of the O'Neil paper). This is supported by the correlation of weight changes with specific microbiota genera which differed between WT and cKO mice after RF (O'Neil et al., 2017).

5.1.4 Methods of investigation of circadian cycle entrainment

For the experiments performed here various protocols were considered. Light based

entrainment of mouse circadian cycles is often investigated by use of light pulses. Single short pulses of light can induce circadian phase shifts depending on the time at which mice are exposed to the pulse. The use of multiple pulses at different circadian times allows the construction of a detailed phase response curve (PRC) detailing how light pulses at each time point influence phase shifts and potential genotype effects on specific directionality of entrainment (LeGates and Altimus, 2011, Banks and Nolan, 2011). See Figure 5.1 for an example PRC.

The light pulse experimental protocol can be performed in one of two ways. Light pulses are performed at specific times within the behavioural cycle, either after several days in DD based on predicted activity onset or on the first day in DD after LD based on the timing of the lighting schedule. The first protocol can be more efficient as it allows for administration of successive pulses following the same protocol without days of reentrainment to LD while the second protocol removes the need for calculation immediately prior to the light pulse and does not subject mice to unique timed light pulses. These are referred to as *Aschoff* type I and type II protocols respectively (Jud et al., 2005).

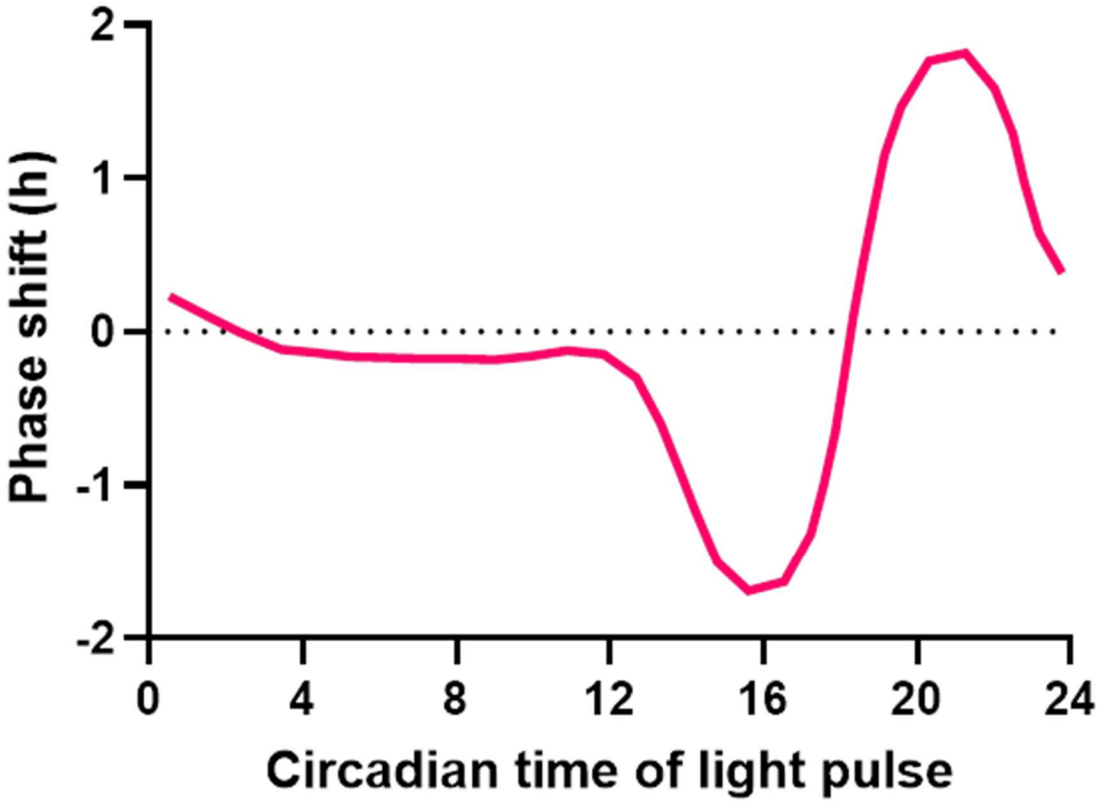

Figure 5.1: An example phase response curve (PRC) for mice

Created based on the phase response curve by LeGates and Altimus (2011). A light pulse during the subjective day (CT0-12) does not induce a significant shift. A light pulse in early subjective night (CT12-19) causes a phase delay and late in subjective night (CT19-24) a phase advance. Investigation by light pulse allows identification of the pattern of the PRC and can show differences in phase shift based on where in the circadian cycle the light pulse is administered.

The investigation of circadian entrainment to feeding is more constrained than investigation of light as unlike light, food is essential for survival, meaning most light entrainment procedures are impossible with food provision. Food entrainment by the FEO is often analysed by use of time restriction of food availability and monitoring daily activity for the development of entrained FAA. Under LD conditions this can appear as a distinct peak of activity or extension of previous activity to include the window prior to food provision while in DD mice phase shift so their active period begins in advance of food provision (see Figure 5.2) (Takasu et al., 2012).

Food restriction under DD will show the entrainment to the timing of food provision, however these results can be complicated by free-running meaning any change in free-running behaviour may be observed as an impact on RF entrainment. For example, a shorter free-running period would mean a mouse could shift faster to an earlier active phase as entrained by food (assuming no effect on the FEO). Testing RF under LD will not cause an obvious phase shift as the primary synchronisation of behaviour by the SCN to the light cycles remains intact. RF under LD can disassociate and desynchronise the FEO from the SCN cycles if the food is provided during the inactive light phase. The phase shifting of the FEO will present as the appearance of a FAA peak separate to the normal activity. This has the benefit of the peak during the light being isolated as a response of the FEO entrainment (Pendergast and Yamazaki, 2018). See Figure 5.2 for example potential actograms.

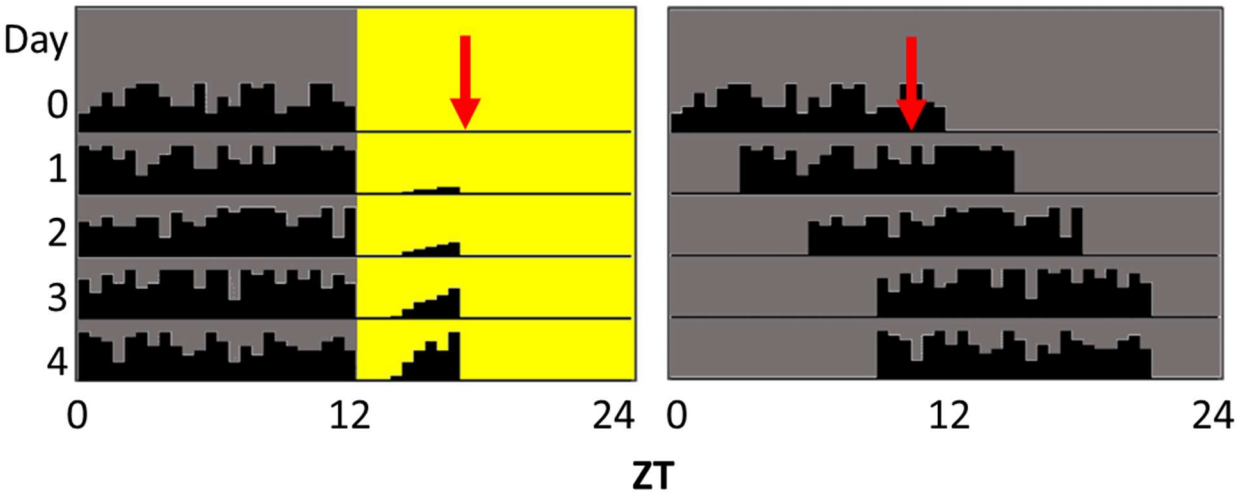

Figure 5.2: Example actograms showing FAA

These actograms show how behaviour patterns may look under RF while in LD (left) or DD (right) conditions. Red arrows mark times of food provision and the background colours represent the lighting, yellow means lights on and grey means lights off. In the LD example activity is not presented after food provision to keep the representation simple. This is very similar to what would be seen if activity were recorded for wheel running as the animal would stop wheel running to eat, while for general activity low level would be seen with peaks at the points of food provision and removal due to this process agitating or waking the mice.

5.1.5 Aims, experimental justification and hypotheses

The aim of these experiments was to investigate the impact of the liver NPAS2 cKO on circadian behaviour and entrainment. The investigations here are complimentary to those performed on constitutive NPAS2 KO mice by Dudley et al. (2003) to identify how their findings compare to those of the liver-specific cKO and address the specificity of the role of NPAS2 in liver peripheral clocks. Two behavioural experiments are detailed here; Experiment 1 investigated the free-running behaviour of the mice while under DD conditions within the circadian cages. The aim of this experiment was to validate that circadian behaviour could be measured in the experimental set-up and also identify any potential change in free-running period length which would represent changes in the endogenous circadian function. Experiment 2 investigated the response of the mice to both light and food entrainment in repeated tests of the same mice throughout. The behaviour of the mice recorded across experiment 2 was also used to examine the circadian variation in locomotor activity under both LD and DD.

Light pulse testing was performed following the *Aschoff* type II protocol which involves reentrainment to 12h:12h LD between light pulses. This was adopted as under our procedures 4 mice are exposed to the same light pulse. This means any variance in free-running periods using an *Aschoff* type I protocol would mean some mice would have to be excluded from the analysis due to light pulse exposure occurring at different circadian times. This has been noted as a problem that required exclusion of up to 3 mice out of 5 in previously published studies (Morin and Studholme, 2014). The timing of the two different light pulses were chosen based on timings which should give a peak phase advance or delay based on phase response curves reported by LeGates and Altimus (2011).

The RF procedure was performed under LD, isolating the influence of behavioural free-running on the experiment. Food availability was restricted to a comparably long 8-hour

window (compared to the 4-6-hour windows used more often in RF investigations) and included mash supplement due to concerns as to how food restriction would affect the health of these mice. These concerns were based on observation in prior experiments in our laboratory that both the control and cKO models showed substantial weight loss upon movement of the mice into the circadian cages (Ruby Chrisp, pers. comm.) and that NPAS2 constitutive KO mice showed a severe phenotype when food availability was limited to only 4 hours (2 deaths and 7 severe conditions out of 11 mice) (Dudley et al., 2003).

We hypothesised that there would be no difference between our control and cKO mice in both free-running and daily patterns of locomotor activity as both of these are hypothesised to be primarily mediated within the SCN and other brain regions. While we anticipated no difference, it was still of interest to confirm these as a comparison to that observed in the constitutive KO model.

It was hypothesised that there would be no effect of the liver NPAS2 cKO on entrainment to light (considered to be mediated by the SCN), but that there would be an attenuation of the food anticipatory response to RF (considered to be mediated by peripheral clocks including the liver). The cKO model used here should avoid some compensatory effects which may have occurred in the constitutive KO mice due to lack of NPAS2 expression in development. This means we may observe more substantial effects than in the constitutive KO due to the absence of these compensatory effects.

5.2 Materials and Methods

5.2.1 Animals

Mice were bred and housed as detailed in section 4.2.1.1 (page 152) prior to movement into circadian cages for experimentation. Mice were used at 3-6 months of age. Identical cohorts of 16 mice were used for each of the two experiments, 8 cKO and 8 control mice counter-balanced for sex (see section 5.2.6).

5.2.2 Circadian cages

Activity recording was performed in identical cages (16 cm x 19 cm x 26 cm) with the mice in semi-social isolation. There were four cages per chamber, (80 cm x 61 cm x 71 cm, ENV-018, MED Associates Inc., St Albans, VT, USA) shown in Figure 5.3. Each chamber contained a fluorescent strip bulb, under the control of a programmable timer, and an IR light (BW® 48 LED Illuminator Light), which is not visible to mice, remained on at all times for video capture. A camera at the roof of the chamber in conjunction with the Video Tracking Interface software (Version 1, MED associates inc) recorded the current tracking location of each individual mouse from each cage. This footage was converted into distance travelled (in cm), by the Activity Monitor software (Version 5, MED associates inc). Each chamber also contained a fan to provide air exchange, which also provided background noise (55dB). A radio in the room was also permanently on to provide background noise (~70 dB).

Mice were provided *ad libitum* water and 2018 Rodent diet (Envigo) and weighed weekly to ensure general good health. This diet was supplemented with ~3.5 g 2019s Teklad mash (Envigo) twice weekly to counter substantial weight loss upon movement of mice into the circadian cages, which had previously been noted in these mice (Ruby Chrisp, pers. comm.). The 2019s mash is similar in nutritional makeup to the 2018 diet but is made into mash by soaking in water making it easier to eat.

Activity data was output from the Activity Monitor Software in multiple data bins of distance travelled in 10-minute periods. The data is formatted in Excel as required for analysis (see 5.2.5).

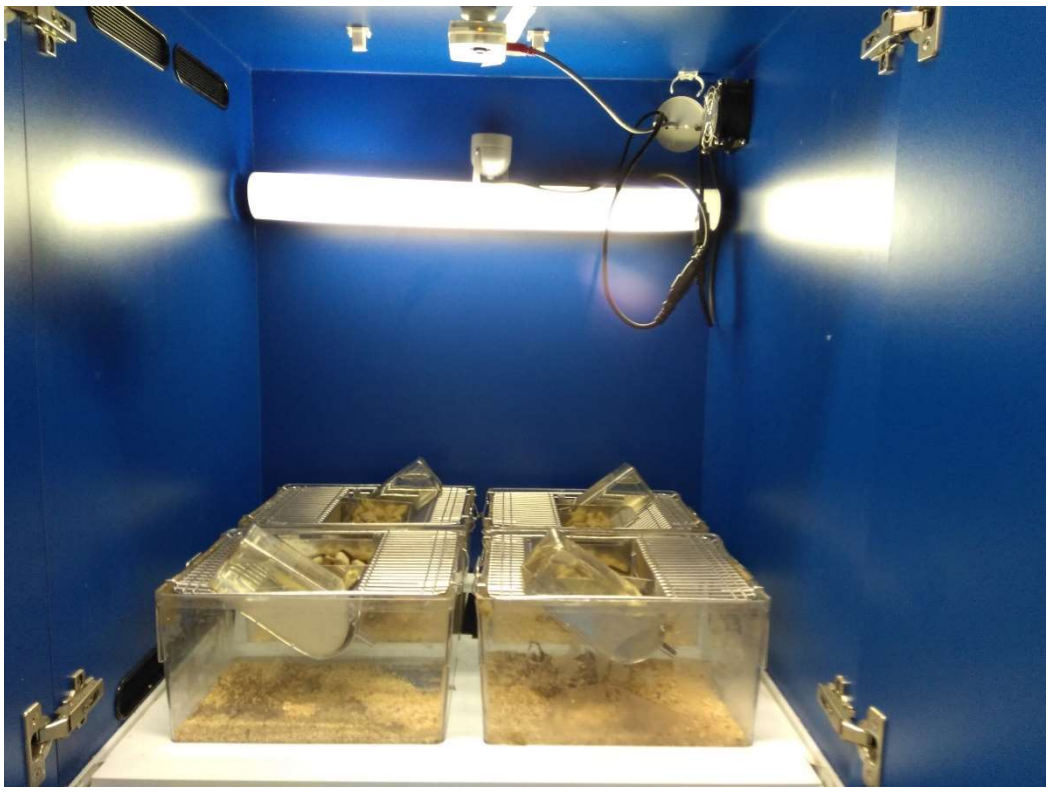

Figure 5.3: Circadian activity recording chamber

Note the camera placed above the cages to record activity, the strip white light and the grey IR lamp placed on the strip light fitting. The IR lamp is pointed away from the cages preventing glare and shadows as the reflection of the IR is sufficient for activity tracking.

5.2.3 Experiment 1 – Free-running investigation

The activity of mice was investigated while circadian free-running under constant darkness using data from experimentation performed by PhD student Ruby Chrisp. Mice were housed in the circadian cages shown in Figure 5.3 under cycling 12h:12h LD conditions (lights on 7am and off at 7pm) for 7 days to adjust to the housing. The lighting condition was then changed to DD for 10 days for activity to be recorded.

5.2.4 Experiment 2 – Entrainment investigation

Experiment 2 investigated light pulse and RF entrainment in the same mice. The light entrainment experimental procedure (section 5.2.4.1) was performed first and as soon as this procedure ended the RF entrainment procedure (section 5.2.4.2) immediately began. Activity recorded on days throughout this experiment were used for investigation of daily locomotor activity (see section 5.2.5.3).

5.2.4.1 Light entrainment by light pulses

Mice were housed in the circadian cages shown in Figure 5.3 under cycling 12h:12h LD conditions (lights on 7am and off at 7pm) for 6 days to adjust to the housing. The lighting condition was then changed to DD with a light pulse at CT16 (11pm), 4 hours into the active phase (LP1). Mice were kept in DD for 7 days for activity to be recorded and then the lighting was returned to LD and the procedure repeated with a light pulse at CT 20 (3am), 4 hours prior to the end of the active phase (LP2). The lighting cycles across days are shown in Figure 5.4.

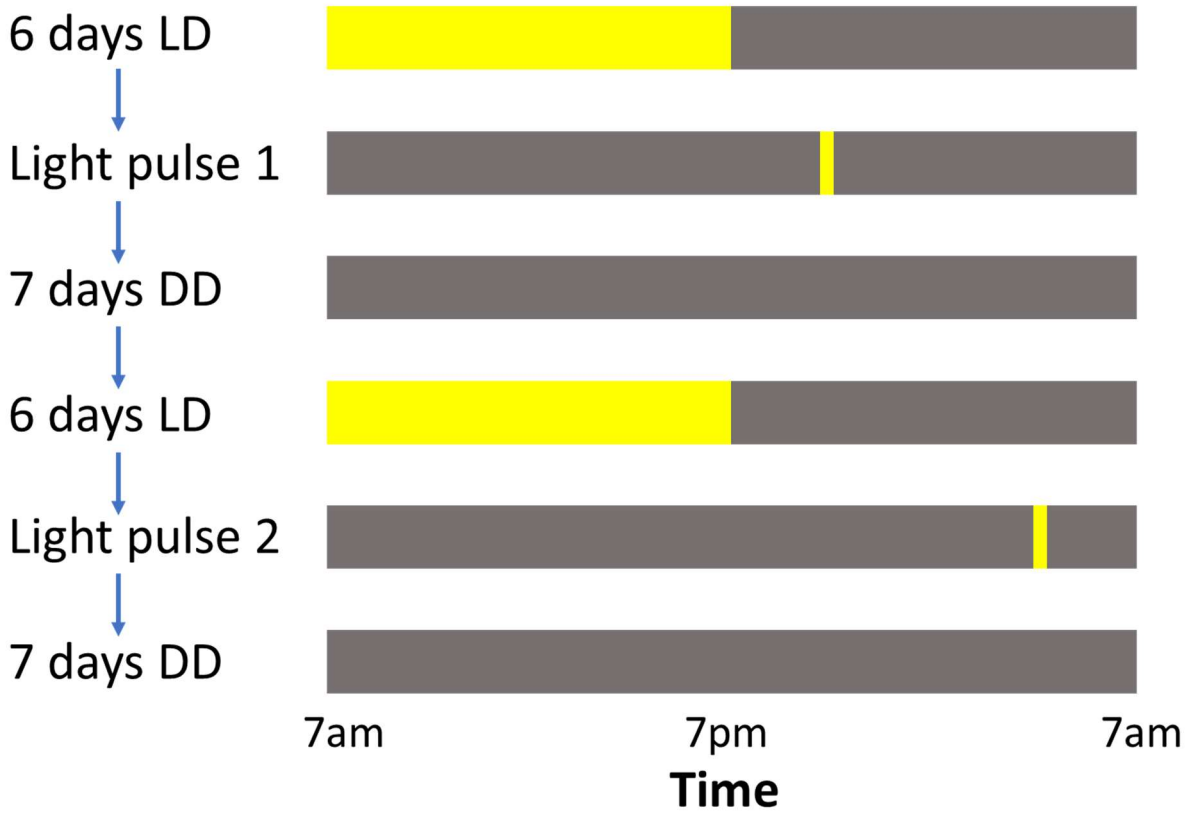

Figure 5.4: Lighting conditions of days for the light pulse experiment

The lighting procedure follows that detailed above. Each row represents a single lighting pattern for one day. Yellow represents times that the lights are on and grey times lights are off.

5.2.4.2 Restricted feeding entrainment

The same mice used for light pulse testing (detailed above in 5.2.4.1) were used for the RF experiment. The mice were reentrained to a 12h:12h light:dark cycle following light pulse testing, with lights on at 6am and off at 6pm. After nine days in LD with *ad libitum* food, the food was removed from the cages at 5pm (ZT11). Food was provided within the light hours every day at 9am (ZT3) along with a ~1.5 g of 2019s Teklad diet (Envigo) and available for 8 hours until 5pm (ZT11). This RF schedule was maintained for 9 days. While under RF mice were weighed every 2-3 days to monitor for maintenance of healthy weight.

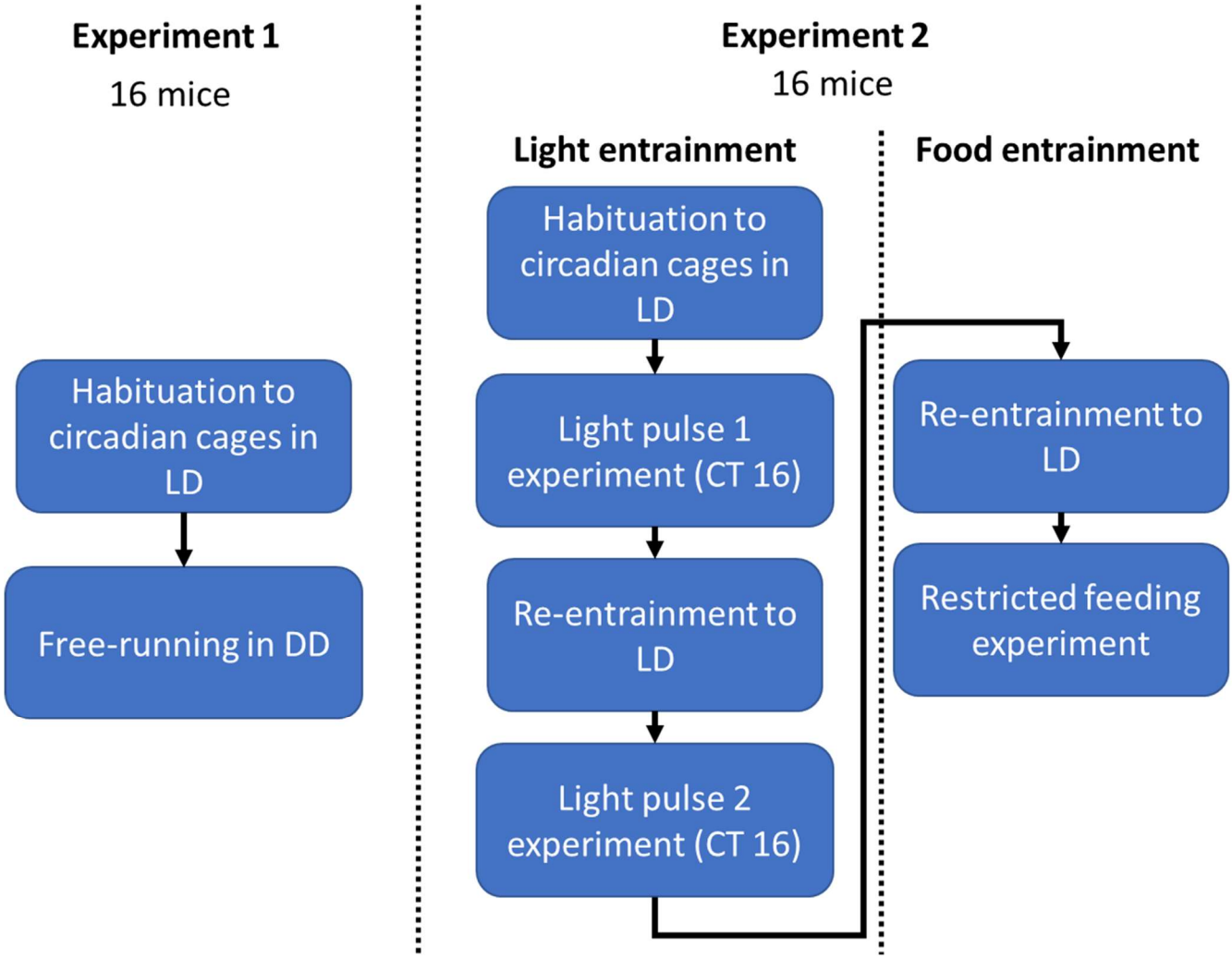

Figure 5.5: Mouse experimental design for investigation of circadian behaviour

Two identical cohorts of 16 mice were used. The cohort in experiment 1 was used to investigate free-running. The other cohort was used in light and then RF entrainment investigation, performed sequentially.

5.2.5 Activity analysis

5.2.5.1 Actograms

Activity is presented in double plotted actograms, produced by use of the ImageJ plugin software, ActogramJ, produced by Schmid et al. (2011). The actograms were normalised to total activity levels for the individual mice for comparison. For activity in RF entrainment average actograms were produced using the functionality of ActogramJ. The background highlighting shows time of lights on (yellow), lights off (grey) and food provision during RF (orange).

5.2.5.2 Period estimates

To generate period estimates the recorded data of distance travelled in 10 minute windows was analysed using online BioDare2 software (Zielinski et al., 2014) using FFT-NLLS analysis. In this analysis initially a Fast Fourier Transformation (FFT) is performed on the data to generate initial period values by fitting a complex cosine curve to the data set. These initial values are then improved on by the Non-Linear Least Squares (NLLS) iterative numerical search, adding cosine components until the addition of a cosine term does not improve the resulting fit significantly. The analysis ends having modelled the data by a sum of cosine functions, the cosine function with a period within the defined window of 18-34 hours is then used to give output values for activity period, amplitude, phase, and the relative amplitude error (RAE), a measure of rhythm robustness which increases from 0 to 1 as the cosine fit to the data nears statistical insignificance. If more than one function falls within this window then the function is manually selected, generally the function with the lowest RAE, supported by observation of the fit to the data.

5.2.5.3 Daily locomotor activity

Daily activity was investigated on days throughout experiment 2. Activity under LD was investigated using activity on 10 days, excluding days in which mice are habituating to the

cages (the first 4 days), resynchronising to the light cycle (the first day when the mice are returned to LD) or were weighed (various days throughout the experiment). Total daily activity under DD was investigated on a selection of 10 days within the light entrainment investigation, excluding those where the mice were exposed to a light pulse or weighed. Hourly daily activity under DD was investigated on a single day as the unsynchronised behaviour in DD will vary day to day so cannot be grouped for a meaningful analysis. The first day of darkness following light pulse 2 was used for this. For this activity investigation, in LD or DD, activity within the 10-minute bins were summed to provide total activity within larger windows of 1, 12 and 24 hours.

5.2.5.4 Light pulse phase shifting

The phase shifts caused by the light pulses were calculated using the ClockLab Analysis 6 software (Actimetrics), this process in the software is shown in Figure 5.6. The software produced least squares regression lines from the activity onset times for the 6 days in LD prior to the light pulse and the 7 days following the light pulse. The phase shift was calculated by comparing the difference in the timings of each of these lines when extrapolated into the last day of LD. A positive value reflects a phase advance, and a negative value reflects a phase delay.

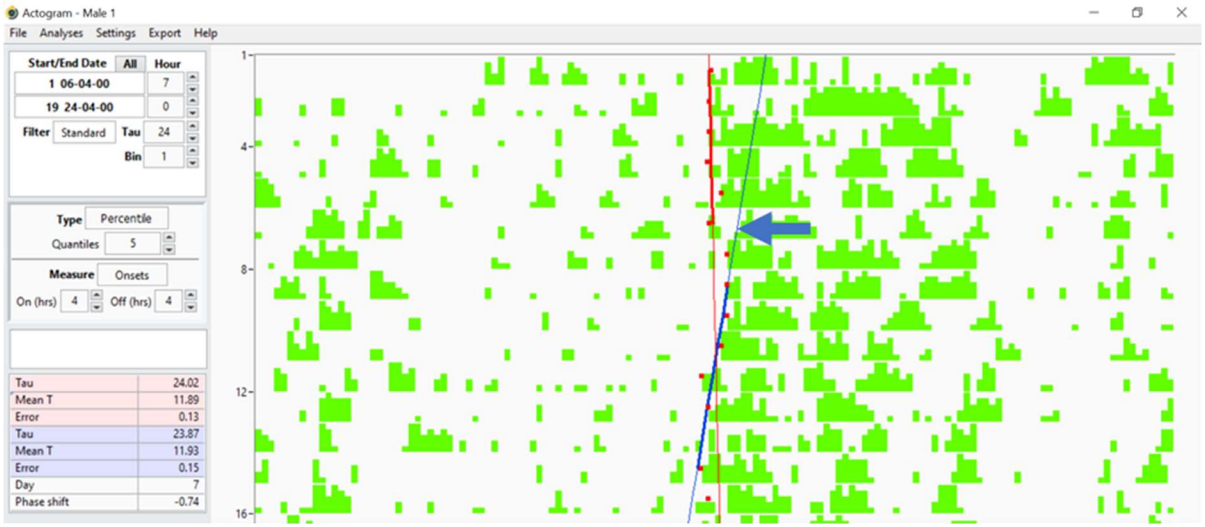

Figure 5.6: Example phase shift calculation in ClockLab

Best fit lines are drawn based on activity onsets for the days prior to and the days following the light pulse. Phase shift is calculated based on the difference between the fit lines on the last day of LD, marked with an arrow. Note that the onset of one of the later days in DD is excluded in this example (no red dot) due to the lack of clarity as to when this should fall based on the activity data.

5.2.5.5 Restricted feeding - FAA measurement

FAA was defined as activity within the window after lights turn on and before food provision that was not caused by a stimulus such as someone entering the room. For this reason, the 30 minutes immediately before food provision are not included in the FAA analysed time frame of 2.5 hours (ZT0-ZT2.5). Percentage FAA activity is calculated using the activity within this window as a percentage of the daily total distance travelled, from lights off to the next lights off, 6am-6am.

Alternate measures of activity included FAA as above, without correction to the daily activity, and the time of onset of FAA prior to food provision. FAA onset prior to food was calculated as the number of minutes prior to food provision where activity was consistently recorded. This was the time of the earliest active data bin within the FAA window that was not separated from the time of food provision by two or more consecutive inactive bins (distance travelled < 50 cm). If no activity is recorded in the two bins prior to food provision the timing of activity onset prior to food provision was defined as zero.

5.2.6 Experimental design

The circadian set-up available limited the testing to cohorts of 16 mice simultaneously with the potential to repeat experiments to increase the n numbers. In both experiments the 16 mice were made up of a balance of the two genotypes: 8 control mice and 8 cKO mice. Due to restrictions in availability of appropriately aged mice and the fact that there was hypothesised to be no sex difference on circadian behaviour (Krizo and Mintz, 2014, Kuljis et al., 2013) both experiments were counter-balanced for sex within each genotype.

Experiment 1 (detailed in 5.3) investigated the functioning of the set up in excluding mice from zeitgebers and investigated the effect of genotype on the free-running period. No genotype effect on free-running period was predicted of a mutation in a peripheral clock so this experiment was considered an appropriately sized pilot study to identify if the free-running

period was of interest for further investigation.

Based on calculations in G power, the 16-mouse cohort provides sensitivity for a Cohen's d effect size of 1.745 or greater for t-tests investigating light pulse effect with an alpha of 0.05 and power of 0.9. For a mixed ANOVA investigating RF entrainment using the same alpha and power, non-sphericity correction of 1 and an estimated repeated measures correlation of 0.5, based on 10 within-subjects measurements G power identified a Cohen's f effect size of 0.281.

Based the reported investigation of entrainment by Dudley et al. (2003), the effect sizes were calculated using the G power software, and Formula 5.1 for F testing. For genotype influence on light entrainment Cohen's d was identified as 0.805 and on RF entrainment the Cohen's f effect size was 0.976. As such the group numbers used here are sufficient to identify a similar effect on RF entrainment but insufficient for a similar effect of light entrainment. It should be noted that the experiment investigating light entrainment performed here differs from the light entrainment protocol used in this publication and it was hypothesised that if liver NPAS2 cKO reflects the constitutive KO effect it would be more subtle. As such the experiments performed here were considered preliminary and power calculations can be used based on the data generated here to plan future cohorts to be investigated to contribute to the available data.

$$\eta_p^2 = \frac{F \times df_{num}}{F \times df_{num} + df_{den}}$$

Formula 5.1: Calculation of partial eta squared from F and df values (Lakens, 2013)

5.2.7 Statistical analysis

Statistical tests were performed using SPSS software as described in Chapter 3, section 3.2.3 (page 123). Where required, data was log transformed to meet the assumption of normality, detailed if performed in the results sections. For mixed repeated measures ANOVAs sphericity was assessed by Mauchly's test of sphericity. If the assumption of sphericity was not

met Greenhouse-Geisser correction was used.

Confirmation of the experimental result in free-running period and light pulse phase shift was performed by one sample t-test comparing the data for all mice to the 'null' value (24 for free-running period, representing maintained daily entrainment, and 0 for phase shift, representing no shift). Investigation of the effects of the factors of sex and genotype on those measures were performed using two-way ANOVAs.

Investigation of daily locomotor activity data was performed using mixed measures ANOVAs with between-subjects factors of genotype and sex and the within-subjects factors of time of day, lighting phase and lighting condition as appropriate. Day was included as a within-subjects factor to permit accurate modelling of the data but not analysed.

Investigation of the activity profiles used hourly data and were analysed using mixed ANOVAs including the within-subjects factor of hour and the between-subjects factors of genotype and sex. For the LD hourly analysis, the between-subjects factor of day was included for modelling purposes. Due to the number of repeated measures being greater than the number of mice, Mauchly's test of sphericity was inappropriate, and Greenhouse-Geisser correction used. This also prevented Bayesian analysis of this data.

Investigation of FAA data was performed by use of mixed ANOVAs and ANOCVA with within-subjects effect of day and between-subjects effects of genotype and sex and weight as a covariate where appropriate. Correlational mouse weight data was analysed using Pearson's correlation coefficient. The FAA onset, calculated based on the discrete 10 minute bins of activity, is non-parametric data and was analysed in SPSS using generalised linear analysis, for repeated measures this takes the form of generalised estimating equations (GEE) which allows for mixed repeated measures analysis (Hardin, 2005). GEE was performed using an unstructured correlation matrix and modelling a linear response. Analysis of genotype effect within each day was performed using generalised linear modelling.

Frequentist testing was supported by Bayesian statistical testing. Frequentist testing cannot distinguish between a true null effect and insensitivity of the experiment whereas Bayesian analysis can identify whether data presents evidence in support of the null hypothesis. Bayesian tests were performed using the JASP software (Version 0.13.1) using default equal prior probabilities for all factors in each analysis. The analysis of effects was performed across matched models. BF values <1 are considered evidence against a model or factor while >1 are evidence for. BF values between 1/3 and 3 are considered inconclusive/weak evidence, unsuitable for drawing a conclusion however these values can identify whether the data is suggestive for or against an effect. Values between 3 and 10 represent substantial evidence, between 10 and 30 strong evidence and >30 decisive evidence in favour of a factor/model, with the inverse values having the same reliability as evidence against (Dienes, 2014). Where performed, Bayesian tests matching the frequentist tests were used (i.e., Bayesian ANOVA, Bayesian repeated measures ANOVA).

5.3 Free-running behaviour

5.3.1 Results

Average periods lengths of the mice under DD are presented in Figure 5.7. The average identified period was 23.88 hours (SEM = ±0.051) across all 16 mice. This was significantly different to 24 by one sample t-test $t(15)=-2.369$, $p=0.032$. This demonstrates that we observed the free-running periods and these mice were not entrained to 24-hour cycles.

ANOVA showed no significant main effect of sex ($F(1,12)=0.953$, $p=0.348$) or genotype ($F(1,12)=0.048$, $p=0.830$) on the free-running period nor of a sex x genotype interaction ($F(1,12)=1.673$, $p=0.220$). A Bayesian ANOVA using default priors favoured the null hypothesis of no effect of sex or genotype ($BF_{10}=1.692$ compared to the next best model; the individual effect of sex, indicating weak evidence). Individual effect analysis showed weak evidence suggestive of no effect of genotype ($BF_{incl}=0.380$) and sex ($BF_{incl}=0.495$) and the sex x genotype interaction ($BF_{incl}=0.402$). This analysis suggests our data, while suggestive against, is unable to be used to confidently conclude as to the effect of genotype on free-running period.

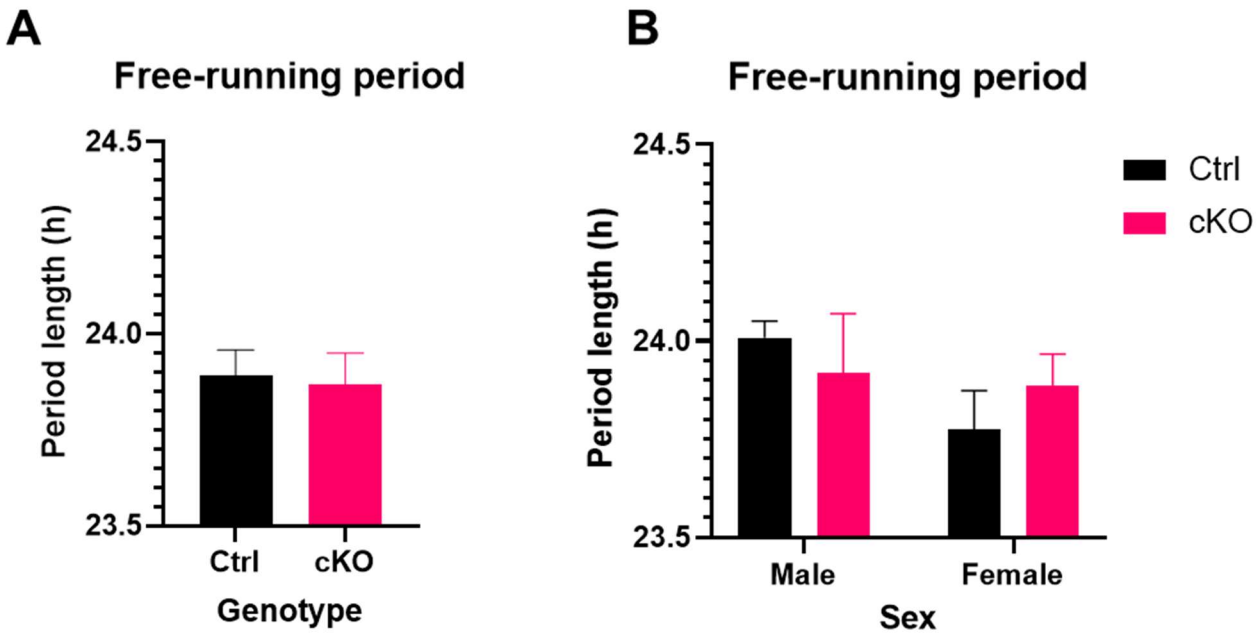

Figure 5.7: Free-running behavioural period of control and cKO mice under DD

Mean free-running period (±SEM) in constant darkness showing the effects of genotype (A) and sex and genotype (B) within the same data. Experimentation performed by PhD student Ruby Chrisp.

5.3.2 Discussion

This experiment successfully validated the set-up and experimental process, as we were able to observe free-running behaviour (see Figure 5.7).

Investigation of the factor of genotype within the ANOVA suggested no effect of the loss of liver NPAS2 on circadian behavioural period. This is in contrast to the shortened period previously observed in constitutive NPAS2 KO mice (Dudley et al., 2003). This suggests that, as predicted, the loss of NPAS2 in the liver may not have contributed to the effect observed in constitutive NPAS2 KO mice.

This experiment is underpowered to appropriately investigate sex interaction effects. Although not significant, graphically we appear to observe a longer average free-running period in control male mice compared to control female mice. Within the female mice an increased period length appears to be observed in cKO mice compared to the control mice (see Figure 5.7 B). This is unexpected as it has been reported previously that there are no sex differences in period length of C57BL/6 mice (Krizo and Mintz, 2014, Kuljis et al., 2013), suggesting a difference may be specific to this floxed mouse strain. Using the same experimental set up in our laboratory we confirmed no sex influence on the DD free-running period in C57BL/6 mice (Ruby Chrisp, pers. comms.). More experimentation would be required to be confident of the small potential sex-specific genotype effect.

In experiments using other liver-specific circadian gene KO models (PER2 and BMAL1) no difference in free-running period compared to WT mice was reported. In PER2 liver-specific KO mice the period was observed to not vary significantly from WT mice while constitutive and neuronal PER2 KO shortens the period length (Chavan et al., 2016). In BMAL1 liver KO mice it has also been reported that the circadian behaviour was unaffected, however no period analysis is shown and visually the actograms for liver BMAL1 KO mice do appear to present a shorter free-running period (Lamia et al., 2008). In mice with a constitutive

BMAL1 KO, restoration of BMAL1 expression to the brain specifically recovers circadian behaviour. However, the period is still shorter than mice retaining constitutive BMAL1 expression, showing a delaying effect of loss of circadian function in peripheral tissues outside of the brain on neural circadian rhythms (McDearmon et al., 2006). This is suggestive of an influence of peripheral clocks on between tissue clock entrainment to influence behavioural cycles.

5.4 Daily locomotor activity

Using activity data recorded throughout experiment 2 we investigated daily locomotor behaviour in the mice. This behaviour can provide insight into effects on circadian patterns outside of zeitgeber influence due to the genetic modifications.

5.4.1 LD results

The collected activity data under LD allowed analysis of the daily activity and average hourly LD activity (see Figure 5.8).

5.4.1.1 LD total daily activity

Daily total activity is presented in Figure 5.8 A. Analysis was performed using log transformed data. A significant main effect of sex on total activity was identified ($F(1,12)=27.542$, $p=0.00021$). There was no significant effect of genotype ($F(1,12)=0.088$, $p=0.772$) nor an interaction effect of sex x genotype ($F(1,12)=0.376$, $p=0.551$). This supports previous reports that female mice show higher daily activity than males (Broida and Svare, 1984) and suggests no genotype effect on total activity is observed. Bayesian mixed ANOVA identified a model with an independent effect of sex as the favoured model ($BF_{10}=229.0$ compared to the null model, indicating decisive evidence). Individual effect analysis showed decisive evidence for an effect of sex ($BF_{incl}=186.2$) and weak evidence suggestive against an effect of genotype ($BF_{incl}=0.702$) and a sex x genotype interaction ($BF_{incl}=0.776$).

5.4.1.2 LD dark phase activity

As activity can be separated into high (dark) and low (light) activity phases based on the lighting cycles, analysis was performed to see if any genotype effect was associated with specific activity phases.

Analysis of activity within the dark phase was performed using log transformed data. There was a significant effect of sex on activity ($F(1,12)=30.511$, $p=0.00013$). No significant effect was identified due to genotype ($F(1,12)=0.106$, $p=0.750$) nor an interaction effect of sex

x genotype ($F(1,12)=0.093$, $p=0.765$). Bayesian analysis favoured a model with an independent effect of sex ($BF_{10}=399.4$ compared to the null model, indicating decisive evidence). Individual effect analysis showed decisive evidence for an effect of sex ($BF_{incl}=335.7$) and weak evidence suggestive of no effect of genotype ($BF_{incl}=0.692$) or a sex x genotype interaction ($BF_{incl}=0.775$). These analysis results are similar to those for total daily activity, which was expected as activity in the dark phase will account for the significant majority of daily activity.

5.4.1.3 LD light phase activity

Analysis of activity within the light phase was performed as above on the log transformed data. There was no significant effect identified of sex ($F(1,12)=1.991$, $p=0.184$) or genotype ($F(1,12)=0.333$, $p=0.575$) but there was a significant sex x genotype interaction ($F(1,12)=5.735$, $p=0.034$). To follow up on the significant interaction effect, simple main effects analysis of the impact of genotype identified no significant effect within male ($p=0.223$) or female mice ($p=0.057$), but a simple main effect of sex was identified between male and female cKO mice ($p=0.020$) which was not observed in control mice ($p=0.500$). This suggests a sex effect on activity in the light phase specifically in the cKO mice. Bayesian analysis favoured the null model ($BF_{10}=1.557$ compared to the next best model; sex effect only, indicating weak evidence). Individual effect analysis supported the frequentist analysis identifying substantial evidence in favour of a sex x genotype interaction ($BF_{incl}=3.022$). However, the analysis found only weak evidence against the main effects of sex ($BF_{incl}=0.765$) and genotype ($BF_{incl}=0.521$). This suggests no effect of the main factors of sex and genotype however these data are inconclusive.

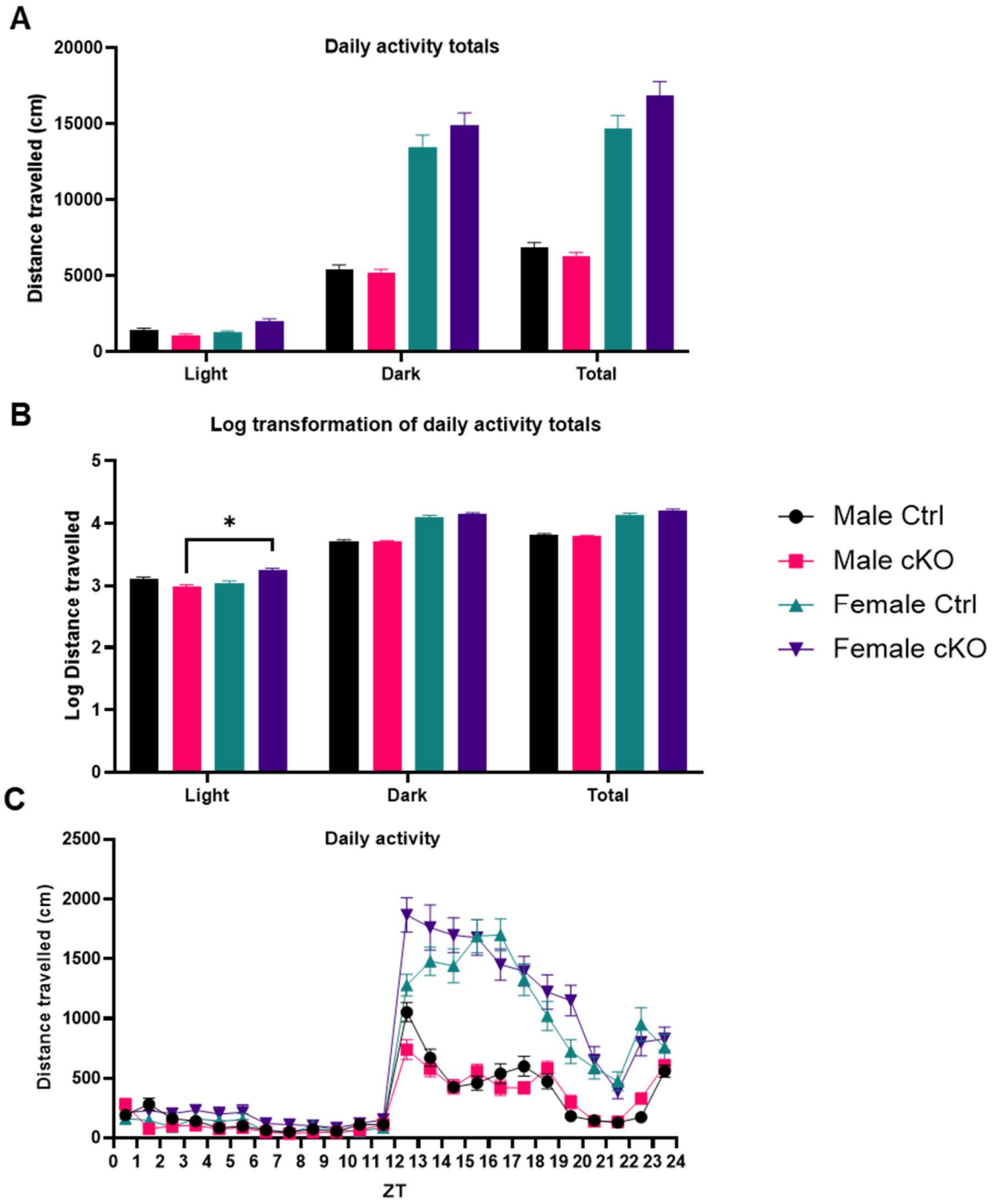

Figure 5.8: Home cage activity of mice under LD measured by total distance travelled. **A:** Mean total distance (±SEM) travelled within the 12-hour light and dark phases and the total day, based on ten days of activity. **B:** Log transformation of the distance travelled data in A. A significant pairwise effect between sexes was observed in cKO mice on activity in the light phase (*=$p<0.05$). **C**: Activity profile of mean distance travelled (±SEM) within each hour.

5.4.1.4 LD hourly activity profile

Average activity per hour over 10 days is presented in Figure 5.8 C. The pattern of most activity occurring in the dark phase can be clearly seen along with the clear sex difference in activity levels. Distance travelled data was log transformed after addition of 1 to each value due to the presence of multiple 0 values for hours in light where no movement was detected. Significant effects were identified of hour ($F(6.663,79.951)=79.661$, $p<0.00001$) and the interaction effect of hour x sex ($F(6.663,79.951)=5.122$, $p=0.00010$) (Greenhouse-Geisser corrected). No significant effects were identified due to the interaction of hour x genotype ($F(6.663,79.951)=1.301$, $p=0.262$), or the interaction of hour x sex x genotype ($F(6.663,79.951)=1.593$, $p=0.153$). Thus, the analysis suggests that the activity varies with hour of day and sex influences the presentation and pattern of this activity, but genotype does not.

5.4.2 DD results

As behavioural patterns are influenced by lighting conditions, locomotor activity was also investigated in conditions of constant darkness. Total activity per day and hourly activity were investigated (Figure 5.9).

5.4.2.1 DD total daily activity

The data for total 24-hour activity was log transformed for analysis. We identified a significant main effect of sex ($F(1,12)=21.831$, $p=0.00054$), but no effect of genotype ($F(1,12)=0.116$, $p=0.740$), nor a significant interaction effect of the two ($F(1,12)=0.247$, $p=0.629$). Bayesian analysis supported this, favouring a model with only an effect of sex ($BF_{10}=78.016$ compared to the null model, indicating decisive evidence). Individual effect analysis showed decisive evidence for an effect of sex ($BF_{incl}=35.081$) and weak evidence suggesting no effect of genotype ($BF_{incl}=0.414$) or a sex x genotype interaction ($BF_{incl}=0.630$). This analysis is similar to that of the LD data, showing that we see a sex effect but no genotype

effect on the amount of activity in DD, however for DD conditions the Bayesian analysis suggests that we are unable to conclude with confidence that there is no genotype effect on activity.

5.4.2.2 DD hourly activity profile

The hourly activity from a single day in DD is presented in Figure 5.9 C. The patterns of low and peak activity presenting a similar pattern to the behaviour under LD can clearly be seen, as well as the sex difference in activity levels. Analysis was performed using distance travelled data log transformed after the addition of 1 as for the LD hourly activity. Due to the variability of hour-to-hour activity, the only significant effect observed on activity was that of hour ($F(6.931,2.020)=10.749$, $p<0.00001$) with no significant interactions of hour x sex ($F(6.931,2.020)=1.001$, $p=0.436$), hour x genotype ($F(6.931,2.020)=0.955$, $p=0.469$) or hour x sex x genotype ($F(6.931,2.020)=0.770$, $p=0.613$) found.

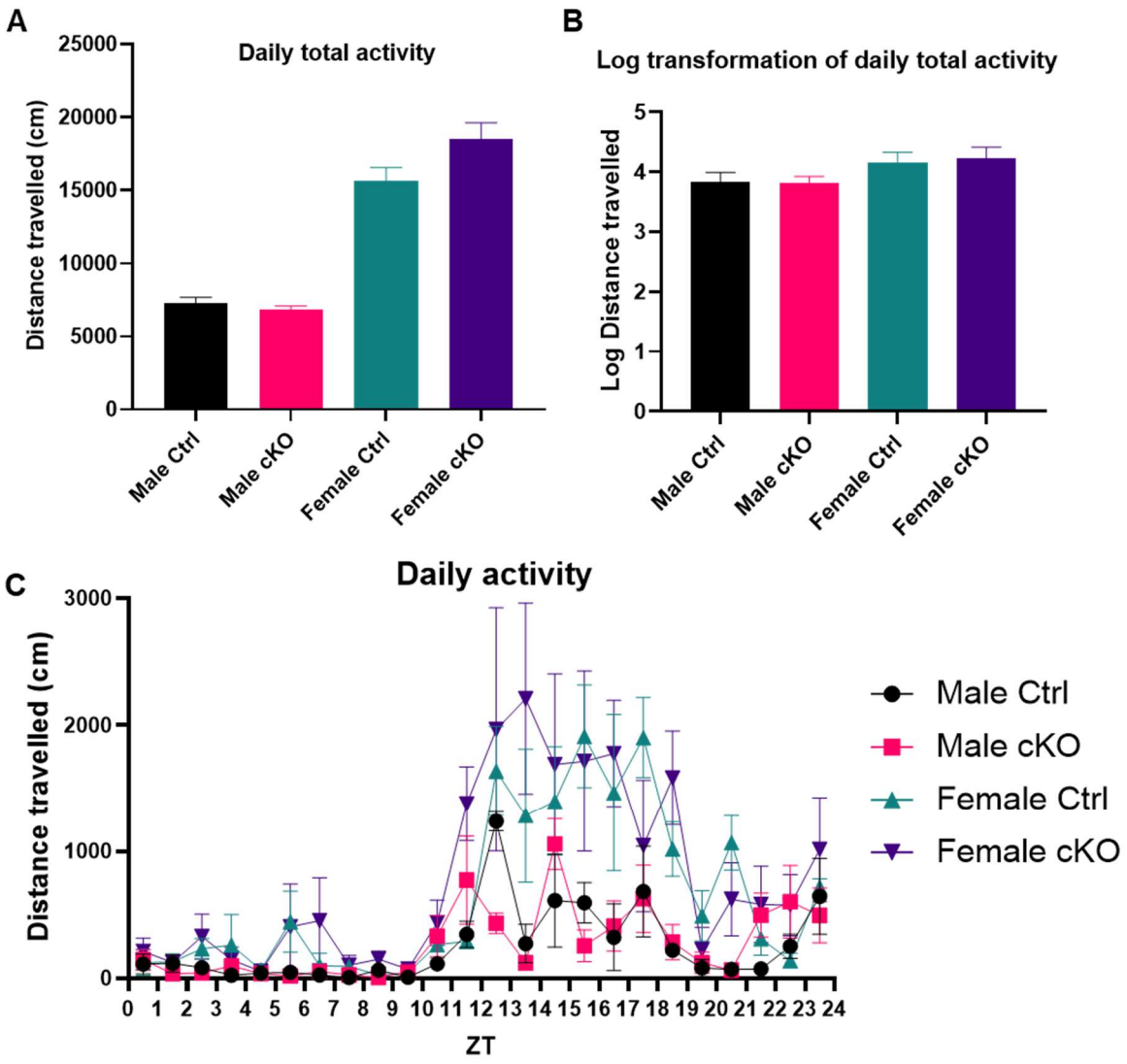

Figure 5.9: Home cage activity of mice under DD measured by total distance travelled **A:** Mean total distance travelled (±SEM) within 24 hours based on 10 days of activity. **B:** Log transformation of the distance travelled data in A. **C:** Activity profile of mean distance travelled (±SEM) within each hour. Note this is based on activity from a single day rather than 10 days hence the SEM values are much greater than those shown in Figure 5.8.

While less obvious due to the larger variability, and again lacking a significant difference, similar daily patterns are presented under DD to that observed for the mice under LD. We see the peak of activity coincided with activity onset in cKO female mice while control female mice showed a later peak of activity. In male mice a single hour of very high activity with activity onset is observed in the control mice while a clear peak is not observed for the cKO mice. This suggests the influence of the loss of liver NPAS2 on the patterns of behaviour were a reflection of the rhythmic behaviour of the mice, independent of a lighting effect as we observed the same in LD and DD.

5.4.3 Comparing LD and DD

The data used above for the LD and DD total day activity analysis were compared together to interrogate the effect of the lighting on total activity, shown in Figure 5.10. Light acts to supress activity, as well as a zeitgeber, so we would expect to see reduced activity in LD compared to DD (Banks and Nolan, 2011). The data was log transformed for analysis. The analysis identified a significant main effect of the lighting condition on daily activity ($F(1,12)=9.223$, $p=0.010$), but no significant interaction effect of lighting condition x sex ($F(1,12)=0.041$, $p=0.842$), lighting condition x genotype ($F(1,12)=0.12$, $p=0.735$), or lighting condition x sex x genotype ($F(1,12)=0.039$, $p=0.847$). Bayesian analysis favoured a model with an effect of the factors lighting condition, and sex ($BF_{10}=5.89x10^3$ compared to the null model, indicating decisive evidence). Individual effect analysis showed decisive evidence for an effect of lighting condition ($BF_{incl}=43.925$), substantial evidence against interaction effects of lighting condition x genotype ($BF_{incl}=0.191$) or lighting condition x sex ($BF_{incl}=0.189$) and lighting condition x sex x genotype ($BF_{incl}=0.212$). Taken together, this analysis shows a significant effect of lighting condition on activity as expected, with higher activity in mice under DD. The Bayesian analysis means we are confidently able to conclude no effect of the loss of liver NPAS2 on how total activity is changed by lighting condition.

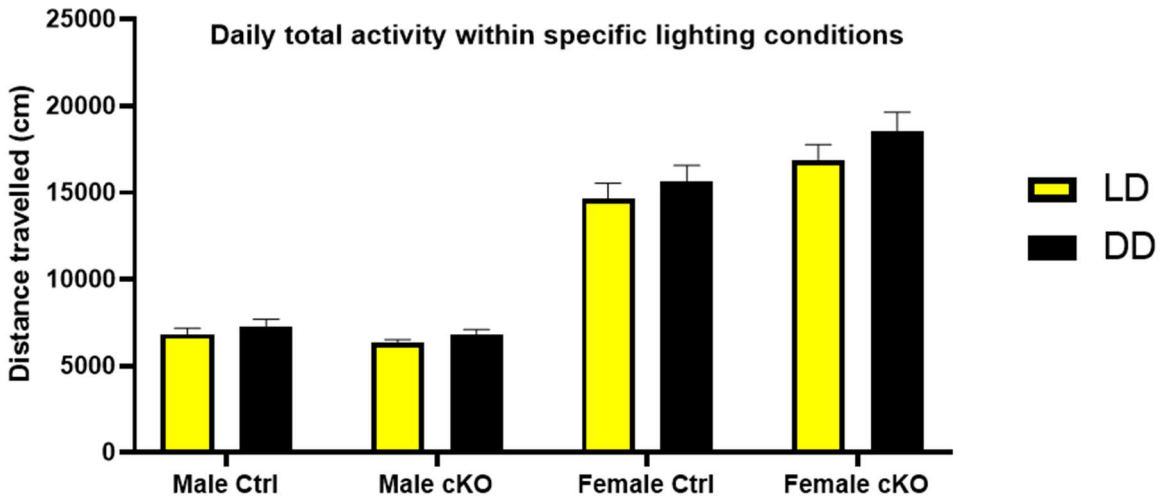

Figure 5.10: Effect of lighting condition on activity levels

Mean total daily home cage activity (±SEM) of mice under LD and DD measured by distance travelled. The higher activity level of female mice can be clearly observed as well as the subtle increase in total activity under DD compared to LD due to loss of light suppression of activity.

5.4.4 Discussion

Analysing general locomotor activity, we observed expected differences in patterns and levels of activity. Female mice were more active than male mice and mice were more active under DD conditions compared to LD, as has been previously reported (Broida and Svare, 1984, Banks and Nolan, 2011). We observed no effect of liver NPAS2 on general activity levels under LD or DD for full day activity although we see a sex-specific genotype effect on behaviour within the light phase in LD conditions with a sex difference of higher activity in female mice only observed within cKO mice. Under other conditions we observe this sex difference without a genotype influence. The change in results of analysis of activity in the light phase is because we are unable to observe the sex difference in control mice. This appearance of a significant sex effect within cKO mice suggests subtle modulation of activity levels in the cKO mice, increased in female and decreased in male mice, enhancing the sex difference meaning it is observable even at low activity levels. We did not observe any significant simple main effect of genotype within the sex groups so are unable to conclude as to the differing genotype effect within sexes.

5.5 Investigation of light entrainment

5.5.1 Results

Example representative actograms for individual mice over the course of the light pulse experimentation are presented in Figure 5.11. These show activity patterns and also the lighting pattern mice were exposed to, including both light pulses.

5.5.1.1 Light pulse 1

The first light pulse at CT16 caused an average phase shift of -0.66 hours (SEM = ±0.075) across all 16 mice (Figure 5.12 A). This shift was significantly different to zero by one sample t-test $t(15)=-8.696$, $p<0.00001$. This demonstrates a phase delaying effect of the light pulse on activity onset as predicted.

ANOVA showed no significant main effect of sex ($F(1,12)=0.433$, $p=0.523$) or genotype ($F(1,12)=1.261$, $p=0.283$) on the phase shift nor of a sex x genotype interaction ($F(1,12)=0.433$, $p=0.523$). A Bayesian ANOVA using default priors favoured the null hypothesis of no effect of sex or genotype ($BF_{10}=1.486$ compared to the next best model; the individual effect of genotype, indicating weak evidence). Individual effect analysis showed weak evidence suggestive of no effect of genotype ($BF_{incl}=0.673$), sex ($BF_{incl}=0.497$) and the sex x genotype interaction ($BF_{incl}=0.587$). This analysis suggests our data is unable to be used confidently conclude as to the effect of genotype on light entrainment.

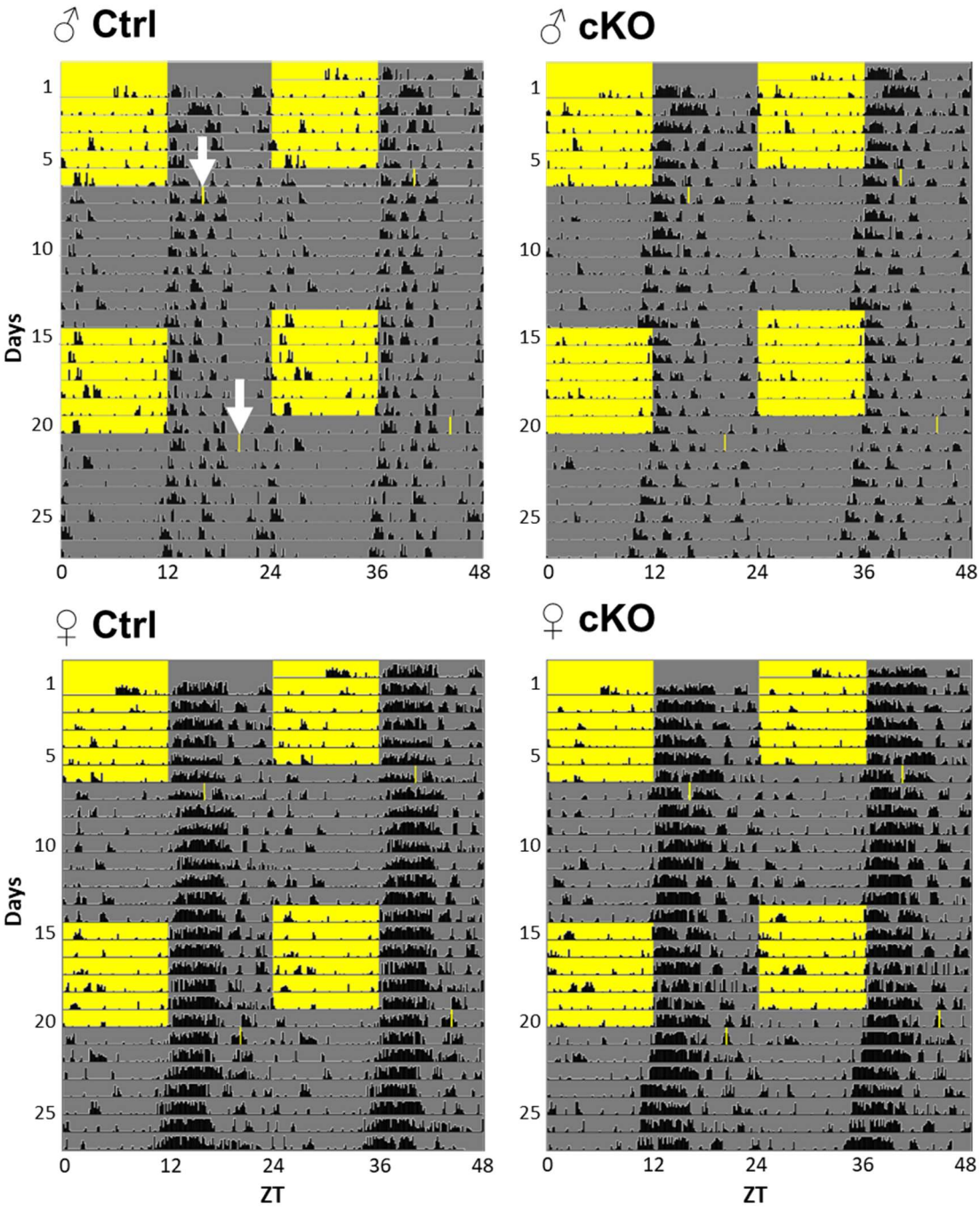

Figure 5.11: Activity of mice exposed to light pulse entrainment

Representative double plotted actograms of individual mouse activity. Lighting conditions are displayed in the background colour. Yellow represents lights on and grey IR light only. The light pulses are short periods of light marked as small yellow sections on the actograms highlighted by a white arrow on the left of the male control actogram. The actograms begin prior to the mice being placed in the cages and a burst of activity in the first light section can be seen when the mice were active having just been moved to a new environment.

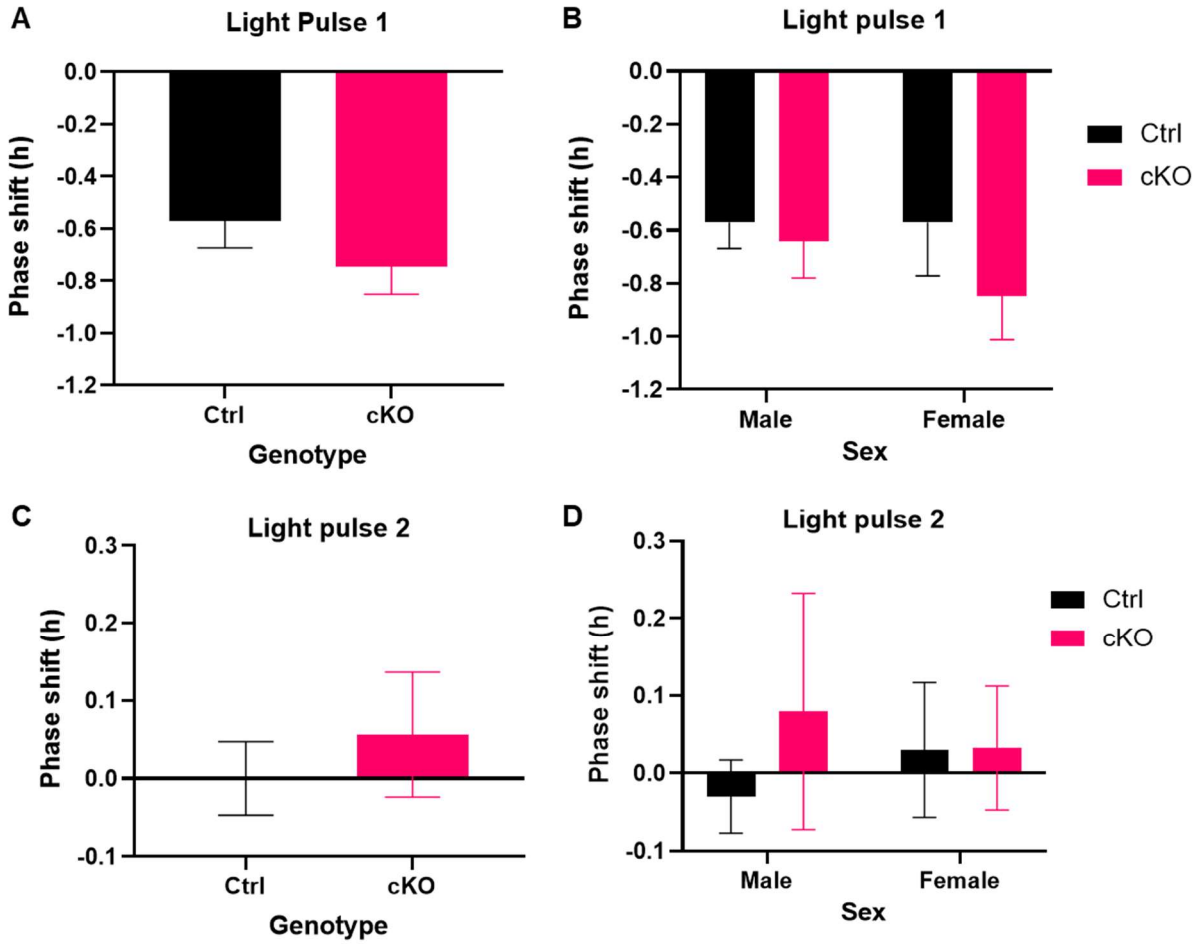

Figure 5.12: Phase shift in activity onset due to light pulses

A positive value reflects a phase advance and a negative value a phase delay. **A & B:** Mean phase shift (±SEM) in response to light pulse 1 showing the effects of genotypes (A) and sex and genotype (B) within the same data. **C & D:** Mean phase shift (±SEM) in response to light pulse 2 showing the effects of genotypes (C) and sex and genotype (D) within the same data. Note the change in scale of the y axes.

5.5.1.2 Light pulse 2

The phase shift following the second light pulse at CT20 caused an average phase advance of 0.028 hours (SEM = ±0.045) across all 16 mice (Figure 5.12 C). This data did not show a significant difference from zero by one sample t-test ($t(15)=0.618$, $p=0.546$) suggesting the light pulse at ZT20 was not able to produce an effect on activity onset as was seen for the light pulse at ZT16.

5.5.2 Discussion

The first light pulse induced a predicted delay in the onset of activity. No significant effect of the liver NPAS2 cKO was identified. While Bayesian analysis favoured the null model, suggestive of no genotype effect as predicted, this result was inconclusive.

The second light pulse did not affect the phase of activity onset. The timings of the light pulses were based on a methods paper by LeGates and Altimus (2011) but it may be that for the delaying shift the light pulse would be more effective at a later time, such as ZT22, based on other publications by Schwartz and Zimmerman (1990) and Banks and Nolan (2011).

This data suggests there is no effect of loss of NPAS2 in the liver on entrainment to light, however, the data supports further investigation to validate this, and we were unable to investigate phase advancing entrainment.

Within this experiment the order of the light pulses was not varied. It is possible that different effects to those observed here would be seen in mice exposed to the light pulses in the opposite order due to a potential lasting effect of the first light pulse influencing the response to the second. Experiments of this nature, where possible within the mouse groups tested, would benefit from counterbalanced groups exposed to the light pulses in different orders due to this possibility.

5.6 Investigation of feeding entrainment

5.6.1 Results

5.6.1.1 Food anticipatory activity

The appearance of FAA in mice under an RF schedule can be seen highlighted in average actograms in Figure 5.13. Note average actograms after normalisation are presented here, rather than representative actograms, as mice under 12h:12h LD remain synchronised with each other making this possible.

The mean FAA percentage of total activity across the days of RF are presented in Figure 5.14. Analysis of the data found a significant main effect of number of days under RF ($F(9, 126)=3.898$, $p=0.0002$) showing we observe RF entrainment. There was no significant effect of the interaction of days x genotype ($F(9, 126)=0.789$, $p=0.627$) suggesting no genotype effect on the entrainment.

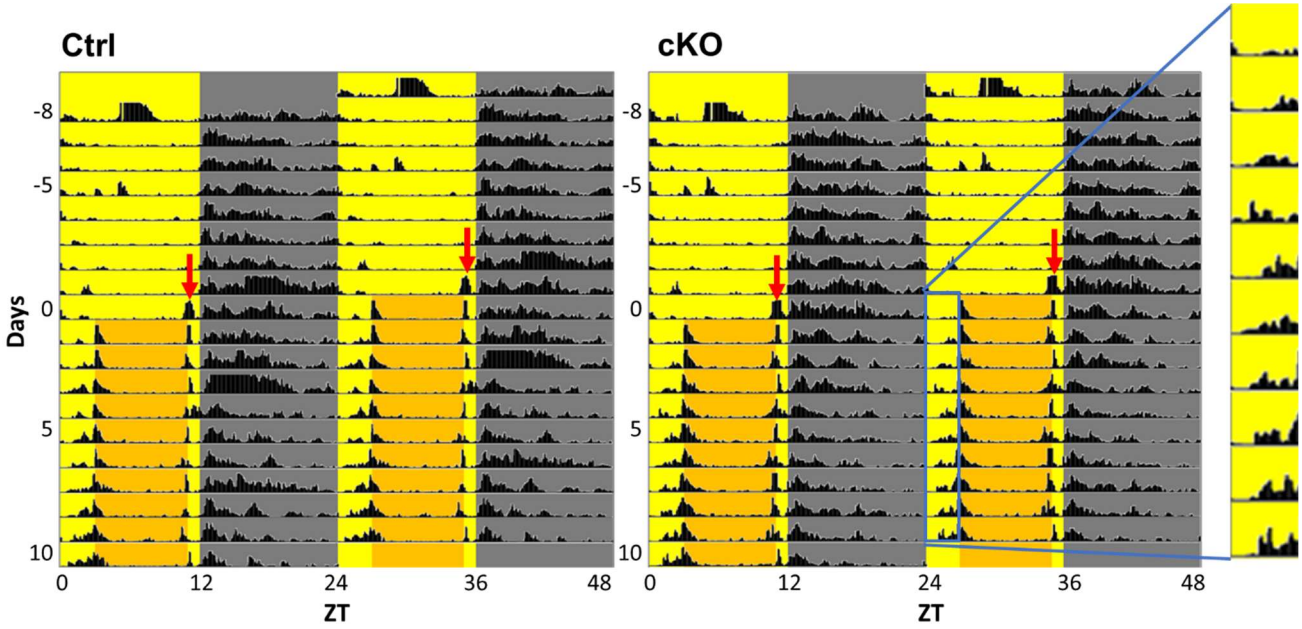

Figure 5.13: Activity of mice under restricted feeding

Average double plotted actograms for each genotype. Lights on or off are marked by yellow or grey, the beginning of food restriction is marked with a red arrow and the times of food availability when food restriction was underway is marked in orange. Note high activity was recorded when the food was provided or taken off each day due to this process being picked up by the tracking cameras as activity. The actograms show the appearance of FAA active periods prior to food provision while the lights were on (highlighted in the cKO actogram) when the animals were inactive on previous days.

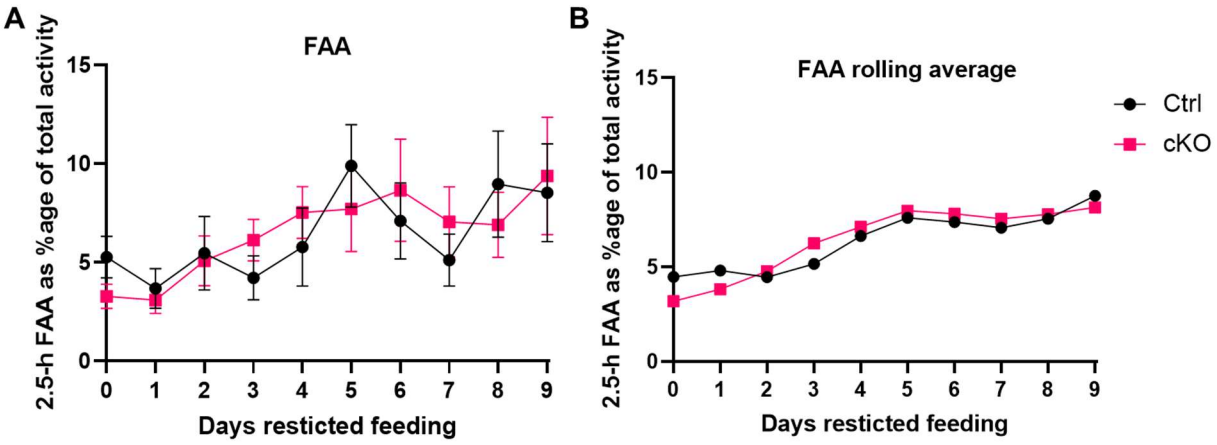

Figure 5.14: Food anticipatory activity

A: The mean percentage of daily activity which falls within the 2.5-hour FAA window (±SEM). **B:** Rolling average of the recorded data for visualisation only. Each data point here is the mean of the three values of the day and the two days either side except days 0 and 9 which were the mean of two days. An upward trend is seen as the animals adjust to the feeding schedule.

Average actograms of mice split by sex and genotype groups are presented in Figure 5.15. FAA percentage data including the factor of sex are presented in Figure 5.16. These data showed a significant main effect of number of days under RF ($F(9, 108)=4.925$, $p=0.00002$) and of the interaction of days x sex ($F(8, 96)=5.046$, $p=0.00001$), but not days x genotype ($F(9, 108)=0.997$, $p=0.447$) or the interaction of all three ($F(9, 108)=0.642$, $p=0.759$).

As there was an interaction, we split the data by sex for analysis. There was no significant effect of day for female mice ($F(3.537, 24.760)=0.964$, $p=0.437$) but there was for male mice ($F(3.895, 27.267$, $p=0.009$) (Greenhouse-Geisser corrected). This means that the behaviour change due to RF is only observed in male mice and we were not able to see an effect of RF on anticipatory behaviour in female mice even over 9 days.

The male data was analysed using a Bayesian mixed factor ANOVA with equal prior probabilities for each model. The analysis determined that the data were best represented by a model using days under RF as the only factor ($BF_{10}=2.16\text{x}10^4$ compared to the null model, indicating decisive evidence). Analysis of effects showed decisive evidence for the main effect of days under RF ($BF_{incl}=2.22\text{x}10^4$), and substantial evidence against the effect of the interaction of number of days x genotype ($BF_{incl}=0.242$). This supports the frequentist ANOVA in showing a clear effect of number of days under RF as expected. More importantly, the Bayesian analysis identifies that our data confidently implies no effect of an interaction of day x genotype in male mice rather than being underpowered to identify such an effect. We conclude that the liver-specific loss of NPAS2 expression does not have an effect on RF entrainment in male mice. This measure was however unable to identify RF entrainment in female mice.

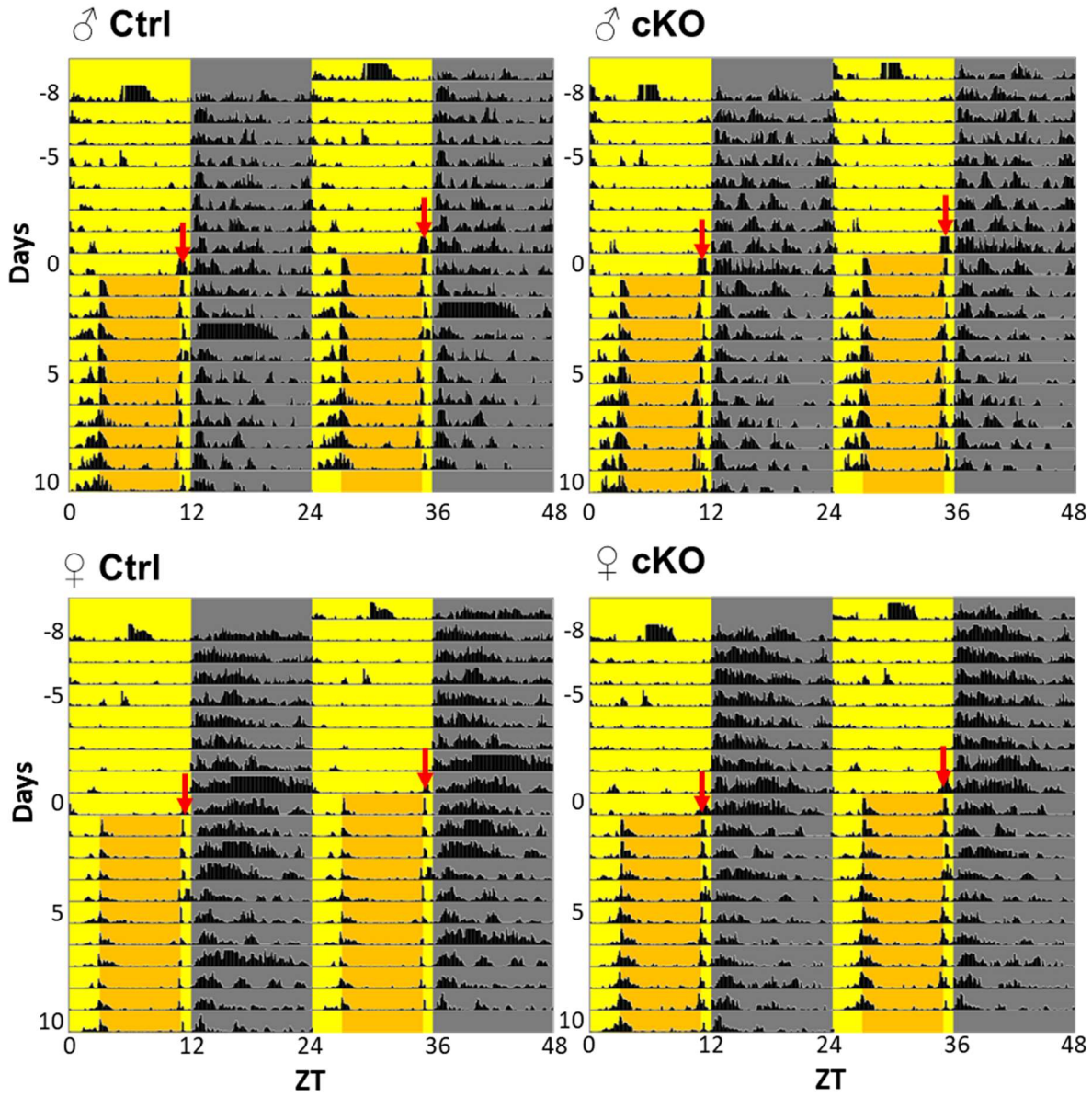

Figure 5.15: Activity of male and female mice under restricted feeding

Average double plotted actograms for each of the genotype and sex mouse groups. Lights on or off are marked by yellow or grey, the beginning of food restriction is marked with an arrow and the times of food availability when food restriction was underway is marked in orange. Note high activity recorded when the food was provided or taken off each day due to this process being picked up by the tracking cameras as activity.

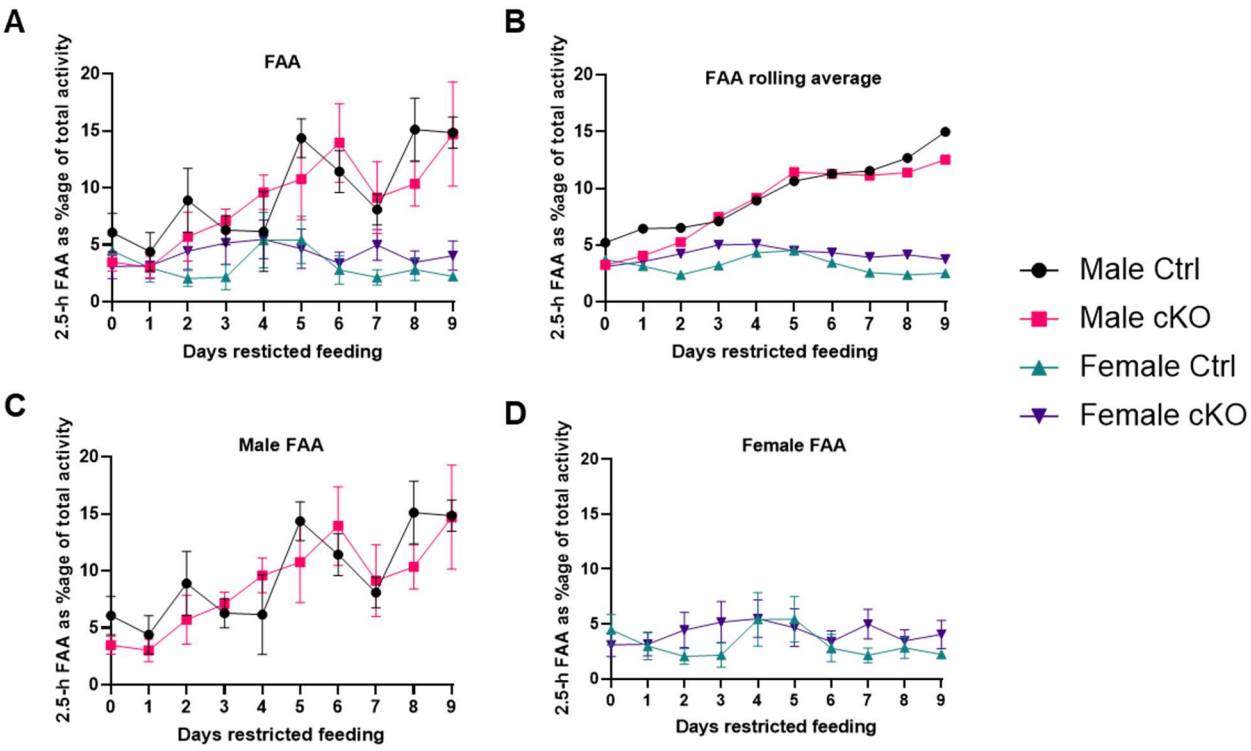

Figure 5.16: Food anticipatory activity of male and female mice

The mean percentage of daily activity which fell within the 2.5-hour FAA window (±SEM). **A:** All data across days of RF. **B:** Rolling average of the recorded data to smooth out daily fluctuations as described in Figure 5.14. **C & D:** Sex separated graphs of the data presented in A to allow clear visualisation of the behaviour of each sex group. Activity of male mice showed the upward trend while the activity of female mice remained consistent across days with only minor fluctuation.

5.6.1.2 Weight

The effect of the RF procedure on mouse weight is shown in Figure 5.17. It appears that the inclusion of mash and the 8-hour feeding window countered any weight loss and prompted weight to be put on by some mice under the procedure. Analysis of weight changes compared to initial weight by Pearson's analysis showed a significant negative correlation ($r=-0.854$, $p=0.00003$) showing that mice with a lower weight put on more weight over the course of RF as shown in Figure 5.17 D. This effect is likely because the amount of wet mash diet was provided equally to all mice meaning lighter mice were provided much more per body weight.

As weight is a potential confounding variable, the FAA percentage data was analysed by mixed measures ANCOVA with initial weight as a covariate. There was no significant interaction of initial weight x days under RF on presentation of FAA activity for all mice or sex separated data (all mice: $F(1,11)=0.442$, $p=0.520$, female mice: $F(1,5)=1.133$, $p=0.336$, male mice: $F(1,5)=0.46$, $p=0.838$).

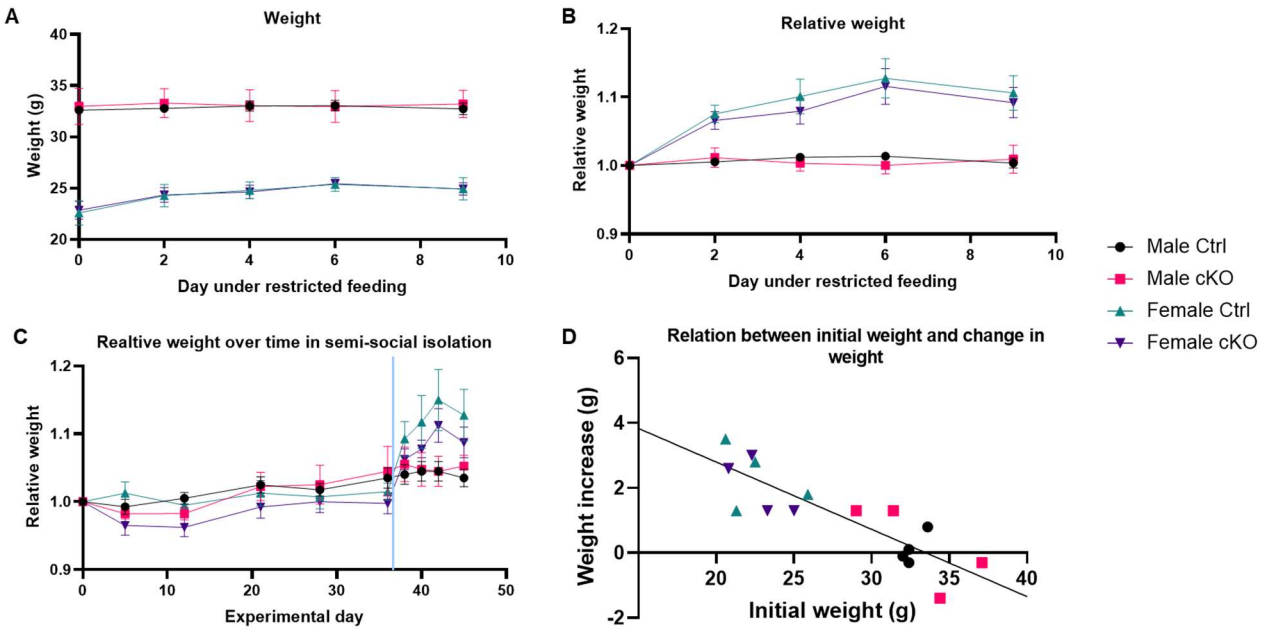

Figure 5.17: The effect of the restricted feeding procedure on mouse weights

A: Mean mouse weights (±SEM) over the RF procedure for each group distinct by genotype and sex **B:** Mean weights relative to the weight when RF began (±SEM). **C:** Mean weights relative to the day the mice were placed into the circadian cages (±SEM). The blue line marks the beginning of RF. **D:** Mean change in weight (±SEM) over the 10 days of RF compared to weight at the beginning of RF. Under RF significant weight loss was prevented in male mice and female mice increased weight. This is likely due to the initial lower weight of the female mice rather than a pure sex difference as higher initial weight is correlated with weight change.

5.6.1.3 Additional FAA measures investigated

We were unable to see entrained FAA behaviour in female mice using the standard percentage activity measure, despite some FAA still appearing to be present in individual female mice actograms (Figure 5.15). We investigated two other measures to investigate whether these showed greater sensitivity to detect FAA in our data. First, the total activity in the FAA window without correction to total activity, as it was possible that the higher level of general total daily activity in female mice obscured the appearance of FAA when used as a percentage measurement. The second measure was the time of onset of activity prior to food provision which should shift earlier as the FEO is entrained to the feeding schedule (detailed in methods section 5.2.5.5). Note that the experiment ended on the tenth day meaning it could not be included in the FAA percentage analysis due to the lack of a full tenth day required for percentage calculation. However, when assessing the activity prior to food provision without respect to the full day, data from all 10 days can be included. The analysis of the raw FAA data is not detailed here as it showed similar data to that of the percentage FAA. Analysis identified no effect of day on female activity while this effect was still observed for male mice suggesting that the high level of daily activity in female mice was not obscuring an entrainment effect.

For time of onset, data fluctuations and variability make this measure unclear graphically, however an upward trend can be seen in all groups when a rolling average is used (Figure 5.18). The GEE analysis showed a significant main effect on activity onset of number of days under RF ($\chi^2(1)=62.921$, $p<0.00001$) and the interaction of days x sex x genotype ($\chi^2(1)=4.261$, $p=0.039$) without significant interaction effects of days x genotype ($\chi^2(1)=0.009$, $p=0.925$) or days x sex ($\chi^2(1)=0.409$, $p=0.523$).

To follow up on the significant interaction, the same analysis was performed on the male and female data individually. In male mice the analysis showed a significant effect of day ($\chi2(1)=32.002$, $p<0.0001$) without a significant interaction effect of day x genotype

($\chi2(1)=3.499$, $p=0.061$) on the time of activity onset. This is consistent with the finding in male mice using the FAA percentage of activity measure as detailed in 5.6.

Analysis of female mice identified a significant effect of day ($\chi2(1)=31.711$, $p<0.00001$) and a significant interaction effect of genotype x day ($\chi2(1)=17.166$, $p=0.00003$). This suggests both that we are observing the effect of RF entrainment, as well as a genotype effect on this entrainment. To further investigate this effect the GEE analysis was used to confirm that a significant effect of day was observed in both genotypes of female mice. A significant effect of day on activity onset was observed for both control ($\chi2(1)=13.298$, $p=0.00027$) and cKO mice ($\chi2(1)=18.635$, $p=0.00002$). This confirms that RF entrainment is still observed in both genotypes.

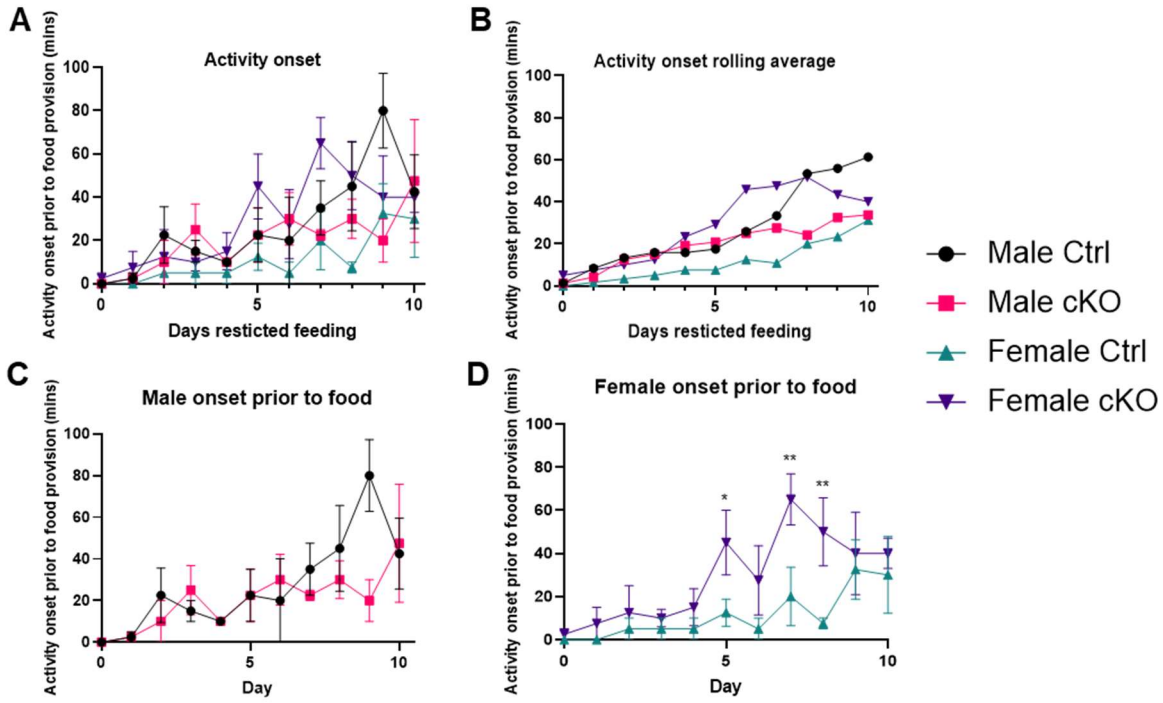

Figure 5.18: Time of activity onset as a measure of behavioural response to restricted feeding.

Onset is presented as the number of minutes prior to food provision from which consistent activity was observed. **A:** Mean time of activity onset prior to food provision (±SEM) for each sex and genotype group **B:** Rolling average of the time of activity onset data based on 3 days **C & D:** Mean onset data (±SEM) as presented in A showing only male (C) and female (D) data to allow clearer comparison. Significance of genotype comparisons within each day for female mice (from Table 5.1) are presented on figure D.

Post hoc analysis was performed comparing the effect of genotype on time of activity onset in female mice on each day, the results of these comparisons are shown in Table 5.1.

These analyses identified significant genotype differences on days 5, 7 and 8. Looking at the data in Figure 5.18 D it can be seen that this is due to earlier activity onset in cKO mice on those days and the significance is lost in the later days as the control mice begin to present an earlier time of activity onset. This suggests faster entrainment of cKO female mice to the feeding schedule.

Table 5.1: Post hoc comparison of genotype effect on activity onset timing in female mice in each day of restricted feeding entrainment using generalised linear modelling

Day	Genotype effect on activity onset
0	$\chi2(1)=1.333$, p=0.248
1	$\chi2(1)=1.333$, p=0.248
2	$\chi2(1)=0.414$, p=0.520
3	$\chi2(1)=0.800$, p=0.371
4	$\chi2(1)=1.333$, p=0.248
5	$\chi2(1)=5.323$, p=0.021*
6	$\chi2(1)=2.400$, p=0.121
7	$\chi2(1)=8.308$, p=0.004*
8	$\chi2(1)=9.398$, p=0.002*
9	$\chi2(1)=0.135$, p=0.713
10	$\chi2(1)=0.364$, p=0.546

5.6.2 Discussion

5.6.2.1 Genotype effects on RF entrainment

In our initial investigation using percentage activity as a measure of the main genotype effect across both sexes we observed RF entrainment and analysis suggested no effect of the loss of liver NPAS2 on this entrainment. This is in contrast to the delayed RF entrainment previously observed in constitutive NPAS2 KO mice (Dudley et al., 2003).

We found a significant effect of sex on the entrainment to RF as female mice did not display a change in percentage FAA over the experimental days. This means this data measurement could not be used to investigate a genotype effect in female mice. Based on Bayesian analysis, the data from male mice provides substantial evidence against an effect of genotype on entrainment to RF. It is concluded therefore that there is no significant effect of loss of liver expression of NPAS2 on behavioural response to RF in male mice specifically.

Measurement of FAA based on the time of onset of activity showed that an earlier shift in activity onset across the repeated days exposed to RF was observed for both male and female mice. There was no main genotype effect found on this measure in males. However, an enhancement of entrained response to RF was observed in cKO female mice. This suggests that in female mice the RF entrainment was enhanced by the loss of NPAS2 expression in the liver when measured by time of onset of activity.

The finding that we did not see delayed RF entrainment as reported in constitutive KO mice (Dudley et al., 2003) suggests that the previously reported effect is due to loss of NPAS2 in other tissues or may be a developmental effect avoided in this model. It should be noted that the study performed by Dudley et al. (2003) was on male mice only and we have observed effects in female mice (and only in one measure). Since this experimentation observed this effect purely in female mice, there may also be a sex effect of the response in the constitutive model that remains unknown.

5.6.2.2 Sex differences

Using activity as a measure of FAA we did not find a RF effect in female mice. It has been reported that female mice present a blunted FAA response compared to male mice. In published research measuring activity by cage activity female mice took longer to show high FAA than males although FAA was still observed after 7 days (Aguayo et al., 2018). Based on this it is possible that we would be able to observe FAA using the standard percentage of total day activity measure (presented in Figure 5.16) in females if they remained under RF for longer. However, our data for female mice does not appear to show even a subtle increasing of FAA so we are unable to conclude with confidence that it would develop given more time. It is possible that the effect would present in the percentage FAA measure for female mice under a stricter RF regimen. The longer window of food availability should not have prevented FEO entrainment as a change in activity would still be required for the mice to be active at an abnormal time to eat. It may however have prevented a significant presentation of FAA, as any active period within that window would have allowed the mice to eat.

We found an RF effect in female mice using a measure of onset of FAA only, while in male mice both measures detected the RF effect. This suggests that we did not observe a change in female activity levels within the 2.5-hour FAA window but a clustering of the activity to the time immediately prior to food provision. The weakness of the percentage FAA measure appears to be the high background level of activity of female mice, even in the light phase.

Using the onset of activity measure of FAA, our data shows a genotype effect specifically within female mice. We also observed the findings using this measure in male mice were consistent with those of the FAA percentage of activity measure. The enhancement of FEO entrainment within the cKO female mice suggests NPAS2 in the liver of control mice may act counter to the FEO entrainment in female mice specifically. Oestrogen signalling in female mice has been identified to influence timing of activity onset (Royston et al., 2014,

Hatcher et al., 2020). Ovariectomised females have also been shown to present enhanced 4-hour RF entrainment (Li et al., 2015) which is posited as presenting a role of oestrogen, although a study where a restricted amount of food was provided at a set time each day observed no effect of ovariectomy on entrainment (Aguayo et al., 2018). While this data is contradictory it suggests that it may be that the loss of liver NPAS2 influences behaviour via an effect on oestrogen signalling. A potential mechanism of this, through an effect on the liver, would be modification of the metabolism of oestrogen. Oestrogen metabolism is performed primarily by the liver expressed cytochromes P450 enzymes CYP1A1, CYP1A2 and CYP3A4 (homologous to CYP3A11, CYP3A16, CYP3A41A, CYP3A41B and CYP3A44 in mice) (Tsuchiya et al., 2005, Renaud et al., 2011). CYP1A1, CYP1A2 and CYP3A11 have all been identified to show rhythmic expression in the female mouse liver (Lu et al., 2013, Lin et al., 2019). If loss of NPAS2 modulates the expression of these enzymes in the liver, then the modification of oestrogen metabolism may be behind a sex-specific effect. Alternatively, it is known that oestrogen can influence metabolism in the liver and the liver shows circadian expression of oestrogen receptors which are under an E-box promotor (Eagon et al., 1986, Cai et al., 2008). If NPAS2 influences the expression of the oestrogen receptors in the liver this may influence metabolic cycles specifically in female mice. This may then influence behavioural entrainment to RF.

We found that loss of NPAS2 expression in the liver is not associated with a negative impact on weight loss recovery when the mice were kept under RF conditions. Our findings are consistent the observations of O'Neil et al. (2017) using these mice. A negative impact of weight loss recovery would be expected if the cKO mice took longer to develop FAA, regardless of any other metabolic associated effect, as slower FEO entrainment would cause extreme weight loss. This finding also suggests that the improved weight recovery in male mice observed by O'Neil et al. (2017) was not due to faster circadian entrainment compared to

controls, which the male mice did not present, but due to another mediating effect such as that on the microbiome. For female mice we did observe accelerated entrainment while O'Neil et al. observed no effect on weight recovery. This supports the weight recovery being independent of an effect on FEO entrainment.

5.7 Conclusions

5.7.1 Results summary

Investigations of the free-running periods, daily locomotor activity and entrainment of behavioural cycles to light pulses in control and cKO mice found no evidence for an effect of the cKO of NPAS2 in the liver. However, potential sex x genotype interactions were suggested by the results of these tests. In male mice we showed no effect of the cKO on entrainment of behavioural cycles to restricted feeding while in female cKO mice a significant enhancement of the entrainment to restricted feeding was observed.

5.7.2 Free-running period

We observed no effect of the liver cKO on free-running behaviour (based on general cage activity analysed by FFT-NLLS), although the data supports further investigation of a potential sex x genotype interaction effect with a potential lengthening of the free-running period in female mice. If supported this would suggest a contribution of the liver clock to behavioural period when food is available *ad libitum* under DD. A sex influence on this effect may suggests a contribution of oestrogen signalling in between clock entrainment as suggested in 5.6.2.2.

5.7.3 Daily locomotor activity

Overall activity is modulated by sex, but we found no evidence of a genotype effect on daily activity levels. We did observe that a significant sex difference in activity levels in the light phase was only observed in cKO mice. A sex-specific effect of the cKO on total daily activity is suggested by the data and may be of interest for further investigation.

The investigation of daily activity patterns was underpowered, but the data suggested potential sex-specific effects of the cKO which may warrant further investigation.

5.7.4 Light and food entrainment

We observed no effect of loss of liver NPAS2 on entrainment to either light or RF in male mice. This is in contrast to Dudley et al. (2003) using constitutive KO mice, who found inhibited RF and enhanced light entrainment. These findings suggest that these entrainment impairments following NPAS2 KO may not have been dependant on a role of NPAS2 in the liver.

In female mice we observed the loss of NPAS2 expression in the liver enhanced behavioural entrainment to feeding when measured as time of onset of activity. Female mice were not used in prior studies of entrainment in constitutive KO mice, it is possible that a sex effect may have been observed if they were. A possible explanation of this effect is an influence of liver NPAS2 on oestrogen signalling in circadian cycles (see section 5.6.2.2).

5.7.5 Future work

Further investigation of free-running behaviour will provide further insight into the potential sex effect observed.

While we were able to observe the effect of an early light pulse in the delaying shift in activity, we were unable to experimentally observe a light pulse induced phase advance. Repetition of the experimental procedure with light pulse performed at different times may be of interest to fully characterise the light response in the cKO mice, especially light pulses causing a phase advance.

Under RF we were able to see entrainment influencing time of activity onset in female mice and an enhancement of the response in cKO females. While this effect was clearly observed it would be preferable to observe this effect in the more robust percentage FAA measurement. As such it may be useful to perform a similar experiment with a reduced window of food availability as this may encourage the appearance of this behaviour and we have seen that these mice do not appear to be at risk of severe weight loss. Investigation of this effect

may be aided by investigation of gene expression in tissues of animals under RF. Tissues collected at multiple times on multiple days would allow observation of the entrainment process but would require a large number of mice. Tissues collected after a substantial number of days where FAA is clearly presented could be compared to mice under normal *ad libitum* feeding to potentially provide insight. It would also be of interest to identify the effect on the expression of genes related to metabolism especially those also related to NPAS2 such as Shp (Lee et al., 2015)

Chapter 6: Latent inhibition of cued fear conditioning in *NPAS2*$^{fl/fl}$/*Alb-cre* liver knockout mice

6.1 Introduction

6.1.1 Circadian cycles and cognition

Circadian cycles have been shown to impact on cognition, as detailed in Chapter 1 sections 1.10 (page 43) and 1.11 (page 44). This can be observed in cycling patterns in the performance of cognitive tasks, performance is generally optimal within the first 8 hours of activity in humans and mice, however this does depend on the specific task. For example, mice showed improved performance in contextual fear conditioning in the dark phase of a 12h:12h LD cycling environment (Valentinuzzi et al., 2001) however performance in tone-cued fear conditioning is improved when mice are trained in the light phase (Chaudhury and Colwell, 2002). Chronic disruption of circadian cycles leads to a deficit in cognitive function in both humans and animals (Krishnan and Lyons, 2015, Cho et al., 2000, Marquie et al., 2015) and KO of various core circadian genes has an impact on cognitive function in different ways (Wang et al., 2009, Kondratova et al., 2010) as detailed in section 1.11 (page 44).

6.1.2 Role of NPAS2 in cognitive tasks – studies in constitutive KO mice

Constitutive NPAS2 KO mice present defective long-term memory of cued and contextual fear conditioning, identified in male mice by Garcia et al. (2000). In this study mice were exposed to a repeated auditory cue and associated foot shock, to induce fear association. Either 30 minutes or 24 hours later, mice were exposed to the auditory cue (cued fear conditioning) or the conditioning cage (contextual fear conditioning) and freezing behaviour was assessed by overhead camera tracking. There was a clear conditioning effect but no genotype difference in freezing response to either cue or context when mice were tested after 30 minutes. However, 24 hours after exposure, mice with a constitutive KO of NPAS2 showed reduced freezing behaviour in response to both the cue and context, compared to controls. This suggests a deficit in long-term memory consolidation of the conditioning in the NPAS2 KO

mice. The effect of loss of NPAS2 function on memory is proposed to be mediated outside of the hippocampus as NPAS2 KO mice also showed no change in performance in the Morris water maze (Garcia et al., 2000), which has been associated with hippocampal function (Vorhees and Williams, 2006), see section 1.11 (page 44).

In a separate study, decreased anxiety-like behaviour has been demonstrated in NPAS2 constitutive KO mice in elevated plus maze, light/dark box, and open field assays (Ozburn et al., 2017). In mice with a selective viral vector shRNA knockdown of NPAS2 specifically within the nucleus accumbens, similar anxiolytic effects on these tests were observed (Ozburn et al., 2017). This suggests the role of NPAS2 in the nucleus accumbens is important for anxiolytic effects.

Within the nucleus accumbens *NPAS2* expression is highly enriched in specifically Drd1 dopamine receptor containing neurons, identified by RT-qPCR of neurons sorted by FACS for Drd1 expression. This is broadly consistent with the finding that NPAS2 expression is also required for rhythmic expression of dopamine receptors (Ozburn et al., 2015). Dopamine signalling pathways have also been shown to be important for both cued and contextual fear conditioning (Fadok et al., 2009, Ikegami et al., 2014). This may suggest that the loss of NPAS2 expression influences dopamine signalling, causing changes contributing to the observed behavioural phenotypes.

6.1.3 Latent inhibition

Latent inhibition (LI) is a process of learning to ignore irrelevant stimuli. The process is a measure of how past experience with a stimulus modulates the attention to, or readiness to form associations with, that stimulus (Lubow, 2005, Weiner and Arad, 2009). Experimentally LI is tested in mice by comparing two experimental groups. One group is pre-exposed to a stimulus such as a tone or light without consequence i.e., pre-exposed (PE) and one group is not pre-exposed to the stimulus i.e., non-pre-exposed (NPE). Both groups are then conditioned

to associate the stimulus with an outcome (e.g., footshock). LI is demonstrated as the PE group showing reduced fear conditioning to the stimulus compared to the NPE group.

In rats, circadian modulation of LI of learning of taste aversion has been observed. Rats pre-exposed and conditioned at a different time of day to testing showed loss of LI effect (Manrique et al., 2004). This suggests LI of association of stimuli is enhanced by matching time of day context. As such the circadian system contributes to LI and modulation of the circadian system may affect LI performance.

LI appears to rely on signalling within the nucleus accumbens, as shown by the disruption of LI by amphetamine when introduced both systemically and by microinjection to the NAc shell (Nelson et al., 2011). The Drd1 and Drd2 dopamine receptors play different roles in of LI. It has been shown that in mouse models with a KO of Drd1, normal disruption of LI induced by D-amphetamine was attenuated, while a Drd2 KO had no effect (Bay-Richter et al., 2013). It has also been shown there are opposite effects of dosing with Drd1 or Drd2 receptor antagonists on LI, with Drd2 antagonists associated with increased LI effect and Drd1 antagonists reduced LI effect (Diaz et al., 2015). This suggests a potential link between LI and NPAS2.

The LI paradigm measures both contextual control of conditioning and cued conditioning. As constitutive NPAS2 KO models have shown a modulation of fear conditioning activity indicating an influence of the KO on associative learning, possibly via a circadian influence, it was hypothesised that an effect may also present in LI of this learning. It was therefore considered to be a useful assay to further evaluate the influence of the loss of NPAS2.

6.1.4 Aims and Hypothesis

The following experiment was intended to establish whether KO of NPAS2 in the liver affects cued fear conditioning and the influence of LI on the fear conditioning. This experiment

was planned as a control for future brain specific NPAS2 KO mice to compare roles of NPAS2 both in and outside of the brain. It was hypothesised that there would be no effect of liver-specific KO of NPAS2 on either fear conditioning or LI of fear conditioning, as general brain function was predicted to be unaffected. It has however been noted that expression of the circadian genes within the brain are modified in the liver NPAS2 cKO mice (section 4.3.3.2, page 167), as such this investigation will inform whether this change affects LI of fear conditioning.

6.2 Materials and Methods

6.2.1 Animals

Mice were bred and housed as detailed in section 4.2.1.1 (page 152). Mice were used at 3-6 months of age. For mouse numbers see Table 6.1 below.

6.2.2 Conditioning chamber set-up

Training and testing occurred in six identical conditioning chambers (21.6 cm x 17.8 cm x 12.7 cm, ENV-307W; Med Associates Inc., St Albans, VT, USA) housed in light and sound-attenuating boxes (ENV-022V, Med Associates Inc.). The conditioning chambers were composed of Plexiglas walls in the front and back, stainless steel sides, and a metal grid floor connected to a shock scrambler and generator. Each box contained a house light, a ventilation fan, mounted at the back to provide air exchange and background noise (69 dB), and a sonalert mounted on the right wall for delivering the conditioned stimulus (CS) (85 dB) (ENV-323AW, Med Associates Inc.). Each chamber was equipped with a removable drink spout located in the left wall of the chamber. The lick spout was connected to a lickometer (ENV-250, Med Associates Inc.) which recorded the number of licks. The chambers were interfaced with a PC computer running MED-PC software (SOF-735, Med Associates Inc.) to control stimulus presentation and record data. The software programs ran are detailed in the appendix (section A.8, page 316).

6.2.3 Cued fear conditioning and latent inhibition of conditioning

The LI protocol was based on that of Bay-Richter et al. (2009) and consisted of six stages: water restriction, pre-training, pre-exposure/no pre-exposure, conditioning, re-establishment of drinking, and testing (summarised in Figure 6.1). Within this experimental protocol we were able to investigate fear conditioning and the LI separately to identify any specific effects as well as investigate the effect of extinction on both by inclusion of repeated

test days. Mouse testing in conditioning chambers commenced at approximately the same time within the morning each day.

Water restriction (days 1-7) - Mice were placed on a 22-h water restriction schedule 7 d before pre-training began. A daily ration of 2 h of water availability was provided in the home cages at the same time each morning.

Pre-training (days 8-13) - Mice were placed in the conditioning chambers and allowed to drink freely from a water sipper for 15 min. The number of licks made and latency to lick was recorded. After the training, the mice were provided a daily ration of 1 hour of water availability in the home cages, the procedure of post-training water provision was followed for the rest of the procedure.

Pre-exposure (day 14) - Mice were placed in the conditioning chambers without access to the water sipper. PE mice were given 60 presentations of an 85-dB 5 s tone with a 15 s interstimulus interval. NPE control mice were placed in the chambers for the same amount of time but received no pre-exposures to the tone.

Conditioning (day 15) - Mice were placed in the experimental chambers without access to the water sipper. After 5 min, two tone-footshock pairings were presented. Each tone (CS) was of 5 s duration and was followed by a 1 s 0.38 mA footshock. There was a 2.5-minute interval between pairings and mice remained in the chamber for 5 minutes following the second tone-shock presentation.

Rebaseline lick training (days 16-17) - Mice were placed in the conditioning chambers for 15 minutes and given free access to the water sipper to re-establish licking in the chamber prior to testing. The same software script was used as that for pre-training.

Testing (day 18-21) - Mice were placed in the conditioning chambers with access to the water sipper. The number of licks and the time to complete licks 90-100 (lick time; LT) were recorded electronically. After the first 90 licks, the tone CS was presented until the mouse

reached lick 100. The measure in seconds (s) of time taken to complete licks 90-100 in the presence of the CS (LT) can be compared across to mice to investigate effects on conditioned suppression. Testing on following days investigated the effect of extinction on the acquired fear conditioning. Extinction was measured by repeating the test phase three days beyond the initial day to give a total of 4 test sessions.

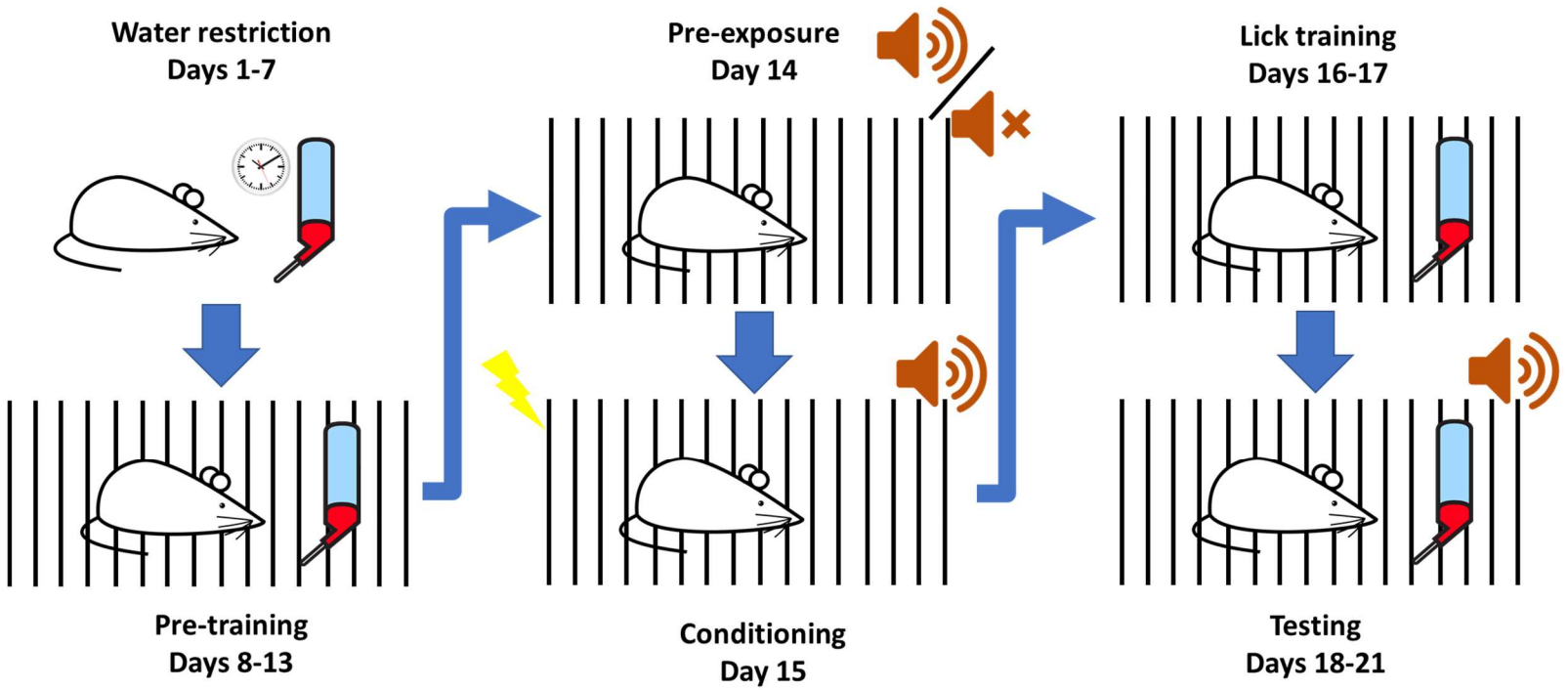

Figure 6.1: Latent inhibition of fear conditioning experimental protocol

Mice were placed on water restriction 7 days prior to, and throughout, the experiment. Over 6 days pre-training the mice were habituated to the test chamber. On the day of pre-exposure, the PE group were exposed repeatedly to the tone while the NPE group were simply placed in the chamber for the same amount of time. On the conditioning day all mice were exposed to two tone-footshock pairings. Two rebaseline lick training days then allowed restoration of normal drinking behaviour in the chambers. On the four test sessions mice were exposed to the tone immediately on reaching lick 90 and the tone continued until they reached lick 100. Conditioning is measured as slowing or cessation of drinking during the tone presentation. LI is shown as reduced conditioning in the group of mice pre-exposed to the stimulus compared to the group not pre-exposed.

6.2.4 Experimental design

Mice were tested across two experimentally identical cohorts (Table 6.1). Sexes were pooled as previous work by our lab group identified no sex effect on fear conditioning and LI in WT C57BL/6 mice (Bay-Richter et al., 2013). The experiment was approximately counter-balanced for sex and equally distributed between PE and NPE mice for each genotype as much as was possible with mouse numbers available.

Power calculations were performed based on reported effect of mutation of the *Disc1* gene on LI which was investigated using a similar protocol (Haque et al., 2012). Based on the reported values, using Formula 5.1 and the G power software the Cohen's f for the genotype effect on LI was determined as 0.287. Using an alpha value of 0.05, power of 0.9, non-sphericity correction of 1 and an estimated repeated measures correlation of 0.5, G power analysis identified that an experiment would be suitably powered to identify a similar sized effect with a total of 36 mice based on a mixed model ANOVA of four groups across four repeats. Based on this at least 9 mice were used for each group, influenced by mouse availability.

Table 6.1: LI mouse sample sizes

Sex and genotype	Cohort 1		Cohort 2		Total	
	NPE	PE	NPE	PE	NPE	PE
♂ cKO	2	2	3	3	5	5
♂ Ctrl	2	3	4	3	6	6
♀ cKO	3	3	1	2	4	5
♀ Ctrl	4	3	1	2	5	5

The data was analysed to separately consider the behavioural outcomes of fear conditioning, LI, and extinction as these reflect separate behavioural mechanisms which, while we were able to investigate within one procedure, are of interest independently to evaluate the effect of the NPAS2 liver cKO.

6.2.5 Statistical analysis

Frequentist statistical tests were performed using SPSS software as described in Chapter 3, section 3.2.3 (page 123). For mixed repeated measures ANOVAs sphericity was assessed by Mauchly's test of sphericity. Independent t-tests were used for investigation of the between-subjects factor of genotype, factorial ANOVAs are used for analysis of combinations of the between-subjects factors of genotype, sex, and pre-exposure on the first test day and mixed ANOVAs were used for investigations of extinction including the within-subject factor of test day. Due to the identification of non-normal distributions of the data, log transformations were used to generate normally distributed data for all analyses in this chapter. Matching Bayesian tests were performed in JASP to supplement frequentist tests and identify support for the null hypothesis as described in Chapter 5, section 5.2.7 (page 156).

6.3 Results

6.3.1 Latent inhibition of fear conditioning behaviour

Fear conditioning was measured using the time taken (s) to complete licks 90-100 while being exposed to the CS tone stimulus (LT). The LI effect is observed as decreased log LT in PE mice as these mice do not form as strong fear association with the stimulus compared to the NPE groups (Figure 6.2).

The results of the statistical analysis are presented in Table 6.2**Error! Reference source not found.**. Interaction effects which include the factor of pre-exposure condition reflect effects on the LI, while other factors and interactions reflect effects on fear conditioning. A significant effect of pre-exposure and a significant effect of sex were identified but there was no significant effect of genotype. No interaction of sex with genotype was identified and nor any significant effect of sex or genotype on LI (interaction terms including pre-exposure).

Bayesian analysis favoured a model consisting of the factors of both pre-exposure and sex independently (BF_{10}=12.848 compared to the null model, indicating strong evidence). Analysis of effects, shown in **Error! Reference source not found.**, identified substantial evidence for the effect of pre-exposure. Substantial evidence was identified against a main effect of genotype suggesting no genotype effect on fear conditioning while evidence was inconclusive regarding interaction effects.

This analysis shows a sex effect in fear conditioning behaviour. While the Bayesian investigation suggests only weak evidence for the effect of sex, taken together with the frequentist analysis, as it does still favour an effect, this conclusion stands. The analysis is suggestive against an interaction of sex x genotype. This experiment was not designed to explicitly test genotype and sex comparison, so was underpowered to investigate these interaction effects. However, it appears graphically that improved learning was seen in cKO male mice compared to control male mice in NPE groups (see Figure 6.2 B**Error! Reference**

source not found.).

The significant effect of the pre-exposure condition shows the LI of fear conditioning. The lower fear conditioning response in male ctrl mice means that the reduction of fear response in this group due to PE is less obvious as the behaviour most likely approaches a baseline. We observe no significance for a sex x pre-exposure interaction and the Bayesian analysis shows the data provides only weak evidence against the interaction, so we are restricted by the power of this study to conclude an effect of sex on the LI of fear conditioning. The analysis suggests we observe only weak evidence that liver-specific NPAS2 cKO does not influence LI of fear conditioning.

Table 6.2: Results of frequentist and Bayesian three-way ANOVA analysis of LI of fear conditioned behaviour in mice and the effects of genotype and sex

Effect	Frequentist ANOVA	Bayesian ANOVA	Bayesian conclusion
Pre-exposure	F(1,33)=8.524, p=0.006*	BF_{incl}=6.894	Substantial evidence for
Genotype	F(1,33)=0.057, p=0.812	BF_{incl}=0.318	Substantial evidence against
Sex	F(1,33)=4.959, p=0.033*	BF_{incl}=2.383	Weak evidence for
Pre-exposure x Genotype	F(1,33)=0.454, p=0.505	BF_{incl}=0.459	Weak evidence against
Pre-exposure x Sex	F(1,33)=0.632, p=0.432	BF_{incl}=0.507	Weak evidence against
Genotype x Sex	F(1,33)=0.356, p=0.555	BF_{incl}=0.443	Weak evidence against
Pre-exposure x Genotype x Sex	F(1,33)=0.486, p=0.491	BF_{incl}=0.503	Weak evidence against

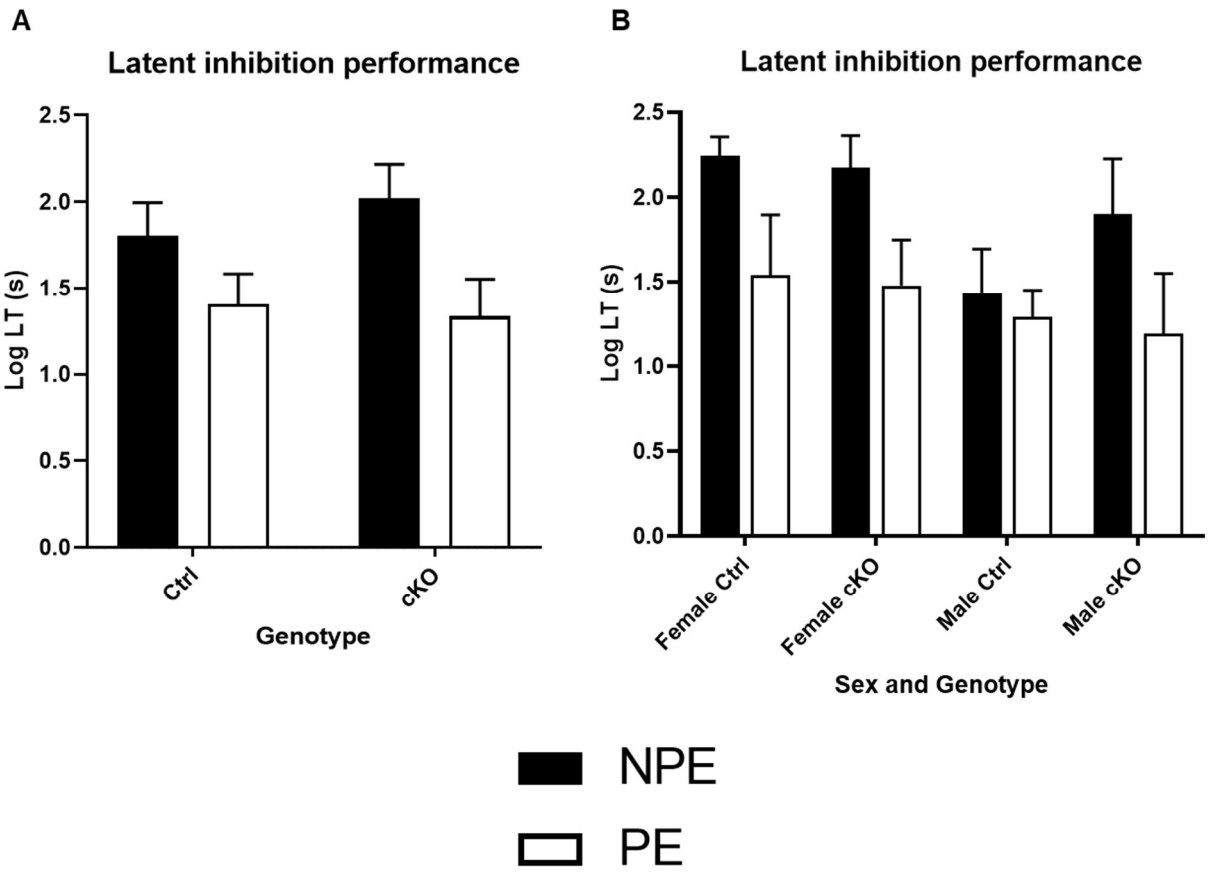

Figure 6.2: Latent inhibition of fear conditioned lick behaviour

A&B: Log mean time taken to perform 10 licks (±SEM) while exposed to the conditioned stimulus (LT) of mice pre-exposed (PE, ○) and not pre-exposed (NPE, ●) to the stimulus. **A:** The effect of pre-exposure condition and genotype. **B:** The effect of pre-exposure condition, genotype, and sex. Decreased LT is apparent for all PE groups in comparison to NPE except the male ctrl mice, due to lesser fear conditioning of male NPE mice.

6.3.2 Extinction of learned behaviour

Extinction is the gradual loss of the learned fear response with repeated exposure of the conditioned stimulus without negative reinforcement. The extinction of fear conditioned behaviour in, both PE and NPE mice, is shown in Figure 6.3, the results of the analysis are presented in Table 6.3. The extinction due to test day showed a significant effect on log LT and significant effects of pre-exposure condition and sex were identified, without a significant genotype effect. No significant interaction effects were identified. Graphically we see the log LT decrease most obviously between the early days, as extinction of the fear conditioning occurs, and little change between day 3 and 4, as behaviour approaches a baseline.

Bayesian analysis favoured a model of independent effects of day, sex, and pre-exposure (BF_{10}=4.51x10^7 compared to the null model, indicating decisive evidence). Analysis of effects are shown in Table 6.3. The Bayesian analysis supports the frequentist identification of significant factors identifying substantial or stronger evidence in favour of those effects. Strong evidence against a genotype x test day interaction and substantial evidence against sex x day and sex x genotype x day interactions suggest sex and genotype had no effects on the extinction of the fear conditioning. Similarly substantial evidence against pre-exposure x sex x day and pre-exposure x genotype x sex x day was identified. For other factors and interactions only weak evidence against them was identified. Taken together the data confirms the occurrence of the extinction of the conditioned fear. However, the data is not conclusive but suggestive against any difference in fear conditioning, LI and LI influenced extinction of fear conditioning presentation in mice with a liver-specific NPAS2 cKO.

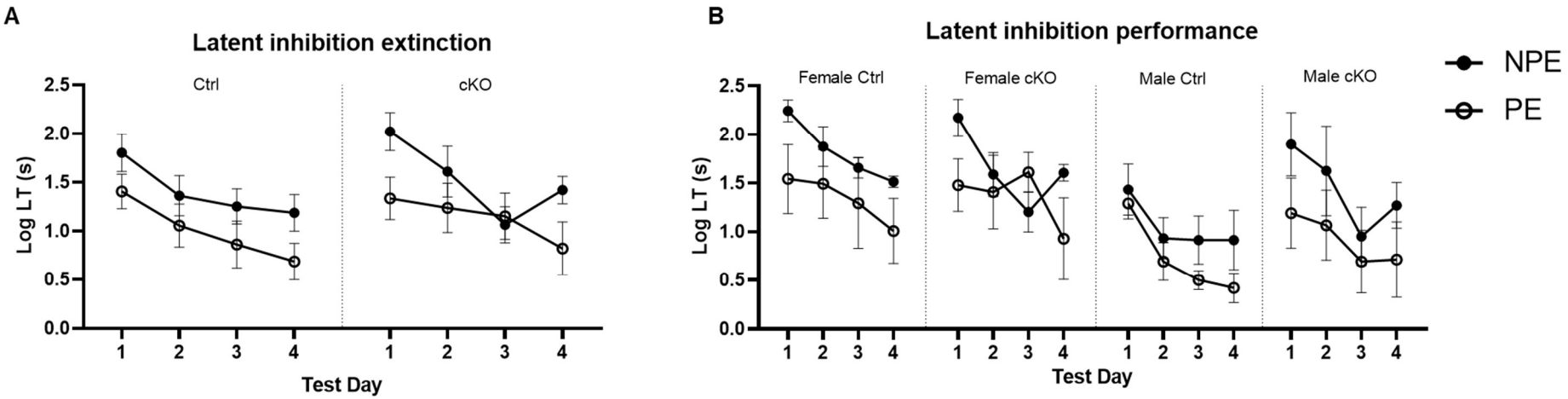

Figure 6.3: Latent inhibition and extinction of fear conditioned lick behaviour

A&B: Log mean time taken to perform 10 licks (±SEM) while exposed to the conditioned stimulus (LT) of mice pre-exposed (PE, ○) and not pre-exposed (NPE, ●) to the stimulus, showing the extinction of the learning over repeated days. **A:** The effect of pre-exposure condition and genotype. **B:** The effect of pre-exposure condition, genotype, and sex. For almost all groups the reduction in LT is clearly observed on test day 1 in mice which were pre-exposed. As extinction of the training occurs over the test days the performance of NPE and PE mice becomes similar, approaching a baseline. The only group where this is not clearly apparent is for the male ctrl mice which as previously noted did not present as clear fear conditioning as that observed in the other groups.

Table 6.3: Results of frequentist and Bayesian mixed ANOVA analysis of extinction of fear conditioned behaviour in mice and the effects of genotype and sex

Effect	Frequentist ANOVA	Bayesian ANOVA	Bayesian conclusion
Pre-exposure	F(1,33)=6.604, p=0.015*	BF_{incl}=4.765	Substantial evidence for
Day	F(1,99)=14.532, p<0.00001*	BF_{incl}=7.53x10^5	Decisive evidence for
Genotype	F(1,33)=0.425, p=0.519	BF_{incl}=0.426	Weak evidence against
Sex	F(1,33)=10.669, p=0.003*	BF_{incl}=24.459	Strong evidence for
Pre-exposure x Day	F(1,99)=1.764, p=0.159	BF_{incl}=0.347	Weak evidence against
Pre-exposure x Genotype	F(1,33)=0.001, p=0.978	BF_{incl}=0.437	Weak evidence against
Pre-exposure x Sex	F(1,33)=0.008, p=0.929	BF_{incl}=0.408	Weak evidence against
Genotype x Day	F(1,99)=0.297, p=0.827	BF_{incl}=0.092	Strong evidence against
Sex x Day	F(1,99)=0.672, p=0.571	BF_{incl}=0.166	Substantial evidence against
Genotype x Sex	F(1,33)=1.338, p=0.256	BF_{incl}=0.718	Weak evidence against
Pre-exposure x Genotype x Day	F(1,99)=1.188, p=0.318	BF_{incl}=0.387	Weak evidence against
Pre-exposure x Sex x Day	F(1,99)=0.938, p=0.426	BF_{incl}=0.318	Substantial evidence against
Pre-exposure x Genotype x Sex	F(1,33)=0.387, p=0.538	BF_{incl}=0.556	Weak evidence against
Genotype x Sex x Day	(F(1,99)=0.727, p=0.538	BF_{incl}=0.243	Substantial evidence against
Pre-exposure x Genotype x Sex x Day	F(1,99)=0.339, p=0.797	BF_{incl}=0.284	Substantial evidence against

6.4 Discussion

6.4.1 Results summary

Our data identified a significant effect of pre-exposure showing that we have demonstrated LI of fear conditioning. We also observed a significant effect of sex, this is likely due to lower baseline fear conditioning of male mice, clearly visible in NPE ctrl mice. This data is evidence against a main effect of genotype on fear conditioning but is inconclusive regarding a genotype x sex interaction. We observe only weak evidence that liver-specific NPAS2 cKO does not influence LI of fear conditioning.

Investigation over repeated days similarly identified significant effects of pre-exposure and sex as well as a significant effect of the factor of day showing the effect of extinction. The data was found to provide evidence against sex, genotype and sex x genotype interaction effects on the extinction.

6.4.2 Fear conditioning, LI, and extinction

No difference was identified in either the fear conditioning or the LI response between genotypes. This supports loss of liver expression of NPAS2 having no effect on fear conditioning behaviour. This was expected but means we do see a successful experimental set up for use with any future brain specific tissue KO models using this floxed line and suggests that the disruptive effect of NPAS2 as reported by Garcia et al. (2000) were not due to effects within the liver.

Extinction of the learning appeared as expected, with a greater decrease in log LT across the earlier days which became a much lesser decrease as the behaviour approached a baseline for lick speed. Mice with a lower initial log LT due to LI showed similar decreases of behaviour approaching a baseline the only difference observed being the log LT was lower on test day 1 for pre-exposed mice. The extinction of the behaviour was not significantly modified in the

liver-specific NPAS2 cKO mice suggesting that NPAS2 in the liver and any effects on brain regions have no influence on the extinction effect.

It should be noted that the experimental process used here was slightly different to that performed by Garcia et al. (2000) on constitutive NPAS2 KO mice where the impact was originally identified. The original experiment identified the fear conditioning through freezing behaviour, while we investigated fear conditioning via cessation of drinking behaviour. In the Garcia paper the fear conditioned behaviour was investigated 24 hours after conditioning while our experimental conditions investigate lick behaviour in the presence of the CS 72 hours after conditioning. This is due to two days of lick training after fear conditioning, required to prevent contribution of contextual fear effects of the test chamber on behaviour, and isolate the effect of the cue on drinking behaviour.

6.4.3 Sex-specific effects

In these data we identified a significant sex effect in fear conditioning with male mice showing reduced fear conditioning compared to female mice. Previous work from our lab using this experimental procedure had identified no sex difference in presentation of fear conditioning and LI of the conditioning in wild type C57BL/6 mice, so this sex effect was unexpected (Bay-Richter et al., 2013, O'Callaghan et al., 2014). Other fear conditioning protocols have however identified a sex difference in mouse behaviour with females showing more freezing when trained by cued and contextual fear conditioning (Borkar et al., 2020, Keiser et al., 2017), while other studies have shown with greater shock intensity male mice present greater freezing behaviour (Villasana et al., 2010).

Possibly a difference in this colony compared to WT C57BL/6 mice means that the sex difference normally observed in freezing behaviour was observed in drinking behaviour for these experiments. While the modification introducing the LoxP sequences in the floxed control mice does not cause any change in gene expression, these mice are not from pure

C57BL/6 stock and have been bred as a separate colony for a large number of generations meaning some genetic drift and differences would be expected (Eraly, 2014). Variation in LI of fear conditioning has been recorded across different mouse strains (Lipina et al., 2011). As such it is fortunate that for our experimentation, we are able to compare litter mate mice as underlying differences would appear as an effect of the genetic modification if compared to a separate control colony.

Experimentally our design was underpowered to identify sex interactions without additional cohorts. While Bayesian analysis was suggestive against a sex x genotype interaction, it was only weak evidence, and it appears that we do see a genotype effect within male mice when viewed graphically (Figure 6.2**Error! Reference source not found.** B). This appears to be an increase in log LT in cKO mice, bringing the behaviour closer to the baseline for female mice. It may be that this increased conditioning would be seen in genotypes for both sexes if the control female mice had a similar low fear conditioning behaviour as it may be that any increase in log LT in the cKO mice is lost due to a ceiling effect. This conclusion would require further experimentation however before it could be upheld.

The potentially increased log LT reflects enhanced fear learning in the male cKO mice, this is the opposite effect to that observed in male constitutive NPAS2 KO mice which showed impaired fear conditioning (Garcia et al., 2000).

As we have observed modified circadian gene expression within the brain, this suggested a pathway through which a liver-specific modification of circadian cycles can influence a memory test, an unexpected outcome. While we have only observed modification of circadian gene expression in the forebrain other brain regions may be similarly affected. As detailed in the introduction section 6.1.1, various circadian disruptions lead to deficits in cognitive function across a variety of tasks, and circadian influences in fear conditioning entrainment have been reported (Albrecht and Stork, 2017).

Investigation of the extinction of the learned behaviour and the effect of LI found that we observe no influence of sex or genotype on these, other than the noted effect on fear conditioning. The lack of change in extinction suggests the reduced fear conditioning in males was not due to faster extinction of the learning in the days between the training and testing, which was one possible mechanistic explanation behind the difference.

Taken together these findings show we have found no significant evidence to support a role of the NPAS2 protein in the liver which influences fear conditioning behaviour. However, our findings suggest the possibility of a genotype effect within male mice specifically which our data is insufficient to conclusively support or oppose, which may warrant further independent investigation.

6.4.4 Future work

These data support further experiments using additional cohorts of male mice to further investigate a potential male specific effect of the cKO on fear conditioning. To support this molecular work, similar to that detailed in Chapter 4, in the tissues of male mice looking at more brain regions would also be useful.

A modification of the procedure such that baseline female fear conditioning is lower could also be developed to investigate if a lower response in control mice permits observation of an increased response in the cKO mice irrespective of sex. This may however have presented in this experiment as a slower extinction of the learning in the female cKO mice or as an increase in the fear conditioning of cKO PE mice compared to control PE mice, neither of which were observed. This does not however rule out that a genetic effect may be seen in female mice under a different protocol.

This potential sex-specific enhancement of LI does not appear to reflect the reported effects in constitutive NPAS2 KO mice but a novel effect of KO of NPAS2 liver expression influencing brain regions. If significantly identified it would also be of interest to further

investigate potential liver influences on circadian cycles in the brain, as suggested in section 4.4.6 (page 179). It is also possible that other cognitive tasks, influenced by circadian cycles, are affected so it would be of interest to investigate how the mice perform in these assays.

Concluding remarks

This project focused on investigating the functions of the transcription factor NPAS2 in modulation of core clock gene transcription *in vitro* and also its contribution to the liver peripheral clock *in vivo*. Previous gene KO studies in mice have found that NPAS2 contributes to the maintenance of circadian cycles in the SCN and peripheral clocks (DeBruyne et al., 2007a, Landgraf et al., 2016). NPAS2 appears to have both overlapping and distinct functions with its paralog CLOCK and ablation of both genes is required to fully abolish circadian cycles *in vivo* (DeBruyne et al., 2007a). NPAS2 has been proposed to play a role in restricted feeding entrainment (Dudley et al., 2003) although the mechanisms of this entrainment mechanism are poorly understood. Food entrainment of circadian behaviour is known to be closely linked to entrainment of peripheral clocks (Damiola et al., 2000), so it was unknown whether the role of NPAS2 in feeding entrainment was primarily within brain or peripheral tissues. As such we investigated the role of NPAS2 in peripheral tissue clocks.

To investigate NPAS2 function in cells, CRISPR-Cas9 gene editing technology was used to genetically edit NIH3T3 fibroblast cells, producing clonal lines deficient in NPAS2 or CLOCK (see Chapter 2). Two clonal lines; NIH3T3-NPAS2-1F1 (ΔNPAS2) comprising a functional KO of NPAS2 and NIH3T3-CLOCK-2H8 (ΔCLOCK) exhibiting depleted CLOCK protein expression were utilised. Transient synchronisation of the control and edited cell lines was successfully achieved via the serum shock method and following release, RT-qPCR at multiple time points established the induction of oscillation in transcript levels of core clock genes (see Chapter 3). In ΔNPAS2 cells, expression of the *REV-ERBα* (*NR1D1*) and *REV-ERBβ (NR1D2)* genes, were found to be significantly increased compared to control levels, with the increase coinciding with the time of peak expression. *CRY2* and *CLOCK* also showed enhanced transcriptional oscillation in this experiment, whereas *BMAL1* expression was

reduced compared to control levels. In ΔCLOCK cells, expression of *REV-ERBα* was similar to control levels, while *BMAL1*, *CLOCK*, and *REV-ERBβ* showed similar changes in expression to that in the ΔNPAS2 cells, although less substantial. The increase in *REV-ERBβ* expression especially was much more substantial in the ΔNPAS2 cells.

To summarise, these results represent (to our knowledge) a novel observation that NPAS2 may function to repress transcription of *REV-ERBα* and *REV-ERBβ* genes (directly or indirectly) in some cellular contexts. Current models invoke a feedback loop where CLOCK:BMAL1 or NPAS2:BMAL1 activate REV-ERBα and REV-ERBβ expression, which in turn repress transcription of the *NPAS2* and *BMAL1* genes. Thus, the results from this study suggest the existence of an additional level of interplay involving context-dependent NPAS2-mediated repression of *REV-ERBα* and *REV-ERBβ*. It will be important to investigate if this is also seen in other cell types and to establish the mechanism involved.

It is important to state some of the limitations of these experiments, for example, we were unable to find clones in which CLOCK expression was completely ablated, thus low level of WT CLOCK was detectable in the ΔCLOCK cell line, which may explain the more moderate effects on core clock gene expression. In addition, the quality of available antibodies for NPAS2 is poor, although we were able to establish with reasonable confidence the absence of NPAS2 protein in the ΔNPAS2 cell line. It would also be important to see if the 'derepression' of *REV-ERBα* and *REV-ERBβ* upon NPAS2 ablation is observed in other cell lines, and to explore if this is a direct or indirect mechanism, e.g., due to the moderately increased *CLOCK* expression in ΔNPAS2 cells.

We also established an *in vivo* model to investigate NPAS2 function, a liver-specific NPAS2 conditional KO mouse colony was established from NPAS2^{TM2AAGAA} and NPAS2$^{TM2.1AAGAA}$ mice imported from the Baylor Institute generated by O'Neil et al. (2017) (see Chapter 4). This model was used for both analysis of core clock gene transcription in the

liver and brain and for behavioural studies. RT-qPCR of mRNA extracted from liver or PFC at opposite time points indicated that expression of *REV-ERBα* and *REV-ERBβ* expression was also altered in liver NPAS2 cKO mice, showing a trend towards reduced levels. A caveat here is that due to restricted mouse availability, influenced by COVID-19 work conditions requiring temporary colony downsizing, we were only able to analyse gene expression at two time points within the experiment. While the result suggests an opposing effect to that seen in the NIH3T3 cells, it does again implicate NPAS2 in regulation of *REV-ERBα* and *REV-ERBβ* genes and may reflect tissue specific effects. Future studies should ideally incorporate additional time points to get a clearer picture of the circadian expression of the genes tested.

The differences between the two models do highlight that the change in gene expression is likely a complex effect, involving mediating effects on the expression of other CCGs which then influence the expression of the circadian genes (see Figure 3.7 D), as without the influence of other factors NPAS2 should act as a transcription factor for the *REV-ERB* genes in a consistent manner across tissues. In both *in vitro* and *in vivo* models, it appears that the circadian expression patterns of the genes were unmodified, this is as expected as the timing of the circadian clock should be maintained as CLOCK is still expressed.

In the *in vivo* model we found that the expression of core circadian genes in the brains of cKO mice were also altered with significant changes to the rhythmic expression of *REV-ERBβ*, *CLOCK* and *BMAL1* observed in cKO mice (see Chapter 4). A similar change to that of *REV-ERBβ* expression was noted for expression of *REV-ERBα*, although this fell below the threshold for significance. These findings show both that the output of the liver circadian clock can influence the circadian clock in other tissues and that within the liver, NPAS2 contributes to the output of synchronising signals in a way which cannot be fully performed when reliant on the expression of CLOCK alone. It is especially of note that in the liver, without NPAS2 contribution, we did not appear to observe a comparable change in rhythmic expression

to the effect we observed the PFC. This may suggest NPAS2 is closely involved at the level of output signalling, so the liver circadian cycles are maintained due to the presence of CLOCK, but without NPAS2 output signals are modified in such a way to have a more substantial effect in other tissues. Various potential mechanisms of how the liver might influence the PFC such as via an effect on liver glucose levels are presented in Chapter 4, section 4.4.5 (page 178).

Investigation of the entrainment to feeding as a zeitgeber identified unanticipated sex-specific effects of the NPAS2 cKO (see Chapter 5). Through investigation of RF entrainment measured by time of FAA onset, this experiment suggested that the cKO of NPAS2 in the liver enhanced FEO entrainment in female mice specifically but not any effect in male mice. As an overall effect, enhanced entrainment in cKO mice would suggest that NPAS2 in the liver either acts to delay circadian entrainment in the liver or that the modulation of circadian rhythms throughout the organism mean that the mice are more susceptible to entrainment to food timing. The sex-specificity of the effect may suggest that the underlying mechanism is more to do with the signalling between the liver and other tissues, as circadian rhythms have a noted association with oestrogen signalling (Royston et al., 2014, Hatcher et al., 2020) which may be responsible for the sex differences.

Investigation of the free-running period, activity levels and patterns, and light entrainment were underpowered statistically to investigate sex effects, however, findings reported here support further investigation with respect to potential sex-specific differences. The lack of observed genotype effect was consistent with our predictions as these behaviours should rely more on circadian gene expression in the brain. However, as experiments in Chapter 4 found that the liver cKO is associated with modified circadian gene expression in the PFC of female mice, this change would provide a potential mechanism for an influence on these behaviours.

Constitutive NPAS2 KO mice have previously been shown to present deficits in fear

conditioning (Dudley et al., 2003). To investigate the contribution of NPAS2 in peripheral clocks to this effect, experiments investigating fear conditioning, LI, and extinction were performed. Again, we observed unexpected sex differences. We found a significant sex difference due to male mice presenting reduced fear conditioning compared to female mice which had not been previously observed in our group using this procedure. While the experiment was underpowered to investigate sex interaction effects the data was suggestive of increased fear conditioning in NPAS2 cKO male mice compared to control male mice. A lower fear conditioning baseline in male mice may have permitted observation of an increase in fear conditioning, with a ceiling effect on the genotype contribution obscuring the effect in female mice. While an effect on a memory task of a liver-specific KO would not be expected, our findings suggest that circadian gene expression in the brain was modified in female mice.

Taken together our findings present three conclusions: 1) Loss of NPAS2 function in peripheral clocks affects the expression of genes which are part of the core transcription feedback loop in a way which is not fully compensated for by CLOCK, especially the *REV-ERB* genes. This suggests specific unique functions of NPAS2 in peripheral clocks which are not seen in the SCN. 2) Loss of NPAS2 in the liver clock modulates the rhythmic expression of circadian genes in the brain, suggesting a possible role of NPAS2 in synchronisation of clocks between the liver and different tissues. 3) Circadian entrainment to restricted feeding is influenced by loss of NPAS2 in a sex-specific manner and sex-specific behavioural effects warrant further investigation for free-running behaviour and fear conditioning.

Appendix

A.1 Generation of BET mutant triple negative breast cancer cells

As part of a collaborative effort to investigate the role of the BET proteins in the hypoxia response in breast cancer, I was responsible for the generation of clones with modified BET protein expression. The BET proteins are epigenetic regulators containing the bromodomain. These function as coactivators for many transcription factors, including members of the bHLH-PAS family which includes HIF, AHR, NPAS, SIM and CLOCK proteins. It is likely that BET proteins are essential for control of circadian gene regulation, and interactions with REV-ERBs have been reported (Kim et al., 2018b)

This work was part of collaborative study between our group and Dr Alan McIntyre, funded by Breast Cancer Now. Guides were designed for, and clones were produced, in which mutations were targeted in the bromodomain and extra-terminal proteins BRD2-4 in two breast cancer cell models, HCC1806 and MDA231, as part of research into tumour hypoxia. The BRD genes are of interest as the BET inhibitor JQ1, which has been shown impair tumour response to hypoxia and downregulate angiogenesis in breast cancer (da Motta et al., 2017) inhibits BRD2, 3 and 4 non-specifically. The KO cells will be used to investigate the role of each BRD protein individually.

A.1.1 Methods

Materials and methods used are as those detailed in Chapter 2 with the exceptions shown below. Targeted clones were generated, and initial PCR analysis was performed. Based on this initial analysis specific clones were selected for western blotting investigation of protein expression which was performed in collaboration with Leonardo da Motta (pers. comms.). Based on western blotting specific clones were chosen and sequencing was performed to identify the specific mutations for the selected BRD3 and BRD4 clones. These processes were

performed following the methods sections in Chapter 2.

A.1.1.1 Culturing of adherent cells

The human breast cancer (MDA231 and HCC1806) cells were maintained in Dulbecco's Modified Eagle Medium (DMEM). This medium was supplemented with 10% (v/v) heat-inactivated fetal calf serum (FCS) plus 1% (v/v) 0.2 M L-glutamine and 1% Penicillin/Streptomycin antibiotics. Cells were cultured in sterile plastics at 37 °C, 5% CO_2 and passaged when at approximately 80% confluency. When passaging and/or collecting cells the medium was aspirated, and cells washed with 1 x PBS. Following this MDA-MB-231 cells were incubated for 5 minutes at 37 °C in 1 x trypsin and fresh media then added and HCC1806 cells were incubated for 10 minutes at 37 °C in 2 x trypsin and fresh media then added. At this point, the cell suspension was diluted and split into other sterile plasticware and/or collected into 15 ml tubes if being used for other processes.

A.1.1.2 Calcium phosphate-mediated transfection of MDA231 and HCC1806 cells

For transfection MDA231 and HCC1806 cells were seeded at a density of 5 x 10^5 cells per well in a 6 well plate, 24 hours prior to transfection. Transfection was performed as detailed for HEK293 cells in section 2.2.5.5 (page 63).

A.1.1.3 Cell sorting of transfected cells

After harvesting cells were sorted by use of fluorescence-activated cell sorting (FACS) for GFP expression with single cells expressing GFP sorted into 96 well plates with prewarmed media.

A.1.1.4 Targeting guides

Guides were designed for the human *BRD2-4* genes as described in section 2.2.3 (page 55), sequences are detailed in Table A.1 (page 296) and targeting information is shown in the relevant following sections. BRD3 and 4 both have only one consensus start codon for all transcripts and guides were designed targeting the start codon in exon 2 for both genes. The

human *BRD2* gene has multiple possible start codons. As such two pairs of guides were designed to target different start codons at different locations within the gene in exon 2 and exon 4. This then meant that targeted effects at the two sites had to be identified individually.

A.1.2 Generated mutant clones

A.1.2.1 BRD2

The targeting information for *BRD2* is shown in Figure A.1, two different sites within the gene were targeted. The mutant HCC1806 clone 2F5 and the MDA-MD-231 clone 1F11 were selected due to the loss of BRD2 protein expression. Western blots showing the modified protein expression compared to single guide transfected control cells are shown in Figure A.2. Sequencing identification of these mutations has not been performed at this time.

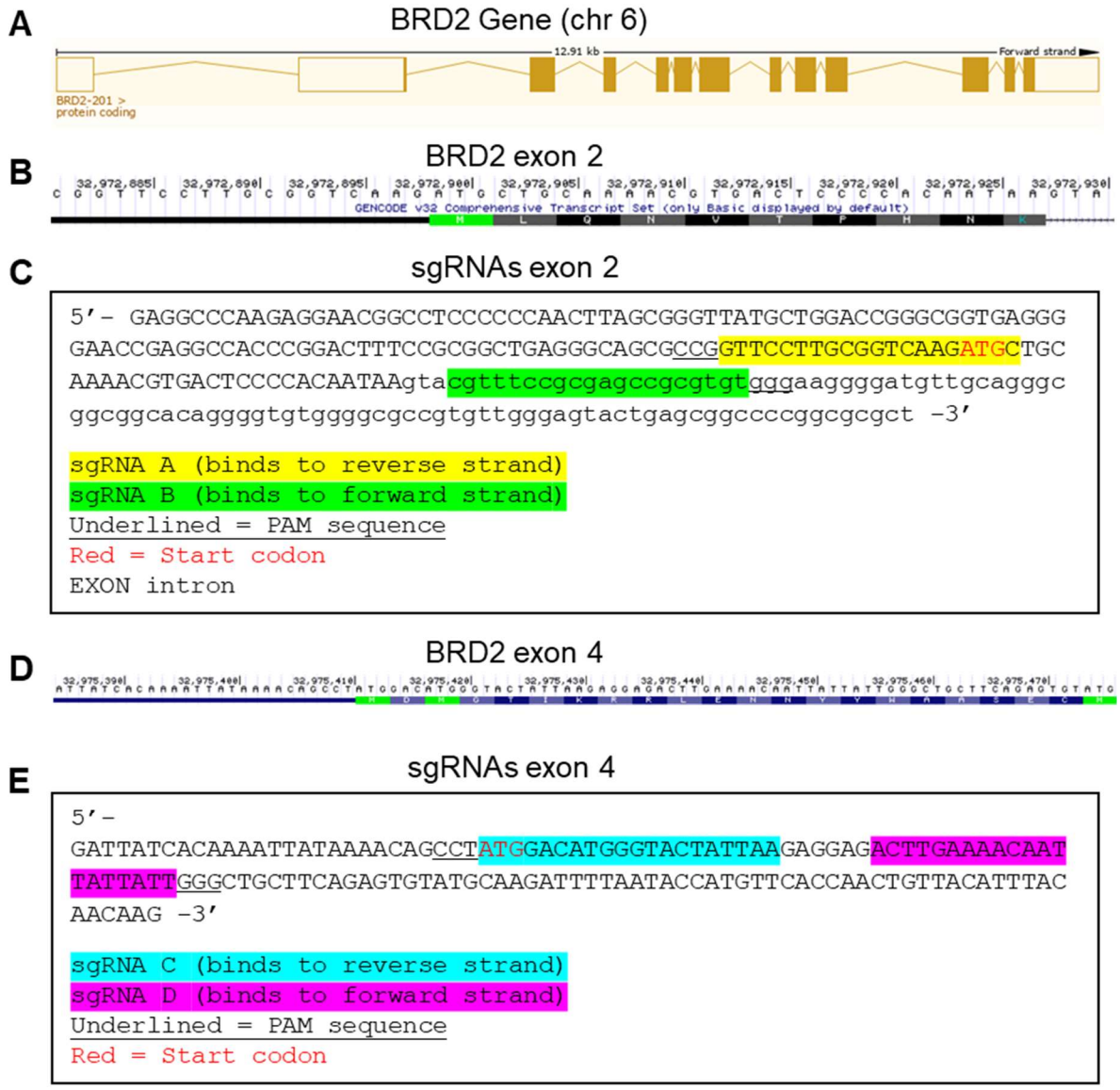

Figure A.1: Targeting the *BRD2* gene

A: Exon structure of the *BRD2* gene from the Ensembl database, note alternate splice variants exist utilising start codons in exons 3 and 4. **B:** Sequence of a section of exon 2 of the *BRD2* gene from the UCSC genome browser showing the initiation coding. **C:** sgRNA designs targeting opposite strands of exon 2 of *BRD2* and the following intron. Guide pairs were selected close to the ATG in a PAM-out arrangement with a 68 bp spacing. **D:** Sequence of a section of exon 4 of the *BRD2* gene from the UCSC genome browser showing the alternate splice form initiation coding. **E:** sgRNA designs targeting opposite strands of exon 4 of *BRD2*. Guide pairs were selected close to the ATG in a PAM-out arrangement with a 46 bp spacing.

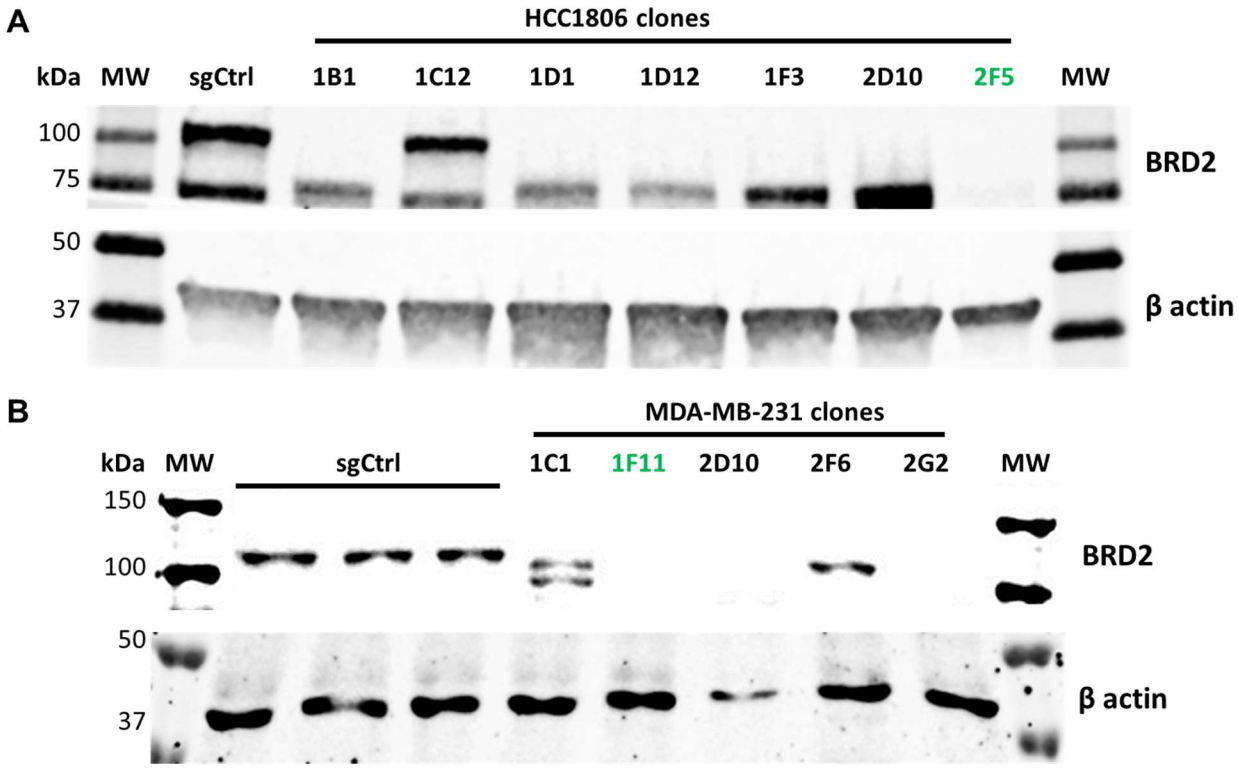

Figure A.2: BRD2 protein expression in targeted HCC1806 and MDA-MB-231 clones

Western blot of protein extracts from *BRD2* targeted clones performed by Leonardo da Motta. Membranes were probed for detection of BRD2 (Cell Signalling, D89134, predicted MW 110 kDa) and β actin (Santa Cruz, sc-1615, predicted MW 42 kDa) proteins of HCC1806 (**A**) and MDA-MB-231 (**B**) clones. Clones highlighted in green were chosen for future work due to the loss of BRD2 expression.

A.1.2.2 BRD3

The targeting information for *BRD3* is shown in Figure A.3, targeting exon 2. The mutant HCC1806 clone 2E2 and the MDA-MD-231 clone 2D9 were selected as successfully targeted cells. Western blots showing the modified protein expression compared to single guide transfected control cells are shown in Figure A.4. The genetic sequence information is shown in Figure A.5. For both clones only one unique allele was identified, this may mean only one allele was present, which is not impossible for triple negative breast cancer cultured cells, or homologous repair was used between the chromosomes so two alleles are present, but both show the same sequence.

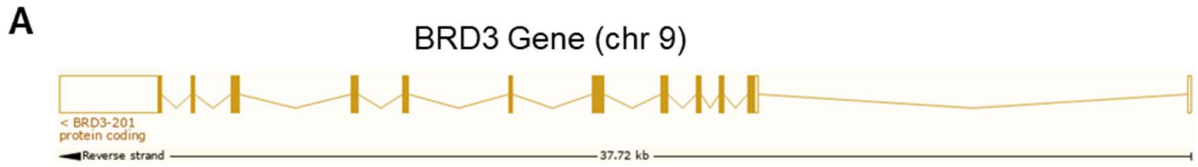

C

sgRNAs

5′- CTGTCGCCTGGTTGGGCCCGGAAATGGGACGTCGCGCTTTCTCAGGGAGCGTAGAAGCAGCCA
GGGCCTCTCCAAGCCGCTGCTGTGACAGAAAGTGAGTGAGCTGCCGGAGGATGTCCACCGCCACGAC
AGTCGCCCCCGCGGGGATCCCGGCGACCCCGGGCCCTGTGAACCCACCCCCCCCGGAGGTCTCCAAC
CCCAGCAAGCCCGGCCGCAAGACCAACCAGCTGCAGTACATGCAGAATGTGGTGGTGAAGACGCTCT
GGAAACACCAGTTCGCCTGGCCCTTCTACCAGCCCGTGGACGCAATCAAATTGAACCTGCCG -3′

sgRNA A (binds to reverse strand)
sgRNA B (binds to forward strand)
Underlined = PAM sequence
Red = Start codon

Figure A.3: Targeting the *BRD3* gene

A: Exon structure of the *BRD3* gene from the Ensembl database **B:** Sequence of a section of exon 2 of the *BRD3* gene from the UCSC genome browser showing the initiation coding. **C:** sgRNA designs targeting opposite strands of exon 2 of *BRD3*. Guide pairs were selected close to the ATG in a PAM-out arrangement with a 41 bp spacing.

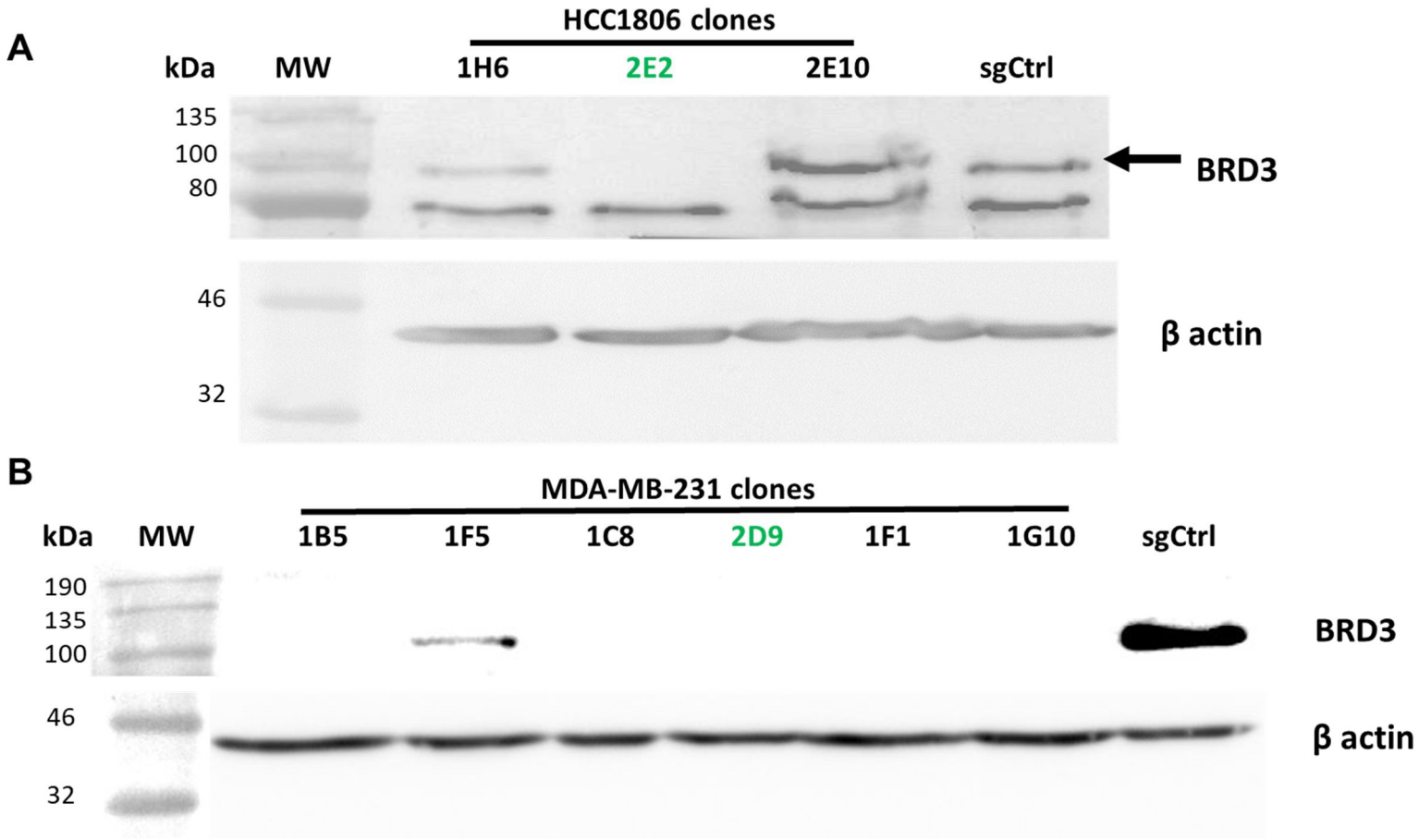

Figure A.4: BRD3 protein expression in targeted HCC1806 and MDA-MB-231 clones

Western blot of protein extracts from *BRD3* targeted clones. Membranes were probed for detection of BRD3 (Cell Signalling, D89134, predicted MW 100 kDa) and β actin (Sigma-Aldrich, A2066, predicted MW 42 kDa) proteins of HCC1806 (**A**) and MDA-MB-231 (**B**) clones. The selected clones of interest are highlighted in green both slowing loss of BRD3 expression.

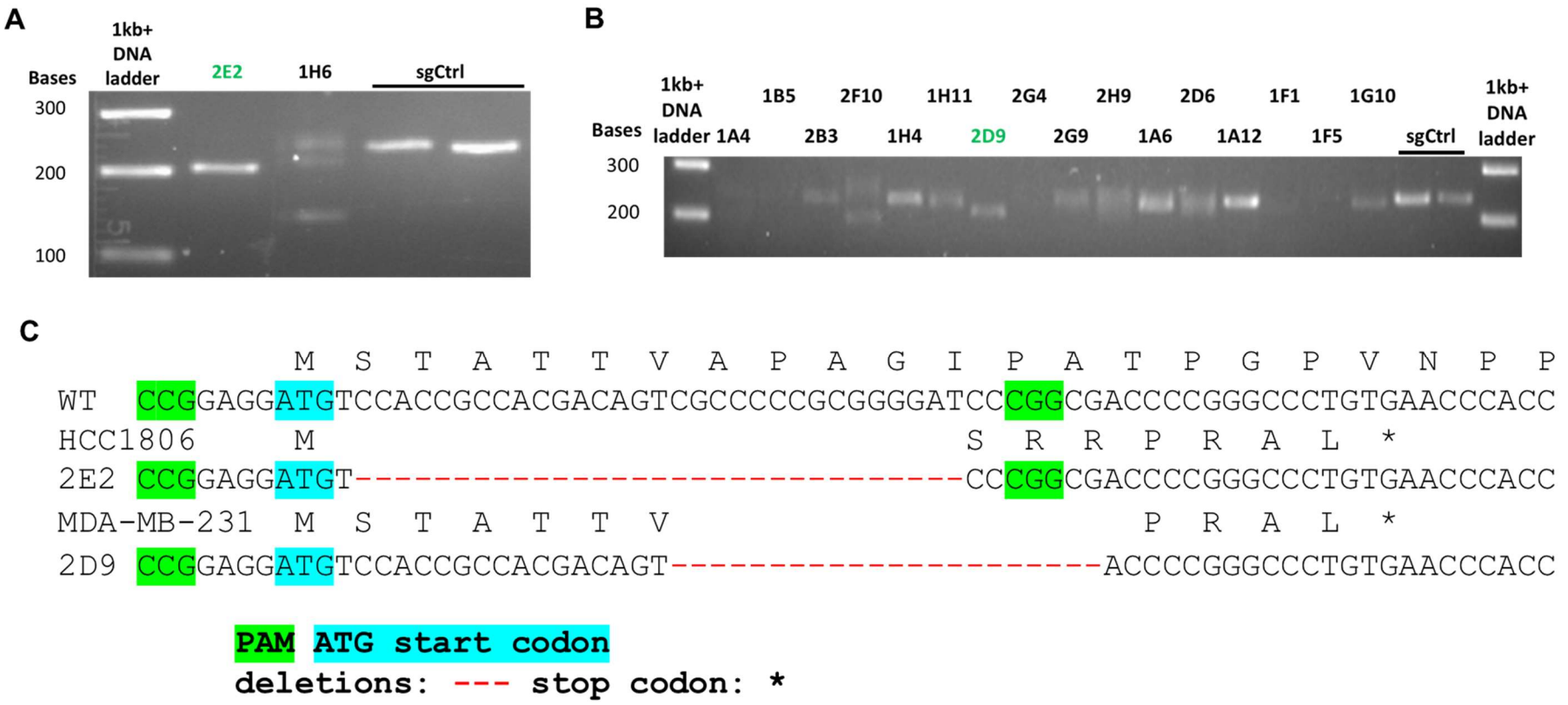

Figure A.5: Sequencing of modifications to the *BRD3* gene in targeted clones

A&B: Agarose gel of PCR products amplified using *BRD3* F1,R2 primers (WT product size: 235 bp) showing a single product of reduced size compared to control unmodified DNA for HCC1806 clone 2E2 in **A** and MDA-MB-321 clone 2D9 in **B**. **C:** Sequences of the target region deletions in the clones leading to frame shift mutations and premature stop codons. Deletion of 31 bases in clone 2E2 and 22 bases in clone 2D9.

A.1.2.3 BRD4

The targeting information for *BRD4* is shown in Figure A.6, targeting exon 2. The mutant HCC1806 clone 1A11 and the MDA-MD-231 clone 2D6 were selected as successfully targeted cells. Western blots showing the modified protein expression compared to single guide transfected control cells are shown in Figure A.7. The genetic sequence information is shown in Figure A.8. For both clones only one unique allele was identified, as for the BRD3 clones. It makes sense that clones which showed most severe effects on protein expression would be cells which only have one allele of the target gene. Both selected clones still retain some expression by western blot despite the sequences identified suggesting that complete loss of the protein would occur. We observed a subtle difference in size of the band in 2D6 which is still larger than a change that an insertion of 4 amino acids would be responsible for. As such it may be that another variant of BRD4 may exist which is dependent on an alternate start codon in these modified clones. While transcript variants for *BRD4* are listed on the Ensembl database which use alternate start codons these transcripts lack the majority of the *BRD4* transcript and any protein produced from these transcripts would have a significantly reduced molecular weight compared to the consensus BRD4 protein, as such these are not responsible for the observed western blot bands and we may be observing a previously unreported isoform. If the western blot bands are due to functional BRD4 or a functional isoform we still see clear reduction in expression meaning the clones are still models which can be used for investigation of BRD4 function.

A

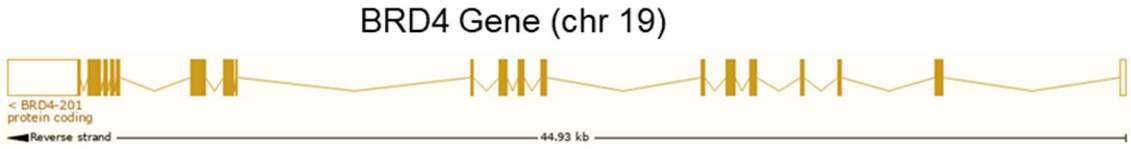

B

C

sgRNAs

5′– AGTGCCTGGTGAAGAATGTGATGGGATCACTAGCATGTCTGCGGAGAGCGGCCCTGGGACGA
GATTGAGAAATCTGCCAGTAATGGGGGATGGACTAGAAACTTCCCAAATGTCTACAACACAGGCCC
AGGCCCAACCCCAGCCAGCCAACGCAGCCAGCACCAACCCCCCGCCCCCAGAGACCTCCAACCCTA
ACAAGCCCAAGAGGCAGACCAACCAACTGCAATACCTGCTCAGAGTGGTGCTCAAGACACTATGGA
AACACCAGTTTGCATGGCCTTTCCAGCAGCCTGTGGATGCCGTCAAGCTGAACCTCCCT –3′

sgRNA A (binds to reverse strand)
sgRNA B (binds to forward strand)
Underlined = PAM sequence
Red = Start codon

Figure A.6: Targeting the *BRD4* gene

A: Exon structure of the *BRD4* gene from the Ensembl database. **B:** Sequence of a section of exon 2 of the *BRD4* gene from the UCSC genome browser showing the initiation coding. **C:** sgRNA designs targeting opposite strands of exon 2 of *BRD4*. Guide pairs were selected close to the ATG in a PAM-out arrangement with a 41 bp spacing.

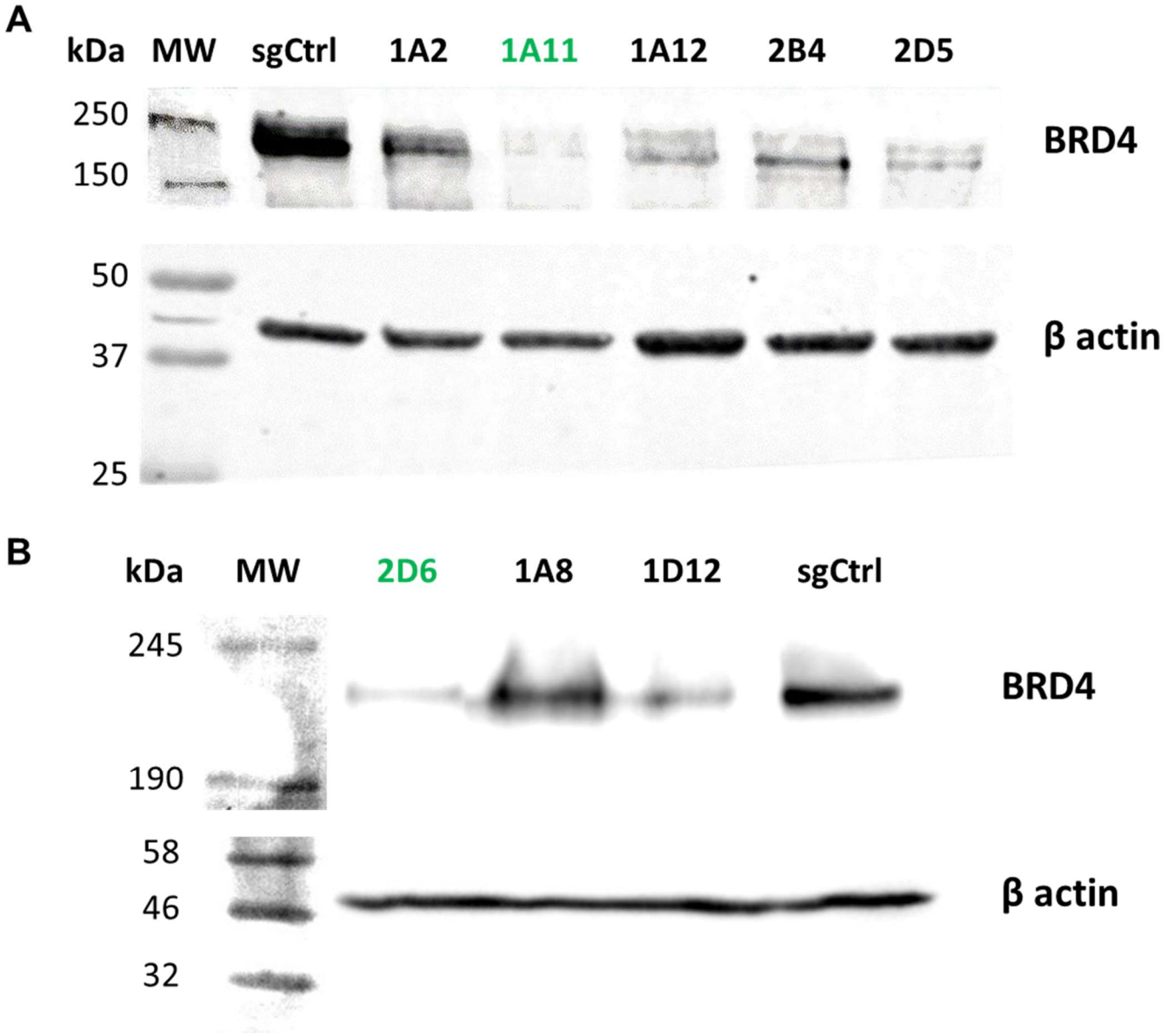

Figure A.7: BRD4 protein expression in targeted HCC1806 and MDA-MB-231 clones

Western blot of protein extracts from *BRD4* targeted clones. Membranes were probed for detection of BRD4 (Cell Signalling, E2A7X, predicted MW 200 kDa) and β actin (Santa Cruz, sc-1615 in **A**, Sigma-Aldrich, A2066 in **B**, predicted MW 42 kDa) proteins of HCC1806 (**A**, performed by Leonardo da Motta) and MDA-MB-231 (**B**) clones. Clones selected for use are highlighted in green. Both selected clones retain the presence of a protein band for BRD4 although notably reduced. For 2D6 it also appears that the band is of a slightly different size.

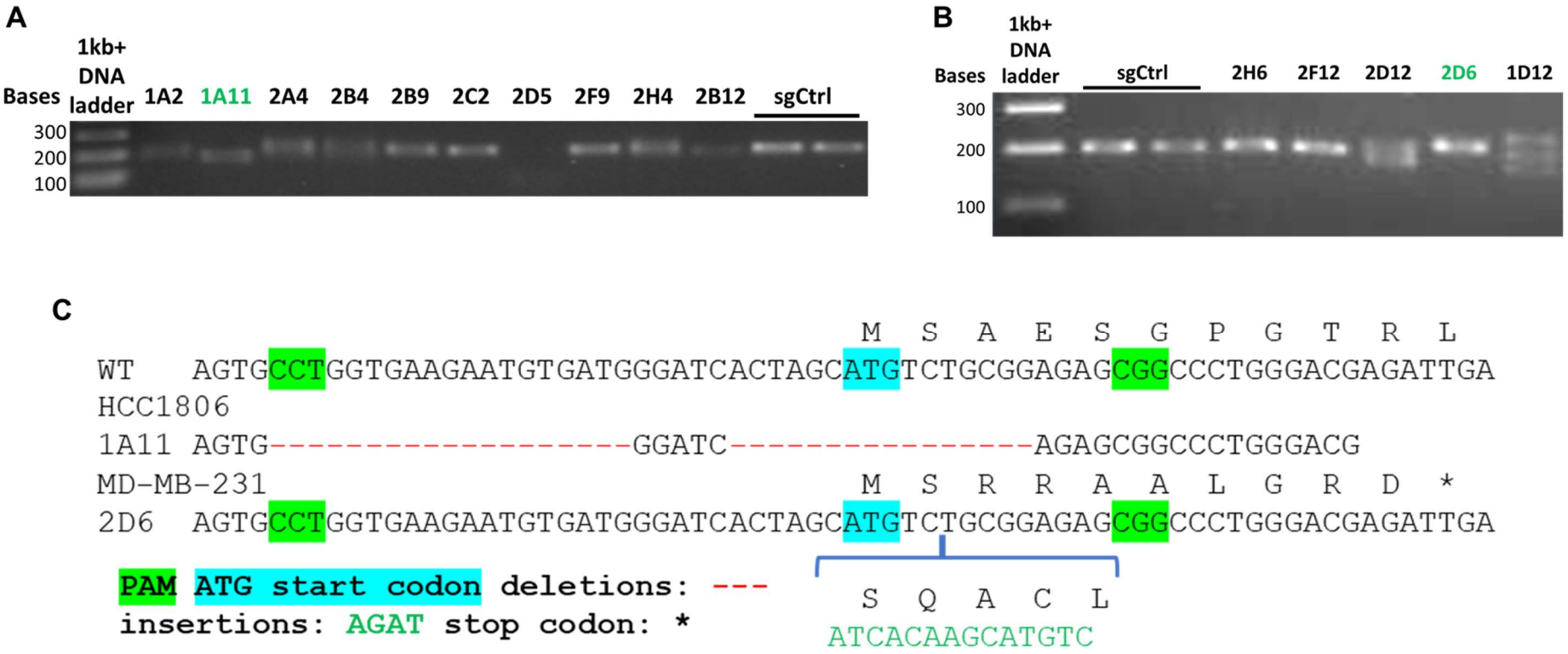

Figure A.8: Sequencing of modifications to the *BRD4* gene in targeted clones

A&B: Agarose gel of PCR products amplified using *BRD4* F1,R2 primers (WT product size: 201 bp) showing a single product of reduced size compared to control unmodified DNA for HCC1806 clone 1A11 in **A** and a single product comparable to the control unmodified DNA project MDA-MB-321 clone 2D9 in **B**. **C:** Sequences of the target region modifications in the clones. In clone 1A11 25 bases were lost which includes the start codon and in clone 2D9 an insertion of 14 bases occurred which introduces a frame shift mutation.

A.2 Rhythmic expression of a *PER2-dLuc* reporter in serum shock synchronised NIH3T3 cells

A.2.1 Introduction

To assess the efficacy of serum shock in establishing circadian gene synchronisation in our cell model, I employed a luciferase reporter system previous described in the literature (Fang et al., 2015, Fang et al., 2017). This system involves a reporter plasmid carrying a destabilised luciferase gene under the control of the human *PER2* promoter. After transient transfection of wild type NIH3T3 cells with the *PER2-dLuc* expression plasmid, stably transfected cells were isolated by selecting for cells resistant to the antibiotic (G418) marker carried on the plasmid. These cells were used to validate the serum shock synchronisation protocol.

A.2.2 Methods

The pGL[*hPer2P*/*Luc2P*/Neo] plasmid was a gift generously provided by Mingzhu Fang (Fang et al., 2017, Fang et al., 2015). This plasmid was used to transform bacteria which were grown for large-scale purification of the plasmid as detailed in Chapter 2 methods 2.2.4.9 (page 60). A map of the plasmid is shown in Figure A.14.

NIH3T3 cells were cultured and transfected with the pGL[*hPer2P*/*Luc2P*/Neo] plasmid as described for the Cas9n plasmid transfection in 2.2.5.6 (page 64). Three days after transfection the cell media was changed to media including 1 mg/ml of G418, selecting for cells expressing neomycin resistance from the transfected plasmid. The media was replaced every 3-4 days to maintain the G418. A control plate of untransfected cells was subjected to the same treatment to validate that complete cell death occurred (Fang et al., 2017). After 2 weeks the cells were plated in duplicate well in 6 x 12-well plates for the serum shock procedure as detailed in 3.2.1.4 (page 118) including control cells exposed to a media change to serum free media when the 50% horse serum media was removed from the serum shocked

cells. Cells were collected into the lysis buffer of the luciferase reporter assay kit 0-, 6-, 12-, 18-, 24- and 30-hours after the treatment and the lysate stored at -80 °C until the analysis was performed.

The luciferase assays were performed in duplicate for each sample using the ThermoFisher Dual-Light™ Luciferase & β-Galactosidase Reporter Gene Assay System per the manufacturer's protocol. The luminescence read was measured using a GloMax® 96 Microplate Luminometer and the two technical replicates from each sample averaged together. The reads were corrected to the total protein mass of the assay volume based on the protein concentrations for the samples assessed by Bradford assay performed as described in 2.2.6.4 (page 66).

A.2.3 Results

A clear rhythmic variation in luciferase activity was detected post serum shock, that showed an approximate 24-hour period, consistent with synchronisation and circadian regulation of the reporter, while cells exposed to only a media change saw an early induction of luciferase expression which then dropped and remained at a low level without circadian expression (Figure A.9). Thus, we concluded serum shock technique to have successfully induced synchronisation of circadian gene regulation in the stable WT cells. However, as the amplitude of dLuc activity was relatively modest, and due to the potential for variability in stable-expression clones due to different reporter integration sites, we did not consider this system would be sufficiently sensitive to enable us to ascertain subtle differences in circadian gene expression between wild type and ΔNPAS2 or ΔCLOCK cells. Thus, it was decided not to proceed further with this system.

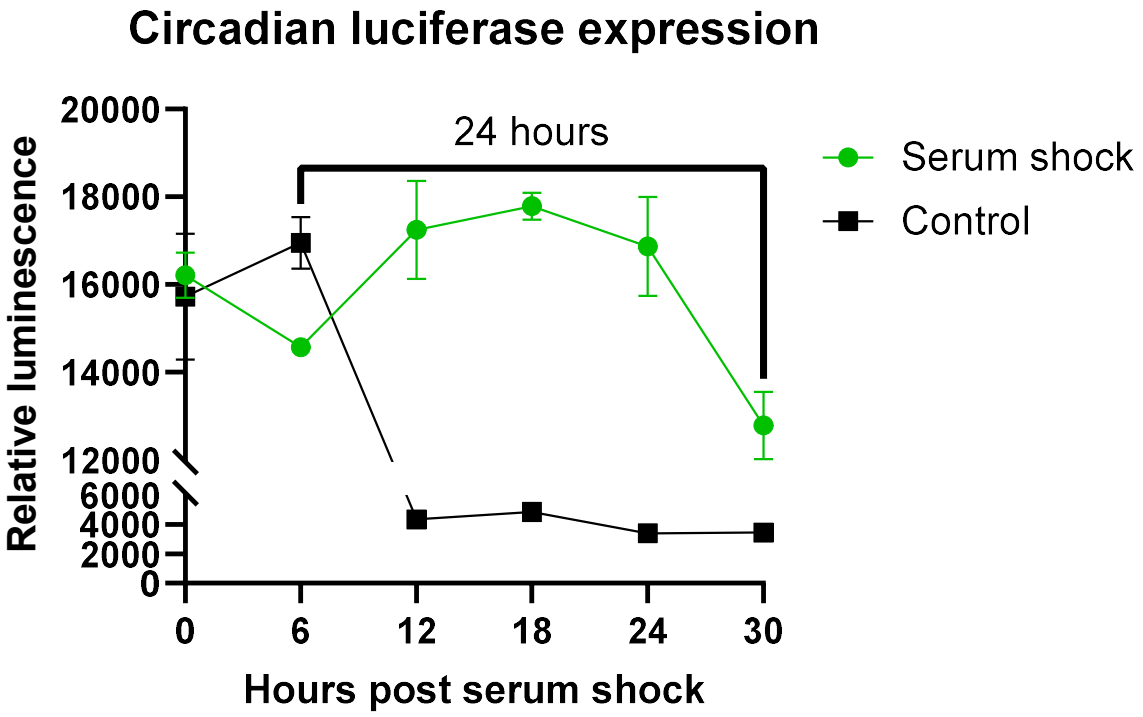

Figure A.9: Expression of dLuc under a *PER2* promotor following a serum-shock.

Mean relative luminescence (±SEM). Bioluminescence assays were performed on protein collected from NIH3T3 cells stably transfected with a *PER2-dLuc* expression vector following either a serum shock (green) or a media change (black). Samples were collected every 6 hours immediately following the treatment up to 30 hours. The luminescence reads were normalised to total protein mass based on protein concentrations determined by Bradford assay. In the serum shock data, the clearest marker of the circadian cycle is the low expression at 6 hours and 24 hours later at 30 hours marked on the graph. In the media change control, while initial induction of the dLuc expression by the media appears to occur, this is not then followed by cycling behaviour as the luminescence read drops and stays at a constant low level. For points without error bars, the SEM was within the size of the point.

A.3 NPAS2 polyclonal antibody

As introduced in Chapter 2 NPAS2 western blots were initially performed using a different polyclonal antibody directed against NPAS2 (Mouse anti-NPAS2, PACO0029654, Antibody Genie). Using this antibody however, multiple bands were identified that were inconsistent with the expected MW of the NPAS2 protein (see Figure A.10). Notably even the 1F1 clone which is selected as the clone used for research due to the change in NPAS2 protein levels appears consistent with all other clones in band intensity.

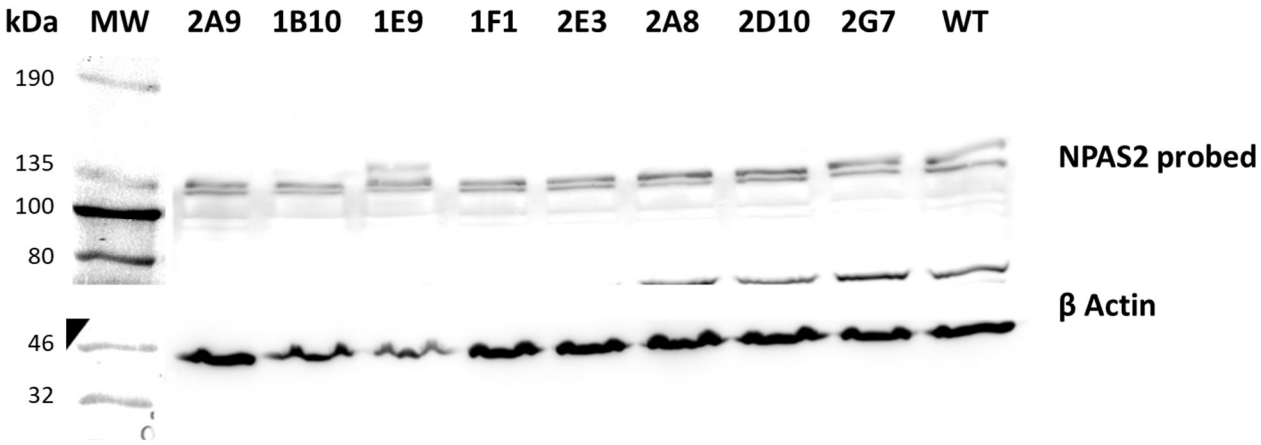

Figure A.10: Western blotting of NPAS2 targeted NIH3T3 clones using a polyclonal NPAS2 antibody

Western blot of protein extracts from selected NPAS2 targeted NIH3T3 clones, probed for NPAS2 (Antibody genie, PACO0029654, predicted MW 91 kDa, 1:500) and β actin (Sigma-Aldrich, A2066, batch: 018M4853V, predicted MW 42 kDa, 1:1000 dilution, 60 sec exposure) as a loading control. The bands detected by use of the NPAS2 antibody do not reflect the appropriate size, the lower bands are not visible for all clones as they are close to the edge of the membrane which was cut at ~58 kDa. All protein extracts show similar intensity of the bands identified by the NPAS2 antibody, notably including 1F1 which showed clear reduction of the NPAS2 band in Figure 2.7 (page 81).

A.4 RT-qPCR primer validation

The various qPCR primers used in Chapters 3 and 4 before use were validated by investigation of the reaction efficiency and specificity of produced products. Primer sequences are detailed in Table A.1 (page 296).

Dilution series were performed to validate the reaction efficiency shows a linear relationship with the cDNA concentrations. cDNA was produced from WT NIH3T3 cells and serial dilutions were used in qPCR for each of the primer sets following procedures presented in 3.2.2.4 (page 121). Graphs of the output values are presented in Figure A.11. The dilution series are not identical across all primer sets; for *18S* rRNA, *CLOCK*, *BMAL1* and *REV-ERBβ* amplification was observed for each of 4 dilutions from 1x to 0.001x however for the other genes, amplification was not observed at lower dilutions, so a more sensitive dilution series was used up to 0.01x, for some of these genes the most diluted sample remained below the detection limit so is also missing from the graphs. For each series the relationship between the Ct and relative quantity of cDNA was analysed by semi-log least squares fit using the prism software. The equation of the linear line on the graph and the R^2 value is presented, R^2 values greater than 0.98 reflect high correlation between the cDNA relative amount and the Ct showing the reaction efficiency does not change with cDNA concentration.

To validate the primer specificity products from the highest concentration of the serial dilution qPCRs were ran on 2% agarose gels following the procedure in 2.2.4.4 (page 58). Gels with products for each of the primer sets are presented in Figure A.12. For all primer sets the expected product sizes, detailed in the figure legend are observed.

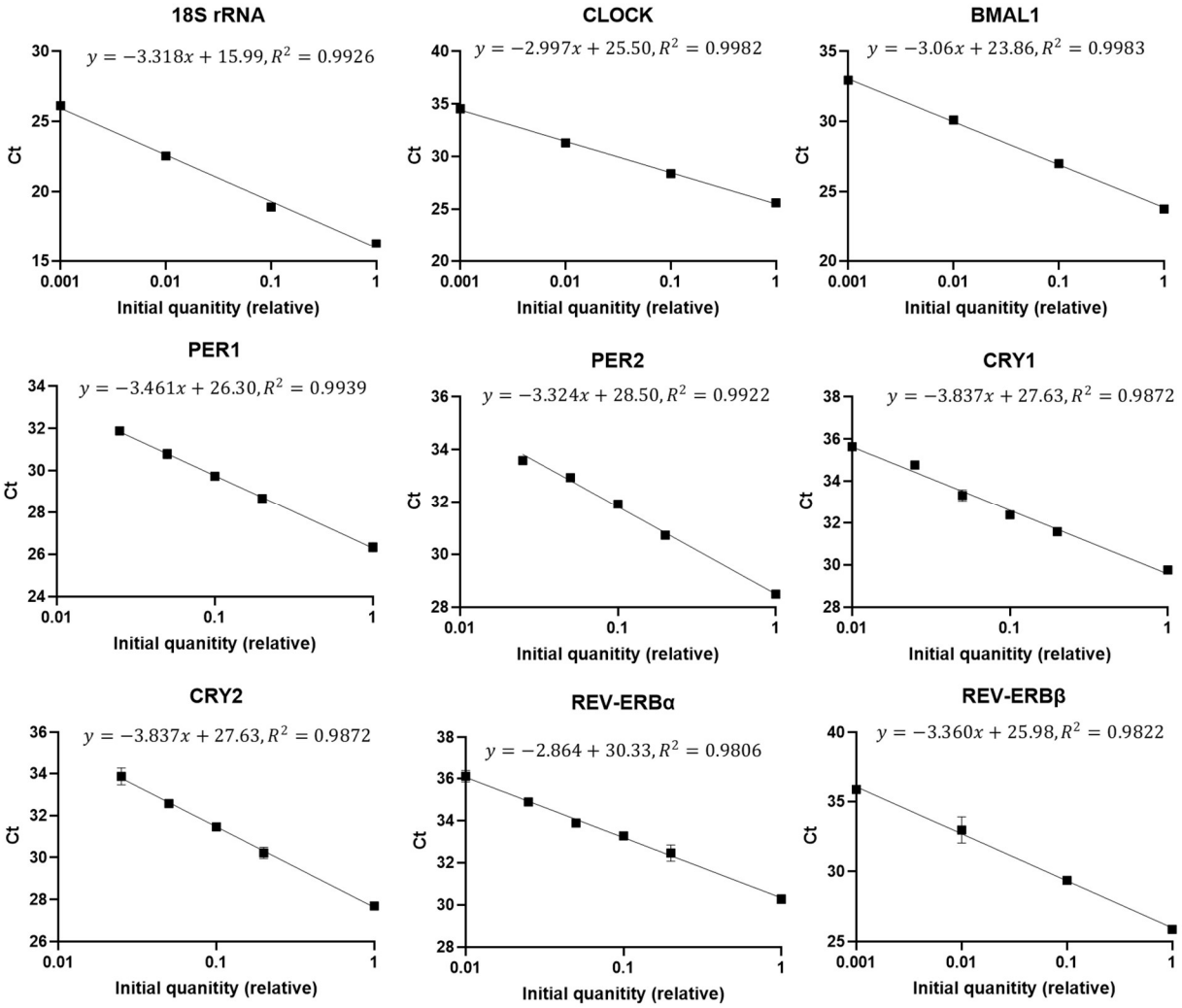

Figure A.11: cDNA dilution series RT-qPCR to test amplification by primer pairs

For each primer set initially a 4-step dilution from 1 to 0.001 relative quantity was used, the expression levels of some genes were too low for identification at these dilutions, so a more sensitive dilution series was used.

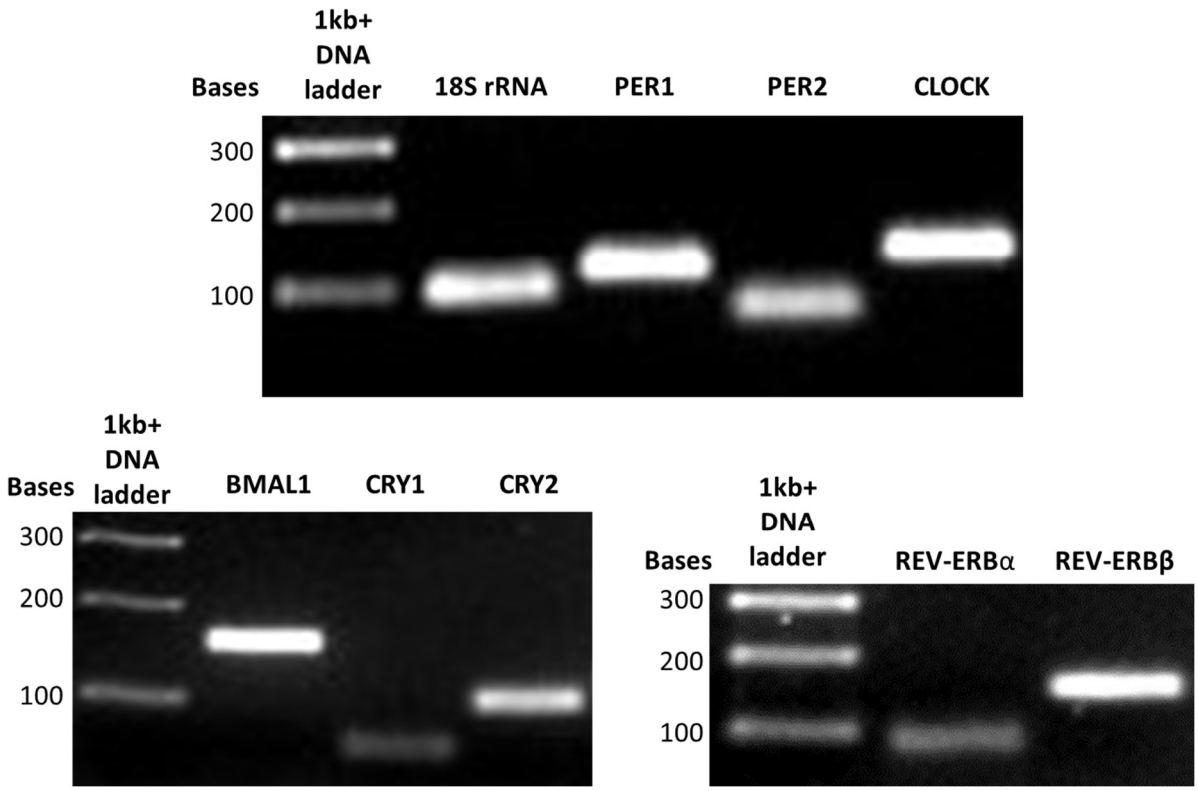

Figure A.12: Agarose gels of RT-qPCR products for specific primer pairs

Three different gels showing the products of qPCR using primers for the various circadian genes investigated. All expected product sizes were observed; *18S* rRNA: 93 bp, *PER1*: 116 bp, *PER2*: 70 bp, *CLOCK*: 135 bp, *BMAL1*: 154 bp, *CRY1*: 60 bp, *CRY2*: 98 bp, *REV-ERBα*: 84 bp, *REV-ERBβ*: 150 bp.

A.5 PCR genotyping

Primers designed for PCR genotyping and sequencing of mutations introduced, use is detailed throughout Chapter 2 and section A.1. Not all primers included here were used as multiple were initially designed in case of issues with specific primers and some were designed specifically for sequencing. In all of the genomic sequence information below exon sequences are presented in capitals and introns in lower case PAMs are marked in blue highlight and ATG start codons where present are underlined.

A.5.1 Murine NPAS2

ATG PAM EXON intron

FORWARD PRIMERs actgggttgaggtgtgcat F1
acatgcctgtacctgatccc F2
REVERSE PRIMERs gcccgccatgttgagtttaa R1
acttcactggtgaggtgcaaa R2

PRODUCT SIZE: F1,R1: 242 F2,R2: 449

tccaacagtgtgctgccctgttaggttagacatgcctgtacctgatcccctaatggcatggatgcttgaatccaaa
caagtctgcttaaactcacatggacaagaactttggaatcctcagtgcattttgggcacacagcaggctgctgtg
acctgtaaggtcaagaatcactgggttgaggtgtgcatgttagataagaccaacatagtgacaaccatcaaaacc
tgtaagaaagatctagaagcagaccactatcatcagattccttttctgttttatttagCAGGCAAGACTGCATA
GAAACTCTAATGGACGAAGATGAGAAGGATAGAGCAAAGAGgtgagtgaagactgcccctgcctcatggtgcatg
agacatttccacgctattaaactcaacatggcgggcagctgtgggatgcggctccctgaaacatttcacagtagc
tttaagatttgcacctcaccagtgaagtgtcgttgtgtgagacttggcaagaagtctgtgtttttagtgtgcct
atgtgctaccctgatgacaatggtcaccatccagaggcctccagtttctgcttttacaagacaggtgctgcttgg

A.5.2 Murine CLOCK

ATG PAM EXON intron

FORWARD PRIMER	ccattaatgttttcttttctcacaagG	F1
	ctcaagataatgttgtagaagtgttttaga	F2
	tgcagccagtttgtagttacg	F3
	tccccatccaaagatatttgct	FS
	ggttgcttcttgtctgggtg	F4
REVERSE PRIMER	tgtcactgtattaaaccacccac	R1
	aaaccagtatgaaattatgtcactgt	R2
	tgaaggcagtgatactcagct	R3
	tttcaaaatggccttcactttt	RS
	tcaaggaaacaagctcggga	R4

PRODUCT SIZE: F1, R1: 186 F1, R2: 203 F2, R1: 226 F2, R2: 243 F3,R3: 551 F4,R4: 1133

tggttgcttcttgtctgggtgataaccactgggcagtatagcttcattgtgtattttgttttcattgtttagata
tctgtttccttgatcagtatagatttctgcctatagaactgagcctctcatccttagaggtacaaggaatatgta
ctgtttagcagaaaataaaatctcaacaaatatttgttagaccatattattgcagccagtttgtagttacgtagt
caaagcatatactgaagattaaaaatgatattttattgctttatagaaatataatttgaattttccatatatctt
ttagaagaaaaaaaagcttaaaatattccccatccaaagatatttgcttgaaaataatataccagcttcatttga
aatctgcatagtaacaatagtattctcaagataatgttgtagaagtgttttagaaaactaataaccattaatgtt
ttcttttctcacaagGAGAAGTACAAATGTCTACCACAAGACGAAAACATAATGTGTTATGGTGTTTACCGTAAG
CTGTAGTAAAATGAGCTCAATTGTTGACAGgtatgtttttaaaatcattattagaatagtgattcttataattcc
aagtgggtggtttaatacagtgacataatttcatactggtttttatatagattttcagtaaaaagtgaaggccatt
ttgaaataagatatttaaactaaataaattcttgtttagcctgatatatacatatagctgagtatcactgccttc
agagttcatgtgtggaaaacttaaaatatagttaactgtaattaaactttgttagaaagtaagttaatggttccc
gagcttgtttccttgatcacctgggacgcaggcgcgtgtgcgtggactcgcctgtggctt

A.5.3 Human CLOCK

PAM EXON intron

FORWARD PRIMERs	acaaaaatcatagggcataactgagttg	F1
	ctgttgcttagtgagtctgct	F2
	accgttactaaaagtttgaaacaag	F3
	tcttgtttagcatgatgtgttc	FS
REVERSE PRIMERs	cacatagcttttggaaatcatttattcac	R1
	cagtttctgtttaagcaaagca	R3
	tctaagttcttccaccttgct	RS

PRODUCT SIZE: F1, R1: 256 F2, R1: 205 F3,R3: 575

taccgttactaaaagtttgaaacaagatatttaaactggttaaattcttgtttagcatgatgtgttcataatata
gctaagtataaatacttttacaatttatgtaataagcttaaaaatataattattactgaattttgatttttgaat
gtttactaggaaataggttagtagtttgaatgttataactcattaacttttacaaaaatcatagggcataactgag
ttgatttacatgtcactttagtattgctgttgcttagtgagtctgctcttactttctctatccgctttcttttag
AGATGACAGTAGTATTTTTGATGGGTTGGTGGAAGAAGATGACAAGGACAAAGCGAAAAGGtagtttgattagag
atataaaatagtaaatgaatgaataatagataaatataatggtaaataaatagtgaataaatgatttccaaaagc
tatgtgctttaggagtttagatatattagcaaggtggaagaacttagaatattggtatgtagtttataaattaaa
tatcttctgacctttggaaaagtattatgctttgcttaaacagaaactgaattagaaaatctgacttcaaagca
gataattacaggtatcataaaatgattgttttataaataatcaagtttttctcaatagct

A.5.4 Human BMAL1

ATG PAM EXON intron

F1 or F2 with R1, F3 with R3

FORWARD PRIMERs	tccagATCATCCAATGGCAGA	F1
	tctccaccacttttgagagct	F2
	ctttccattctatcacatgcctg	F3
	ggggtgtgagagatgcattag	FS
REVERSE PRIMERs	agaggaagacatgccccaaa	R1
	aaggctccttcttgcttacaa	R3
	tgtcgccacctagagttgg	RS

PRODUCT SIZE: F1, R1: 181 F2, R1: 240 F3,R3: 525

tatgatgctctttccattctatcacatgcctgttctgggtccggggtgtgagagatgca
ttagtgctgctgtaaaccagccccgggtctccccccccggcccccccaccaccaaaccccc
aagcaccaacctgggttctccaccacttttgagagctcatcgaaataaacacacctttgt
gcctcttgtaacaattccagATCATCCAATGGCAGACCAGAGAATGGACATTTCTTCAAC
CATCAGTGATTTCATGTCCCCGGGCCCCACCGACCTGCTTTCCAGCTCTCTTGGTACCAG
TGGTGTGGATTGCAACCGCAAACGGAAAGGCAGCTCCACTGACTACCAgtaaggcctttg
gggcatgtcttcctcttgttaaacttggtgtcagttctcgggcatggaacatctagcagc
cagctactgtttcatcctggaaaaggggatgggaataaaaaaccaactctaggtggcga
cacagttggtttttggctttaccttcccctagtttgtaagcaagaaggagccttcagcag

A.5.5 Human NPAS2

ATG PAM EXON intron

FORWARD PRIMERs	agaccaaaatgacaacaacctga	F1
REVERSE PRIMERs	agagtgaaagccagcgagat	R1
	aaaacccagaccactcagcc	R2

PRODUCT SIZE: F1,R1: 233 F1, R2: 390

taagaccaaaatgacaacaacctgaaagacttttaagaaagatgtagaagcagacagtaa
ttatccattctttttaatttttttttttttttgcagGAAAAACTGCATAGAAAATCTA
ATGGATGAAGATGAGAAAGACAGAGCCAAGAGgtaagatgcagctgtccccctgctcagc
agagctctctggcccccggggtctgcctggcagaatctcgctggctttcactctgtgca
ggtgaggccaccagcaagataggcagctgtaggacacactctctgtgacatattgcagtg
ctccatgagaaaccttctagagagctcactcagccctgcccctcactgtgaaatgacaca
ttgtctaggactggctgagtggtctgggttttgtcatgctcctgtgtacccctgttgac

A.5.6 BRD2

Exon 2

```
FORWARD PRIMER ggttatgctggaccgggc      AF1
               gaggccacccggactttccg    AF2
               gagaggccccaaagagactg    AF3
REVERSE PRIMER ccgctcagtactcccaaca     AR1
               agtactcccaacacggcgcc    AR2
               aaaaccgtcgctcaattccc    AR3

PRODUCT SIZE AF1,AR1: 202 AF2,AR2: 165 AF3,AR3: 583

TCCGAGAGGCCCCAAAGAGACTGCTTTCGTGCCGGCCAGGCAGGGGGTTTGTCGCCTGGAGGCCCAAGAGGAACG
GCCTCCCCCCAACTTAGCGGGTTATGCTGGACCGGGCGGTGAGGGGAACCGAGGCCACCCGGACTTTCCGCGGCT
GAGGGCAGCGCCGGTTCCTTGCGGTCAAGATGCTGCAAAACGTGACTCCCCACAATAAgtacgtttccgcgagcc
gcgtgtgggaaggggatgttgcagggcggcggcacaggggtgtggggcgccgtgttgggagtactgagcggcccc
ggcgcgctgctgttgcggcgcagctgtcgactcggtcgcgcggagggaattgagcgacggttttggaacggtgg
```

Exon 4

```
FORWARD PRIMER tcggtagtctccctataagca   BF1
               aattggggccgcagtttaag     BF2
REVERSE PRIMER actgtttctccccacctact     BR1
               agagctctgaagtcacatcact   BR2

PRODUCT SIZE BF1,BR1: 244 BF1,BR2: 388 BF2,BR2: 471

ttatttatttattttgtcccacagtttaattggggccgcagtttaagtaactgttcctttgatgcataggggggg
tgtgtgtgtgtgtgtgtgtgtgagagtcggggatcggtagtctccctataagcatttatttttctgtggttct
gacctaacatttttttatttagGATTATCACAAAATTATAAAACAGCCTATGGACATGGGTACTATTAAGAGGAG
ACTTGAAAACAATTATTATTGGGCTGCTTCAGAGTGTATGCAAGATTTTAATACCATGTTCACCAACTGTTACAT
TTACAACAAGgtgagtttttctgtgtgttcatttagtaggtggggagaaacagtaacttctattattgctggata
tgttgtctacataaagtttaaatcctttgctactgaaggtgttatccaggtagggtagtcggagtcttaaaaacc
tgactctagatggtactattgaacacagtgatgtgacttcagagctctagttgaaggttatttagaa
```

A.5.7 BRD3

```
FORWARD PRIMER gctttctcagggagcgtaga    F1
               ctccaagccgctgctgtgac    F2
               ctttcccgacagcctctca     F3
               gactggccttcctctctgtt    FS
REVERSE PRIMER gcttgctggggttggaga      R1
               gtttccagagcgtcttcacc    R2
               caaattcccaaggccagagg    R3
               agaacgtggctcttgggg      RS

PRODUCT SIZE F1,R1: 172 F1,R2: 235 F2,R1: 138 F2,R2: 201 F3,R3: 597

cttcgcctgagcagctttcccgacagcctctcacctgggtggctgggcaatgggggtgagtgagtggagcaggcc
ctgctgaggcccgacaggtgccctcaggagcccgccgaggctgggagaggtgggggtccccggggtgactggcct
tcctctctgttgtgcttcctcctctgcagCTGTCGCCTGGTTGGGCCCGGAAATGGGACGTCGCGCTTTCTCAGG
GAGCGTAGAAGCAGCCAGGGCCTCTCCAAGCCGCTGCTGTGACAGAAAGTGAGTGAGCTGCCGGAGGATGTCCAC
CGCCACGACAGTCGCCCCCGCGGGGATCCCGGCGACCCCGGGCCCTGTGAACCCACCCCCCCCGGAGGTCTCCAA
CCCCAGCAAGCCCGGCCGCAAGACCAACCAGCTGCAGTACATGCAGAATGTGGTGGTGAAGACGCTCTGGAAACA
CCAGTTCGCCTGGCCCTTCTACCAGCCCGTGGACGCAATCAAATTGAACCTGCCGgtgcgtagctgctgcctccc
caagagccacgttctgctgctgccgtcctctgtccccctcctgctgcccccatcctggaaagactgcctctggcc
ttgggaatttgctgctaagctggggacagcctgtgcctcaggaagtccacagcacagaggcgcacagggg
```

A.5.8 BRD4

FORWARD PRIMER	ggacttgtcattctgagcgg	F1
	tgctgactgatatctcacggg	F2
	ttcagtcaaagcatggggtg	F3
	caacttggctagctaccgc	FS
REVERSE PRIMER	ggaagtttctagtccatcccc	R1
	cctgggcctgtgttgtaga	R2
	ccctgcccacactactcac	R3

PRODUCT SIZE F1,R1: 176 F1,R2: 201 F2,R1: 148 F2,R2: 173 F3,R3: 492

accacctcactctgcctcctctgttggtttgtggtctcctccctgctggagggtaagtctttggggagaggagac
attggaacccttcagtcaaagcatggggtggtccctctggccaacttggctagctaccgccagggaactcagtc
cttggagaccacagccagaggacttgtcattctgagcggtgcccatctgctgactgatatctcacgggggctct
tctcttcctttgtagAGTGCCTGGTGAAGAATGTGATGGGATCACTAGCATGTCTGCGGAGAGCGGCCCTGGGAC
GAGATTGAGAAATCTGCCAGTAATGGGGGATGGACTAGAAACTTCCCAAATGTCTACAACACAGGCCCAGGCCCA
ACCCCAGCCAGCCAACGCAGCCAGCACCAACCCCCCGCCCCCAGAGACCTCCAACCCTAACAAGCCCAAGAGGCA
GACCAACCAACTGCAATACCTGCTCAGAGTGGTGCTCAAGACACTATGGAAACACCAGTTTGCATGGCCTTTCCA
GCAGCCTGTGGATGCCGTCAAGCTGAACCTCCCTgtgagtagtgtgggcagggcccagggtggccgtcctggagg
tcgtctcctgcatgtctcctggtcagggcagttcctgggggggagggtaggagatgcattt

A.6 Oligonucleotides, vectors and plasmids

Table A.1: Oligonucleotides: primers and sgRNA sequences

Name	Gene	Specifics	Purpose	Sequence
U6 Promotor F	Human U6 Promotor	F	Plasmid sequencing	ACTATCATATGCTTACCGTAAC
MuCLOCK sgRNA AT	Mouse CLOCK	Guide A Top	Cas9n targeting	CACCGCACATTATGTTTTCGTCTTG
MuCLOCK sgRNA AB	Mouse CLOCK	Guide A Bottom	Cas9n targeting	AAACCAAGACGAAAACATAATGTGC
MuCLOCK sgRNA BT	Mouse CLOCK	Guide B Top	Cas9n targeting	CACCGAAATGAGCTCAATTGTTGAC
MuCLOCK sgRNA BB	Mouse CLOCK	Guide B Bottom	Cas9n targeting	AAACGTCAACAATTGAGCTCATTTC
HuCLOCK sgRNA AT	Human CLOCK	Guide A Top	Cas9n targeting	CACCGCTGTCATCTCTAAAAGAAAG
HuCLOCK sgRNA AB	Human CLOCK	Guide A Bottom	Cas9n targeting	AAACCTTTCTTTTAGAGATGACAGC
HuCLOCK sgRNA BT	Human CLOCK	Guide B Top	Cas9n targeting	CACCGATGACAAGGACAAAGCGAAA
HuCLOCK sgRNA BB	Human CLOCK	Guide B Bottom	Cas9n targeting	AAACTTTCGCTTTGTCCTTGTCATC
HuBMAL1 sgRNA AT	Human BMAL1	Guide A Top	Cas9n targeting	CACCGAGCTGGAAAGCAGGTCGGT
HuBMAL1 sgRNA AB	Human BMAL1	Guide A Bottom	Cas9n targeting	AAACACCGACCTGCTTTCCAGCTC
HuBMAL1 sgRNA BT	Human BMAL1	Guide B Top	Cas9n targeting	CACCGTGTGGATTGCAACCGCAAA
HuBMAL1 sgRNA BB	Human BMAL1	Guide B Bottom	Cas9n targeting	AAACTTTGCGGTTGCAATCCACAC
HuNPAS2 sgRNA AT	Human NPAS2	Guide A Top	Cas9n targeting	CACCGGACAGCTGCATCTTACCTCT
HuNPAS2 sgRNA AB	Human NPAS2	Guide A Bottom	Cas9n targeting	AAACAGAGGTAAGATGCAGCTGTCC
HuNPAS2 sgRNA BT	Human NPAS2	Guide B Top	Cas9n targeting	CACCGCAGAGCTCTCTGGCCCCCGG
HuNPAS2 sgRNA BB	Human NPAS2	Guide B Bottom	Cas9n targeting	AAACCCGGGGGCCAGAGAGCTCTGC
MuNPAS2 sgRNA AT	Mouse NPAS2	Guide A Top	Cas9n targeting	CACCGAAAAAGGAATCTGATGATAG

MuNPAS2 sgRNA AB	Mouse NPAS2	Guide A Bottom	Cas9n targeting	AAACCTATCATCAGATTCCTTTTTC
MuNPAS2 sgRNA BT	Mouse NPAS2	Guide B Top	Cas9n targeting	CACCGAGACTGCATAGAAACTCTAA
MuNPAS2 sgRNA BB	Mouse NPAS2	Guide B Bottom	Cas9n targeting	AAACTTAGAGTTTCTATGCAGTCTC
BRD2 sgRNA AT	Human BRD2	Guide C Top	Cas9n targeting	CACCGGCATCTTGACCGCAAGGAAC
BRD2 sgRNA AB	Human BRD2	Guide C Bottom	Cas9n targeting	AAACGTTCCTTGCGGTCAAGATGCC
BRD2 sgRNA BT	Human BRD2	Guide D Top	Cas9n targeting	CACCGCGTTTCCGCGAGCCGCGTGT
BRD2 sgRNA BB	Human BRD2	Guide D Bottom	Cas9n targeting	AAACACACGCGGCTCGCGGAAACGC
BRD2 sgRNA CT	Human BRD2	Guide E Top	Cas9n targeting	CACCGTTAATAGTACCCATGTCCAT
BRD2 sgRNA CB	Human BRD2	Guide E Bottom	Cas9n targeting	AAACATGGACATGGGTACTATTAAC
BRD2 sgRNA DT	Human BRD2	Guide F Top	Cas9n targeting	CACCGACTTGAAAACAATTATTATT
BRD2 sgRNA DB	Human BRD2	Guide F Bottom	Cas9n targeting	AAACAATAATAATTGTTTTCAAGTC
BRD3 sgRNA AT	Human BRD3	Guide A Top	Cas9n targeting	CACCTCGTGGCGGTGGACATCCTC
BRD3 sgRNA AB	Human BRD3	Guide A Bottom	Cas9n targeting	AAACGAGGATGTCCACCGCCACGA
BRD3 sgRNA BT	Human BRD3	Guide B Top	Cas9n targeting	CACCAGTCGCCCCCGCGGGGATCC
BRD3 sgRNA BB	Human BRD3	Guide B Bottom	Cas9n targeting	AAACGGATCCCCGCGGGGGCGACT
BRD4 sgRNA AT	Human BRD4	Guide A Top	Cas9n targeting	CACCATCCCATCACATTCTTCACC
BRD4 sgRNA AB	Human BRD4	Guide A Bottom	Cas9n targeting	AAACGGTGAAGAATGTGATGGGAT
BRD4 sgRNA BT	Human BRD4	Guide B Top	Cas9n targeting	CACCACTAGCATGTCTGCGGAGAG
BRD4 sgRNA BB	Human BRD4	Guide B Bottom	Cas9n targeting	AAACCTCTCCGCAGACATGCTAGT
MuNPAS2 F1	Mouse NPAS2	Exon2 F1	Primer - genotyping	ACTGGGTTGAGGTGTGCAT
MuNPAS2 R1	Mouse NPAS2	Exon2 R1	Primer - genotyping	GCCCGCCATGTTGAGTTTAA
MuNPAS2 F2	Mouse NPAS2	Exon2 F2	Primer - genotyping	ACATGCCTGTACCTGATCCC

MuNPAS2 R2	Mouse NPAS2	Exon2 R2	Primer - genotyping	ACTTCACTGGTGAGGTGCAAA
MuCLOCK F1	Mouse CLOCK	Exon4 F1	Primer - genotyping	CCATTAATGTTTTCTTTTCTCACAAGG
MuCLOCK F2	Mouse CLOCK	Exon4 F2	Primer - genotyping	CTCAAGATAATGTTGTAGAAGTGTTTTAGA
MuCLOCK R1	Mouse CLOCK	Exon4 R1	Primer - genotyping	TGTCACTGTATTAAACCACCCAC
MuCLOCK R2	Mouse CLOCK	Exon4 R2	Primer - genotyping	AAACCAGTATGAAATTATGTCACTGT
MuCLOCK F3	Mouse CLOCK	Exon4 F3	Primer - genotyping	TGCAGCCAGTTTGTAGTTACG
MuCLOCK FS	Mouse CLOCK	Exon4 FS	Primer - genotyping	TCCCCATCCAAAGATATTTGCT
MuCLOCK R3	Mouse CLOCK	Exon4 R3	Primer - genotyping	TGAAGGCAGTGATACTCAGCT
MuCLOCK RS	Mouse CLOCK	Exon4 RS	Primer - genotyping	TTTCAAAATGGCCTTCACTTTT
MuCLOCK F4	Mouse CLOCK	Exon4 F4	Primer - genotyping	GGTTGCTTCTTGTCTGGGTG
MuCLOCK R4	Mouse CLOCK	Exon4 R4	Primer - genotyping	TCAAGGAAACAAGCTCGGGA
HuCLOCK F1	Human CLOCK	Exon5 F1	Primer - genotyping	ACAAAAATCATAGGGCATAACTGAGTTG
HuCLOCK F2	Human CLOCK	Exon5 F2	Primer - genotyping	CTGTTGCTTAGTGAGTCTGCT
HuCLOCK R1	Human CLOCK	Exon5 R1	Primer - genotyping	CACATAGCTTTTGGAAATCATTTATTCAC
HuCLOCK F3	Human CLOCK	Exon5 F3	Primer - genotyping	ACCGTTACTAAAAGTTTGAAACAAG
HuCLOCK FS	Human CLOCK	Exon5 FS	Primer - genotyping	TCTTGTTTAGCATGATGTGTTC
HuCLOCK R3	Human CLOCK	Exon5 R3	Primer - genotyping	CAGTTTCTGTTTAAGCAAAGCA
HuCLOCK RS	Human CLOCK	Exon5 RS	Primer - genotyping	TCTAAGTTCTTCCACCTTGCT
HuBMAL1 F1	Human BMAL1	Exon5 F1	Primer - genotyping	TCCAGATCATCCAATGGCAGA
HuBMAL1 F2	Human BMAL1	Exon5 F2	Primer - genotyping	TCTCCACCACTTTTGAGAGCT
HuBMAL1 R1	Human BMAL1	Exon5 R1	Primer - genotyping	AGAGGAAGACATGCCCCAAA
HuBMAL1 F3	Human BMAL1	Exon5 F3	Primer - genotyping	CTTTCCATTCTATCACATGCCTG

HuBMAL1 FS	Human BMAL1	Exon5 FS	Primer - genotyping	GGGGTGTGAGAGATGCATTAG
HuBMAL1 R3	Human BMAL1	Exon5 R3	Primer - genotyping	AAGGCTCCTTCTTGCTTACAA
HuBMAL1 RS	Human BMAL1	Exon5 RS	Primer - genotyping	TGTCGCCACCTAGAGTTGG
HuNPAS2 F1	Human NPAS2	Exon2 F1	Primer - genotyping	AGACCAAAATGACAACAACCTGA
HuNPAS2 R1	Human NPAS2	Exon2 R1	Primer - genotyping	AGAGTGAAAGCCAGCGAGAT
HuNPAS2 R2	Human NPAS2	Exon2 R2	Primer - genotyping	AAAACCCAGACCACTCAGCC
BRD2 AF1	Human BRD2	Exon2 AF1	Primer - genotyping	GGTTATGCTGGACCGGGC
BRD2 AF2	Human BRD2	Exon2 AF2	Primer - genotyping	GAGGCCACCCGGACTTTCCG
BRD2 AR1	Human BRD2	Exon2 AR1	Primer - genotyping	CCGCTCAGTACTCCCAACA
BRD2 AR2	Human BRD2	Exon2 AR2	Primer - genotyping	AGTACTCCCAACACGGCGCC
BRD2 AF3	Human BRD2	Exon2 AF3	Primer - genotyping	GAGAGGCCCCAAAGAGACTG
BRD2 AR3	Human BRD2	Exon2 AR3	Primer - genotyping	AAAACCGTCGCTCAATTCCC
BRD2 BF1	Human BRD2	Exon4 BF1	Primer - genotyping	TCGGTAGTCTCCCTATAAGCA
BRD2 BF2	Human BRD2	Exon4 BF2	Primer - genotyping	AATTGGGGCCGCAGTTTAAG
BRD2 BR1	Human BRD2	Exon4 BR1	Primer - genotyping	ACTGTTTCTCCCCACCTACT
BRD2 BR2	Human BRD2	Exon4 BR2	Primer - genotyping	AGAGCTCTGAAGTCACATCACT
BRD3 F1	Human BRD3	Exon2 F1	Primer - genotyping	GCTTTCTCAGGGAGCGTAGA
BRD3 F2	Human BRD3	Exon2 F2	Primer - genotyping	CTCCAAGCCGCTGCTGTGAC
BRD3 R1	Human BRD3	Exon2 R1	Primer - genotyping	GCTTGCTGGGGTTGGAGA
BRD3 R2	Human BRD3	Exon2 R2	Primer - genotyping	GTTTCCAGAGCGTCTTCACC
BRD3 F3	Human BRD3	Exon2 F3	Primer - genotyping	CTTTCCCGACAGCCTCTCA
BRD3 FS	Human BRD3	Exon2 FS	Primer - genotyping	GACTGGCCTTCCTCTCTGTT

BRD3 R3	Human BRD3	Exon2 R3	Primer - genotyping	CAAATTCCCAAGGCCAGAGG
BRD3 RS	Human BRD3	Exon2 RS	Primer - genotyping	AGAACGTGGCTCTTGGGG
BRD4 F1	Human BRD4	Exon2 F1	Primer - genotyping	GGACTTGTCATTCTGAGCGG
BRD4 F2	Human BRD4	Exon2 F2	Primer - genotyping	TGCTGACTGATATCTCACGGG
BRD4 R1	Human BRD4	Exon2 R1	Primer - genotyping	GGAAGTTTCTAGTCCATCCCC
BRD4 R2	Human BRD4	Exon2 R2	Primer - genotyping	CCTGGGCCTGTGTTGTAGA
BRD4 F3	Human BRD4	Exon2 F3	Primer - genotyping	TTCAGTCAAAGCATGGGGTG
BRD4 FS	Human BRD4	Exon2 FS	Primer - genotyping	CAACTTGGCTAGCTACCGC
BRD4 R3	Human BRD4	Exon2 R3	Primer - genotyping	CCCTGCCCACACTACTCAC
Cre F1	Cre	F1	Primer - genotyping	GCGGTCTGGCAGTAAAAACTATC
Cre R1	Cre	R1	Primer - genotyping	GTGAAACAGCATTGCTGTCACTT
Cre F2	Cre	F2	Primer - genotyping	GCATTACCGGTCGATGCAACGAGTGATGAG
Cre R2	Cre	R2	Primer - genotyping	GAGTGAACGAACCTGGTCGAAATCAGTGCG
Cre F3	Cre	F3	Primer - genotyping	CGGTCGATGCAACGAGTGATGAGG
Cre R3	Cre	R3	Primer - genotyping	CCAGAGACGGAAATCCATCGCTCG
NPAS2 LoxP 5'F	NPAS2 LoxP site	5'F	Primer - genotyping	TGGCCAAAGTCTAGCAAAA
NPAS2 LoxP 5'R	NPAS2 LoxP site	5'R	Primer - genotyping	GGAACACACAAGGCACAGGTTA
NPAS2 LoxP 3'R	NPAS2 LoxP site	3'R	Primer - genotyping	GGATGAGTTCCAGGGGATTATG
qPCR PER1 F	Mouse PER1	F	Primer - qPCR	TCGAAACCAGGACACCTTCTCT
qPCR PER1 R	Mouse PER1	R	Primer - qPCR	GGGCACCCCGAAACACA
qPCR PER2 F	Mouse PER2	F	Primer - qPCR	GCTCGCCATCCACAAGAAG
qPCR PER2 R	Mouse PER2	R	Primer - qPCR	GCGGAATCGAATGGGAGAATA

qPCR CLOCK F	Mouse CLOCK	F	Primer - qPCR	CGGCGAGAACTTGGCATT
qPCR CLOCK R	Mouse CLOCK	R	Primer - qPCR	AGGAGTTGGGCTGTGATCA
qPCR BMAL1 F	Mouse BMAL1	F	Primer - qPCR	TGACCCTCATGGAAGGTTAGAA
qPCR BMAL1 R	Mouse BMAL1	R	Primer - qPCR	GGACATTGCATTGCATGTTGG
qPCR CRY1 F	Mouse CRY1	F	Primer - qPCR	ATCGTGCGCATTTCACATAC
qPCR CRY1 R	Mouse CRY1	R	Primer - qPCR	TCCGCCATTGAGTTCTATGAT
qPCR CRY2 F	Mouse CRY2	F	Primer - qPCR	CCATTATGAAGATGGCCAAGGA
qPCR CRY2 R	Mouse CRY2	R	Primer - qPCR	CTGCCCATTCAGTTCGATGATT
qPCR REV-ERBα F	Mouse REV-ERBα	F	Primer - qPCR	TGGCATGGTGCTACTGTGTAAGG
qPCR REV-ERBα R	Mouse REV-ERBα	R	Primer - qPCR	ATATTCTGTTGGATGCTCCGGCG
qPCR REV-ERBβ F	Mouse REV-ERBβ	F	Primer - qPCR	GGAGTTCATGCTTGTGAAGGCTGT
qPCR REV-ERBβ R	Mouse REV-ERBβ	R	Primer - qPCR	CAGACACTTCTTAAAGCGGCACTG

Table A.2: Vectors and plasmids

Vector/Plasmid Name	Insert	Restriction Site Used	Antibiotic Resistance	Source
pSpCas9n(BB)-2A-GFP (PX461)	N/A	N/A	Ampicillin	A gift from Feng Zhang (Addgene plasmid #48140)
PX461-Mus musculus CLOCK sgRNA A	MuCLOCK sgRNA A	BbsI (BpiI)	Ampicillin	Mitchell Masterson
PX461-Mus musculus CLOCK sgRNA B	M**u**CLOCK sgRNA B	BbsI (BpiI)	Ampicillin	Mitchell Masterson
PX461-Homo sapiens CLOCK sgRNA A	HuCLOCK sgRNA A	BbsI (BpiI)	Ampicillin	Mitchell Masterson
PX461-Homo sapiens CLOCK sgRNA B	HuCLOCK sgRNA B	BbsI (BpiI)	Ampicillin	Mitchell Masterson

PX461-Homo sapiens BMAL1 sgRNA A	HuBMAL1 sgRNA A	BbsI (BpiI)	Ampicillin	Mitchell Masterson
PX461-Homo sapiens BMAL1 sgRNA B	HuBMAL1 sgRNA B	BbsI (BpiI)	Ampicillin	Mitchell Masterson
PX461-Homo sapiens NPAS2 sgRNA A	HuNPAS2 sgRNA A	BbsI (BpiI)	Ampicillin	Mitchell Masterson
PX461-Homo sapiens NPAS2 sgRNA B	HuNPAS2 sgRNA B	BbsI (BpiI)	Ampicillin	Mitchell Masterson
PX461-Mus musculus NPAS2 sgRNA A	MuNPAS2 sgRNA A	BbsI (BpiI)	Ampicillin	Mitchell Masterson
PX461-Mus musculus NPAS2 sgRNA B	MuNPAS2 sgRNA B	BbsI (BpiI)	Ampicillin	Mitchell Masterson
pGL[hPer2P/Luc2P/Neo]	Per 2 promotor	SacI/HindIII	Ampicillin / Neomycin	A gift from Mingzhu Fang (Fang et al., 2017)
PX461-Homo sapiens BRD2 sgRNA A	BRD2 sgRNA C	BbsI (BpiI)	Ampicillin	Mitchell Masterson
PX461-Homo sapiens BRD2 sgRNA B	BRD2 sgRNA D	BbsI (BpiI)	Ampicillin	Mitchell Masterson
PX461-Homo sapiens BRD2 sgRNA C	BRD2 sgRNA E	BbsI (BpiI)	Ampicillin	Mitchell Masterson
PX461-Homo sapiens BRD2 sgRNA D	BRD2 sgRNA F	BbsI (BpiI)	Ampicillin	Mitchell Masterson
PX461-Homo sapiens BRD3 sgRNA A	BRD3 sgRNA A	BbsI (BpiI)	Ampicillin	Mitchell Masterson
PX461-Homo sapiens BRD3 sgRNA B	BRD3 sgRNA B	BbsI (BpiI)	Ampicillin	Mitchell Masterson
PX461-Homo sapiens BRD4 sgRNA A	BRD4 sgRNA A	BbsI (BpiI)	Ampicillin	Mitchell Masterson
PX461-Homo sapiens BRD4 sgRNA B	BRD4 sgRNA B	BbsI (BpiI)	Ampicillin	Mitchell Masterson

Figure A.13: Map of the PX461 Cas9n vector

The BbsI double restriction site where the guides are inserted is just prior to the blue marked gRNA scaffold after the U6 promotor.

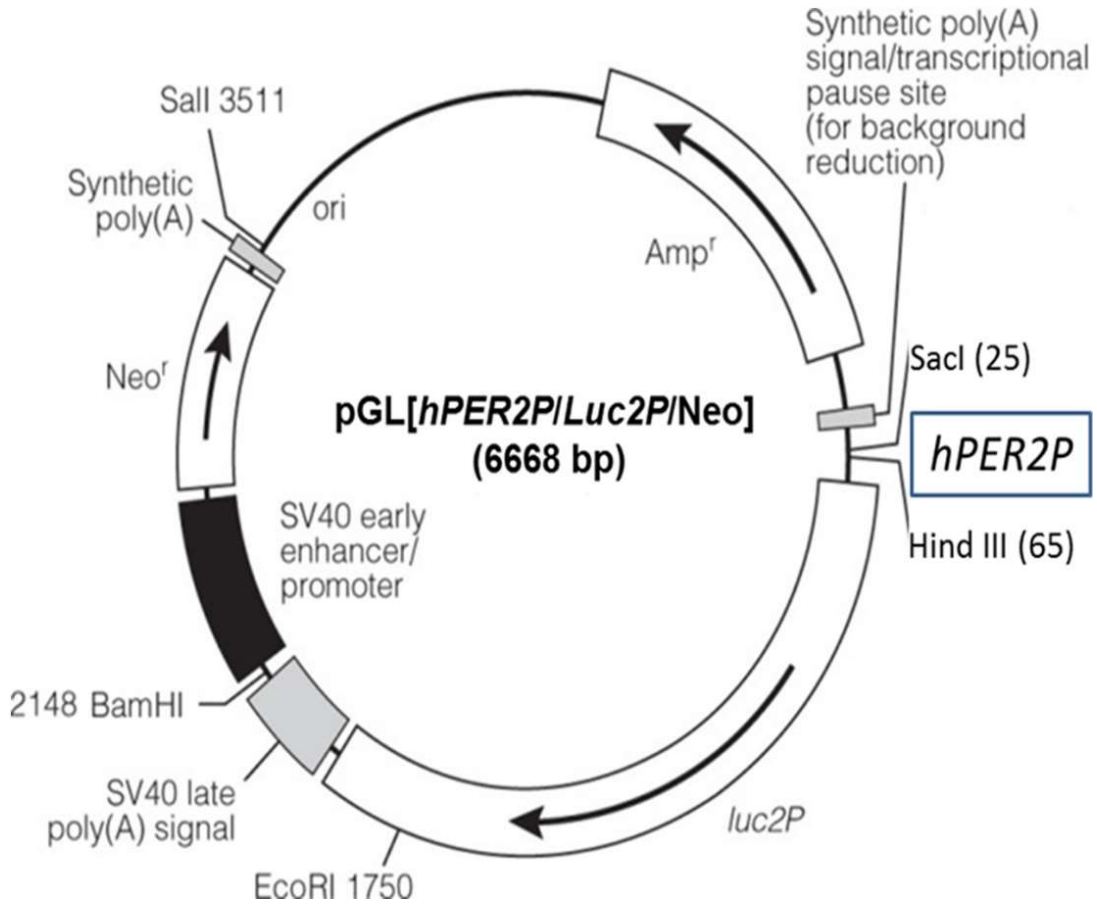

Figure A.14: Map of the pGL[*hPer2P*/*Luc2P*/Neo] plasmid

Image taken from Fang et al. (2017). Important regions are the human PER2 promotor region (hPER2P) upstream of the dLuc gene (luc2P), the neomycin resistance gene (Neo^r) for selection in the mammalian cultured cells and the ampicillin resistance gene (Amp^r) for selection in bacterial cell culture for cloning.

A.7 Target genes of BMAL1, CLOCK and NPAS2 identified by ChIP-seq

Unique and overlapping target genes of BMAL1, CLOCK and NPAS2, gene lists behind Figure 3.1. Based on ChIP-seq data from Koike et al. (2012) organised by use of Venny software (Oliveros, 2007).

NPAS2: BC067010, Zyg11a, Aox3, Slc20a2, Sh3bp5l, Ppox, BC054353, AK202580, AK133333, Npsr1, 9230115E21Rik, Polr3b, Gm10451, Trpc7, Spatc1, Usp49, Syvn1, Rnls, Refbp2, Lcn12, Mybl2, AK076665, Cldn11, Pgrmc2, Ubxn2b, AK050144, AK142614, D4Bwg0951e, Faah, D4Ertd22e, Kif1b, Fam20c, Nxph1, Chchd3, AK215237, D6Ertd474e, Prr24, Opa3, Gsk3a, Plekhf1, Polr3e, Slc5a11, Mfhas1, Gm10649, Lipc, BC048403, 2310004N24Rik, Serpina3k, Larp4b, Cmah, Gcm2, Bmp1, AK084954, Fgd4, AK015664, Ptprm, Il17b, Pkd2l1, Lgsn, Hibch, Cflar, Pdcd1, AK147021, Nr6a1, Abcb11, Trim69, Gss, Lbp, Pigt, Slc9a8, Trim55, AK076759, Grhpr, Alad, Orm1, Tle1, Btf3l4, AK148461, Rnf11, Luzp1, Arhgef19, Pex10, Ept1, Tfip11, P2rx7, Zkscan1, Kdelr2, BC044870, Gngt1, Cml5, Atp2b2, Anubl1, AK143902, AK156678, Zfp444, Mctp2, E230029C05Rik, Mrps31, BC035532, DQ704652, Gfod2, Smpd3, Dpep1, Agt, Ttc36, Med23, Ifi47, Zfp692-ps, Spag7, Abcc3, Fbxo47, Brca1, Baiap2, AK020496, AB349192, AK015341, C230035I16Rik, Hist1h4h, AK144747, Papd4, Bhmt2, Gcnt4, Itga1, Ints9, AK015937, C1qtnf3, Cyp2d40, Trmu, AK019614, Serpind1, Acat3, Fam120b, Chd1, Zfp40, BC003965, LOC100415784, Wac, Gata6, Mir1948, Apbb3, Zfp608, Grpel2, Zfp236, BC021614, 2010003K11Rik, AK048878, 9130011E15Rik, Apool, Gm7157, Rs1

CLOCK: Cyld, Cdk5, AK040640, Cldn3, Espl1, C80913, Yap1, Rufy3, Cd9, Txn2, Ndufb3, Mrpl34, Ndufv1, AK054442, Ttll5, Klhl20, Ubxn1, Ogfod2, BC033430, Gldn, Slc33a1, Ethe1, AK005539, Rev1, Gtpbp1, Rpl3, Nenf, C85492, Gm10094, Pno1, AK037512, Alkbh7, AK020619, Zbtb7b, Pias1, AK017586, Agfg2, Papln, Rd3, 4933434E20Rik, Ergic3, Lpcat2b, Wdr45l, Vnn3, Proc, Atf6, Eif4ebp1, Blk, Tead4, Acp6, Spns1, Cxadr, Vaultrc5, Ptges, Radil, Ttc33, AK027935, DQ707749, AK050069, Gypc, Ppp4r2, Prtg, Slc22a6, Iars, Gtpbp4, Prss22, Grb10, AK146888, AK043285, C3, Mir721, Slc44a1, Skp2, Scd1, Lgr4, Pyroxd1, Cutc, Gsta4, AK149260, Crp, Uqcc, Evi5, Hmgcl, Slc26a11, Myoc, Il1rn, Alx4, Grem1, Kin, Nfam1, Erp44, Lrrn4, Zfp788, Coq6, Ints4, Apoa2, Dusp5, Taf6l, 2410001C21Rik, Snx32, Diap3, Erlin1, Nop14, Plcz1, U09772, Gm826, Rfesd, Mep1b, Apobec1, AK158157, Kif13a, Polr3gl, Slc39a9, Mustn1, Ift140, H2-K2, Pacsin2, Pigr, Immt, Cdk17, Lpin2, Eri2, Rpap3, Skiv2l2, Prph, Fam78a, Tfrc, Chek2, Sp4, Rnf5, Slc17a1, Txnl4b, Ube2l6, Fabp5, AK133167, AK144274, Nfyc, Arhgap21, AK039014, Serpina12, 1810031K17Rik, AK078979, Fbxw11, Rab18, 9930013L23Rik, Tspan15, Il12a, AK036551, C8b, Mir592, E2f7, Lrfn3, Stt3a, Atp6v0e, H2-Q10, Zcchc7, C2cd4a, Gm6792, Fam108c, Rhbdf2, Mrpl37, Acacb, Ldhd, Nudt2, Pecr, Myh14, 8430410K20Rik, 1700009P17Rik, B3galnt1, Cd1d1, Rnf186, Lins, Chid1, Morc2a, Mycn, Ankrd33b, Hnrnpul2, AK090268, Mpp4, 5830433M19Rik, Tbc1d2b, Pion, Zfp354b, Akr1b7, Themis, AK147070, Anp32b, Arhgap24, AK143758, AK043365, Cldn5, Rps2, Srsf7, Fam154a, Bag3, Acly, Gtf2f2, Wdr91,

Ablim3, Tlk1, 1700034H15Rik, Bahd1, Qprt, Mphosph6, Adamts7, Pole4, Gsta2, Gm16515, Tmem102, Ccdc43, Dsg2, N4bp2l1, Slc24a1, P4ha1, Atg2b, Morn4, Kcnq1ot1, Cnot1, AK085480, 1600002K03Rik, AK028549, Tat, Tsta3, Haus6, Morn3, Colec12, Tmem186, AK036616, Mir3065, Med18, Tmem150a, AK133650, Nrap, Mcart1, Chrna2, Ehbp1, Stom, Fxyd1, 2410006H16Rik, AK007214, Pi4k2a, Vcpip1, Stau1, BC029726, Umod, Slco2a1, Grsf1, Grm2, Ubxn11, Igf2bp3, Dera, Pcm1, AK035573, AK145139, Scp2, 1300017J02Rik, Rfk, Tmem185b, Commd9, AK076716, Taf2, Mir33, Srsf1, AK040684, Dnaja2, Sp2, 4930579G24Rik, 4933406I18Rik, DQ564716, AK083606, Rps6kb1, Mir346, Copz1, Gm7550, Bambi, 2900060B14Rik, Pamr1, Alg6, Hps4, Cdkn2aip, Trim71, Zfp354c, Prrx1, 9130409I23Rik, AK040173, Creld1, Qpctl, Gtf2a2, Ifi27l2b, Puf60, Olfr1423, Kif6, Gpr153, Golga7, Tmem107, Cgrrf1, Kng2, Necab1, Pnpla1, AK188812, Inadl, Fam151a, Cyp2b10, Ogt, Mir375, Spon2, Lphn3, C330005M16Rik, Hmox1, BC005537, Ccdc90a, Sall3, Fam107b, Cdk9, AK008166, Vgf, Mast3, Lrig3, Calml3, Med10, Pxt1, Capn10, Gclc, Ppm1l, Cep57, Dnaja3, Nfkbia, Ift57, Cdh26, Selenbp1, Ccin, Pax4, Tmem209, Hes7, Hexim2, Ifngr2, C030016D13Rik, Raly, Zc3hav1, C1ra, 2310033P09Rik, Wfikkn2, Timm9, Rgs6, Cdh6, Mir193b, AK029591, Veph1, Usp1, AK076709, Lig3, Myt1l, Med17, BC004004, Gabarapl1, Rock2, Taf4a, Ube2u, Ptch2, Tpk1, Hrg, Hdlbp, Fmn2, AK006766, Myl10, Anxa4, 8430419L09Rik, Chd2, Ifitm2, Wdr18, AK041537, Dscam, AK208354, Rhod, Cep350, 5730590G19Rik, Leap2, A230051G13Rik, DQ703913, Cd96, Fen1, Ubap2, Usp24, Gatc, AK006167, Hmg20b, AA987161, Kctd9, Rap2a, Mtm1, Tgs1, Sh3bp4, Smpdl3a, Dpys, AK011877, Shroom3, Tcerg1l, Nudcd3, Rnu12, Wnt8b, Txndc9, Csf1, Ank1, Cybrd1, Tuba3b, Med21, Wdr72, AK089981, Dcn, AK047676, Fam181a, BC068229, Rsph9, Tmem146, Kcnh6, Hk2, Pde4a, Tcam1, Prodh, Slc26a6, Fcho2, Atp5g2, AK192544, Nfatc3, Cx3cr1, Cirbp, Dnahc6, Hp1bp3, Ccdc126, Clip1, Terf2, AK077428, Sep-10, Mycl1, AK018911, Hpcal1, Olfr655, Dctn6, 1700071K01Rik, Mtrf1, DQ686437, Prdx3, 2810008D09Rik, Unc45a, Rabep1, Greb1, Bicd2, Mrps6, Pkig, AK037419, Mphosph10, Smg7, Angel2, Acot11, Fbrsl1, Lnx2, Myst3, Tagln, Zfp521, Wwp2, Ky, Fez2, Hist4h4, Slc25a19, 3110001I22Rik, Zfp35, Efcab4b, BC019943, Fam73b, AK215842, Ahctf1, Tmem63a, Setmar, Sult2a6, Asf1b, Cpn2, Fndc3a, Ado, Abp1, Apoc1, Maff, Ppp1r10, Mir30a, Gpatch1, AK019722, Ifi35, Golt1a, Gpr37l1, Rgl1, Gnb2l1, Trp53, Erc2, AK132729, Zfp760, Atp5c1, Cog8, Ppil1, Zfp39, AK028012, 1700016K19Rik, Sntn, Poc1b, Phf20, Sik3, Robo1, 1700034H14Rik, 5031425F14Rik, Epha7, 2610528J11Rik, AK087942, Plxna1, AK005115, Ptk2b, Cxcl13, Acer3, Ell2, Arl16, Hrk, Fam149b, Adam30, Tomm6, A730017L22Rik,

BMAL1: Etfa, Hnrnph3, Nr2f2, Lss, A930001N09Rik, Vkorc1, Arrb2, Tdo2, D2Wsu81e, Mir1931, Mknk1, BC048393, Mapk8, Ninj1, Ccne1, Pgm2l1, Abcf1, 2310016C08Rik, Xpot, Usp3, Acbd3, Ccne2, Trappc10, Macrod1, Eif5a2, Hspb8, Rnf19b, Rps6ka5, Clcn2, Ppfibp2, Pa2g4, AK086741, Aimp2, C230081A13Rik, AK017040, Stk40, Tlcd1, Ndel1, Ntpcr, Top1mt, Aph1c, Mafk, Parp1, AK019691, Galt, Hspbap1, Wdr89, Hnrnpf, Pex14, AK031221, Ptpn3, Srp14, Phf19, Ttc25, Triobp, Hexa, AK133925, Vps13a, Mir1943, BC024139, Chsy3, Ptplad1, AK053084, Tcfap4, Mtrr, Mir499, Slc30a1, Cpm, Lsm4, Ptprs, Ncl, Lcorl, Usp28, Nab2, AK144265, Pola2, Unc5b, Psmg3, Pepd, Kremen1, Ccnh, Rcbtb1, Btbd3, Mpped1, Fbxo15, BC050972, Fads6, Gm15348, Ccdc33, Edn3, Cbara1, DQ568657, Chchd8, Mccc2, Mbp, BC082591, Lactb2, F930015N05Rik, Polr2j, AK039686, Dhx29, AK052590, Znhit6, Agpat6, Irs1, AK030052, Tcfap2c, Mar-08, Fam26f, Mlec, Dact3,

Chst14, Pde9a, Acaca, Glul, Dnajc1, Naa30, Lrig1, Zbed4, Srsf11, AK005363, Bop1, Xylb, Acyp1, Dcp2, Fam164c, D17Wsu92e, Sigmar1, Elovl1, Nars2, Comtd1, Rassf5, 4933400F21Rik, Clcn4-2, Acads, Elovl3, Naaa, Adamts1, 2810407C02Rik, Irgm1, Mirlet7c-2, Zmym6, Stk24, Tanc2, Zfyve21, Nrtn, Pmf1, AK019366, Phf1, Zyx, Lipt1, Paqr3, Cdh15, Pcbd1, Bcl2l11, Hnrnpul1, Gpr137, Fzr1, Pih1d1, Smyd3, 1700029J11Rik, Polr3g, Rad51l1, Got1, AK006413, Pou2f1, Ccno, Rmrp, BC031361, Zfp623, Jazf1, Rps17, Ormdl3, Ptges2, Foxred2, Fam113b, Snhg10, Pus7l, Apitd1, Mgst1, 6030446N20Rik, Cd300lg, Dhps, Nudt6, BC048644, Rpl13a, Pfn1, Gm6772, Eprs, Rybp, Ccdc134, Cyp46a1, Mir30d, Sec11a, Lsm1, Tnfsf14, Cntd1, Pla1a, Lmx1a, Per3, Cops7a, Stub1, Nbas, Fbl, BC068281, Slc39a8, Egfr, Ptp4a2, Gpsm2, Mthfd1l, Camta1, Acat1, Cml2, Bckdha, Gtf2b, 2010305A19Rik, Rreb1, AK019719, Efna3, Ubtf, Zcchc24, Ubl3, Abca3, Lmf1, Cldn14, Nt5c3, Pvr, D15Ertd621e, Kctd3, Nop10, AK043303, Slc27a1, Stag1, Rsph1, Kctd13, Slc37a1, AK012595, Scara5, Setd1b, Adrbk2, AK085371, Kidins220, 4930583K01Rik, Btbd9, Spnb3, Gm5544, Atl3, Tle6, Nat15, Xpo4, Tmub1, Erap1, Il6ra, Prcp, AK090150, Naglu, Ddx31, Supt4h1, Hmgb1, Sep-09, Vldlr, Dlc1, Bri3bp, Xkr9, Fam45a, Eif2c3, 1700018L24Rik, Irf8, Rhobtb2, Ntan1, 4930471G03Rik, Laptm4a, C1qtnf6, Vwce, Idua, Rmnd5a, Rps6kc1, Fgl1, Dsc2, 4930592I03Rik, Park7, D10Jhu81e, 1810063B07Rik, Rap1b, Amz2, Spata24, AK146979, Rbm38, Parp2, Foxk2, Rrn3, Hspe1, Pfkfb2, Tapt1, AK043804, Heatr3, AK144055, Tbc1d7, Pdlim1, Myo19, Tmem144, Bfsp1, Dennd4a, Hinfp, Nme4, Gatsl3, Pitx3, Tcerg1, BC029722, Acp5, Arhgap26, Cul3, Rbp7, Tnfrsf25, AK007460, Atxn3, Dyrk3, Vps37d, Mapkapk3, AK040873, AK053246, AK087382, Mex3d, Golga5, Gstm6, Zmat3, Ccdc21, Cks2, Slmap, Dusp4, BC038648, Asb4, Rnaseh2b, 2010107G12Rik, Plxnb1, Aen, Wipi2, Csrp2, Nek7, AK156148, Gstt1, Mina, Mospd4, 4930523C07Rik, Atf3, Gm10684, Mpp7, Cbwd1, Bend3, Mfsd10, Upb1, AI428936, Klhl29, Bbs7, Acadm, Spsb1, Ppm1k, Spg21, 1700012B15Rik, Mir3092, Maz, Wnt4, Nnt, Clcn6, Crkl, 4833442J19Rik, AK133793, Osbpl8, Ptrh1, Immp2l, Fam50b, Sox12, AY512912, Dfna5, Mir23a, 2310035K24Rik, Atp6v1h, Il12rb1, Glo1, Ift172, Rad51c, Abcc4, Mrpl54, AK085274, Rnd3, AK014798, Atp6v1g1, Prkaca, Csda, Rdh13, Mesp1, Mir17, Birc6, Lrrc8d, Sema4b, Smoc1, 4933427E11Rik, AK087736, Slc35c2, Kcns2, Lmna, Slc25a47, Gm16062, En1, Abcb4, Pde8a, AK165776, Paxip1, Prkaa1, Gpd1, BC057079, AK169507, Cstf1, Krtcap2, Nbeal2, Fam185a, Ahcyl2, Sos1, C1qtnf1, Rere, Gpr155, 2210015D19Rik, Taf4b, A630072M18Rik, AK145464, Trim29, Frat2, Armc8, Tmem104, Slc26a2, Ccnl1, 3110070M22Rik, Zhx2, Gamt, Gpx4, AI314180, Aim1l, Akt2, Kdm5b, Zfp639, Ppp3ca, Hgfac, Opn1sw, 2610035D17Rik, Ncoa4, BC029214, Cyp2j6, Kank2, 4933433P14Rik, Chst2, Gm7854, Snx1, 0610012H03Rik, B3gnt3, Get4, Impact, Prex2, BC055402, Gtf2a1, Clcc1, Akr1a4, Uspl1, Rassf7, Dot1l, Scarf2, C4b, AK041972, Stx4a, Mir1942, Fastkd3, Erf, Atg4c, AK017924, AI316807, Cpsf4l, Pdzd8, Itgal, Cyp2a5, Pgm1, Fam105b, Tnfrsf14, Fut10, Rnft2, Rab3il1, Fbxo9, Mettl14, Nol6, Snhg12, Copg, Myh9, Serac1, AK141725, AK017409, Depdc7, Shox2, Cyp3a11, Trim8, Ces1d, Plbd1, Isoc2b, Ccdc12, Stmn1, Cdx4, Ntrk2, Tmem37, Acvr1, Zc3h8, Plk3, Ung, Zfp958, Dhdds, 2810004N23Rik, AK131895, Arhgef37, Srsf4, Gm12597, Mpa2l, Cobl, Ddx50, AK043964, Nuak2, Rasgef1b, Gpr98, Sh3bgrl2, Syne2, Afg3l2, Opn3, AK085768, Nceh1, Tceb3, Wdr62, Casp14, Opn4, AK080350, Matr3, Mcoln1, Nkx6-2, Vtn, Srcin1, Trim37, Galk1, Fam69b, Ces2a, Dll1, Tmem184a, Prok2, Slc30a9, Ube2t, Grik4, Etnk1, Xpo1, Akap10, AK138421, AK011498, AK146230, Cct8, Bad, 4930473A06Rik, Acvr2b, Akap12, Styx, Idh1,

2810006K23Rik, Gabarapl2, Coro6, Habp2, Utp14a, Gpr150, Snap29, St8sia1, Cyb5r3, Slc29a2, Mir128-2, Xirp1, Iqgap2, Ywhaz, AK036422, Fosb, Kdsr, Zc3h4, Zc3h18, Agtrap, Pcyt2, Eny2, 2500003M10Rik, 3110082I17Rik, Eif3b, Pla2g15, Smagp, Mtl5, Syf2, Spen, Naa25, Mtg1, Spcs3, Kcnk16, Dopey2, Ldb1, AK079280, 5031439G07Rik, Cyp2e1, Rnf14, Vstm2l, Kdm2b, Tulp4, AK039373, Capn1, Pitrm1, Cycs, Smad1, Trhde, AK154275, B4galnt4, Ppm1b, Tprkb, Zfp239, Omp, Dcun1d3, Glrx3, Cd164, AK145334, 2010109K11Rik, Tcra, Scaf4, Vmn2r93, BC021953, Ispd, Vps13d, Prodh2, Polr3h, Mir2861, Etaa1, Aspscr1, Tifa, AK076685, Midn, Gabarap, Yars, Tacc1, Ankrd56, Zfp362, Baz1a, AK009785, Phyhd1, Zbtb43, H2afj, Cux1, 1810043G02Rik, Rab34, BC057022, Tab2, Cndp2, Ccng2, 1810029B16Rik, Vamp1, Nip7, Rnf141, Car8, Rtp4, Tuba1c, AK039577, Mir720, Rwdd4a, Prss48, Galnt10, D17Wsu104e, Thada, Sox7, Pold3, Polm, Fzd8, Zzz3, Col25a1, Tie1, Srp72, BC042727, Klf10, DQ714940, Gm2058, Cyb5b, Cep57l1, Kifc1, Pprc1, Gm3646, Pla2g2c, E2f8, Rab11a, AK085428, Spice1, Sgol1, Cxcr4, Prrc2b, Ube3c, Fosl2, AK015545, Fbln2, Bax, 4932414J04Rik, Atp5g1, Pygl, Pigp, Brd2, Rbm4b, Plekhg1, Bach2, Jag1, 1700057K13Rik, Dtx4, Fam159a, Ndufa4l2, Tmem64, 4930555I21Rik, Stk35, Mbtd1, Lgals8, DQ693081, Nup153, Adsl, Hiat1, Tgm1, AK035687, Trim47, Hat1, Msx1, Fam173b, Zadh2, Nup93, Nme6, AK046786, Tmem86b, Tpst2, Hus1, Pbx4, Plekha7, AK048595, Fam102a, Prrg4, Dhrs3, 1810013D10Rik, Cnbp, Nup210, Insc, AK006239, D16Ertd472e, Hps1, 2700078E11Rik, Dusp10, Hdc, Far2, Pnpla2, 4931428F04Rik, Fam54a, Rnd2, Sdc1, Cetn3, Grid1, Socs5, Asb13, Mir684-1, Tmem177, Mfsd4, Acss2, Ece2, Peo1, Osm, Hlcs, Nr2f6, Aldh3b1, Dst, Set, Mir3109, Eif2b5, Uhrf1, Wdr36, BC100494, AK020061, Mt1, Fnip1, Otof, Msx1as, Lin54, AK036547, Nnmt, Wdr61, Ccdc109a, 1300014I06Rik, S100a10, Spcs2, Cenpn, Socs7, Pnldc1, Arhgap32, Bcl10, Emx1, Olfm2, Ublcp1, Baalc, Prr5, AK085609, Bloc1s1, Fbxo33, Fam134b, Cdk18, Oxt, Tgm2, Snapin, Tmem55a, AK007223, Sh2d6, Isy1, Ctdsp2, Nme2, Bik, Igsf11, Thoc1, Fhod3, 4921504E06Rik, Ctcfl, Pklr, Lsm10, Ccar1, 2310003H01Rik, Calm1, Dock5, Acap2, AK133038, AK033147, 1810009A15Rik, Psmg4, Cdk5r1, Mthfd2, Csk, Zfhx3, Peli2, Hn1l, Cd160, Heatr2, AK050516, Adamts4, 4833439L19Rik, E030010A14Rik, Fas, Jph1, Klf7, SH3d19, Letm2, AK007545, Iqch, Ctnna1, Map2k5, AK033049, Grin3b, Fam108a, Akap11, Fgf21, AK144388, AW549877, AK047030, Gm1661, Maml2, E130317F20Rik, Kif1c, Rps6ka4, Ino80d, Apcs, AK144798, Eya3, Nudt9, Hscb, Eln, Hspb1, Mgll, Nfrkb, Pde7b, Mon2, Mmd, Lasp1, Pcnx, Tmem171, Cenpj, Dis3, Yaf2, 9430023L20Rik, Rxrb, Lhfpl1, Shroom2, Auh, Vps26a, Kl, 2700060E02Rik, Mir1962, Adam19, AK141540, Cyp2c55, Lnx1, Aldh1l2, AK039053, Nrn1, Atp6v1e2, Mbl2, Hsp90aa1, Igfn1, Chadl, Slc19a2, AK016837, Papd7, AK085943, Dapp1, 1810046K07Rik, Oit3, Tmpo, Uqcr10, Gpld1, Gart, Mfsd6, Xkr8, Pdk4, Mir139, 1110004F10Rik, Egln1, Apon, Erbb3, B3galnt2, Tert, Rnf19a, Litaf, Klhl24, Olfm1, AK139864, 2010000I03Rik, Rbm19, Ppp2cb, Dnm2, Glyctk, Polr3k, Fubp1, Lingo2, 2610002J02Rik, 4831440E17Rik, AK016046, AK131759, D10920, Mars2, Zfp664, Galc, Tubb2a, Cul4a, Capn7, Tmc6, Ssr1, Wdr43, Ydjc, Robo3, Rheb, Eif2b4, Snai3, Sep-07, AK078931, Metrnl, Zfp277, Ankrd46, Syp, Ing5, Snora65, 0610011L14Rik, Sepsecs, Plcxd1, Smurf1, Pvrl2, Fsd2, AK154190, Ddx6, Snrpf, Fn3k, Lrrc9, Slc25a48, Mast4, Hnrnpa1, Gpr156, Mir99a, Plod3, Ccl2, AK012387, Prr3, Arhgef18, Celf1, C030039L03Rik, AK041339, Serpina1e, Hnrnpa0, Prpf19, AK018156, Barx2, Ankrd9, BC030050, Rela, Negr1, Id3, AK042124, Serpina1b, Ptch1, Tdh, Pop1, Zfp791, Fpgs, Pafah2, Fbxo8, Serpina9, Cd46,

2010016I18Rik, Faf1, AK079675, Polr1a, Lpar2, Herpud2, Msra, AK009639, Mmadhc, Cept1, AK005641, Hdhd3, Zc3h12a, Rab42-ps, AK006202, Usp12, Ctsc, Sox6, Zbtb2, Bbs10, Pex12, Rptor, 1110057K04Rik, Cd83, Tnfrsf19, Ebpl, Mapk14, Rdbp, AB350970, Hirip3, Dct, Pabpc2, Cebpe, Dtd1, Gm11968, Stk32a, Top2b, Kif14, AK046134, Rpl41, Idi1, Uba6, Gsr, Slc12a4, AK006037, Slc25a29, D0H4S114, Skor2, Spred1, BC062821, Lyl1, Atm, Nrbf2, LOC100045653, Pld6, 5430411K18Rik, Kalrn, Utp18, Nid2, Snai1, Mycbp, Rtp3, Jmjd6, Prkcd, Ppfia4, Vamp4, Hnf4a, Ctbs, Gm12633, BC063263, Bet1l, Stt3b, Smarcd2, Tomm20l, AB352963, Chkb, 9930021J03Rik, BC034090, Scand3, Lrrc42, Fbln5, 5330439B14Rik, Cog6, AK087045, Nr4a3, AK085891, AK077358, AK144984, Dpf2, AK138296, Ralgps1, Pmvk, Crcp, Sepw1, Fkbp8, Ier2, Hmg20a, Slc16a10, AK015520, AK016521, Cacna1h, Mdc1, Cdo1, Vmn2r121, Nek2, Slc35a3, Clock, Ccdc9, Aldh3a2, Vash1, Hrh2, Hrasls, Cpox, AK150559, Mir698, Myo1e, Ube2cbp, AK019365, Fry, 2700089E24Rik, Fxyd3, Cpeb1, 9530008L14Rik, Tsc22d3, Cttn, Tnfrsf26, Nprl3, Plekha1, Psd3, Ces2g, Mir1930, Zap70, Bzw1, Dner, Gli2, BC006779, Tcea2, Tgfa, Cadm4, Capn12, Mmp15, Jam3, Poc1a, Tgfbr2, Hivep2, AK007947, Sectm1a, Nup155, Pgam1, Mid1ip1, Ctrc, Impdh2, Mllt10, Sec62, Asna1, Tbata, Slc9a3r1, Exosc2, 2310033E01Rik, Fam83a, Wdr26, Pou2af1, AK156967, Tmem200b, Man2a2, Guk1, Ildr2, Ptk6, 5430416N02Rik, Opcml, Clec10a, AK021004, Plin3, Frat1, Fdxacb1, Adat2, Gpr182, Aarsd1, Dysf, AK017331, Arl15, Ctsz, Gm5506, Capza3, Cdyl, AK087806, D4Wsu53e, Zxdc, Usp5, Ttc21a, Nr4a1, Rce1, Mtx3, Stard7, Slc35a2, Mesdc2, Cgnl1, Tmem14a, 0610007L01Rik, Chchd2, Entpd6, Prdm14, AK084494, Atp10d, Hsf5, BC065997, Tnfrsf18, BC006965, Abcb1a, 1190002N15Rik, Nags, AK080657, Slc35d1, Nat8, AK143760, Dnhd1, Taf5l, Ndrg2, A730085E03Rik, AK217854, Plscr3, Zbtb20, Cdh1, Caprin1, Prpsap1, Hmgcr, Ranbp3, Tmem120a, Top1, Acadl

NPAS2 and CLOCK: Rcbtb2, Osbpl3, Krt23, AK048886, Hnrpll, AK132836, Eif2b3, AK142879, Psmd1, Cr2, Usp8, Fam63a, Dpyd, Cno, Slc25a36, Mafg, Slc45a2, Gm5468, Mpz, Ier5l, Dnajc5b, AK045932, Tgfbr1, AK019798, Aldh2, 2810007J24Rik, ORF61, Eea1, Phlda1, Mettl7b, Accn1, B130006D01Rik, C030044B11Rik, Fam172a, Ndrg1, Gtf2f1, Ndst1, AK019053, Efcab2, Ptgds, Dido1, Prmt6, Klhl9, Rlf, Errfi1, Galntl5, AK006930, Afp, Glt1d1, Chn2, Ccdc61, Tomm40, Saa1, Myo7a, Sbk1, Rbpms, Enpp6, Gcdh, Nlrc5, 1810063B05Rik, BC018242, Tmem25, G630090E17Rik, Lrrc48, Zfyve1, Nol8, Parp4, AK014089, Rfc4, Gp5, Snx4, Hgd, AK083150, Hdgfrp2, Map4k3, Tmem20, Gm7102, Slc10a3, Uchl5, C130074G19Rik, Ints7, 9430008C03Rik, Sox2ot, Asap3, Gm13011, Zfp513, Npffr2, Tmem106b, Creb5, Elmod3, Cic, Gm5595, Tsku, Tpte, Aprt, Birc3, Spc24, Ostb, Fam83b, Pbld2, Tmem220, 1810027O10Rik, Stat3, Hexim1, Fdxr, Arl4a, Scarna13, Cdca7l, Gpx5, Gas1, Rarb, AK015818, Mar-06, Rab40c, Runx2, Khsrp, Kcng3, Ttr, Diap1, AK086315, AK016444, AK075658,

NPAS2 and BMAL1: Hmcn1, 0610007P14Rik, Kif12, Klhdc7b, Lipa, Elk4, Cd302, Tspan9, Ireb2, Usp20, Ptpmt1, Tmem53, Tgfbr3, Vkorc1l1, Fabp1, Lhfpl4, Abcb10, Gopc, Man1a, Eif1, Serpina11, BC024659, Mrpl15, Rab14, Dio1, Pcgf3, Uroc1, AK042445, Plxnd1, Zbtb32, Tmem86a, Dkk3, Cars2, Cln8, Clec18a, Zc3h12c, Fbxo22, Stmn1-rs1, Chac2, Ctage5, Smek1, AK076979, Ror2, Habp4, Kif13b, 9030625A04Rik, Ldhal6b, Sult1c2, Tmc1, Cnnm2, Mobkl3, Nrp2, Dnpep, Dnajb3, Cabc1, Trp53bp2, Il1f9, Gm13498, Fign, Ambra1, Cds2, Nfatc2, Fgg, Slc16a1, Osgin2, Aco1, Edn2, Fndc5, Slc30a2, Pax7, Abcf2, Tmed5, Ephb4, Met, AK080009, Atoh8, Mat2a, Magi1, A230083G16Rik, Bbc3, Lrrk1, Rnf169, St5, Pex11c,

Pde4c, Ces1g, Has3, Zfp872, Dlat, Kdelc2, Sin3a, Edc3, Pkm2, Skor1, Parp16, Manf, Zc3h12d, 2010003K15Rik, Prep, Arid3a, Rfx4, Gas2l3, Sec14l2, Smcr8, Dhrs7b, 1810012P15Rik, Pigw, Akap1, Grb2, Nampt, Mir681, Hist1h2bh, Ankrd55, Dock9, Mir297-1, Ank, Trio, Rnf139, AK020235, AB099516, Acvr1b, Eif4b, Itsn1, Lnpep, Slc22a7, Rasgrp3, Scarna17, Tjp2, Neurl1a, Gm5098

CLOCK and BMAL1: Cdk4, 1700021K19Rik, Ddt, Fhit, Tbc1d15, Lonp1, AK138667, C1rl, Lama3, Pten, Dvl2, Gse1, Gtl3, Art2b, Nlrp6, Dap, Mirlet7a-1, AI462493, AK029768, Nelf, Top3a, Hspg2, 5830415F09Rik, Atf6b, AK146139, Slc25a13, AK168184, D5Ertd579e, Dbx1, Fam101a, 1700001C19Rik, Prhoxnb, Klb, Smad6, Tmem182, AK086793, Phb, Mir3075, Rab44, Celsr2, Sertad1, Irf1, Tmem55b, Gm16516, Cecr2, Rbm17, Fam189b, AK154735, Srbd1, Tmem106a, AK154225, Zbtb40, Elavl3, Cyp2u1, AK035211, Lrrc28, Ubr2, Vps37a, Cdv3, Bhlhe41, Gpx1, Mrpl23, Gpr135, Chd7, E2f2, Tpra1, Ets1, Tm4sf4, Gaa, Alkbh5, Arhgef26, Mettl4, Limd1, Pard3, Rnf43, Adck3, Nptn, Dcaf13, Gprc5c, Tbc1d9b, Ino80, Rpl14, Sc4mol, Tmem212, Nr1d2, Ing2, Arrdc4, Mxd4, Fam187b, Zc3h11a, Slc23a1, Mllt1, P2rx4, Zfp507, Fgb, 1810010H24Rik, 5930403L14Rik, Epn1, Hagh, AK019662, Ell, Bdh1, Ppa1, Angptl3, Wars2, D030047H15Rik, BC044868, Amigo2, 9530091C08Rik, Slc35d2, Tmem174, Myom3, Olfml2a, Tbl2, D10Wsu102e, AK089375, Sdad1, Zfp69, Tatdn2, Bcat2, Arrdc1, Hpn, Cltc, Frmd6, Cln6, Rab3gap2, Ctla4, Ccdc37, Hspa8, 1300001I01Rik, Polr3a, Pmch, Rnf144a, AK046304, Zfp710, Nfib, 2400001E08Rik, Kif21a, Gnat2, Glrx5, Ccdc86, Fbxo30, AK079018, Slc38a3, Ptprj, AK153351, Pfkfb3, Derl3, Rrp8, Ccbp2, 4933439F18Rik, Dclre1a, Mknk2, AK134426, Tor1aip1, Vps37b, Hsd17b2, Sumo3, Gpt, AK017620, Polr2i, Pard6b, Comp, AK005707, Rnf38, Pnpla7, Zbtb17, Adam2, Zfp62, Acaa2, Slc16a12, Cat, Tada1, Cebpa, Mvd, 1810055G02Rik, 2310047M10Rik, Prlr, Tbl1xr1, Cfb, AK040741, Ltbr, 0610007C21Rik, Ccdc121, Yif1b, St13, Mst1, OTTMUSG00000024510, Kdm4b, Alg9, Fbxo31, Ralb, Narg2, Bat1a, Slc6a6, Tsc22d2, Ccdc3, Bcl7a, Mrpl36, Hspa9, Lztfl1, Lrtm1, AK047558, Ddi2, Kdm4a, Sqrdl, Atf7ip, BC031781, Cyp2d13, Chat, 2210417A02Rik, Psmd9, Ccdc132, Gast, Btd, Mtmr7, Foxa3, H47, Rcc2, Calr3, Grn, AK006039, Clcn7, Gm9159, Kifc5b, Hhex, Mobkl1a, Hnrnpu, Celf2, Igfbp5, Dntt, Psmb3, Narf, Dync2li1, Mir1901, Krcc1, Sertad2, Uqcrq, 9230116N13Rik, Tomm20, Bcas1, Shb, Raf1, Dync1li1, Bves, Ttll8, Zfp36l2, Ptprf, Chpt1, Wnt10a, Eif5a, Qtrtd1, 0610030E20Rik, Gzmk, Neu3, AK162599, Dyrk1a, Slc22a1, Cxcl12, Slc12a3, Polr2h, Tpd52l1, AK002663, Gmfb, F7, Hyal1, Pnrc1, Med11, Ptbp1, Mat1a, Pcsk9, Tjp3, Meig1, AK016682, Max, Aqp8, Sucla2, Slc19a1, Cyth1, Mtf1, Tnfaip8l2, Zfp933, Zfp292, Rhou, Lamc1, Fbxo46, Sgms1, BC024978, AK079377, Taf8, Spata2L, St3gal5, Pkp4, B230312A22Rik, BC055111, AK018302, Ubqln1, Nagpa, Atp1a1, Dhdh, Pip5k1c, AK076673, Lonrf1, Zfp457, Mettl13, Lrig2, AK006664, Zfp609, Myrip, AK014704, Edf1, Slco1b2, Atp8b1, Pdia4, AK029587, Naa10, Sucnr1, Birc5, 1700084E18Rik, Trp53inp1, Cdk7, Tnfrsf1a, Rin3, AK139806, Tcf7l2, Arid2, Dsp, 1700029F12Rik, Neil2, Tmem100, Qtrt1, Rab17, C4bp, Mical2, Mgat1, Fkbp5, Pdcd11, Prkca, AK155560, AK140161, AK006070, AK018984, Mcl1, Gcc2, Tubg1, Cdc42bpa, Apoc2, Rps14, BC024479, AK049871, Ddhd1, Ap1b1, ADAM22, Fbxl22, Wdr81, AK139053, Gtf2ird1, Dyrk1b, Tshz1, Rhof, Praf2, Mreg, AK010767, Parp11, Chrd, Casr, Pdp2, Dpy19l1, Hist1h1c, Ctsf, Egr1, Abtb1, Gtpbp2, E130203B14Rik, Niacr1, Prkag2, Trim56, Akr1c14, Agpat2, Krt18, Tarbp1, Phf15, Sec22a, Fzd1, Cadm1, Fgfr4, Bid, Tmed2, Rassf1, Znrf4, AK144632, Stxbp5l, Tpp2,

Snd1, AK014435, Arhgap12, Pikfyve, Ttpal, Mpzl2, AK021325, Nkx2-2, AK087755, Mtdh, Gcat, Tmem44, Cdh2, Eif6, Fam25c, Slc38a2, Ahsg, 2810055F11Rik, Slc38a9, Fam46c, Whamm, 2610101N10Rik, Pelo, Gpr110, Slc4a3, Gdpd4, Tmem126a, AK020861, Nolc1, A530013C23Rik, Utrn, 1810011O10Rik, Ercc6, Umps, Gtf2i, Entpd5, Igfals, Neurl2, 2610002D18Rik, Lrp5, Ddb1, Pdgfa, Ppargc1a, 1600002H07Rik, Ywhae, Psapl1, Reep3, Hmx1, Shmt1, Idh3a, Ankrd28, Rnase10, BC016495, Klhdc3, Stab2, Ddx39, AK044432, E2f1, AK160416, AK141187, 1110003E01Rik, AK086149, Kbtbd11, Ocln, Atf7, AK010245, Nfix, Ndfip1, Nr4a2, Xylt1, Vprbp, Gm829, Adck4, Cyp4v3, Ticam1, Arhgef1, Scn3a, Egr3, Pnpla5, Ikbke, C330006K01Rik, Lipg, Slc26a1, AK043789, Rpp38, AK076318, Pvrl1, AK144897, Setd4, Engase, Sec31a, Cldn2, Gnl3, Commd8, Fa2h, Gm2a, Dnajb9, Txnip, Mcm7, AK015284, Ppp1r3g, Usp16, Pnpo, AK146386, Fam100a, Crybg3, Tmem183a, Pdhb, Nadk, AK039589, AK015526, Zfp91, Fdx1l, Sidt2, Rad9, AK205379, Agps, Rbms1, Rhobtb3, Ptp4a1, Wdfy3, Rpl29, Zfp827, Papola, Rnase13, Wfikkn1, Ak2, Vsig10l, Tet2, Wnt5b, Homer2, Fam81a, Ccdc148, Tnfsf10, Atg3, Ube2i, Ppp1r15b, Cnst, Exosc5, Ehhadh, AK085201, Lass2, Slc25a22, Prdm4, Daam1, AK044449, AK076253, Rrp12, Gtf3a, Bbox1, Cbfa2t2, Serbp1, Cdcp1, Tpo, Kdm3a, Fxn, Rasl11b, Mrps12, Sc5d, Nsd1, C030006K11Rik, Zfp174, AY512943, Epb4.1, Areg, Akr1b3, Tnpo2, Gng7, Bptf, Bfar, Agxt, Bmp8b, Cbr4, Plekhg3, 1110018J18Rik, B4galt5, Sec13, BC049352, Maml3, Alpk1, Cpsf4, Grlf1, AK021232, Fam50a, Tox, Bod1, AA388235, Irak1bp1, Slc35a4, BC002163, Cyp4f15, Pmpcb, Cry1, AK046160, Mki67ip, Bahcc1, AK039829, Ankrd33, Lyzl1, D19Ertd386e, Nudt16l1, Angptl4, Mtfr1, Fntb, AK044426, AK136047, Scarb2, Orai1, Ctse, Zfp750, Lin52, Ankrd23, AK046316, Glt28d2, Rrp9, H2afy2, AK050866, Atp5sl, Sacs, Frmd4b, 1810020D17Rik, Insig2, AK029599, Gpr84, AK017143, Foxk1, Foxq1, Synpo, Snx18, Mapkap1, Slc36a1, AK051055, Trip6, AK020095, Banp, Derl2, Acer2, Hs3st3b1, Nab1, Serf2, AK160548, Ptprg, Glt25d2, Zbtb34, Asgr2, Zfp36l1, Derl1, Cbs, AK142949, Pde1a, Pebp1, Hip1r, Snrnp27, Ceacam16, Ankrd27, Elovl5, Tmem17, Ehmt2, A1cf, Rmi1, Creg1, Acvr2a, BC020535, Pgpep1, AK044786, AK090213, Tnrc18, Anapc5, Fchsd2, Tex18, Fzd7, Cstad, AK013883, Dnmbp, Dusp12, Ttc23, Zfp143, Ankrd37, Snx33, AK196141, Bphl, 5730469M10Rik, Ehmt1, Ap1ar, Ncf1, Cdk8, Arhgap18, Armc2, Cdc42ep4, Igsf5, Dclre1c, Lepre1, Gfpt1, Mgmt, Fadd, Trip4, Ddc, Mir365-2, Tnfaip8l1, Fis1, Creb3l3, Slc12a7, Rsad1, Prr22, Dhcr24, Sqstm1, 5730455O13Rik, Dtx2, AK084560, Chac1, Als2cr11, Phospho1, Chchd7, Dtx1, Coq7, Mfn1, 4921507P07Rik, Usp10, Cdkn3, Aven, Gtf2ird2, 6430548M08Rik, BC096441, Kpna2, Tnrc6b, Itgb5, Pisd-ps2, Ncrna00085, Amdhd2, Alpk2, AA408296, Rfx5, Slc12a9, Adamts15, Nme1, Cnot4, Ptprd, Slc35e3, Senp7, Mgst2, Rbbp4, Asgr1, Ampd2, Mapk6, Fgfr2, Alg11, Dock4, Ercc6l, Gldc, Trak1, Dnajc12, Riok2, AK054493, Mrgprg, Pabpc1, Rnf149, Tm4sf1, Fga, AK006245, 8430408G22Rik, Icam1, Ube2b, D030028A08Rik, Phf2, Mrpl14, Foxn2, AK016120, Tmem2, BC114417, AK040090, 1810008A18Rik, Camk1d, Pmp2, Shfm1, Ahi1, Dctpp1, BC030398, Fos, Pdcd2, Tlr5, Mul1, Tpcn1, Kctd21, Nmnat3, Btbd2, Mir29b-1, Got2, Psma4, Myl7, Med31, Tnks1bp1, Tmem189, AK009335, Aars, Calm3, Bcl3, Sil1, Lamp1, AK032654, Eif2ak3, Acat2, Sar1b, Serpina10, Tcf3, Srebf1, Scap, Dhx9, AA881470, Capg, Xpo7, Zfp871, Zbtb10, Med13l, Hpgd, Dynlrb2, Gdnf, Fst, AK042990, BC035947, Spata5, Gstm1, Slc25a42, AK038627, Extl3, Tars, Etv5, Rps4x, Gpatch4, Taok3, Fkbp4, AK084599, Zfp566, Parva, AK215526, Mcph1, Mir3471-1, Zfyve26, Samd4, Mbnl2, Cuta, Fth1, Fmo5, Nit2, Ccdc85b, Vamp5, Dip2c, Farp1, Samm50, Parp9, BC024582, Mir148a, Socs3, Madd,

AK011482, Sntb1, Tnks, Serpina4-ps1, Cald1, Pcsk4, Slc1a4, Shank2, Hnrnpa3, Vav2, Ldlrad3, 3230401D17Rik, Mfsd1, Plk5, Myst4, Tsc1, Cisd2, Samd8, Trpc4ap, Snx14, Pias4, Mir183, Shkbp1, Cabyr, Prkaa2, A430107O13Rik, Arhgef7, Bag4, 9030617O03Rik, BC048601, 4933403F05Rik, A930007I19Rik, Kif26b, AK049838, Ilvbl, Ddit4l, Cidec, Hsbp1l1, Nnat, Tubb2c, Nmd3, Cxcl14, A630055G03Rik, Epc1, Golm1, Dclk3, Prf1, Agphd1, Hsd17b3, Spp2, 1700037H04Rik, Vps33a, Aqp11, Slc39a10, Igfbp2, Serpinc1, Gga2, Esrp2, Trcg1, Nktr, Esr1, 6720456H20Rik, Mcfd2, Tpst1, Cherp, Cdadc1, Ccdc112, 6330403A02Rik, Dusp23, Xrn2, Carhsp1, Shroom1, Tgds, Tmem175, Dedd2, Arap1, AK087886, P4hb, Aco2, Lrrc58, AK018858, Ddah1, Atf1, Stim2, AK053124, Cdc25a, H6pd, Ankrd12, Kcnh1, AK133032, Mapkapk2, Optc, Chd1l, Baiap2l1, Tjp1, AK019657, Acot4, 2010107H07Rik, AK132723, Clpp, Smap2, Pink1, Pgd, Aqp1, P2ry2, Zfp809, Trpv2, E130012A19Rik, Slc34a1, Slc25a30, Sec14l5, Crisp2, Banf1, Dtymk, Abhd11, Abcc12, AK039624, Pfkl, Elane, Itih1, Cyp4f17, A330023F24Rik, Arfgap2, Tmppe, B4galnt1, Rad50, Axin2, Klf11, Mir23b, Jak1, Chrna4, Tprgl, Rhbdd2, Spop, Bche, Tmem38b, Mir455, AK005667, Plscr2, Smcr7, 4933426M11Rik, 4930539E08Rik, Ppic, AK082757, Dab2ip, Gpr88, Mir709, Smad3, Abca8a, Ubr5, Rab5a, Esco1, D1Bwg0212e, Traf3ip3, Ugdh, Spry2, Ola1, Zfp462, Dcp1b, Tecr, AK050336, Hdac5, Hes6, Qsox1, Rabgap1l, Fabp2, Ap1m1, Il34, Chchd10, Slc16a6, C1ql4, Ctdp1, Atrnl1, 6030422M02Rik, BC023483, Zmynd12, Ubp1, Jarid2, AK082325, Tcp11, Dusp1, Paqr7, Trpv4, Ntsr2, Mir582, Telo2, Gm4906, Ccdc25, Mrps9, Ubiad1, Dpy19l3, Pdgfrl, AK132865, Ube2ql1, St8sia3, Arhgef17, Fance, AK160850, Senp2, 4930528F23Rik, Stard13, Mir203, Plxnb2, Rims1, Add2, Gemin4, Nrip1, Gnmt, Gchfr, Sox4, 4930562C15Rik, 1190005I06Rik, Rangap1, Nedd4l, AK149321, AK144662, Gna14, Secisbp2l, Rtn4rl1, Mef2a, Map2k7, Ndufs7, Als2, Drd4, Arid5b, A330040F15Rik, Spag4, Itpripl1, EG232599, Plcg2, Gm6924, Rffl, Slc7a15, Gpbp1, St7, AK087264, AK085341, Pomc, Fam18a, Brpf3, AK046150, Snrk, Usp22, AK136034, Ganab, AK006712, Csrnp1, 2610203C22Rik, 1700030F18Rik, Srm, Cacng1, Gpr68, Hnrnpm, Slc35f5, Iffo2, AK160141, Bcor, AK043922, Cisd1, Cxxc5, Tle4, Clint1, Mylk, Ccdc41, AK008767, Slc7a6, Nfic, Gas7, Ccdc114, Ttyh2, Gm5294, Ccnb2, Rrp1, Ap3m1, Rogdi, Irf2bp1, Dolk, Kcnv2, Enpp2, Ihh, Mansc1, Tfdp1, Pemt, Kcnj12, Sgpp1, Il15ra, Slc24a3, 2210403K04Rik, Usp6nl, Tmem50a, Cbx8, Hsd17b12, Arhgdia, AK019751, Zfhx2, Mir802, 2900079G21Rik, Lrp3, Gm628, Tmem56, Chchd4, Nhlrc2

NPAS2, CLOCK and BMAL1: Per1, Dcun1d4, Myo10, Srd5a2, Nr1d1, Mpp6, Klf13, Thrsp, Upp2, BC037703, Tenc1, Chka, AK020914, Synj2, Inmt, AK036974, Nav2, Fads1, Phf17, Ubap1, Pitpnm2, Dbp, AK158188, Gm129, Fam47e, Pdk1, Decr1, Por, Anks4b, Eepd1, Tbcel, Tha1, Slc25a37, Furin, Usp36, Agxt2, Mgrn1, Hoga1, Hjurp, Mafb, Acot7, Nr3c2, Il17rd, AK086749, Ndufb9, Memo1, Pax2, Mir26b, Grem2, Cubn, Ccdc141, Cry2, Utp11l, Gys2, Xrcc1, Ccnd1, Hlf, Matn2, Eif4g1, Rtp1, ORF63, AK019601, Ppp2r5a, Mcm10, Rapgef1, 0610037L13Rik, Slc45a1, Wipf3, Prss8, Gpt2, St3gal4, Gnat1, Nfil3, Wdfy2, Gm7325, Cps1, A730008H23Rik, Per2, Aqp12, Atp1b1, Rapgef2, Col27a1, Prkg2, Herpud1, 4931406C07Rik, Car12, Pctk2, Plk2, Abcd2, Ergic1, Fgd2, AK077157, Ugt1a1, Rgs8, Igsf8, Lrp4, AK042900, AU019990, Bcl2l1, Tshz2, Abcd3, Pla2g12a, Ppap2b, Adc, Nr0b2, Gpatch3, Gm16532, AK042797, Nup62, 2700029M09Rik, Maf, AK078316, Fdx1, Adarb1, Nudt4, Fam19a2, Igfbp4, AK136877, Gch1, 1700108F19Rik, Trib1, Slc38a4, Pim1, Ttc7, Ammecr1l, Ppargc1b, D18Ertd653e, Mamdc2, Gm815, AK171953, Etnk2, BC050122, AK053216,

Ralgapa2, Ahcy, AK027991, Cp, Ccrn4l, Ptgfr, Thrap3, Agmat, Atxn2, Smyd1, Kbtbd8, Itpr2, Stard5, Xpo6, Slc22a16, AK169506, Cnot8, Slc13a2, Map2k6, Hbp1, Gphb5, AK200600, Nln, AK016040, Gnpnat1, Azin1, Tef, Nup50, AK007854, AK050349, Eif1a, Zfp407, Cyp17a1, Il1r1, Dis3l2, Rgs16, Mir103-2, Nrsn2, Gclm, AK047309, Hyi, Padi1, Dnajc16, Afm, Bri3, Akr1d1, Plekha8, Znrf2, Itpr1, Clec2d, AK043814, Irgq, AK007376, Pcsk6, Trpc2, Psma1, Sephs2, Lhpp, AK021128, AK032387, Nudt7, Rab6b, Reep6, Tmem19, Tbc1d10a, Tmem93, Tob1, AK143961, 4831426I19Rik, Wrnip1, AK007100, Fam107a, Gjb2, Lifr, Pim3, Nr1i2, Prr18, Vegfa, Cfh, Prdx6, AK042551, Bend7, Plcb1, 0610008F07Rik, Zmynd8, Adh6b, Uox, B4galt1, Epb4.1l4b, Sgip1, AK144477, Pum1, Mtor, Cpeb2, Slc4a4, Alb, 2900026A02Rik, 2410137F16Rik, D6Ertd527e, AK029023, Slco1a4, Ppfibp1, Zfp36, Fam196a, Tmem80, Tspan4, Hook3, Helt, 4930567H12Rik, Ldlr, Bmper, Usp2, Mfrp, Tle3, Trf, Alas1, AK006189, Arg1, Prdm1, Nap1l1, Sdr9c7, BC019819, Cyfip2, G3bp1, Trim11, Pipox, Slc35b1, Slc25a39, Tbc1d16, Id2, Tssc1, Sh3yl1, Arhgap5, AK034421, AK014028, Txndc5, 9430083A17Rik, Smad5, Agtpbp1, Dmgdh, Scamp1, Chdh, Ctsb, Tmem184b, AK045688, 1700001L05Rik, Nfe2, Nmral1, Vps8, 1110020A21Rik, Epas1, Rnf125, Lman1, Flrt1, Smarca2, Papss2, Ppp1r3c, Tectb, Gm8883, Agap1, Zcchc2, AK039419, Chit1, Fam20b, Mpzl1, Psen2, Mir1981, Plxna2, AK075572, Ass1, Abl1, Cobll1, D2Ertd750e, Sord, Slc27a2, Gm14164, Matn4, Fndc3b, Ensa, Adh5, Gabbr2, St3gal3, C77080, Klhdc7a, Epha2, Fhad1, Slc25a33, Arhgef16, Crot, Lgi2, 0610040J01Rik, Rbm47, Prkab1, Pptc7, Gpr146, Gna12, 1700001J03Rik, Slc46a3, AK076827, AK008560, Snx10, 9130019P16Rik, Fam176a, Klf15, Hdac11, AK002866, Vgll4, Pik3c2g, Ehd2, Cblc, Mogat2, Wee1, Eps8l2, Odz3, Isyna1, Junb, Sall1, AK015712, Bcar1, Galnt2, AK041328, Apoa1, 1700017B05Rik, Ip6k2, Cnksr3, Cited2, DQ696813, Aifm2, Gstt2, AB251164, Pah, Plxnc1, Rdh9, Gm12034, Slit3, Wwc1, Vdac1, Rara, G6pc, Fam20a, Tk1, AK192194, 2310015A10Rik, Clmn, Aspg, Atp6ap1l, AK043460, AK087292, Anxa7, Pbrm1, Txndc16, 1700129C05Rik, Fdft1, Sorbs3, Mtss1, Asap1, Rbfox2, Ppara, Tymp, Krt8, Tbccd1, AI480653, Wdr4, Ddr1, Svil, Pcdh1, A930012L18Rik, Gm672, Acy3, Neat1, AK019124, AK039361, Blnk, Marveld1, Abcc2, AK087340, Tbl1x, Tram1, Hs6st1, Cnnm4, AK041998, Ptma, Rbm44, Epb4.1l5, Slc41a1, Plekha6, Ivns1abp, Adcy10, Gfi1b, AK011205, B3galt1, Dhrs9, Gorasp2, AK044780, Bmf, AK134652, Slc25a44, Efna1, Mrps21, Cnn3, Agxt2l1, Ripk2, Ifnk, Dnajb5, Tnfsf15, Fggy, Lepr, Dab1, Eif4g3, Camk2n1, Efhd2, AK135377, Hopx, Mn1, Pxn, AK162140, 0910001L09Rik, Cyp2w1, Gpr12, AK046388, Zfp467, Fam13a, Aldh1l1, Lpcat3, 4930417O13Rik, Etv6, Sox5, Zfp526, Lipe, Cyp2f2, Eif3k, 4930432E11Rik, AK149394, Akap13, Uvrag, AK016032, Irs2, Slc7a2, Mlf1ip, Myo9b, Prdx2, Ces1e, 4933407C03Rik, Car5a, Trhr2, Fanca, Sipa1l2, Irf2bp2, Rgl3, Imp3, Glce, Dapk2, AK076831, Uba7, 1700102P08Rik, P4htm, Acaa1b, Cyp8b1, AK008417, Supv3l1, Cdk1, 1110038D17Rik, Pttg1ip, Slc17a8, Dusp6, Tns3, Rnf145, Slc22a4, Larp1, Dhx33, Mnt, Med13, AK003943, Mir152, Nol11, 2900041M22Rik, AK089512, Lpin1, Egln3, Arid4a, 4930403N07Rik, Ttc8, Mir3073, Adssl1, Peci, AK155516, Gfod1, Thoc3, Dapk1, Slc30a5, Acox2, AK047978, Htr2a, Zfp622, Col22a1, Adcy6, Csad, Ap2m1, Gramd1c, Cd47, Gbe1, Urb1, Ifnar2, AK038602, Clic6, Ripk4, Arid1b, AK006572, Srsf3, Abcg1, AK080425, Man2a1, Tgif1, Ypel5, Haao, Abcg8, Onecut2, Mir122a, Fads2, Cyp26a1, Pik3ap1, Avpi1, Gm10768, Pdcd4, Acsl5, Prps1, Gsta3, Fzd5, Tns1, 2810459M11Rik, Lrrfip1, Tor3a, Dpt, Nos1ap, Hlx, Mir669i, Sardh, Wdr38, AK007819, Serping1, Fnbp4, Slc20a1, Hao1, Id1, Plcg1, Sgk2, Sdc4, Ptpn1, Pck1, Slc17a9, Slc2a2, Lekr1, Fnip2, Trim45, Sort1,

A930005H10Rik, Mir760, Elovl6, Hadh, Bdh2, Cyr61, AK077587, 2610301B20Rik, Ddx58, Nfx1, Aldob, Zfp618, Plin2, E130114P18Rik, Ak4, Slc6a9, Artn, Khdrbs1, Tmem222, Rpl11, Tmco4, B330016D10Rik, Slc25a34, Gm10565, AK147071, AK033051, Srpk2, Agbl5, Yes1, Tbc1d14, Slc2a9, Stbd1, Fras1, Fgfrl1, Slc24a6, Gpn3, Aacs, Gusb, Baz1b, Mepce, Cyp3a13, BC046508, Slc13a4, Hipk2, AK016225, Asprv1, Suclg2, Lmod3, AK039720, Oxtr, Adipor2, Mical3, Clstn3, BC048546, Leng9, Slc7a10, Fcgrt, Ftl1, AK085337, Abhd2, Mrpl48, Acsm5, Acsm3, Zfp747, AK041267, AK031861, Echs1, BC052524, F10, Zfp703, Irf2, Man2b1, Fto, Ranbp10, Taf1c, Klhl36, Gins2, Ilf3, Gm6484, Fam55b, Zbtb16, 1600029D21Rik, AK018968, BC031353, Eef1a1, Amotl2, Dusp7, Gpd1l, Acaa1a, Hhatl, Map3k5, Sesn1, 1700040L02Rik, AK046981, Dazap1, Rps15, 1190007I07Rik, Ccdc38, AK002250, Wif1, Rassf3, Xrcc6bp1, Inhbe, Nxph4, Sec14l4, Xbp1, Adra1b, Maml1, Clk4, B9d1, Kdm6b, Aldoc, Utp6, Acsf2, Pdk2, Arhgap23, Thra, Msl1, Dnmt3a, Cys1, Adi1, Efcab10, Ifrd1, Sos2, Dhrs7, AK085818, Hif1a, Foxn3, Ttc7b, Serpina6, Meg3, Dio3os, Dnahc11, AK046182, Gm11346, Slc22a23, Bmp6, Gm10790, Il6st, Mocs2, Abhd6, Ecd, Arhgef3, Il17rb, Tkt, Sfmbt1, Zfhx2as, Gucy1b2, Slc39a14, Lrrc63, Gpc6, Cox6c, Eppk1, Rbx1, Tob2, 2210021J22Rik, Rhebl1, Tmbim6, Lima1, Cbx5, BC046487, Fetub, AK018484, Fam43a, BC027231, Cryzl1, Ets2, B930003M22Rik, Hmga1, Cryaa, Plin5, Alk, Galm, Prkce, 3110002H16Rik, Npc1, Osbpl1a, Aqp4, Gm5820, Cabp4, Lrfn4, Pank1, 1500017E21Rik, Sorbs1, Cpn1, Pcgf6, Sh3pxd2a, Mxi1, Rbm20, Coq10b, Pinc, Ngef, Usp40, Phlpp1, Lax1, Adora1, Nr5a2, Nmnat2, AK154552, BC039791, Olfml2b, Ephx1, AK076929, Crat, Psmb7, Lass6, AK143789, Zfp106, Trpm7, Atrn, Bmp2, Rrbp1, Pax1, 1110008F13Rik, Sys1, A630075F10Rik, Osbpl2, Gm5148, Slc25a31, AK040671, Rnf13, Igsf10, Mbnl1, Mef2d, Tchhl1, Car14, Stxbp3a, Agl, Palmd, F3, Bcar3, AB351921, Lpar3, Ndufaf4, Susd1, Rgs3, Mpdz, Ttc39b, Podn, Btbd19, Ece1, Pqlc2, Aldh4a1, Arhgef10l, Tnfrsf1b, Slc2a5, Morn1, Akap9, Slc4a2, Fgfr3, Htra3, Med28, Sel1l3, Pds5a, AK078705, Paics, AK050091, Klhl8, Hsd17b13, C130026L21Rik, 2210016L21Rik, 2410131K14Rik, Ncor2, Scarb1, Ubc, Slc15a4, Mlxipl, E130309D02Rik, AK038791, DMR, Mtif3, Hsph1, Aass, Gprin3, Rtkn, Bhlhe40, Irak2, Zfp422, Il17ra, Slc6a13, Gapdh, Lrp6, Hebp1, Slco1a1, Abcc9, Rassf8, LOC100303645, Rps9, Zfp446, Napa, Apoe, 2210010C17Rik, Cyp2g1, Cebpg, E130304I02Rik, Ruvbl2, Sphk2, Saa3, Ldha, Mir211, Adamts17, Polg, Lrrc32, Dgat2, Slco2b1, Tmc7, Cln3, Bnip3, Syce1, Insr, AK047141, AK162519, Proz, Sfrp1, Ppp1r3b, 6430573F11Rik, Adam24, Mtus1, Klkb1, Chd9, Lcat, Ctrb1, AK085459, BC021891, Nrp1, Ecsit, C2cd2l, Nrg4, AK028224, Snx22, Aqp9, Nedd4, Onecut1, Ctgf, Wisp3, AI317395, Foxo3, Tmem26, AK143813, Pdxk, Jsrp1, Gadd45b, Slc41a2, Tcp11l2, Fgd6, Tmcc3, Acss3, Slc16a7, Ddit3, Rdh7, Gls2, Rps26, Lif, Znrf3, Igfbp1, Agxt2l2, Sec24a, Tom1l2, AK140192, Aldh3a1, Ube2g1, Tmem97, 1100001G20Rik, Hnf1b, Tex14, Dusp3, Snord104, Wipi1, 4933422H20Rik, Wbp2, AK084679, Hectd1, 2310044G17Rik, Serpina3n, Hhipl1, B930059L03Rik, Inf2, Slc17a2, BC025054, Agtr1a, DQ685120, BB123696, Fbp1, Ctsl, Cdk20, Adcy2, Glrx, AK144545, 4833420G17Rik, Adk, AK016284, Dcp1a, Ubb, Atg14, Rabggta, Cbln3, Cryl1, Spata13, AK215081, Clu, 1300010F03Rik, Sepp1, Rai14, Ext1, AK007154, Pla2g6, Atf4, Cyp2d10, Arsa, Lmbr1l, Zfp263, Ppl, Dexi, BC106179, Uts2d, Hes1, Tmem39a, AK165366, AK087725, Brp44l, AK015714, Igf2r, Tbc1d24, AK149278, Myom1, Prkd3, AK041408, Ttc39c, Stard4, AK158482, Ccdc68, Smad7, Cyb5, Pcx, Pacs1, Pga5, 1110059E24Rik, AK076909, Tnks2, Cyp2c44, Gpam, Fam160b1, Gfra1, Obfc2a, Pgap1, Trak2, Als2cr4, AK040166, Gm15456,

AK079660, Pid1, Dgkd, Ube2f, AK039635, Dbi, 3110009E18Rik, Dars, Zfp281, Abl2, Fmo3, Mgst3, Pfdn2, Mir350, Degs1, Mosc2, Hsd11b1, Phyh, 5430407P10Rik, Rexo4, Rxra, Tor1b, Lhx6, Nek6, Mettl8, AK079188, Chrna1, Nfe2l2, AK078367, F2, Nat10, Catsper2, Mall, Slc23a2, 1110034G24Rik, Foxa2, Ncoa3, Sulf2, Atp9a, Fabp4, Fabp12, Foxo1, Tlr2, D930015E06Rik, Fam160a1, Hdgf, AK007191, Rorc, AK052161, Hsd3b5, Slc22a15, Sars, S1pr1, Enpep, Papss1, BC046436, Adh1, AK029620, Dnajb4, Cth, Asph, Ttpa, Aptx, Gne, Abca1, AI427809, Akap2, E130308A19Rik, Pgm2, AK021368, Leprot, C8a, Ssbp3, Hectd3, Mfsd2a, Rragc, Fam76a, Wdtc1, Rps6ka1, Gale, Alpl, Fam131c, Tnfrsf8, Mthfr, Klhl21, Ski, Prkcz, Phtf2, 2900005J15Rik, Insig1, AK189432, Ywhah, Zfyve28, AK076853, Qdpr, Rell1, Klf3, AK007290, Gc, Rassf6, Cxcl1, Aff1, Ulk1, Tmem211, Fbxo21, Tctn2, Wbscr25, Stx1a, Serpine1, 4930432F04Rik, Pan3, Lrrc4, BC145649, AK020588, AK039826, Pcyox1, Eefsec, AK083777, AK154635, Foxp1, Pex26, Nop2, Ntf3, Pzp, Erp27, Plekha5, Aebp2, Ifltd1, Lypd4, Egln2, Snrpa, Blvrb, Dpf1, AK087850, Nudt19, Rras, Rps11, Abcc6, Csrp3, Mesp2, Anpep, Ap3s2, AK155169, Fah, Clpb, Gde1, Pdilt, Crym, Eef2k, Lcmt1, Zfp768, Tacc2, Fam53b, D7Ertd443e, Ppp2r2d, Olfr541, BC024386, Rplp2, Ctsd, Gas6, Rasa3, F11, Acsl1, Stox2, Eps15l1, 0610038B21Rik, Hook2, 9330175E14Rik, Slc38a7, Nol3, Mir3108, Hp, AK008488, Wwox, Sdr42e1, Osgin1, Crispld2, Fam92b, Zfpm1, AK040202, 2310022B05Rik, AK143934, Raver1, AK048946, Dcps, Oaf, AK143856, Slc37a4, Apoa5, AI118078, Cyp1a2, Rplp1, Myo6, Paqr9, Dnajc13, Tlr9, Abhd14a, Ifrd2, Ip6k1, Mtap4, Cmtm8, Gorasp1, Ctnnb1, Tspyl1, Ddo, Pbld1, Rtkn2, Rhobtb1, AK044689, Bcr, Col18a1, Ap3d1, Lmnb2, Nfyb, AK006461, Ric8b, Fhl4, Hsp90b1, 1700113H08Rik, Nr1h4, Krr1, AK089123, Cand1, Gns, R3hdm2, Lrp1, Hsd17b6, Pes1, Ugp2, Smek2, Snrnp25, Npm1, Mat2b, 3010026O09Rik, Slc22a5, Flcn, Map2k3, Chd3, Eif4a1, Senp3, Aspa, Dph1, Myo18a, Wsb1, AK019731, Ccl9, Dusp14, Aatf, Ypel2, 1700106J16Rik, Tns4, Stat5b, Dhx8, G6pc3, Abca8b, Cdk3, Cbx4, Actg1, Slc25a10, Gcgr, Atxn7l1, Snx13, Psma6, Mia2, Ppm1a, Fut8, Gphn, Actn1, 1700052I22Rik, Mir3067, Dpf3, 6430527G18Rik, 3300002A11Rik, Slc17a3, Uqcrfs1, Mylk4, Gcnt2, AK006512, Atxn1, Fam120a, Gadd45g, Klhl3, AK038606, BC051665, Pcsk1, Col4a3bp, Utp15, Pik3r1, Adamts6, Zswim6, Actr8, Eaf1, Gm3219, AK020680, Zfp395, Reep4, Ghr, BC048765, BC048519, St3gal1, Plec, Adck5, Lrrc14, BC100417, Cdc42ep1, Ndufa6, Pnpla3, Atxn10, AK041762, 1300018J18Rik, Scaf11, Fkbp11, Gm10035, Adcy9, 1810013L24Rik, AK028773, Txndc11, Mkl2, Bcl6, AK039760, AK053957, Gm1968, AK029404, Senp5, Pdia5, Plcxd2, Cblb, Mrpl39, Bach1, Dscr3, Cldn20, Plg, Dact2, Mapk13, Pknox1, Sik1, Brd4, Neu1, 2310039H08Rik, Mrps10, DQ716672, Dpp9, Twsg1, Lclat1, Fam98a, AK153584, Lrpprc, AK085972, AK016027, Fam59a, Mapre2, Nr3c1, Fech, Poli, AK036329, DQ548994, Pqlc1, Cpt1a, Gstp1, Esrra, Zfand5, Klf9, Mir101b, B430203M17Rik, Mir107, Hectd2, AK082813, Loxl4, As3mt, Nt5c2, Adra2a, AK045643

A.8 Software protocols for fear conditioning and latent inhibition

These programs were used to run inputs and record lick data from the cages used for fear conditioning/latent inhibition investigation in Chapter 6.

A.8.1 Pre-training

```
\filename, cecilie_li_pretraining
\the following test paradigm is divided into 4 parts: pre-training, pre-exposure, conditioning and test. This part is the pre-training. It runs for 15 mins as follow: start program. Record time of first lick. Record total number of licks AND record number of licks every minute.

\inputs
^lick = 2      \lickometer

\variables
\L = lick_to        licks total
\A = lick_a              lick array counting licks pr. minute
\F = first_l        time of first lick
\P = array minute timer
\M = minutes
\S = seconds
\T = seconds counting until first lick
\U = minutes counting until first lick
\Q = count of licks in array

\state sets
\S.S.1 = start program and count response


DISKVARS=L,A,T,U

\_____________________________________________

DIM A = 14

S.S.1     \start program and count response

S1,
#START: ---> S2

S2,
#R^lick: ADD L; ADD Q ---> S2

\_____________________________________________
```

```
S.S.2     \session timing

S1,
#START: ---> S2          \the start command ensures that timing
will begin concurrently with S.S.1

S2,
1": ADD S; IF S<60 [@sec, @min]    \check every second for the
count to 60
     @sec: ---> S2
     @min: ADD M; SET S = 0; IF M < 15 [@cont, @stop]
     \after 60" count one minute and reset to zero. Session time
is set for 15 minutes.
     @cont: ---> S2
     @stop: ---> S3

S3,
1": ---> STOPABORTFLUSH

\_____________________________________________________

S.S.3     \Screen display
S1,
0.1": SHOW 1,lick_to,L,2, Mins,M, 3, Secs,S, 4,lick_a,P, 5,
first_S, T, 6, first_M, U  ---> S1

\_____________________________________________________

S.S.4     \Recording amount of licks pr. minute

S1,
#START: ---> S2

S2,
1': SET A(P) = Q, Q = 0; ADD P ---> S2

\_____________________________________________________

S.S.5     \time of first lick

S1,
#start: ---> S2

S2,
#R^lick: ---> S3   \when first lick, stop timing by jumping to
S3

1": ADD T; IF T<60 [@sec, @min]    \check every second for the
count to 60
     @sec: ---> S2
```

```
     @min: ADD U; SET T = 0 ---> S2
S3,
0.1": ---> SX
```

A.8.2 Pre-exposure

```
\filename, cecilie_li_preexposure
\the following test paradigm is divided into 4 parts: pre-
training, pre-exposure, conditioning and test. This part is the
preexposure. A
\stimulus is presented repeatedly without consequences.  Here,
the
\parameters are set to 60 pre-exposures (PEs) of 5 sec tones at
an inter-stimulus interval
\(ISI) of 15 seconds.

\_____________________________________________________________

\outputs
^tone = 1      \tone

\_____________________________________________________________

\_________________Other constants-------\

^StimDuration = 5                              \Duration of each
stimulus (5s)
^ISI           = 15                              \inter-stimulus
interval(15s)
^PE          = 60                           \No. of PEs

\----Descriptions of variables------------\

\S = number of stimuli (ss1)

\----Declarations of array variables------\

\-----Control procedure-------------------\

s.s.1,                                            \Delivers pre-
exposures and
s1,                                         \starts and ends the
program.
#Start: ---> s2
s2,
^ISI": ON ^Tone; ADD S; show 1, NUM_PE, S ---> s3      \Waits
for ISI, sounds tone,
                                  \increments number of PEs and
                                       \displays that on screen

s3,                                  \After stimulus duration has
^StimDuration": OFF ^Tone ---> s4          \passed, switch off
the tone.
```

```
s4,
0.1": IF S = ^PE [@Finished, @Unfinished]   \If the required
number of PEs
         @Finished:  ---> s5                \have been given,
jump to stop the
         @Unfinished: ---> s2            \program end, otherwise
loop back to
                                            \give the next PE.
s5,
15": ---> STOPKILL                        \stop the program
```

Note for NPE mice no outputs were used or inputs recorded so no script is used

A.8.3 Conditioning

```
\filename, cecilie_li_conditioning
\date, august 17 2006
\the following test paradigm is divided into 4 parts: pre-
training, pre-exposure, conditioning and test. This part is the
conditioning phase. Two
\stimulus-shock pairings are presented.  Here, the parameters
are set to
\5 sec tone followed immediately by 1 sec shock (0.5 mA), given
5 and 7.5 mins into
\a 12.5 minute session.

\_____________________________________________________

\outputs
^tone = 1      \tone
^shock = 8          \shock (check that this is the right output
number)
^shockmode = 2          \ delivers shock together with 8

\----Definitions of other constants-------\

^StimDuration = 5                              \Duration of each
stimulus (5s)
^ShockDuration = 1                            \Duration of shock
(1s)
^ISI          = 150                         \Time between stimuli
(2.5 min = 150s)
^Conds        = 2                            \Number of stimulus-
shock pairings

\----Descriptions of variables------------\

\S = number of stimuli (ss1)

\----Declarations of array variables------\

\-----Control procedure-------------------\

s.s.1,                                        \Delivers tone-shock
pairings and
s1,                                           \starts and ends the
program.
#Start: ---> s2                          \Waits for start signal

s2,
5': ON ^Tone; ADD S; show 1, NUM_PE, S ---> s3
\Waits for ISI, sounds tone,
                                                    \increments
```

```
number of PEs and
                                                    \displays
that on screen

s3,                                                 \After
stimulus duration has
^StimDuration": OFF ^Tone; ON ^Shock, ^shockmode ---> s4
     \passed, switch off the tone
                                                    \and   switch
on the shock.

s4,
^ShockDuration": OFF ^Shock, ^shockmode ---> s5         \After
shock duration has passed,
                                              \switch   off   the
shock.

s5,
0.1": IF S = ^Conds [@Finished, @Unfinished]  \If the required
number of
         @Finished: ---> s6                    \pairings have been
given, jump
         @Unfinished: ---> s7                \to where the program
will stop,
                                               \otherwise loop back
to give the
                                               \next pairing.

s6,
5': ---> STOPKILL                            \after 5 minutes, stop
the program.

s7,                            \if   the   required   number   of
pairings are not given, go to ISI and do same procedure


^ISI": ON ^Tone; ADD S; show 1, NUM_PE, S ---> s3        \Waits
for ISI, sounds tone,
                                                    \increments
number of PEs and
                                                    \displays
that on screen
```

A.8.4 Testing

```
\filename, cecilie_li_pretraining
\date, august 17 2006
\the following test paradigm is divided into 4 parts: pre-
training, pre-exposure, conditioning and test. This part is the
test phase.\ Licks are counted,
\and after a set number of licks a conditioned stimulus (CS) is
presented
\until a certain number of licks have been completed. A keyboard
signal is
\given to stop the program. The time of every lick is recorded.
Here, the parameters are set to
\tone given after 90 licks until 10 more licks have been
completed.
\_____________________________________________________

\inputs
^lick = 2      \lickometer

\outputs
^tone = 1      \tone

DISKVARS=A,B,C,D,E,F,G,H,R,T,X

\_____________________________________________________

\----Definitions of other constants-------\

^CSOn         = 90                        \Lick no. at which CS
comes on (90)
^CSStaysOn    = 10                            \No. of licks for
which CS stays on

\----Descriptions of variables------------\

\A = time A (10 licks)
\B = time B  (10 licks)
\H = lick number that is start of time A (i.e. ^CSOn minus
^CSStaysOn)
\D = lick number that is end of time B (i.e. ^CSOn plus
^CSStaysOn)
\E = time at which lick H is made
\F = time at which lick ^CSOn is made
\G = time at which lick D is made

\T = total number of licks
\R = suppression ratio (10 licks)

\----Declarations of array variables------\
```

```
dim C = 9900                                  \Up to 9901 lick times
recorded

\-----Control procedure-------------------\

s.s.1,                                        \Delivers CS, counts
licks and
s1,                                           \starts and ends the
program.
#Start: SET H = ^CSOn - ^CSStaysOn;
        SET D = ^CSOn + ^CSStaysOn ---> s2
                                              \Waits for start and
works out
                                              \start of time A and
end of time B
                                              \for    both    lick
periods
s2,
1#R^Lick: ADD T; SET C(T) = X/10; show 1, LICKS, T ---> s3
                                  \Waits for a lick,
                                  \records the time of the lick
                           \increments and displays lick
                           \total on screen
s3,
0.1": IF T = H [@TimeA,@NotTimeA]           \Check for start of
time A
        @TimeA: SET E = X/10 ---> s2
        @NotTimeA: IF T = ^CSOn [@TimeB,@NotTimeB]
                                                  \If   lick   that
starts CS
         @TimeB: ON ^Tone; SET F = X/10 --->s2 \and time B has
been
                                                     \made,
start the CS and
                                                 \record the time
         @NotTimeB: IF T = D [@EndTimeB10, @NotEndTimeB10]
           @EndTimeB10: OFF ^Tone; SET G = X/10; \If yes, switch
off tone
            SET A = F - E, B = G - F;           \calculate 10-
lick SR
            SET R = A/(A + B);
            SHOW 2, SR_10, R---> s2
           @NotEndTimeB10:    ---> s2          \If no, go back
and wait for next lick


\-----End of session procedure-------------\
s.s.31,

s1,
```

```
#Start: ---> s2                              \Wait for start signal

s2,
#K2:  ---> s3                                \Wait for K2 signal

s3,
0.1": SET C(T+1) = -987.987 ---> STOPABORTFLUSH \Put stop value
into array,
                                             \stop       program,
writing data to disk.

\-----Program timer procedure -------------\
s.s.32,

s1,
#Start: ---> s2                              \Wait for start signal

s2,
0.1": ADD X ---> s2                             \Every 10th of a
second,
                                             \increment  a  timer
variable
```

A.9 PIP reflective statement

Note to examiners:

This statement is included as an appendix to the thesis in order that the thesis accurately captures the PhD training experienced by the candidate as a BBSRC Doctoral Training Partnership student.

The Professional Internship for PhD Students is a compulsory 3-month placement which must be undertaken by DTP students. It is usually centred on a specific project and must not be related to the PhD project. This reflective statement is designed to capture the skills development which has taken place during the student's placement and the impact on their career plans it has had.

Phenotyping ZFHX3 mouse models

From 30/08/2019 to 20/12/2020 I was on placement at MRC Harwell working with the Nolan group. My work was as part of a project investigating conditional deletion of the hypothalamic transcription factor ZFHX3 in mice. Previous work by the group had revealed an important role for the transcription factor ZFHX3 in circadian biology. A dominant missense mutation in the gene (*Zfhx3*^{Sci}) results in a short circadian period in constant conditions and altered sleep homeostasis (Parsons et al., 2015, Balzani et al., 2016). Mice with an inducible ZFHX3 KO have been found to show acute shortening of circadian period and/or loss of rhythmicity in constant conditions (Wilcox et al., 2017). My work in the inducible ZFHX3 KO model was work in further characterisation of effects within these mice through Harwell's phenotyping suite.

My work identified an anxiety phenotype in the mice observed in open field exploration and a change in social dominance behaviour specifically within male mice assessed by dominance tube testing. I was also able to perform other assays which identified no effect of the gene KO in these trials.

During my time at Harwell, I was also able to shadow or assist in a variety of other procedures I would not have been exposed to over the course of my PhD including experience working at a world class animal facility. I was able to receive training and experience in various mouse assays as well as ex vivo brain slice culture in which live luminescence was followed. While at Harwell I was first trained on the ClockLab software which I then used in my own PhD work for the investigation of light pulse behavioural effects. I was fortunate enough to also join a LASA course led by scientists at Harwell on generation of transgenic mice and embryo electroporation.

Bibliography

AGUAYO, A., MARTIN, C. S., HUDDY, T. F., OGAWA-OKADA, M., ADKINS, J. L. & STEELE, A. D. 2018. Sex differences in circadian food anticipatory activity are not altered by individual manipulations of sex hormones or sex chromosome copy number in mice. *PLOS ONE,* 13**,** e0191373.

AGUILAR-ARNAL, L. & SASSONE-CORSI, P. 2015. Chromatin Dynamics of Circadian Transcription. *Current molecular biology reports,* 1**,** 1-9.

AKASHI, M. & NISHIDA, E. 2000. Involvement of the MAP kinase cascade in resetting of the mammalian circadian clock. *Genes Dev,* 14**,** 645-9.

ALBRECHT, A. & STORK, O. 2017. Circadian Rhythms in Fear Conditioning: An Overview of Behavioral, Brain System, and Molecular Interactions. *Neural Plast,* 2017**,** 3750307.

ALLEN, G., RAPPE, J., EARNEST, D. J. & CASSONE, V. M. 2001. Oscillating on Borrowed Time: Diffusible Signals from Immortalized Suprachiasmatic Nucleus Cells Regulate Circadian Rhythmicity in Cultured Fibroblasts. *The Journal of Neuroscience,* 21**,** 7937-7943.

ALLEN, G. C., FARNELL, Y., BELL-PEDERSEN, D., CASSONE, V. M. & EARNEST, D. J. 2004. Effects of altered Clock gene expression on the pacemaker properties of SCN2.2 cells and oscillatory properties of NIH/3T3 cells. *Neuroscience,* 127**,** 989-999.

ALONSO-VALE, M. I., ANDREOTTI, S., MUKAI, P. Y., BORGES-SILVA, C., PERES, S. B., CIPOLLA-NETO, J. & LIMA, F. B. 2008. Melatonin and the circadian entrainment of metabolic and hormonal activities in primary isolated adipocytes. *J Pineal Res,* 45**,** 422-9.

ASHER, G., GATFIELD, D., STRATMANN, M., REINKE, H., DIBNER, C., KREPPEL, F., MOSTOSLAVSKY, R., ALT, F. W. & SCHIBLER, U. 2008. SIRT1 regulates circadian clock gene expression through PER2 deacetylation. *Cell,* 134**,** 317-28.

ASHER, G., REINKE, H., ALTMEYER, M., GUTIERREZ-ARCELUS, M., HOTTIGER, M. O. & SCHIBLER, U. 2010. Poly(ADP-ribose) polymerase 1 participates in the phase entrainment of circadian clocks to feeding. *Cell,* 142**,** 943-53.

BAINS, R. S., WELLS, S., SILLITO, R. R., ARMSTRONG, J. D., CATER, H. L., BANKS, G. & NOLAN, P. M. 2017. Assessing mouse behaviour throughout the light/dark cycle using automated in-cage analysis tools. *J Neurosci Methods*.

BALLESTA, A., INNOMINATO, P. F., DALLMANN, R., RAND, D. A. & LÉVI, F. A. 2017. Systems Chronotherapeutics. *Pharmacol Rev,* 69**,** 161-199.

BALSALOBRE, A., BROWN, S. A., MARCACCI, L., TRONCHE, F., KELLENDONK, C., REICHARDT, H. M., SCHÜTZ, G. & SCHIBLER, U. 2000. Resetting of circadian time in peripheral tissues by glucocorticoid signaling. *Science,* 289**,** 2344-7.

BALSALOBRE, A., DAMIOLA, F. & SCHIBLER, U. 1998. A serum shock induces circadian gene expression in mammalian tissue culture cells. *Cell,* 93**,** 929-37.

BALZANI, E., LASSI, G., MAGGI, S., SETHI, S., PARSONS, M. J., SIMON, M., NOLAN, P. M. & TUCCI, V. 2016. The Zfhx3-Mediated Axis Regulates Sleep and Interval Timing in Mice. *Cell Rep,* 16**,** 615-21.

BANKS, G. T. & NOLAN, P. M. 2011. Assessment of Circadian and Light-Entrainable Parameters in Mice Using Wheel-Running Activity. *Curr Protoc Mouse Biol,* 1**,** 369-81.

BAY-RICHTER, C., O'CALLAGHAN, M. J., MATHUR, N., O'TUATHAIGH, C. M. P., HEERY, D. M., FONE, K. C. F., WADDINGTON, J. L. & MORAN, P. M. 2013. D-amphetamine and antipsychotic drug effects on latent inhibition in mice lacking

dopamine D2 receptors. *Neuropsychopharmacology : official publication of the American College of Neuropsychopharmacology,* 38**,** 1512-1520.
BAY-RICHTER, C., O'TUATHAIGH, C. M. P., O'SULLIVAN, G., HEERY, D. M., WADDINGTON, J. L. & MORAN, P. M. 2009. Enhanced latent inhibition in dopamine receptor-deficient mice is sex-specific for the D1 but not D2 receptor subtype: implications for antipsychotic drug action. *The international journal of neuropsychopharmacology,* 12**,** 403-414.
BAYLIES, M. K., BARGIELLO, T. A., JACKSON, F. R. & YOUNG, M. W. 1987. Changes in abundance or structure of the per gene product can alter periodicity of the Drosophila clock. *Nature,* 326**,** 390-2.
BERTOLUCCI, C., CAVALLARI, N., COLOGNESI, I., AGUZZI, J., CHEN, Z., CARUSO, P., FOÁ, A., TOSINI, G., BERNARDI, F. & PINOTTI, M. 2008. Evidence for an Overlapping Role of CLOCK and NPAS2 Transcription Factors in Liver Circadian Oscillators. *Molecular and Cellular Biology,* 28**,** 3070-3075.
BEYTEBIERE, J. R., TROTT, A. J., GREENWELL, B. J., OSBORNE, C. A., VITET, H., SPENCE, J., YOO, S. H., CHEN, Z., TAKAHASHI, J. S., GHAFFARI, N. & MENET, J. S. 2019. Tissue-specific BMAL1 cistromes reveal that rhythmic transcription is associated with rhythmic enhancer-enhancer interactions. *Genes Dev,* 33**,** 294-309.
BORKAR, C. D., DOROFEIKOVA, M., LE, Q.-S. E., VUTUKURI, R., VO, C., HEREFORD, D., RESENDEZ, A., BASAVANHALLI, S., SIFNUGEL, N. & FADOK, J. P. 2020. Sex differences in behavioral responses during a conditioned flight paradigm. *Behavioural Brain Research,* 389**,** 112623.
BOTHMER, A., PHADKE, T., BARRERA, L. A., MARGULIES, C. M., LEE, C. S., BUQUICCHIO, F., MOSS, S., ABDULKERIM, H. S., SELLECK, W., JAYARAM, H., MYER, V. E. & COTTA-RAMUSINO, C. 2017. Characterization of the interplay between DNA repair and CRISPR/Cas9-induced DNA lesions at an endogenous locus. *Nat Commun,* 8**,** 13905.
BROIDA, J. & SVARE, B. 1984. Sex differences in the activity of mice: modulation by postnatal gonadal hormones. *Horm Behav,* 18**,** 65-78.
BROWN, L. A., HASAN, S., FOSTER, R. G. & PEIRSON, S. N. 2016. COMPASS: Continuous Open Mouse Phenotyping of Activity and Sleep Status. *Wellcome Open Res,* 1.
BUGGE, A., FENG, D., EVERETT, L. J., BRIGGS, E. R., MULLICAN, S. E., WANG, F., JAGER, J. & LAZAR, M. A. 2012. Rev-erbα and Rev-erbβ coordinately protect the circadian clock and normal metabolic function. *Genes Dev,* 26**,** 657-67.
BUIJS, R. M., SCHEER, F. A., KREIER, F., YI, C., BOS, N., GONCHARUK, V. D. & KALSBEEK, A. 2006. Organization of circadian functions: interaction with the body. *Prog Brain Res,* 153**,** 341-60.
BUNGER, M. K., WILSBACHER, L. D., MORAN, S. M., CLENDENIN, C., RADCLIFFE, L. A., HOGENESCH, J. B., SIMON, M. C., TAKAHASHI, J. S. & BRADFIELD, C. A. 2000. Mop3 is an essential component of the master circadian pacemaker in mammals. *Cell,* 103**,** 1009-1017.
BURDAKOV, D., GERASIMENKO, O. & VERKHRATSKY, A. 2005. Physiological changes in glucose differentially modulate the excitability of hypothalamic melanin-concentrating hormone and orexin neurons in situ. *J Neurosci,* 25**,** 2429-33.
CAI, W., RAMBAUD, J., TEBOUL, M., MASSE, I., BENOIT, G., GUSTAFSSON, J. A., DELAUNAY, F., LAUDET, V. & PONGRATZ, I. 2008. Expression levels of estrogen receptor beta are modulated by components of the molecular clock. *Mol Cell Biol,* 28**,** 784-93.
CARLBERG, C. 2000. Gene regulation by melatonin. *Ann N Y Acad Sci,* 917**,** 387-96.

CARNEIRO, B. T. & ARAUJO, J. F. 2009. The food-entrainable oscillator: a network of interconnected brain structures entrained by humoral signals? *Chronobiol Int,* 26**,** 1273-89.
CHAUDHURY, D. & COLWELL, C. S. 2002. Circadian modulation of learning and memory in fear-conditioned mice. *Behavioural Brain Research,* 133**,** 95-108.
CHAVAN, R., FEILLET, C., COSTA, S. S., DELORME, J. E., OKABE, T., RIPPERGER, J. A. & ALBRECHT, U. 2016. Liver-derived ketone bodies are necessary for food anticipation. *Nat Commun,* 7**,** 10580.
CHEN, D., ZHANG, T. & LEE, T. H. 2020. Cellular Mechanisms of Melatonin: Insight from Neurodegenerative Diseases. *Biomolecules,* 10.
CHEN, H., LIN, R. J., SCHILTZ, R. L., CHAKRAVARTI, D., NASH, A., NAGY, L., PRIVALSKY, M. L., NAKATANI, Y. & EVANS, R. M. 1997. Nuclear receptor coactivator ACTR is a novel histone acetyltransferase and forms a multimeric activation complex with P/CAF and CBP/p300. *Cell,* 90**,** 569-80.
CHIANG, T. W., LE SAGE, C., LARRIEU, D., DEMIR, M. & JACKSON, S. P. 2016. CRISPR-Cas9(D10A) nickase-based genotypic and phenotypic screening to enhance genome editing. *Sci Rep,* 6**,** 24356.
CHO, K., ENNACEUR, A., COLE, J. C. & SUH, C. K. 2000. Chronic jet lag produces cognitive deficits. *J Neurosci,* 20**,** RC66.
CHUN, L. E., WOODRUFF, E. R., MORTON, S., HINDS, L. R. & SPENCER, R. L. 2015. Variations in Phase and Amplitude of Rhythmic Clock Gene Expression across Prefrontal Cortex, Hippocampus, Amygdala, and Hypothalamic Paraventricular and Suprachiasmatic Nuclei of Male and Female Rats. *J Biol Rhythms,* 30**,** 417-36.
CONSORTIUM, T. U. 2019. UniProt: a worldwide hub of protein knowledge. *Nucleic Acids Res,* 47**,** D506-d515.
COPPARI, R., ICHINOSE, M., LEE, C. E., PULLEN, A. E., KENNY, C. D., MCGOVERN, R. A., TANG, V., LIU, S. M., LUDWIG, T., CHUA, S. C., JR., LOWELL, B. B. & ELMQUIST, J. K. 2005. The hypothalamic arcuate nucleus: a key site for mediating leptin's effects on glucose homeostasis and locomotor activity. *Cell Metab,* 1**,** 63-72.
COX, C. 2012. *The Circadian Clock and The Cell Cycle.* Cell and Developmental Biology, UCL.
CROSBY, P., HAMNETT, R., PUTKER, M., HOYLE, N. P., REED, M., KARAM, C. J., MAYWOOD, E. S., STANGHERLIN, A., CHESHAM, J. E., HAYTER, E. A., ROSENBRIER-RIBEIRO, L., NEWHAM, P., CLEVERS, H., BECHTOLD, D. A. & O'NEILL, J. S. 2019. Insulin/IGF-1 Drives PERIOD Synthesis to Entrain Circadian Rhythms with Feeding Time. *Cell,* 177**,** 896-909.e20.
CUNNINGHAM, F., ACHUTHAN, P., AKANNI, W., ALLEN, J., AMODE, M R., ARMEAN, I. M., BENNETT, R., BHAI, J., BILLIS, K., BODDU, S., CUMMINS, C., DAVIDSON, C., DODIYA, K. J., GALL, A., GIRÓN, C. G., GIL, L., GREGO, T., HAGGERTY, L., HASKELL, E., HOURLIER, T., IZUOGU, O. G., JANACEK, S. H., JUETTEMANN, T., KAY, M., LAIRD, M. R., LAVIDAS, I., LIU, Z., LOVELAND, JANE E., MARUGÁN, J. C., MAUREL, T., MCMAHON, A. C., MOORE, B., MORALES, J., MUDGE, J. M., NUHN, M., OGEH, D., PARKER, A., PARTON, A., PATRICIO, M., ABDUL SALAM, A. I., SCHMITT, B. M., SCHUILENBURG, H., SHEPPARD, D., SPARROW, H., STAPLETON, E., SZUBA, M., TAYLOR, K., THREADGOLD, G., THORMANN, A., VULLO, A., WALTS, B., WINTERBOTTOM, A., ZADISSA, A., CHAKIACHVILI, M., FRANKISH, A., HUNT, S. E., KOSTADIMA, M., LANGRIDGE, N., MARTIN, F. J., MUFFATO, M., PERRY, E., RUFFIER, M., STAINES, D. M., TREVANION, S. J., AKEN, B. L., YATES, A. D., ZERBINO, D. R. & FLICEK, P. 2019. Ensembl 2019. *Nucleic Acids*

Research, 47**,** D745-D751.
CURTIS, A. M., SEO, S. B., WESTGATE, E. J., RUDIC, R. D., SMYTH, E. M., CHAKRAVARTI, D., FITZGERALD, G. A. & MCNAMARA, P. 2004. Histone acetyltransferase-dependent chromatin remodeling and the vascular clock. *J Biol Chem,* 279**,** 7091-7.
DA MOTTA, L. L., LEDAKI, I., PURSHOUSE, K., HAIDER, S., DE BASTIANI, M. A., BABAN, D., MOROTTI, M., STEERS, G., WIGFIELD, S., BRIDGES, E., LI, J. L., KNAPP, S., EBNER, D., KLAMT, F., HARRIS, A. L. & MCINTYRE, A. 2017. The BET inhibitor JQ1 selectively impairs tumour response to hypoxia and downregulates CA9 and angiogenesis in triple negative breast cancer. *Oncogene,* 36**,** 122-132.
DAMIOLA, F., LE MINH, N., PREITNER, N., KORNMANN, B., FLEURY-OLELA, F. & SCHIBLER, U. 2000. Restricted feeding uncouples circadian oscillators in peripheral tissues from the central pacemaker in the suprachiasmatic nucleus. *Genes Dev,* 14**,** 2950-61.
DEBRUYNE, J. P. 2008. Oscillating perceptions: the ups and downs of the CLOCK protein in the mouse circadian system. *Journal of genetics,* 87**,** 437-446.
DEBRUYNE, J. P., NOTON, E., LAMBERT, C. M., MAYWOOD, E. S., WEAVER, D. R. & REPPERT, S. M. 2006. A clock shock: mouse CLOCK is not required for circadian oscillator function. *Neuron,* 50**,** 465-77.
DEBRUYNE, J. P., WEAVER, D. R. & REPPERT, S. M. 2007a. CLOCK and NPAS2 have overlapping roles in the suprachiasmatic circadian clock. *Nat Neurosci,* 10**,** 543-545.
DEBRUYNE, J. P., WEAVER, D. R. & REPPERT, S. M. 2007b. Peripheral circadian oscillators require CLOCK. *Current Biology,* 17**,** R538-R539.
DÍAZ-MUÑOZ, M., VÁZQUEZ-MARTÍNEZ, O., AGUILAR-ROBLERO, R. & ESCOBAR, C. 2000. Anticipatory changes in liver metabolism and entrainment of insulin, glucagon, and corticosterone in food-restricted rats. *Am J Physiol Regul Integr Comp Physiol,* 279**,** R2048-56.
DIAZ, E., MEDELLÍN, J., SÁNCHEZ, N., VARGAS, J. P. & LÓPEZ, J. C. 2015. Involvement of D1 and D2 dopamine receptor in the retrieval processes in latent inhibition. *Psychopharmacology (Berl),* 232**,** 4337-46.
DIENES, Z. 2014. Using Bayes to get the most out of non-significant results. *Frontiers in Psychology,* 5.
DIOUM, E. M., RUTTER, J., TUCKERMAN, J. R., GONZALEZ, G., GILLES-GONZALEZ, M.-A. & MCKNIGHT, S. L. 2002. NPAS2: A Gas-Responsive Transcription Factor. *Science,* 298**,** 2385-2387.
DOI, M., HIRAYAMA, J. & SASSONE-CORSI, P. 2006. Circadian regulator CLOCK is a histone acetyltransferase. *Cell,* 125**,** 497-508.
DUDLEY, C. A., ERBEL-SIELER, C., ESTILL, S. J., REICK, M., FRANKEN, P., PITTS, S. & MCKNIGHT, S. L. 2003. Altered Patterns of Sleep and Behavioral Adaptability in NPAS2-Deficient Mice. *Science,* 301**,** 379-383.
DUONG, H. A., ROBLES, M. S., KNUTTI, D. & WEITZ, C. J. 2011. A molecular mechanism for circadian clock negative feedback. *Science,* 332**,** 1436-9.
EAGON, P. K., DILEO, A., POLIMENO, L., FRANCAVILLA, A., VAN THIEL, D. H., GUGLIELMI, F. & STARZL, T. E. 1986. Circadian rhythm of hepatic cytosolic and nuclear estrogen receptors. *Chronobiology international,* 3**,** 207-211.
EL-BROLOSY, M. A. & STAINIER, D. Y. R. 2017. Genetic compensation: A phenomenon in search of mechanisms. *PLoS Genet,* 13**,** e1006780.
ERALY, S. A. 2014. Striking differences between knockout and wild-type mice in global gene expression variability. *PloS one,* 9**,** e97734-e97734.
ERREN, T. C., PAPE, H. G., REITER, R. J. & PIEKARSKI, C. 2008. Chronodisruption and

cancer. *Naturwissenschaften,* 95**,** 367-82.
ETCHEGARAY, J. P., LEE, C., WADE, P. A. & REPPERT, S. M. 2003. Rhythmic histone acetylation underlies transcription in the mammalian circadian clock. *Nature,* 421**,** 177-82.
FADOK, J. P., DICKERSON, T. M. K. & PALMITER, R. D. 2009. Dopamine is necessary for cue-dependent fear conditioning. *The Journal of neuroscience : the official journal of the Society for Neuroscience,* 29**,** 11089-11097.
FANG, M., GUO, W. R., PARK, Y., KANG, H. G. & ZARBL, H. 2015. Enhancement of NAD^+-dependent SIRT1 deacetylase activity by methylselenocysteine resets the circadian clock in carcinogen-treated mammary epithelial cells. *Oncotarget,* 6**,** 42879-91.
FANG, M., KANG, H. G., PARK, Y., ESTRELLA, B. & ZARBL, H. 2017. In Vitro Bioluminescence Assay to Characterize Circadian Rhythm in Mammary Epithelial Cells. *J Vis Exp*.
FARSHADI, E., VAN DER HORST, G. T. J. & CHAVES, I. 2020. Molecular Links between the Circadian Clock and the Cell Cycle. *Journal of Molecular Biology,* 432**,** 3515-3524.
FENG, D., LIU, T., SUN, Z., BUGGE, A., MULLICAN, S. E., ALENGHAT, T., LIU, X. S. & LAZAR, M. A. 2011. A circadian rhythm orchestrated by histone deacetylase 3 controls hepatic lipid metabolism. *Science,* 331**,** 1315-9.
FERRELL, J. M. & CHIANG, J. Y. 2015. Circadian rhythms in liver metabolism and disease. *Acta Pharm Sin B,* 5**,** 113-22.
FISHER, S. P., GODINHO, S. I., POTHECARY, C. A., HANKINS, M. W., FOSTER, R. G. & PEIRSON, S. N. 2012. Rapid assessment of sleep-wake behavior in mice. *J Biol Rhythms,* 27**,** 48-58.
GARCIA, J. A., ZHANG, D., ESTILL, S. J., MICHNOFF, C., RUTTER, J., REICK, M., SCOTT, K., DIAZ-ARRASTIA, R. & MCKNIGHT, S. L. 2000. Impaired Cued and Contextual Memory in NPAS2-Deficient Mice. *Science,* 288**,** 2226-2230.
GEKAKIS, N., STAKNIS, D., NGUYEN, H. B., DAVIS, F. C., WILSBACHER, L. D., KING, D. P., TAKAHASHI, J. S. & WEITZ, C. J. 1998. Role of the CLOCK protein in the mammalian circadian mechanism. *Science,* 280**,** 1564-9.
GERSTNER, J. R., LYONS, L. C., WRIGHT, K. P., LOH, D. H., RAWASHDEH, O., ECKEL-MAHAN, K. L. & ROMAN, G. W. 2009. Cycling Behavior and Memory Formation. *The Journal of neuroscience : the official journal of the Society for Neuroscience,* 29**,** 12824-12830.
GOEL, N., BASNER, M., RAO, H. & DINGES, D. F. 2013. Circadian rhythms, sleep deprivation, and human performance. *Prog Mol Biol Transl Sci,* 119**,** 155-90.
HANAHAN, D. 1983. Studies on transformation of Escherichia coli with plasmids. *Journal of Molecular Biology,* 166**,** 557-580.
HAQUE, F. N., LIPINA, T. V., RODER, J. C. & WONG, A. H. C. 2012. Social defeat interacts with Disc1 mutations in the mouse to affect behavior. *Behavioural Brain Research,* 233**,** 337-344.
HARA, R., WAN, K., WAKAMATSU, H., AIDA, R., MORIYA, T., AKIYAMA, M. & SHIBATA, S. 2001. Restricted feeding entrains liver clock without participation of the suprachiasmatic nucleus. *Genes Cells,* 6**,** 269-78.
HARDIN, J. W. 2005. Generalized Estimating Equations (GEE). *Encyclopedia of Statistics in Behavioral Science.*
HATCHER, K. M., ROYSTON, S. E. & MAHONEY, M. M. 2020. Modulation of circadian rhythms through estrogen receptor signaling. *Eur J Neurosci,* 51**,** 217-228.
HERMANSSON, J., GILLANDER GÅDIN, K., KARLSSON, B., LINDAHL, B., STEGMAYR, B. & KNUTSSON, A. 2007. Ischemic stroke and shift work. *Scand J*

Work Environ Health, 33**,** 435-9.
HIRAYAMA, J., SAHAR, S., GRIMALDI, B., TAMARU, T., TAKAMATSU, K., NAKAHATA, Y. & SASSONE-CORSI, P. 2007. CLOCK-mediated acetylation of BMAL1 controls circadian function. *Nature,* 450**,** 1086-90.
HOFFMANN, H. J. & BALSCHUN, D. 1992. Circadian differences in maze performance of C57BI/6 Ola mice. *Behavioural Processes,* 27**,** 77-83.
HOGENESCH, J. B., GU, Y. Z., JAIN, S. & BRADFIELD, C. A. 1998. The basic-helix-loop-helix-PAS orphan MOP3 forms transcriptionally active complexes with circadian and hypoxia factors. *Proc Natl Acad Sci U S A,* 95**,** 5474-9.
HSU, P. D., SCOTT, D. A., WEINSTEIN, J. A., RAN, F. A., KONERMANN, S., AGARWALA, V., LI, Y., FINE, E. J., WU, X., SHALEM, O., CRADICK, T. J., MARRAFFINI, L. A., BAO, G. & ZHANG, F. 2013. DNA targeting specificity of RNA-guided Cas9 nucleases. *Nat Biotechnol,* 31**,** 827-32.
HUGHES, M. E., DITACCHIO, L., HAYES, K. R., VOLLMERS, C., PULIVARTHY, S., BAGGS, J. E., PANDA, S. & HOGENESCH, J. B. 2009. Harmonics of circadian gene transcription in mammals. *PLoS Genet,* 5**,** e1000442.
IIJIMA, O., FUKANO, H., TAKAHASHI, H., SHIRAI, M. & SUZUKI, Y. 2006. A purine at +2 rather than +1 adjacent to the human U6 promoter is required to prepare effective short hairpin RNAs. *Biochem Biophys Res Commun,* 350**,** 809-17.
IKEDA, R., TSUCHIYA, Y., KOIKE, N., UMEMURA, Y., INOKAWA, H., ONO, R., INOUE, M., SASAWAKI, Y., GRIETEN, T., OKUBO, N., IKOMA, K., FUJIWARA, H., KUBO, T. & YAGITA, K. 2019. REV-ERBα and REV-ERBβ function as key factors regulating Mammalian Circadian Output. *Scientific Reports,* 9**,** 10171.
IKEGAMI, M., UEMURA, T., KISHIOKA, A., SAKIMURA, K. & MISHINA, M. 2014. Striatal dopamine D1 receptor is essential for contextual fear conditioning. *Sci Rep,* 4**,** 3976.
IZUMO, M., PEJCHAL, M., SCHOOK, A. C., LANGE, R. P., WALISSER, J. A., SATO, T. R., WANG, X., BRADFIELD, C. A. & TAKAHASHI, J. S. 2014. Differential effects of light and feeding on circadian organization of peripheral clocks in a forebrain Bmal1 mutant. *Elife,* 3.
JAMES, S. M., HONN, K. A., GADDAMEEDHI, S. & VAN DONGEN, H. P. A. 2017. Shift Work: Disrupted Circadian Rhythms and Sleep-Implications for Health and Well-Being. *Curr Sleep Med Rep,* 3**,** 104-112.
JANKOWSKY, J. L., FADALE, D. J., ANDERSON, J., XU, G. M., GONZALES, V., JENKINS, N. A., COPELAND, N. G., LEE, M. K., YOUNKIN, L. H., WAGNER, S. L., YOUNKIN, S. G. & BORCHELT, D. R. 2004. Mutant presenilins specifically elevate the levels of the 42 residue beta-amyloid peptide in vivo: evidence for augmentation of a 42-specific gamma secretase. *Hum Mol Genet,* 13**,** 159-70.
JIN, X., SHEARMAN, L. P., WEAVER, D. R., ZYLKA, M. J., DE VRIES, G. J. & REPPERT, S. M. 1999. A molecular mechanism regulating rhythmic output from the suprachiasmatic circadian clock. *Cell,* 96**,** 57-68.
JOHANSSON, C., WILLEIT, M., SMEDH, C., EKHOLM, J., PAUNIO, T., KIESEPPA, T., LICHTERMANN, D., PRASCHAK-RIEDER, N., NEUMEISTER, A., NILSSON, L. G., KASPER, S., PELTONEN, L., ADOLFSSON, R., SCHALLING, M. & PARTONEN, T. 2003. Circadian clock-related polymorphisms in seasonal affective disorder and their relevance to diurnal preference. *Neuropsychopharmacology,* 28**,** 734-9.
JUD, C., SCHMUTZ, I., HAMPP, G., OSTER, H. & ALBRECHT, U. 2005. A guideline for analyzing circadian wheel-running behavior in rodents under different lighting conditions. *Biological procedures online,* 7**,** 101-116.

KALMBACH, D. A., PILLAI, V., CHENG, P., ARNEDT, J. T. & DRAKE, C. L. 2015. Shift work disorder, depression, and anxiety in the transition to rotating shifts: the role of sleep reactivity. *Sleep Med,* 16**,** 1532-8.

KANG, J. E., LIM, M. M., BATEMAN, R. J., LEE, J. J., SMYTH, L. P., CIRRITO, J. R., FUJIKI, N., NISHINO, S. & HOLTZMAN, D. M. 2009. Amyloid-beta dynamics are regulated by orexin and the sleep-wake cycle. *Science,* 326**,** 1005-7.

KARCZEWSKI, K. J., FRANCIOLI, L. C., TIAO, G., CUMMINGS, B. B., ALFÖLDI, J., WANG, Q., COLLINS, R. L., LARICCHIA, K. M., GANNA, A., BIRNBAUM, D. P., GAUTHIER, L. D., BRAND, H., SOLOMONSON, M., WATTS, N. A., RHODES, D., SINGER-BERK, M., ENGLAND, E. M., SEABY, E. G., KOSMICKI, J. A., WALTERS, R. K., TASHMAN, K., FARJOUN, Y., BANKS, E., POTERBA, T., WANG, A., SEED, C., WHIFFIN, N., CHONG, J. X., SAMOCHA, K. E., PIERCE-HOFFMAN, E., ZAPPALA, Z., O'DONNELL-LURIA, A. H., MINIKEL, E. V., WEISBURD, B., LEK, M., WARE, J. S., VITTAL, C., ARMEAN, I. M., BERGELSON, L., CIBULSKIS, K., CONNOLLY, K. M., COVARRUBIAS, M., DONNELLY, S., FERRIERA, S., GABRIEL, S., GENTRY, J., GUPTA, N., JEANDET, T., KAPLAN, D., LLANWARNE, C., MUNSHI, R., NOVOD, S., PETRILLO, N., ROAZEN, D., RUANO-RUBIO, V., SALTZMAN, A., SCHLEICHER, M., SOTO, J., TIBBETTS, K., TOLONEN, C., WADE, G., TALKOWSKI, M. E., NEALE, B. M., DALY, M. J. & MACARTHUR, D. G. 2020. The mutational constraint spectrum quantified from variation in 141,456 humans. *Nature,* 581**,** 434-443.

KEISER, A. A., TURNBULL, L. M., DARIAN, M. A., FELDMAN, D. E., SONG, I. & TRONSON, N. C. 2017. Sex Differences in Context Fear Generalization and Recruitment of Hippocampus and Amygdala during Retrieval. *Neuropsychopharmacology : official publication of the American College of Neuropsychopharmacology,* 42**,** 397-407.

KENNAWAY, D. J., OWENS, J. A., VOULTSIOS, A. & VARCOE, T. J. 2006. Functional central rhythmicity and light entrainment, but not liver and muscle rhythmicity, are Clock independent. *Am J Physiol Regul Integr Comp Physiol,* 291**,** R1172-80.

KIM, H., KIM, M., IM, S.-K. & FANG, S. 2018a. Mouse Cre-LoxP system: general principles to determine tissue-specific roles of target genes. *Laboratory animal research,* 34**,** 147-159.

KIM, J. & FANSELOW, M. 1992. Modality-specific retrograde amnesia of fear. *Science,* 256**,** 675-677.

KIM, Y. H., MARHON, S. A., ZHANG, Y., STEGER, D. J., WON, K.-J. & LAZAR, M. A. 2018b. Rev-erbα dynamically modulates chromatin looping to control circadian gene transcription. *Science*.

KING, D. P., ZHAO, Y., SANGORAM, A. M., WILSBACHER, L. D., TANAKA, M., ANTOCH, M. P., STEEVES, T. D. L., VITATERNA, M. H., KORNHAUSER, J. M., LOWREY, P. L., TUREK, F. W. & TAKAHASHI, J. S. 1997. Positional Cloning of the Mouse Circadian Clock Gene. *Cell,* 89**,** 641-653.

KNUTSSON, A. & KEMPE, A. 2014. Shift work and diabetes--a systematic review. *Chronobiol Int,* 31**,** 1146-51.

KOIKE, N., YOO, S. H., HUANG, H. C., KUMAR, V., LEE, C., KIM, T. K. & TAKAHASHI, J. S. 2012. Transcriptional Architecture and Chromatin Landscape of the Core Circadian Clock in Mammals. *Science,* 338**,** 349-54.

KONDRATOVA, A. A., DUBROVSKY, Y. V., ANTOCH, M. P. & KONDRATOV, R. V. 2010. Circadian clock proteins control adaptation to novel environment and memory formation. *Aging (Albany NY),* 2**,** 285-97.

KONOPKA, R. J. & BENZER, S. 1971. Clock mutants of Drosophila melanogaster. *Proc Natl Acad Sci U S A,* 68**,** 2112-6.
KORF, H. W., VON GALL, C. & STEHLE, J. 2003. The circadian system and melatonin: lessons from rats and mice. *Chronobiol Int,* 20**,** 697-710.
KORNMANN, B., SCHAAD, O., BUJARD, H., TAKAHASHI, J. S. & SCHIBLER, U. 2007. System-Driven and Oscillator-Dependent Circadian Transcription in Mice with a Conditionally Active Liver Clock. *PLOS Biology,* 5**,** e34.
KORONOWSKI, K. B., KINOUCHI, K., WELZ, P. S., SMITH, J. G., ZINNA, V. M., SHI, J., SAMAD, M., CHEN, S., MAGNAN, C. N., KINCHEN, J. M., LI, W., BALDI, P., BENITAH, S. A. & SASSONE-CORSI, P. 2019. Defining the Independence of the Liver Circadian Clock. *Cell,* 177**,** 1448-1462.e14.
KRIEBS, A., JORDAN, S. D., SOTO, E., HENRIKSSON, E., SANDATE, C. R., VAUGHAN, M. E., CHAN, A. B., DUGLAN, D., PAPP, S. J., HUBER, A. L., AFETIAN, M. E., YU, R. T., ZHAO, X., DOWNES, M., EVANS, R. M. & LAMIA, K. A. 2017. Circadian repressors CRY1 and CRY2 broadly interact with nuclear receptors and modulate transcriptional activity. *Proc Natl Acad Sci U S A,* 114**,** 8776-8781.
KRIEGER, D. T., HAUSER, H. & KREY, L. C. 1977. Suprachiasmatic nuclear lesions do not abolish food-shifted circadian adrenal and temperature rhythmicity. *Science,* 197**,** 398-9.
KRISHNAN, H. C. & LYONS, L. C. 2015. Synchrony and desynchrony in circadian clocks: impacts on learning and memory. *Learning & memory (Cold Spring Harbor, N.Y.),* 22**,** 426-437.
KRIZO, J. A. & MINTZ, E. M. 2014. Sex differences in behavioral circadian rhythms in laboratory rodents. *Front Endocrinol (Lausanne),* 5**,** 234.
KULJIS, D. A., LOH, D. H., TRUONG, D., VOSKO, A. M., ONG, M. L., MCCLUSKY, R., ARNOLD, A. P. & COLWELL, C. S. 2013. Gonadal- and sex-chromosome-dependent sex differences in the circadian system. *Endocrinology,* 154**,** 1501-12.
KUME, K., ZYLKA, M. J., SRIRAM, S., SHEARMAN, L. P., WEAVER, D. R., JIN, X., MAYWOOD, E. S., HASTINGS, M. H. & REPPERT, S. M. 1999. mCRY1 and mCRY2 are essential components of the negative limb of the circadian clock feedback loop. *Cell,* 98**,** 193-205.
LABUN, K., MONTAGUE, T. G., KRAUSE, M., TORRES CLEUREN, Y. N., TJELDNES, H. & VALEN, E. 2019. CHOPCHOP v3: expanding the CRISPR web toolbox beyond genome editing. *Nucleic Acids Res,* 47**,** W171-4.
LAKENS, D. 2013. Calculating and reporting effect sizes to facilitate cumulative science: a practical primer for t-tests and ANOVAs. *Frontiers in psychology,* 4**,** 863-863.
LAMIA, K. A., PAPP, S. J., YU, R. T., BARISH, G. D., UHLENHAUT, N. H., JONKER, J. W., DOWNES, M. & EVANS, R. M. 2011. Cryptochromes mediate rhythmic repression of the glucocorticoid receptor. *Nature,* 480**,** 552-6.
LAMIA, K. A., SACHDEVA, U. M., DITACCHIO, L., WILLIAMS, E. C., ALVAREZ, J. G., EGAN, D. F., VASQUEZ, D. S., JUGUILON, H., PANDA, S., SHAW, R. J., THOMPSON, C. B. & EVANS, R. M. 2009. AMPK regulates the circadian clock by cryptochrome phosphorylation and degradation. *Science,* 326**,** 437-40.
LAMIA, K. A., STORCH, K.-F. & WEITZ, C. J. 2008. Physiological significance of a peripheral tissue circadian clock. *Proceedings of the National Academy of Sciences,* 105**,** 15172-15177.
LANDGRAF, D., WANG, L. L., DIEMER, T. & WELSH, D. K. 2016. NPAS2 Compensates for Loss of CLOCK in Peripheral Circadian Oscillators. *PLoS Genetics,* 12**,** e1005882.
LECLERC, G. M., BOOCKFOR, F. R., FAUGHT, W. J. & FRAWLEY, L. S. 2000. Development of a Destabilized Firefly Luciferase Enzyme for Measurement of Gene

Expression. *BioTechniques,* 29**,** 590-601.
LEE, C., ETCHEGARAY, J.-P., CAGAMPANG, F. R. A., LOUDON, A. S. I. & REPPERT, S. M. 2001. Posttranslational Mechanisms Regulate the Mammalian Circadian Clock. *Cell,* 107**,** 855-867.
LEE, S. M., ZHANG, Y., TSUCHIYA, H., SMALLING, R., JETTEN, A. M. & WANG, L. 2015. Shp/Npas2 Axis in Regulating the Oscillation of Liver Lipid Metabolism. *Hepatology (Baltimore, Md.),* 61**,** 497-505.
LEGATES, T. A. & ALTIMUS, C. M. 2011. Measuring circadian and acute light responses in mice using wheel running activity. *Journal of visualized experiments : JoVE***,** 2463.
LEIBIGER, C., KOSYAKOVA, N., MKRTCHYAN, H., GLEI, M., TRIFONOV, V. & LIEHR, T. 2013. First Molecular Cytogenetic High Resolution Characterization of the NIH 3T3 Cell Line by Murine Multicolor Banding. *Journal of Histochemistry and Cytochemistry,* 61**,** 306-312.
LESAUTER, J., HOQUE, N., WEINTRAUB, M., PFAFF, D. W. & SILVER, R. 2009. Stomach ghrelin-secreting cells as food-entrainable circadian clocks. *Proceedings of the National Academy of Sciences,* 106**,** 13582-13587.
LI, S. & ZHANG, L. 2015. Circadian Control of Global Transcription. *BioMed research international,* 2015**,** 187809-187809.
LI, Z., WANG, Y., SUN, K. K., WANG, K., SUN, Z. S., ZHAO, M. & WANG, J. 2015. Sex-related difference in food-anticipatory activity of mice. *Hormones and Behavior,* 70**,** 38-46.
LIN, Y.-C., BOONE, M., MEURIS, L., LEMMENS, I., VAN ROY, N., SOETE, A., REUMERS, J., MOISSE, M., PLAISANCE, S., DRMANAC, R., CHEN, J., SPELEMAN, F., LAMBRECHTS, D., VAN DE PEER, Y., TAVERNIER, J. & CALLEWAERT, N. 2014. Genome dynamics of the human embryonic kidney 293 lineage in response to cell biology manipulations. *Nature Communications,* 5**,** 4767.
LIN, Y., WANG, S., ZHOU, Z., GUO, L., YU, F. & WU, B. 2019. Bmal1 regulates circadian expression of cytochrome P450 3a11 and drug metabolism in mice. *Communications Biology,* 2**,** 378.
LIPINA, T. V., RASQUINHA, R. & RODER, J. C. 2011. Parametric and pharmacological modulations of latent inhibition in mouse inbred strains. *Pharmacol Biochem Behav,* 100**,** 244-52.
LU, Y. F., JIN, T., XU, Y., ZHANG, D., WU, Q., ZHANG, Y. K. & LIU, J. 2013. Sex differences in the circadian variation of cytochrome p450 genes and corresponding nuclear receptors in mouse liver. *Chronobiol Int,* 30**,** 1135-43.
LUBOW, R. E. 2005. Construct validity of the animal latent inhibition model of selective attention deficits in schizophrenia. *Schizophr Bull,* 31**,** 139-53.
MA, Z., JIANG, W. & ZHANG, E. E. 2016. Orexin signaling regulates both the hippocampal clock and the circadian oscillation of Alzheimer's disease-risk genes. *Sci Rep,* 6**,** 36035.
MADEIRA, F., PARK, Y. M., LEE, J., BUSO, N., GUR, T., MADHUSOODANAN, N., BASUTKAR, P., TIVEY, A. R. N., POTTER, S. C., FINN, R. D. & LOPEZ, R. 2019. The EMBL-EBI search and sequence analysis tools APIs in 2019. *Nucleic Acids Research,* 47**,** W636-W641.
MANRIQUE, T., MOLERO, A., BALLESTEROS, M. A., MORON, I., GALLO, M. & FENTON, A. A. 2004. Time of day-dependent latent inhibition of conditioned taste aversions in rats. *Neurobiol Learn Mem,* 82**,** 77-80.
MAREN, S., AHARONOV, G. & FANSELOW, M. S. 1997. Neurotoxic lesions of the dorsal hippocampus and Pavlovian fear conditioning in rats. *Behav Brain Res,* 88**,** 261-74.
MARQUIE, J. C., TUCKER, P., FOLKARD, S., GENTIL, C. & ANSIAU, D. 2015. Chronic effects of shift work on cognition: findings from the VISAT longitudinal study. *Occup*

Environ Med, 72**,** 258-64.
MARSCHNER, A., KALISCH, R., VERVLIET, B., VANSTEENWEGEN, D. & BÜCHEL, C. 2008. Dissociable Roles for the Hippocampus and the Amygdala in Human Cued versus Context Fear Conditioning. *The Journal of Neuroscience,* 28**,** 9030-9036.
MASRI, S., PATEL, V. R., ECKEL-MAHAN, K. L., PELEG, S., FORNE, I., LADURNER, A. G., BALDI, P., IMHOF, A. & SASSONE-CORSI, P. 2013. Circadian acetylome reveals regulation of mitochondrial metabolic pathways. *Proceedings of the National Academy of Sciences of the United States of America,* 110**,** 3339-3344.
MATSUMURA, R., OKAMOTO, A., NODE, K. & AKASHI, M. 2014. Compensation for intracellular environment in expression levels of mammalian circadian clock genes. *Scientific reports,* 4**,** 4032-4032.
MCDEARMON, E. L., PATEL, K. N., KO, C. H., WALISSER, J. A., SCHOOK, A. C., CHONG, J. L., WILSBACHER, L. D., SONG, E. J., HONG, H. K., BRADFIELD, C. A. & TAKAHASHI, J. S. 2006. Dissecting the functions of the mammalian clock protein BMAL1 by tissue-specific rescue in mice. *Science,* 314**,** 1304-8.
MEIJMAN, T., VAN DER MEER, O. & VAN DORMOLEN, M. 1993. The after-effects of night work on short-term memory performance. *Ergonomics,* 36**,** 37-42.
MENGER, G. J., ALLEN, G. C., NEUENDORFF, N., NAHM, S.-S., THOMAS, T. L., CASSONE, V. M. & EARNEST, D. J. 2007. Circadian profiling of the transcriptome in NIH/3T3 fibroblasts: comparison with rhythmic gene expression in SCN2.2 cells and the rat SCN. *Physiological Genomics,* 29**,** 280-289.
MISTLBERGER, R. E. 1994. Circadian food-anticipatory activity: Formal models and physiological mechanisms. *Neuroscience & Biobehavioral Reviews,* 18**,** 171-195.
MISTLBERGER, R. E. 2005. Circadian regulation of sleep in mammals: role of the suprachiasmatic nucleus. *Brain Res Brain Res Rev,* 49**,** 429-54.
MISTLBERGER, R. E. 2020. Food as circadian time cue for appetitive behavior. *F1000Research,* 9**,** F1000 Faculty Rev-61.
MOORE, R. Y. & EICHLER, V. B. 1972. Loss of a circadian adrenal corticosterone rhythm following suprachiasmatic lesions in the rat. *Brain Research,* 42**,** 201-206.
MORIN, L. P. & STUDHOLME, K. M. 2014. Light Pulse Duration Differentially Regulates Mouse Locomotor Suppression and Phase Shifts. *Journal of Biological Rhythms,* 29**,** 346-354.
MURAYAMA, Y., YAHAGI, N., TAKEUCHI, Y., AITA, Y., MEHRAZAD SABER, Z., WADA, N., LI, E., PIAO, X., SAWADA, Y., SHIKAMA, A., MASUDA, Y., NISHI-TATSUMI, M., KUBOTA, M., IZUMIDA, Y., MIYAMOTO, T., SEKIYA, M., MATSUZAKA, T., NAKAGAWA, Y., SUGANO, Y., IWASAKI, H., KOBAYASHI, K., YATOH, S., SUZUKI, H., YAGYU, H., KAWAKAMI, Y. & SHIMANO, H. 2019. Glucocorticoid receptor suppresses gene expression of Rev-erbα (Nr1d1) through interaction with the CLOCK complex. *FEBS Lett,* 593**,** 423-432.
NAGOSHI, E., BROWN, S. A., DIBNER, C., KORNMANN, B. & SCHIBLER, U. 2005. Circadian gene expression in cultured cells. *Methods Enzymol,* 393**,** 543-57.
NAGOSHI, E., SAINI, C., BAUER, C., LAROCHE, T., NAEF, F. & SCHIBLER, U. 2004. Circadian gene expression in individual fibroblasts: cell-autonomous and self-sustained oscillators pass time to daughter cells. *Cell,* 119**,** 693-705.
NAKAHATA, Y., KALUZOVA, M., GRIMALDI, B., SAHAR, S., HIRAYAMA, J., CHEN, D., GUARENTE, L. P. & SASSONE-CORSI, P. 2008. The NAD+-dependent deacetylase SIRT1 modulates CLOCK-mediated chromatin remodeling and circadian control. *Cell,* 134**,** 329-40.
NELSON, A. J. D., THUR, K. E., MARSDEN, C. A. & CASSADAY, H. J. 2011. Dopamine in nucleus accumbens: salience modulation in latent inhibition and overshadowing.

Journal of psychopharmacology (Oxford, England), 25**,** 1649-1660.
O'CALLAGHAN, M. J., BAY-RICHTER, C., O'TUATHAIGH, C. M., HEERY, D. M., WADDINGTON, J. L. & MORAN, P. M. 2014. Potentiation of latent inhibition by haloperidol and clozapine is attenuated in Dopamine D2 receptor (Drd-2)-deficient mice: do antipsychotics influence learning to ignore irrelevant stimuli via both Drd-2 and non-Drd-2 mechanisms? *Journal of psychopharmacology (Oxford, England),* 28**,** 973-977.
O'LEARY, N. A., WRIGHT, M. W., BRISTER, J. R., CIUFO, S., HADDAD, D., MCVEIGH, R., RAJPUT, B., ROBBERTSE, B., SMITH-WHITE, B., AKO-ADJEI, D., ASTASHYN, A., BADRETDIN, A., BAO, Y., BLINKOVA, O., BROVER, V., CHETVERNIN, V., CHOI, J., COX, E., ERMOLAEVA, O., FARRELL, C. M., GOLDFARB, T., GUPTA, T., HAFT, D., HATCHER, E., HLAVINA, W., JOARDAR, V. S., KODALI, V. K., LI, W., MAGLOTT, D., MASTERSON, P., MCGARVEY, K. M., MURPHY, M. R., O'NEILL, K., PUJAR, S., RANGWALA, S. H., RAUSCH, D., RIDDICK, L. D., SCHOCH, C., SHKEDA, A., STORZ, S. S., SUN, H., THIBAUD-NISSEN, F., TOLSTOY, I., TULLY, R. E., VATSAN, A. R., WALLIN, C., WEBB, D., WU, W., LANDRUM, M. J., KIMCHI, A., TATUSOVA, T., DICUCCIO, M., KITTS, P., MURPHY, T. D. & PRUITT, K. D. 2016. Reference sequence (RefSeq) database at NCBI: current status, taxonomic expansion, and functional annotation. *Nucleic Acids Res,* 44**,** D733-45.
O'NEILL, J. S. & HASTINGS, M. H. 2008. Increased coherence of circadian rhythms in mature fibroblast cultures. *J Biol Rhythms,* 23**,** 483-8.
O'NEIL, D., MENDEZ-FIGUEROA, H., MISTRETTA, T.-A., SU, C., LANE, R. H. & AAGAARD, K. M. 2013. Dysregulation of Npas2 Leads to Altered Metabolic Pathways in a Murine Knockout Model. *Molecular genetics and metabolism,* 110**,** 10.1016/j.ymgme.2013.08.015.
O'NEIL, D. S., STEWART, C. J., CHU, D. M., GOODSPEED, D. M., GONZALEZ-RODRIGUEZ, P. J., SHOPE, C. D. & AAGAARD, K. M. 2017. Conditional postnatal deletion of the neonatal murine hepatic circadian gene, Npas2, alters the gut microbiome following restricted feeding. *American Journal of Obstetrics and Gynecology,* 217**,** 218.e1-218.e15.
OISHI, Y., TAKATA, Y., TAGUCHI, Y., KOHTOH, S., URADE, Y. & LAZARUS, M. 2016. Polygraphic Recording Procedure for Measuring Sleep in Mice. *Journal of Visualized Experiments : JoVE***,** 53678.
OLIVEROS, J. C. 2007. VENNY. An interactive tool for comparing lists with Venn Diagrams.
OSLAND, T. M., FERNØ, J., HÅVIK, B., HEUCH, I., RUOFF, P., LÆRUM, O. D. & STEEN, V. M. 2011. Lithium differentially affects clock gene expression in serum-shocked NIH-3T3 cells. *J Psychopharmacol,* 25**,** 924-33.
OTSUKA, T., THI LE, H., KOHSAKA, A., SATO, F., IHARA, H., NAKAO, T. & MAEDA, M. 2020. Adverse Effects of Circadian Disorganization on Mood and Molecular Rhythms in the Prefrontal Cortex of Mice. *Neuroscience,* 432**,** 44-54.
OYEGBAMI, O., COLLINS, H. M., PARDON, M. C., EBLING, F. J., HEERY, D. M. & MORAN, P. M. 2017. Abnormal clock gene expression and locomotor activity rhythms in two month-old female APPSwe/PS1dE9 mice. *Curr Alzheimer Res*.
OZBURN, A. R., FALCON, E., TWADDLE, A., NUGENT, A. L., GILLMAN, A. G., SPENCER, S. M., AREY, R. N., MUKHERJEE, S., LYONS-WEILER, J., SELF, D. W. & MCCLUNG, C. A. 2015. Direct regulation of diurnal Drd3 expression and cocaine reward by NPAS2. *Biol Psychiatry,* 77**,** 425-433.
OZBURN, A. R., KERN, J., PAREKH, P. K., LOGAN, R. W., LIU, Z., FALCON, E., BECKER-KRAIL, D., PUROHIT, K., EDGAR, N. M., HUANG, Y. & MCCLUNG,

C. A. 2017. NPAS2 Regulation of Anxiety-Like Behavior and GABAA Receptors. *Frontiers in Molecular Neuroscience,* 10**,** 360.

PACK, A. I., GALANTE, R. J., MAISLIN, G., CATER, J., METAXAS, D., LU, S., ZHANG, L., VON SMITH, R., KAY, T., LIAN, J., SVENSON, K. & PETERS, L. L. 2007. Novel method for high-throughput phenotyping of sleep in mice. *Physiol Genomics,* 28**,** 232-8.

PANDA, S., ANTOCH, M. P., MILLER, B. H., SU, A. I., SCHOOK, A. B., STRAUME, M., SCHULTZ, P. G., KAY, S. A., TAKAHASHI, J. S. & HOGENESCH, J. B. 2002a. Coordinated Transcription of Key Pathways in the Mouse by the Circadian Clock. *Cell,* 109**,** 307-320.

PANDA, S., HOGENESCH, J. B. & KAY, S. A. 2002b. Circadian rhythms from flies to human. *Nature,* 417**,** 329-35.

PAPATHEODOROU, I., MORENO, P., MANNING, J., FUENTES, A. M.-P., GEORGE, N., FEXOVA, S., FONSECA, N. A., FÜLLGRABE, A., GREEN, M., HUANG, N., HUERTA, L., IQBAL, H., JIANU, M., MOHAMMED, S., ZHAO, L., JARNUCZAK, A. F., JUPP, S., MARIONI, J., MEYER, K., PETRYSZAK, R., PRADA MEDINA, C. A., TALAVERA-LÓPEZ, C., TEICHMANN, S., VIZCAINO, J. A. & BRAZMA, A. 2019. Expression Atlas update: from tissues to single cells. *Nucleic Acids Research,* 48**,** D77-D83.

PARSONS, M. J., BRANCACCIO, M., SETHI, S., MAYWOOD, E. S., SATIJA, R., EDWARDS, J. K., JAGANNATH, A., COUCH, Y., FINELLI, M. J., SMYLLIE, N. J., ESAPA, C., BUTLER, R., BARNARD, A. R., CHESHAM, J. E., SAITO, S., JOYNSON, G., WELLS, S., FOSTER, R. G., OLIVER, P. L., SIMON, M. M., MALLON, A. M., HASTINGS, M. H. & NOLAN, P. M. 2015. The Regulatory Factor ZFHX3 Modifies Circadian Function in SCN via an AT Motif-Driven Axis. *Cell,* 162**,** 607-21.

PARTCH, C. L., GREEN, C. B. & TAKAHASHI, J. S. 2014. Molecular architecture of the mammalian circadian clock. *Trends Cell Biol,* 24**,** 90-9.

PENDERGAST, J. S., WENDROTH, R. H., STENNER, R. C., KEIL, C. D. & YAMAZAKI, S. 2017. mPeriod2Brdm1and other single Period mutant mice have normal food anticipatory activity. *Scientific Reports,* 7**,** 15510.

PENDERGAST, J. S. & YAMAZAKI, S. 2018. The Mysterious Food-Entrainable Oscillator: Insights from Mutant and Engineered Mouse Models. *Journal of biological rhythms,* 33**,** 458-474.

PETT, J. P., KORENČIČ, A., WESENER, F., KRAMER, A. & HERZEL, H. 2016. Feedback Loops of the Mammalian Circadian Clock Constitute Repressilator. *PLOS Computational Biology,* 12**,** e1005266.

PHILLIPS, R. G. & LEDOUX, J. E. 1992. Differential contribution of amygdala and hippocampus to cued and contextual fear conditioning. *Behav Neurosci,* 106**,** 274-85.

PIMENTA, A. M., KAC, G., SOUZA, R. R., FERREIRA, L. M. & SILQUEIRA, S. M. 2012. Night-shift work and cardiovascular risk among employees of a public university. *Rev Assoc Med Bras (1992),* 58**,** 168-77.

PIZARRO, A., HAYER, K., LAHENS, N. F. & HOGENESCH, J. B. 2013. CircaDB: a database of mammalian circadian gene expression profiles. *Nucleic Acids Res,* 41**,** D1009-13.

PREITNER, N., DAMIOLA, F., LUIS LOPEZ, M., ZAKANY, J., DUBOULE, D., ALBRECHT, U. & SCHIBLER, U. 2002. The Orphan Nuclear Receptor REV-ERBα Controls Circadian Transcription within the Positive Limb of the Mammalian Circadian Oscillator. *Cell,* 110**,** 251-260.

QU, M., DUFFY, T., HIROTA, T. & KAY, S. A. 2018. Nuclear receptor HNF4A

transrepresses CLOCK:BMAL1 and modulates tissue-specific circadian networks. *Proceedings of the National Academy of Sciences,* 115**,** E12305-E12312.
RAGHURAM, S., STAYROOK, K. R., HUANG, P., ROGERS, P. M., NOSIE, A. K., MCCLURE, D. B., BURRIS, L. L., KHORASANIZADEH, S., BURRIS, T. P. & RASTINEJAD, F. 2007. Identification of heme as the ligand for the orphan nuclear receptors REV-ERBalpha and REV-ERBbeta. *Nature structural & molecular biology,* 14**,** 1207-1213.
RALPH, M., FOSTER, R., DAVIS, F. & MENAKER, M. 1990. Transplanted suprachiasmatic nucleus determines circadian period. *Science,* 247**,** 975-978.
RAMANATHAN, C., XU, H., KHAN, S. K., SHEN, Y., GITIS, P. J., WELSH, D. K., HOGENESCH, J. B. & LIU, A. C. 2014. Cell Type-Specific Functions of Period Genes Revealed by Novel Adipocyte and Hepatocyte Circadian Clock Models. *PLOS Genetics,* 10**,** e1004244.
RAN, F. A., HSU, P. D., LIN, C. Y., GOOTENBERG, J. S., KONERMANN, S., TREVINO, A. E., SCOTT, D. A., INOUE, A., MATOBA, S., ZHANG, Y. & ZHANG, F. 2013a. Double nicking by RNA-guided CRISPR Cas9 for enhanced genome editing specificity. *Cell,* 154**,** 1380-9.
RAN, F. A., HSU, P. D., WRIGHT, J., AGARWALA, V., SCOTT, D. A. & ZHANG, F. 2013b. Genome engineering using the CRISPR-Cas9 system. *Nat Protoc,* 8**,** 2281-2308.
REDDY, A. B., MAYWOOD, E. S., KARP, N. A., KING, V. M., INOUE, Y., GONZALEZ, F. J., LILLEY, K. S., KYRIACOU, C. P. & HASTINGS, M. H. 2007. Glucocorticoid signaling synchronizes the liver circadian transcriptome. *Hepatology,* 45**,** 1478-88.
REICK, M., GARCIA, J. A., DUDLEY, C. & MCKNIGHT, S. L. 2001. NPAS2: An Analog of Clock Operative in the Mammalian Forebrain. *Science,* 293**,** 506-509.
RENAUD, H. J., CUI, J. Y., KHAN, M. & KLAASSEN, C. D. 2011. Tissue distribution and gender-divergent expression of 78 cytochrome P450 mRNAs in mice. *Toxicol Sci,* 124**,** 261-77.
RICHTER, C. P. 1922. A Behavioristic Study of the Activity of the Rat. *Comparative Psychology Monographs,* 1, 2**,** 56-56.
ROYSTON, S. E., YASUI, N., KONDILIS, A. G., LORD, S. V., KATZENELLENBOGEN, J. A. & MAHONEY, M. M. 2014. ESR1 and ESR2 differentially regulate daily and circadian activity rhythms in female mice. *Endocrinology,* 155**,** 2613-2623.
RUTTER, J., REICK, M., WU, L. C. & MCKNIGHT, S. L. 2001. Regulation of clock and NPAS2 DNA binding by the redox state of NAD cofactors. *Science,* 293**,** 510-4.
SAINI, C., LIANI, A., CURIE, T., GOS, P., KREPPEL, F., EMMENEGGER, Y., BONACINA, L., WOLF, J. P., POGET, Y. A., FRANKEN, P. & SCHIBLER, U. 2013. Real-time recording of circadian liver gene expression in freely moving mice reveals the phase-setting behavior of hepatocyte clocks. *Genes Dev,* 27**,** 1526-36.
SANDERS, M. J., WILTGEN, B. J. & FANSELOW, M. S. 2003. The place of the hippocampus in fear conditioning. *European Journal of Pharmacology,* 463**,** 217-223.
SASAKI, H., HOKUGO, A., WANG, L., MORINAGA, K., NGO, J. T., OKAWA, H. & NISHIMURA, I. 2020. Neuronal PAS Domain 2 (Npas2)-Deficient Fibroblasts Accelerate Skin Wound Healing and Dermal Collagen Reconstruction. *Anat Rec (Hoboken),* 303**,** 1630-1641.
SATO, M., MURAKAMI, M., NODE, K., MATSUMURA, R. & AKASHI, M. 2014. The role of the endocrine system in feeding-induced tissue-specific circadian entrainment. *Cell Rep,* 8**,** 393-401.
SATO, T. K., PANDA, S., MIRAGLIA, L. J., REYES, T. M., RUDIC, R. D., MCNAMARA, P., NAIK, K. A., FITZGERALD, G. A., KAY, S. A. & HOGENESCH, J. B. 2004. A Functional Genomics Strategy Reveals Rora as a Component of the Mammalian

Circadian Clock. *Neuron,* 43**,** 527-537.
SCHMID, B., HELFRICH-FÖRSTER, C. & YOSHII, T. 2011. A New ImageJ Plug-in "ActogramJ" for Chronobiological Analyses. *Journal of Biological Rhythms,* 26**,** 464-467.
SCHWARTZ, W. J. & ZIMMERMAN, P. 1990. Circadian timekeeping in BALB/c and C57BL/6 inbred mouse strains. *J Neurosci,* 10**,** 3685-94.
SHEARMAN, L. P., SRIRAM, S., WEAVER, D. R., MAYWOOD, E. S., CHAVES, I., ZHENG, B., KUME, K., LEE, C. C., VAN DER HORST, G. T., HASTINGS, M. H. & REPPERT, S. M. 2000. Interacting molecular loops in the mammalian circadian clock. *Science,* 288**,** 1013-9.
SHEARMAN, L. P., ZYLKA, M. J., REPPERT, S. M. & WEAVER, D. R. 1999. Expression of basic helix-loop-helix/pas genes in the mouse suprachiasmatic nucleus. *Neuroscience,* 89**,** 387-397.
SHEN, B., ZHANG, W., ZHANG, J., ZHOU, J., WANG, J., CHEN, L., WANG, L., HODGKINS, A., IYER, V., HUANG, X. & SKARNES, W. C. 2014. Efficient genome modification by CRISPR-Cas9 nickase with minimal off-target effects. *Nat Methods,* 11**,** 399-402.
SHI, S., HIDA, A., MCGUINNESS, O. P., WASSERMAN, D. H., YAMAZAKI, S. & JOHNSON, C. H. 2010. Circadian clock gene Bmal1 is not essential; functional replacement with its paralog, Bmal2. *Current biology : CB,* 20**,** 316-321.
SIEPKA, S. M. & TAKAHASHI, J. S. 2005. Methods to record circadian rhythm wheel running activity in mice. *Methods Enzymol,* 393**,** 230-9.
SNIDER, K. H., SULLIVAN, K. A. & OBRIETAN, K. 2018. Circadian Regulation of Hippocampal-Dependent Memory: Circuits, Synapses, and Molecular Mechanisms. *Neural Plasticity,* 2018**,** 7292540.SMITH, C. M., HAYAMIZU, T. F., FINGER, J. H., BELLO, S. M., MCCRIGHT, I. J., XU, J., BALDARELLI, R. M., BEAL, J. S., CAMPBELL, J., CORBANI, L. E., FROST, P. J., LEWIS, J. R., GIANNATTO, S. C., MIERS, D., SHAW, D. R., KADIN, J. A., RICHARDSON, J. E., SMITH, C. L. & RINGWALD, M. 2018. The mouse Gene Expression Database (GXD): 2019 update. *Nucleic Acids Research,* 47**,** D774-D779.
SO, A. Y., BERNAL, T. U., PILLSBURY, M. L., YAMAMOTO, K. R. & FELDMAN, B. J. 2009. Glucocorticoid regulation of the circadian clock modulates glucose homeostasis. *Proc Natl Acad Sci U S A,* 106**,** 17582-7.
SON, G. H., CHUNG, S. & KIM, K. 2011. The adrenal peripheral clock: glucocorticoid and the circadian timing system. *Front Neuroendocrinol,* 32**,** 451-65.
SONG, B., CHEN, Y., LIU, Y., WAN, C., ZHANG, L. & ZHANG, W. 2018. NPAS2 regulates proliferation of acute myeloid leukemia cells via CDC25A-mediated cell cycle progression and apoptosis. *J Cell Biochem*.
STRAIF, K., BAAN, R., GROSSE, Y., SECRETAN, B., EL GHISSASSI, F., BOUVARD, V., ALTIERI, A., BENBRAHIM-TALLAA, L. & COGLIANO, V. 2007. Carcinogenicity of shift-work, painting, and fire-fighting. *Lancet Oncol,* 8**,** 1065-6.
SUN, X., DANG, F., ZHANG, D., YUAN, Y., ZHANG, C., WU, Y., WANG, Y. & LIU, Y. 2015. Glucagon-CREB/CRTC2 signaling cascade regulates hepatic BMAL1 protein. *J Biol Chem,* 290**,** 2189-97.
TAKAHASHI, J. S., HONG, H.-K., KO, C. H. & MCDEARMON, E. L. 2008. The genetics of mammalian circadian order and disorder: implications for physiology and disease. *Nat Rev Genet,* 9**,** 764-775.
TAKASU, N. N., KUROSAWA, G., TOKUDA, I. T., MOCHIZUKI, A., TODO, T. & NAKAMURA, W. 2012. Circadian Regulation of Food-Anticipatory Activity in Molecular Clock–Deficient Mice. *PLOS ONE,* 7**,** e48892.

TAKEDA, Y., KANG, H. S., ANGERS, M. & JETTEN, A. M. 2011. Retinoic acid-related orphan receptor γ directly regulates neuronal PAS domain protein 2 transcription in vivo. *Nucleic Acids Res,* 39**,** 4769-82.

TROTT, A. J. & MENET, J. S. 2018. Regulation of circadian clock transcriptional output by CLOCK:BMAL1. *PLOS Genetics,* 14**,** e1007156.

TSUCHIYA, Y., AKASHI, M. & NISHIDA, E. 2003. Temperature compensation and temperature resetting of circadian rhythms in mammalian cultured fibroblasts. *Genes to Cells,* 8**,** 713-720.

TSUCHIYA, Y., NAKAJIMA, M. & YOKOI, T. 2005. Cytochrome P450-mediated metabolism of estrogens and its regulation in human. *Cancer Letters,* 227**,** 115-124.

VALENTINUZZI, V. S., KOLKER, D. E., VITATERNA, M. H., FERRARI, E. A. M., TAKAHASHI, J. S. & TUREK, F. W. 2001. Effect of circadian phase on context and cued fear conditioning in C57BL/6J mice. *Animal Learning & Behavior,* 29**,** 133-142.

VETTER, C., DASHTI, H. S., LANE, J. M., ANDERSON, S. G., SCHERNHAMMER, E. S., RUTTER, M. K., SAXENA, R. & SCHEER, F. 2018. Night Shift Work, Genetic Risk, and Type 2 Diabetes in the UK Biobank. *Diabetes Care,* 41**,** 762-769.

VILLASANA, L., ROSENBERG, J. & RABER, J. 2010. Sex-dependent effects of 56Fe irradiation on contextual fear conditioning in C57BL/6J mice. *Hippocampus,* 20**,** 19-23.

VITATERNA, M. H., KING, D. P., CHANG, A. M., KORNHAUSER, J. M., LOWREY, P. L., MCDONALD, J. D., DOVE, W. F., PINTO, L. H., TUREK, F. W. & TAKAHASHI, J. S. 1994. Mutagenesis and mapping of a mouse gene, Clock, essential for circadian behavior. *Science,* 264**,** 719-25.

VOLICER, L., HARPER, D. G., MANNING, B. C., GOLDSTEIN, R. & SATLIN, A. 2001. Sundowning and Circadian Rhythms in Alzheimer's Disease. *American Journal of Psychiatry,* 158**,** 704-711.

VOLLMERS, C., SCHMITZ, R. J., NATHANSON, J., YEO, G., ECKER, J. R. & PANDA, S. 2012. Circadian oscillations of protein-coding and regulatory RNAs in a highly dynamic mammalian liver epigenome. *Cell metabolism,* 16**,** 833-845.

VORHEES, C. V. & WILLIAMS, M. T. 2006. Morris water maze: procedures for assessing spatial and related forms of learning and memory. *Nature protocols,* 1**,** 848-858.

VRIEND, J. & REITER, R. J. 2015. Melatonin feedback on clock genes: a theory involving the proteasome. *J Pineal Res,* 58**,** 1-11.

WANG, F., ZHANG, L., ZHANG, Y., ZHANG, B., HE, Y., XIE, S., LI, M., MIAO, X., CHAN, E. Y., TANG, J. L., WONG, M. C., LI, Z., YU, I. T. & TSE, L. A. 2014. Meta-analysis on night shift work and risk of metabolic syndrome. *Obes Rev,* 15**,** 709-20.

WANG, L. M., DRAGICH, J. M., KUDO, T., ODOM, I. H., WELSH, D. K., O'DELL, T. J. & COLWELL, C. S. 2009. Expression of the circadian clock gene Period2 in the hippocampus: possible implications for synaptic plasticity and learned behaviour. *ASN Neuro,* 1.

WEINER, I. & ARAD, M. 2009. Using the pharmacology of latent inhibition to model domains of pathology in schizophrenia and their treatment. *Behavioural Brain Research,* 204**,** 369-386.

WELSH, D. K. & KAY, S. A. 2005. Bioluminescence imaging in living organisms. *Current Opinion in Biotechnology,* 16**,** 73-78.

WELSH, D. K., LOGOTHETIS, D. E., MEISTER, M. & REPPERT, S. M. 1995. Individual neurons dissociated from rat suprachiasmatic nucleus express independently phased circadian firing rhythms. *Neuron,* 14**,** 697-706.

WERTZ, A. T., RONDA, J. M., CZEISLER, C. A. & WRIGHT, K. P., JR. 2006. Effects of sleep inertia on cognition. *JAMA,* 295**,** 163-4.

WIATER, M. F., LI, A. J., DINH, T. T., JANSEN, H. T. & RITTER, S. 2013. Leptin-sensitive neurons in the arcuate nucleus integrate activity and temperature circadian rhythms and anticipatory responses to food restriction. *Am J Physiol Regul Integr Comp Physiol,* 305**,** R949-60.

WILCOX, A. G., VIZOR, L., PARSONS, M. J., BANKS, G. & NOLAN, P. M. 2017. Inducible Knockout of Mouse Zfhx3 Emphasizes Its Key Role in Setting the Pace and Amplitude of the Adult Circadian Clock. *Journal of Biological Rhythms,* 32**,** 433-443.

WRIGHT, K. P., LOWRY, C. A. & LEBOURGEOIS, M. K. 2012. Circadian and wakefulness-sleep modulation of cognition in humans. *Frontiers in Molecular Neuroscience,* 5**,** 50.

XIE, Y., TANG, Q., CHEN, G., XIE, M., YU, S., ZHAO, J. & CHEN, L. 2019. New Insights Into the Circadian Rhythm and Its Related Diseases. *Front Physiol,* 10.

XUE, X., LIU, F., HAN, Y., LI, P., YUAN, B., WANG, X., CHEN, Y., KUANG, Y., ZHI, Q. & ZHAO, H. 2014. Silencing NPAS2 promotes cell growth and invasion in DLD-1 cells and correlated with poor prognosis of colorectal cancer. *Biochem Biophys Res Commun,* 450**,** 1058-62.

YAMAMOTO, T., NAKAHATA, Y., TANAKA, M., YOSHIDA, M., SOMA, H., SHINOHARA, K., YASUDA, A., MAMINE, T. & TAKUMI, T. 2005. Acute physical stress elevates mouse period1 mRNA expression in mouse peripheral tissues via a glucocorticoid-responsive element. *J Biol Chem,* 280**,** 42036-43.

YAMAZAKI, S., NUMANO, R., ABE, M., HIDA, A., TAKAHASHI, R., UEDA, M., BLOCK, G. D., SAKAKI, Y., MENAKER, M. & TEI, H. 2000. Resetting central and peripheral circadian oscillators in transgenic rats. *Science,* 288**,** 682-5.

YAN, J., WANG, H., LIU, Y. & SHAO, C. 2008. Analysis of Gene Regulatory Networks in the Mammalian Circadian Rhythm. *PLOS Computational Biology,* 4**,** e1000193.

YAN, S., SCHUBERT, M., YOUNG, M. & WANG, B. 2017. Applications of Cas9 nickases for genome engineering. *Integrated DNA Technologies, Application Note.* https://sfvideo.blob.core.windows.net/sitefinity/docs/default-source/application-note/applications-of-cas9-nickases-for-genome-engineering.pdf.

YE, R., SELBY, C. P., CHIOU, Y. Y., OZKAN-DAGLIYAN, I., GADDAMEEDHI, S. & SANCAR, A. 2014. Dual modes of CLOCK:BMAL1 inhibition mediated by Cryptochrome and Period proteins in the mammalian circadian clock. *Genes Dev,* 28**,** 1989-98.

YEUNG, J., MERMET, J., JOUFFE, C., MARQUIS, J., CHARPAGNE, A., GACHON, F. & NAEF, F. 2018. Transcription factor activity rhythms and tissue-specific chromatin interactions explain circadian gene expression across organs. *Genome Res,* 28**,** 182-191.

YI, C.-X., VAN DER VLIET, J., DAI, J., YIN, G., RU, L. & BUIJS, R. M. 2006. Ventromedial Arcuate Nucleus Communicates Peripheral Metabolic Information to the Suprachiasmatic Nucleus. *Endocrinology,* 147**,** 283-294.

YI, C. X., LA FLEUR, S. E., FLIERS, E. & KALSBEEK, A. 2010. The role of the autonomic nervous liver innervation in the control of energy metabolism. *Biochim Biophys Acta,* 1802**,** 416-31.

YOSHII, K., ISHIJIMA, S. & SAGAMI, I. 2013. Effects of NAD(P)H and its derivatives on the DNA-binding activity of NPAS2, a mammalian circadian transcription factor. *Biochem Biophys Res Commun,* 437**,** 386-91.

YOSHITANE, H. & FUKADA, Y. 2009. CIPC-dependent phosphorylation of CLOCK and NPAS2 in circadian clockwork. *Sleep and Biological Rhythms,* 7**,** 226-234.

YUAN, P., LI, J., ZHOU, F., HUANG, Q., ZHANG, J., GUO, X., LYU, Z., ZHANG, H. & XING, J. 2017. NPAS2 promotes cell survival of hepatocellular carcinoma by transactivating CDC25A. *Cell Death Dis,* 8**,** e2704.

ZERBINO, D. R., ACHUTHAN, P., AKANNI, W., AMODE, M R., BARRELL, D., BHAI, J., BILLIS, K., CUMMINS, C., GALL, A., GIRÓN, C. G., GIL, L., GORDON, L., HAGGERTY, L., HASKELL, E., HOURLIER, T., IZUOGU, O. G., JANACEK, S. H., JUETTEMANN, T., TO, J. K., LAIRD, M. R., LAVIDAS, I., LIU, Z., LOVELAND, J. E., MAUREL, T., MCLAREN, W., MOORE, B., MUDGE, J., MURPHY, D. N., NEWMAN, V., NUHN, M., OGEH, D., ONG, C. K., PARKER, A., PATRICIO, M., RIAT, H. S., SCHUILENBURG, H., SHEPPARD, D., SPARROW, H., TAYLOR, K., THORMANN, A., VULLO, A., WALTS, B., ZADISSA, A., FRANKISH, A., HUNT, S. E., KOSTADIMA, M., LANGRIDGE, N., MARTIN, F. J., MUFFATO, M., PERRY, E., RUFFIER, M., STAINES, D. M., TREVANION, S. J., AKEN, B. L., CUNNINGHAM, F., YATES, A. & FLICEK, P. 2018. Ensembl 2018. *Nucleic Acids Research,* 46**,** D754-D761.

ZHANG, R., LAHENS, N. F., BALLANCE, H. I., HUGHES, M. E. & HOGENESCH, J. B. 2014. A circadian gene expression atlas in mammals: implications for biology and medicine. *Proc Natl Acad Sci U S A,* 111**,** 16219-24.

ZHAO, W. N., MALININ, N., YANG, F. C., STAKNIS, D., GEKAKIS, N., MAIER, B., REISCHL, S., KRAMER, A. & WEITZ, C. J. 2007. CIPC is a mammalian circadian clock protein without invertebrate homologues. *Nat Cell Biol,* 9**,** 268-75.

ZHOU, D., WANG, Y., CHEN, L., JIA, L., YUAN, J., SUN, M., ZHANG, W., WANG, P., ZUO, J., XU, Z. & LUAN, J. 2016. Evolving roles of circadian rhythms in liver homeostasis and pathology. *Oncotarget,* 7**,** 8625-39.

ZHOU, Y. D., BARNARD, M., TIAN, H., LI, X., RING, H. Z., FRANCKE, U., SHELTON, J., RICHARDSON, J., RUSSELL, D. W. & MCKNIGHT, S. L. 1997. Molecular characterization of two mammalian bHLH-PAS domain proteins selectively expressed in the central nervous system. *Proceedings of the National Academy of Sciences of the United States of America,* 94**,** 713-718.

ZIELINSKI, T., MOORE, A. M., TROUP, E., HALLIDAY, K. J. & MILLAR, A. J. 2014. Strengths and limitations of period estimation methods for circadian data. *PLoS One,* 9**,** e96462.